

Mark Berlin

Predicting Oral Absorption of Poorly Soluble Weakly Basic Drugs

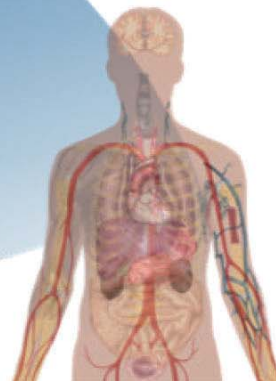
in vitro



in silico



in vivo



Cuvillier Verlag Göttingen
Internationaler wissenschaftlicher Fachverlag



Predicting Oral Absorption of Poorly Soluble Weakly Basic Drugs





Mark Berlin

Predicting Oral Absorption of Poorly Soluble Weakly Basic Drugs



Cuvillier Verlag Göttingen
Internationaler wissenschaftlicher Fachverlag



Bibliografische Information der Deutschen Nationalbibliothek

Die Deutsche Nationalbibliothek verzeichnet diese Publikation in der Deutschen Nationalbibliografie; detaillierte bibliografische Daten sind im Internet über <http://dnb.d-nb.de> abrufbar.

1. Aufl. - Göttingen: Cuvillier, 2015

Zugl.: Frankfurt am Main, Univ., Diss., 2015

© CUVILLIER VERLAG, Göttingen 2015

Nonnenstieg 8, 37075 Göttingen

Telefon: 0551-54724-0

Telefax: 0551-54724-21

www.cuvillier.de

Alle Rechte vorbehalten. Ohne ausdrückliche Genehmigung des Verlages ist es nicht gestattet, das Buch oder Teile daraus auf fotomechanischem Weg (Fotokopie, Mikrokopie) zu vervielfältigen.

1. Auflage, 2015

Gedruckt auf umweltfreundlichem, säurefreiem Papier aus nachhaltiger Forstwirtschaft.

ISBN 978-3-7369-9146-0

eISBN 978-3-7369-8146-1



Acknowledgements

First and foremost my deepest gratitude to Prof. Dr. Jennifer B. Dressman for her continuous guidance, support and encouragement throughout my research work. I want to thank for her time and energy invested in valuable advices, discussions as well as for her admirable care, motivation and open mindedness. I deeply appreciate being given the opportunity to work under the supervision of Prof. Dressman.

I also want to thank my friends and colleagues at the Institute of Pharmaceutical Technology, namely Mr. Cord Andreas, Dr. Marcel Arndt, Ms. Susanne Bayer, Ms. Gerlinde Born, Dr. Miriam Dadparvar, Mr. Yang Fei, Mr. Alexander Fuchs, Ms. Simone Hansmann, Mrs. Christine Janas, Dr. Atsushi Kambayashi, Dr. Murat Kilic, Mr. Andeas Koczwarra, Dr. Edmund "Ed" Kostewicz, Prof. Dr. Jörg Kreuter, Dr. Anna Christine Mieden, Dr. Astrid Mühlstein, Ms. Lisa Nothnagel, Mr. Keiichi Otsuka, Dr. Ina Rosenberger, Mr. Karim Sempf, Dr. Thomas Taupitz, Mr. Julian Thinnies, Dr. Waralee Watcharin, Dr. Matthias Wacker and Dr. Christian Wagner.

My very special thanks go to Dr. Anita Nair, Dr. Stefanie Straub and Mr. Aaron Ruff for the good times we had.

My appreciation goes also to the technical staff of the Institute, Mrs. Hannelore Berger, Ms. Mareike Götz, Mrs. Elisabeth "Sissy" Herbert, Mrs. Birgit Johann, Mr. Kaufmann and Mrs. Sylvia Niederdorf.

Big thanks go to our project partners, Dr. Dieter Baumann, Mr. Karl-Heinz Przyklenk, Mrs. Annette Richtberg (Hennig Arzneimittel GmbH, Flörsheim am Main, Germany), Dr. Filippos Kesisoglou, Mr. Michael Hong Wang and Mrs. Wei Xu (Merck Sharp & Dohme, Kenilworth, New Jersey, USA) for their professional support, valuable discussions and input. Special thanks go also to Prof. Dr. Christos Reppas (National and Kapodistrian University, Athens, Greece) for the valued scientific input and conversations.

My deepest gratitude, appreciation and love go to my dear parents, Henrietta Deborah Ruth and Alexander and to my dear sister Beata Esther Feiga for their incomparable encouragement and motivation throughout my studies and PhD work. Without you it would not have been possible.





Dedicated to my parents,
Henrietta Deborah Ruth and Alexander Berlin

“Stay hungry. Stay foolish.”
Steward Brand





Predicting Oral Absorption of Poorly Soluble Weakly Basic Drugs

Dissertation
zur Erlangung des Doktorgrades
der Naturwissenschaften

Vorgelegt beim Fachbereich 14
Biochemie, Chemie und Pharmazie
der Goethe-Universität
in Frankfurt am Main

von Mark Berlin
aus Vilnius (Litauen)

Frankfurt am Main, 2015
(D30)



vom Fachbereich der Biochemie, Chemie und Pharmazie der Goethe-Universität als
Dissertation angenommen.

Dekan: Prof. Dr. Michael Karas

1. Gutachter: Prof. Dr. Jennifer B. Dressman

2. Gutachter: Prof. Dr. Christos Reppas

Datum der Disputation: 11. November 2015



Index

1	Introduction	1
1.1	Drug transit through the upper GI tract.....	2
1.2	Determinants of drug absorption	4
1.2.1	The biopharmaceutics classification system	4
1.2.2	The biopharmaceutics drug disposition classification system.....	5
1.2.3	The developability classification system	6
1.3	Weak bases and the GI tract.....	7
1.3.1	pH in the GI tract	7
1.3.2	Bile salts and food in the GI tract	9
1.3.3	Gastric emptying	10
1.4	Simulation of <i>in vivo</i> drug dissolution	10
1.4.1	Dissolution media simulating GI fluids	10
1.4.2	Simulation of GI dissolution conditions	11
1.5	Drug permeability assessment	14
1.6	Physiologically based pharmacokinetic modeling	16
1.6.1	PBPK modeling approaches	16
1.6.2	Software for PBPK modeling.....	17
1.6.2.1	<i>MATLAB[®] and STELLA[®]</i>	17
1.6.2.2	<i>Commercial software (Simcyp[®], GastroPlus[®], PK-Sim[®]) and GI-Sim[®]</i>	18
1.7	Aims of this work	20
2	Materials and Methods.....	21
2.1	Materials.....	21
2.1.1	Chemicals	21
2.1.2	Model substance cinnarizine	22
2.1.3	Model substance atazanavir	24
2.2	Methods.....	28
2.2.1	HPLC-UV setup.....	28
2.2.2	Biorelevant media	29
2.2.3	Solubility assessment.....	31
2.2.4	Dissolution experiments	33
2.2.5	“Dumping” experiments.....	33
2.2.6	Transfer experiments	33
2.2.7	WinNonLin [®] - assessment of pharmacokinetics of API formulations	38
2.2.8	STELLA [®]	39
2.2.9	Simcyp [®]	47
2.2.10	Statistical comparison of predicted plasma profiles using different transfer experiment approaches	51



3	Results	52
3.1	Cinnarizine – investigation of <i>in vitro</i> behavior	52
3.1.1	Solubility results	52
3.1.2	Dissolution of cinnarizine tablets in biorelevant media	53
3.1.3	Dumping of pure cinnarizine	57
3.1.4	Investigation of supersaturation and precipitation of cinnarizine during transfer experiments	58
3.2	Cinnarizine - <i>in silico</i> plasma profile simulation	66
3.2.1	Evaluation of distribution and elimination kinetics of various cinnarizine tablets using WinNonLin®	66
3.2.2	STELLA® model - investigation of permeability restrictions of cinnarizine using fed state simulations	67
3.2.3	STELLA® “dissolution-only” vs. “supersaturation and precipitation” PBPK model in cinnarizine fasted state simulations	69
3.2.4	STELLA® statistical comparison analysis of different transfer rates	73
3.2.5	STELLA® sensitivity analysis of cinnarizine plasma profile predictions	74
3.2.6	Summary of cinnarizine plasma profile simulations using Simcyp®	77
3.3	Summary of the cinnarizine investigation and formulation suggestions	78
3.4	Atazanavir sulfate – investigation of <i>in vitro</i> behavior	80
3.4.1	Solubility results	80
3.4.1.1	<i>Equilibrium solubility</i>	80
3.4.1.2	<i>Kinetic solubility</i>	82
3.4.2	Dissolution results of atazanavir sulfate capsules in biorelevant media	83
3.4.3	Dumping results of atazanavir sulfate	87
3.4.4	Investigation of the atazanavir sulfate concentration profile during simulated transfer from the stomach to the intestine	88
3.5	Atazanavir sulfate - <i>in silico</i> plasma profile simulation	95
3.5.1	Evaluation of distribution and elimination kinetics of atazanavir using WinNonLin® analysis of literature PK data	95
3.5.2	Permeability evaluation of atazanavir	96
3.5.3	STELLA® plasma profile predictions of atazanavir capsules in the fasted state	97
3.5.4	STELLA® sensitivity analysis on atazanavir plasma profile predictions	104
3.6	Summary of atazanavir plasma profile simulations using Simcyp®	109
3.7	Summary of the atazanavir investigation and formulation suggestions	110
4	General discussion and conclusions	113
4.1	Choosing the right <i>in vitro</i> investigation approach	113
4.2	Formulation enhancement approaches for weakly basic drugs	120
4.3	Choosing the right PBPK modeling approach	122
4.3.1	Development and evolution of the STELLA® model	122



4.3.2	Self-built versus commercial PBPK models (STELLA [®] versus Simcyp [®])	123
4.3.2.1	<i>Input of release and dissolution profiles</i>	124
4.3.2.2	<i>Opportunities for simulating pharmacokinetics of modified release formulations</i>	125
4.3.2.3	<i>Input of permeability</i>	125
4.3.2.4	<i>Middle-out and Bottom-up modeling approaches</i>	126
4.3.2.5	<i>Virtual populations</i>	127
4.3.2.6	<i>Summary</i>	127
4.4	Outlook	128
5	Summary	131
6	German Summary (Deutsche Zusammenfassung)	137
7	Appendix	143
7.1	STELLA [®] sensitivity analysis of cinnarizine plasma profile predictions	143
7.2	STELLA [®] sensitivity analysis of atazanavir sulfate plasma profile predictions	145
7.3	Simcyp [®] plasma profile predictions of cinnarizine	148
7.3.1	Simcyp [®] plasma profile predictions of cinnarizine in the fasted state	148
7.3.2	Simcyp [®] plasma profile predictions of cinnarizine in the fed state	155
7.3.3	Simcyp [®] sensitivity analysis of cinnarizine plasma profile predictions	161
7.3.4	Simcyp [®] plasma profile predictions of cinnarizine using fitted Vd	172
7.4	Simcyp [®] plasma profile predictions of atazanavir	176
7.4.1	Simcyp [®] plasma profile predictions of atazanavir in the fasted state	176
7.4.2	Simcyp [®] plasma profile predictions of atazanavir in the fed state	184
7.4.3	Simcyp [®] sensitivity analysis of atazanavir plasma profile predictions	188
8	References	203
9	Curriculum Vitae	216
9.1	Personal Information	216
9.2	Professional experience	216
9.3	Education	217
10	Scientific Publications	218
10.1	Papers	218
10.2	Posters	218
11	Academic Teachers	218



List of Figures

Fig. 1.1: Dosage form and drug transit in the upper GI tract.....	3
Fig. 1.2: Categorization of APIs based on the biopharmaceutics classification system.....	4
Fig. 1.3: Categorization of APIs based on biopharmaceutics drug disposition classification system.....	6
Fig. 1.4: Characterization of APIs based on developability classification system. Green bars describe the extension of the dose solubility ratio from 250 ml to 500 ml.	7
Fig. 1.5: pH solubility behavior of weak bases and acids in relation to the upper GI pH.....	8
Fig. 1.6: Possible dissolution scenarios for weak bases upon entering the upper small intestine	9
Fig. 1.7: Transfer model for the <i>in vitro</i> simulation of gastric emptying	13
Fig. 2.1: Structure of cinnarizine.....	23
Fig. 2.2: Structure of atazanavir sulfate.....	26
Fig. 2.3: Evaluation of fraction of drug dissolved (f_d) and precipitation kinetics during and after gastric emptying (k_p). Total mass of drug emptied into intestine at time t is shown as a theoretical concentration curve (\cdots). The observed percentage (mass) of drug dissolved in the intestine at time t and drug precipitation at times after gastric emptying is complete, t' , are presented in the continuous curve ($-$). The vertical line ($--$) represents the time at which gastric emptying is complete, t'	37
Fig. 2.4: Pharmacokinetic model used in WinNonLin [®] : k_{01} : absorption kinetics constant, k_{10} : elimination kinetics constant, k_{12} : deep compartment inflow constant (optional), k_{21} : deep compartment outflow constant (optional).	38
Fig. 2.5: PBPK model for <i>in vivo</i> API formulation behavior, in which only dissolution is accounted for (dissolution-only PBPK model).	39
Fig. 2.6: PBPK model for <i>in vivo</i> API formulation behavior, in which dissolution, supersaturation, subsequent precipitation and efflux/extraction kinetics can be accounted for (supersaturation and precipitation PBPK model).	40
Fig. 2.7: STELLA [®] dissolution-only PBPK model without permeability restrictions; green: pre-absorptive kinetics (gastric and intestinal dissolution, gastric emptying), orange: post-absorptive kinetics (distribution and elimination), dotted square: (optional) deep compartment kinetics.	41
Fig. 2.8: STELLA [®] dissolution-only PBPK model with permeability restrictions; green: pre-absorptive kinetics (gastric and intestinal dissolution, gastric emptying), orange: post-absorptive kinetics (distribution and elimination), red: absorption kinetics, dotted square: (optional) deep compartment kinetics.	43
Fig. 2.9: STELLA [®] supersaturation and precipitation PBPK model with permeability restrictions; yellow: fractioning of dissolved and solid drug during gastric emptying, blue: precipitation, dissolution and re-dissolution of drug after gastric emptying, red: absorption kinetics, orange: post-absorptive kinetics (distribution and elimination), dotted square: (optional) deep compartment kinetics.	46
Fig. 3.1: Solubilities of cinnarizine in biorelevant media (logarithmic scaling). Solubility values in $\mu\text{g/ml}$ along with the standard errors are shown on the bar for each medium.	53
Fig. 3.2: Dissolution of pure cinnarizine and cinnarizine tablets in fasted state gastric (A) and intestinal (B) media (some symbols are bigger than the standard deviation bars): Arlevert [®] (●) and Stugeron [®]	



(■), cinnarizine 20 mg (○) and 25 mg (□) (curves are overlapping) along with the theoretical % dissolved for 20 mg cinnarizine in FaSSIF-V2, based on its solubility (- -)..... 55

Fig. 3.3: Dissolution of pure cinnarizine and cinnarizine tablets in the fed gastric (A) and intestinal (B) biorelevant media (some symbols are bigger than the standard deviation bars): Arlevert[®] (●) and Cinnarizine 30 mg tablets (▲), pure cinnarizine 20 mg (○) and 30 mg (△) along with the maximum theoretical % dissolved for 30 mg cinnarizine in FaSSGF pH 5.0, based on its solubility (- -). 56

Fig. 3.4: Concentration profile of cinnarizine after dumping a solution of 20 mg cinnarizine in 250 ml FaSSGF pH 2.0 into 500 ml FaSSIF-V2(PO₄) along with the maximum theoretical % dissolved for 20 mg cinnarizine based on its solubility in the combination of FaSSGF pH 2.0 and FaSSIF-V2(PO₄) in the ratio of 1:2 (- -). 58

Fig. 3.5: Fasted state transfer of a solution of 20 (◆), 40 (■) and 80 mg (▲) cinnarizine in FaSSGF pH 2.0 into FaSSIF-V2(PO₄) using transfer rates of 3 h⁻¹ (A), 9 ml/min (B), 4 ml/min (C) and 0.5 ml/min (D). The theoretical transfer curve (- -) is displayed along with the maximum theoretical % dissolved for 20 mg cinnarizine based on its solubility in the combination of FaSSGF pH 2.0 and FaSSIF-V2(PO₄) in the ratio of 1:2 (- -). 59

Fig. 3.6: Fasted state transfer of 20 mg cinnarizine as a solution (●), dissolved Arlevert[®] tablets (◆) and intact Arlevert[®] tablets (▲) in FaSSGF pH 2.0 into FaSSIF-V2(PO₄) using transfer rates of 3 h⁻¹ (A), 9 ml/min (B) and 4 ml/min (C). The theoretical transfer curve (- -) is displayed along with the maximum theoretical % dissolved for 20 mg cinnarizine based on its solubility in the combination of FaSSGF pH 2.0 and FaSSIF-V2(PO₄) in the ratio of 1:2 (- -). 61

Fig. 3.7: Fasted state transfer of Arlevert[®] (○) and Stugeron[®] (●) cinnarizine tablets at 3 h⁻¹ (A), 9 ml/min (B), 4 ml/min (C) and 0.5 ml/min (D) transfer rates. The theoretical transfer curve (- -) is displayed along with the solubility (- -) of 25 mg cinnarizine in the combination of FaSSGF pH 2.0 and FaSSIF-V2(PO₄) in the ratio 1:2. 63

Fig. 3.8: Fed state transfer of Cinnarizine 30 mg tablets using the zero order transfer rate of 2 ml/min along with the theoretical transfer curve (- -). 65

Fig. 3.9: Fed state plasma profile predictions of Arlevert[®] (A) and Cinnarizine 30 mg (B) tablets using the dissolution-only PBPK models with and without permeability restrictions based on Caco-2 data. . 69

Fig. 3.10: Fasted state plasma profile predictions of Arlevert[®] (A) and Stugeron[®] (B) tablets using the dissolution-only and supersaturation and precipitation (obtained from transfer experiments at a rate of 3 h⁻¹) PBPK model. 71

Fig. 3.11: Fasted state plasma profile predictions of Arlevert[®] (-) and Stugeron[®] (-) tablets using the supersaturation and precipitation PBPK model after implementing results of different transfer rates. The *in vivo* plasma profiles of Arlevert[®] (○) and Stugeron[®] (●) are displayed against profile predictions for each transfer rate, i.e. 3 h⁻¹ (A), 9 ml/min (B), 4 ml/min (C) and 0.5 ml/min (D). 74

Fig. 3.12: Arlevert[®] in the fasted state - sensitivity analysis of the fraction dissolved constant (A), precipitation constant (B), the gastric emptying rate (C) and the effective permeability (D) on cinnarizine plasma profiles..... 75



Fig. 3.13: Arlever[®] in the fed state - sensitivity analysis of the z value in FeSSGF (A), the z value in FeSSIF-V2 (B) the gastric emptying rate (C) and the effective permeability (D) on cinnarizine plasma profiles 76

Fig. 3.14: Equilibrium solubilities of atazanavir in biorelevant media (logarithmic scaling). Solubility values in µg/ml along with the standard deviations are shown on the bar for each medium (n=3). 82

Fig. 3.15: Kinetic solubilities of atazanavir sulfate in biorelevant media over 24 hours (some symbols are bigger than the standard deviation bars) (n=3)..... 83

Fig. 3.16: Dissolution of different doses of atazanavir sulfate capsules (Reyataz[®]) in fasted state gastric (A) and intestinal (B) media (symbols are bigger than the standard deviation bars): 100 mg (◆), 200 mg (■), 400 mg (▲), 1200 mg (●) and solubility (- -)..... 84

Fig. 3.17: Dissolution of 400 mg atazanavir sulfate capsules (Reyataz[®]) in the fed state biorelevant media (some symbols are bigger than the standard deviation bars): FeSSGEm pH 2.75 (▲) and FeSSGEm pH 5.0 (■) along with the equilibrium solubility in FeSSGEm pH 2.75 (- -) and in FeSSGEm pH 5.0 (- -). Concentrations are presented in a logarithmic scale. 85

Fig. 3.18: Dissolution of 400 mg atazanavir sulfate capsules (Reyataz[®]) in FeSSIF-V2 (◆) (some symbols are bigger than the standard deviation bars) along with the equilibrium solubility (- -). Symbols are bigger than the standard deviation bars. 86

Fig. 3.19: Concentration profile of 200 mg atazanavir after the pre-dissolved compound in 250 ml FaSSGF pH 2.0 into 500 ml of FaSSIF-V2(PO₄) (some symbols are bigger than the standard deviation bars). The dotted line represents the kinetic solubility relative to the 200 mg atazanavir dose. 88

Fig. 3.20: Simulated fasted state transfer results of 100 mg (◆) and 200 mg (■) pre-dissolved atazanavir sulfate using the zero order transfer rate of 9 ml/min. The kinetic solubilities of atazanavir sulfate (solubility value at hour 1 in the 1:2 FaSSGF pH 2.0/FaSSIF-V2(PO₄) mixture) relative to the corresponding dose (- -) are presented along with the theoretical transfer curve (- -). Some of the error bars are smaller than the symbols. 89

Fig. 3.21: Simulated fasted state transfer results of Reyataz[®] 200 mg (amorphous) (▲), 200 mg atazanavir sulfate compound (crystalline) (○) and pre-dissolved 200 mg atazanavir sulfate (crystalline) (□) using the zero order transfer rate of 9 ml/min. The kinetic solubility of atazanavir sulfate (solubility value at hour 1 in the 1:2 FaSSGF pH 2.0/FaSSIF-V2(PO₄) mixture) relative to the 200 mg dose (- -) is presented along with the theoretical transfer curve (- -). Some of the error bars are smaller than the symbols..... 90

Fig. 3.22: Simulated fasted state transfer results of atazanavir sulfate capsules 100 mg (◆), 200 mg (■), 400 mg (▲), 1200 mg (●) using the first order transfer of 4 h⁻¹ (A) and zero order transfer rates of 9 ml/min (B) and 2 ml/min (C). The kinetic solubilities of atazanavir sulfate (solubility value at hour 1 in the 1:2 FaSSGF pH 2.0/FaSSIF-V2(PO₄) mixture) relative to the corresponding dose (- -) are presented along with the theoretical transfer curve (- -). Some of the error bars are smaller than the symbols..... 91

Fig. 3.23: Simulated fed state transfer results of 400 mg (2 x 200 mg) Reyataz[®] capsules using the 4 ml/min zero order transfer rate for 250 ml of FeSSGEm pH 2.75 (▲) and FeSSGF pH 2.75 (▲) as a VI



donor compartment. The solubilities of atazanavir sulfate in mixtures of FeSSGEm pH 2.75/FeSSIF-V2 (1:2) (– –) and FeSSGF pH 2.75/FeSSIF-V2 (1:2) (– –) are presented along with the theoretical transfer curve (– –). Some of the error bars are smaller than the symbols. 93

Fig. 3.24: Fed state transfer results (simulating the high fat meal) of 400 mg (2 x 200 mg) Reyataz[®] capsules using the 2 ml/min zero order transfer rate for 500 ml of FeSSGEm pH 5.0 (◆) as a donor compartment. The solubility of atazanavir sulfate in FeSSIF-V2 (– –) is presented along with the theoretical transfer curve (– –). Error bars are smaller than the symbols..... 93

Fig. 3.25: Observed (●) and predicted fasted state plasma profiles of 100 mg atazanavir sulfate capsules with 90% (–) and without (– –) efflux/extraction kinetics. Coefficient of variation is shown for the C_{max} value (reported as geometric mean (□)). 99

Fig. 3.26: Observed (●) and predicted fasted state plasma profiles of 200 mg (A), 400 mg (B) and 1200 mg (C) atazanavir sulfate capsules (–). Coefficients of variation are shown for the C_{max} values (reported as geometric means (□)). 100

Fig. 3.27: Observed and predicted fed state plasma profiles of 400 mg atazanavir sulfate (2 x 200 mg Reyataz[®]) capsules. Predictions were made using different transfer experiments using either FeSSGF pH 2.75 (“best case”) or FeSSGEm pH 2.75 (“worst case”) as donor media. The solid line shows the average of the best and worst case scenarios..... 103

Fig. 3.28: Sensitivity analysis of the fraction dissolved constant < 5 min (A), the fraction dissolved constant > 5 min (B), the gastric emptying constant (C), the permeability (D) the volume of distribution (E), and the elimination constant (F) on plasma profile predictions of 400 mg (2 x 200 mg) atazanavir sulfate capsules in the fasted state. The observed *in vivo* profile is shown along with coefficient of variation for the C_{max} value (reported as geometric mean). 105

Fig. 3.29: Sensitivity analysis was performed for simulations using data obtained from transfer experiments with FeSSGEm pH 2.75 as the donor compartment (“worst case”). Analysis of the fraction dissolved constant < 10 min (A), the fraction dissolved constant > 10 min (B), the precipitation constant (C), the gastric emptying constant (D), the permeability (E), the elimination constant (F), and the volume of distribution (G) on plasma profile predictions of 400 mg (2 x 200 mg) atazanavir sulfate in the fed state. 107

Fig. 3.30: Sensitivity analysis was performed for simulations using data obtained from transfer experiments with FeSSGF pH 2.75 as the donor compartment (“best case”). Analysis of the fraction dissolved constant < 20 min (A), the fraction dissolved constant > 20 min (B), the gastric emptying constant (C), the permeability (D), the volume of distribution (E) and the elimination constant (F) on plasma profile predictions of 400 mg (2 x 200 mg) atazanavir sulfate in the fed state. 108

Fig. 4.1: Proposed outline of *in vitro* experiments for investigation and development of drug products containing weak bases..... 115

Fig. 4.2: Coupling of *in vitro* data to *in silico* PBPK/PD modeling in order to investigate a therapeutic outcome of an API. 129

Fig. 7.1: Stugeron[®] in the fasted state - sensitivity analysis of the fraction dissolved constant (A), the precipitation constant (B), the gastric emptying rate (C) and the effective permeability (D) on cinnarizine plasma profiles..... 143



Fig. 7.2: Cinnarizine 30 mg tablets in the fed state - sensitivity analysis of the z value in FeSSGF (A), the z value in FeSSIF-V2 (B) the gastric emptying rate (C) and the effective permeability (D) on cinnarizine plasma profiles..... 144

Fig. 7.3: Sensitivity analysis of the fraction dissolved constant < 5 min (A), the fraction dissolved constant > 5 min (B), the gastric emptying constant (C), the permeability (D), the volume of distribution (E), and the elimination constant (F) on plasma profile predictions of 100 mg atazanavir sulfate capsules in the fasted state. 145

Fig. 7.4: Sensitivity analysis of the fraction dissolved constant < 5 min (A), the fraction dissolved constant > 5 min (B), the gastric emptying constant (C), the permeability (D), the volume of distribution (E), and the elimination constant (F) on plasma profile predictions of 200 mg atazanavir sulfate capsules in the fasted state. 146

Fig. 7.5: Sensitivity analysis of the fraction dissolved constant (A), the first order precipitation constant (B), the gastric emptying constant (C), the permeability (D), the volume of distribution (E), and the elimination constant (F) on plasma profile predictions of 1200 mg atazanavir sulfate capsules in the fasted state. 147

Fig. 7.6: Fasted state plasma profile predictions of Arlever[®] 20 mg (A) and Stugeron[®] 25 mg (B) by implementing biorelevant solubility of cinnarizine into the Simcyp[®] gastrointestinal solubility mask. . 149

Fig. 7.7: Fasted state plasma profile predictions of Arlever[®] 20 mg (A) and Stugeron[®] 25 mg (B) using Simcyp[®] predictions of cinnarizine solubility based on its physicochemical properties..... 152

Fig. 7.8: pH solubility profile of cinnarizine predicted by Simcyp[®] 152

Fig. 7.9: Fasted state plasma profile predictions of Arlever[®] 20 mg (A) and Stugeron[®] 25 mg (B) by implementing cinnarizine solubility at different pH values into the Simcyp[®] mask..... 154

Fig. 7.10: Fed state plasma profile predictions of Arlever[®] 20 mg (A) and Cinnarizine 30 mg tablets (B) by implementing dissolution profiles in FeSSGF pH 5.0 and FeSSIF-V2 into Simcyp[®] 156

Fig. 7.11: Fed state plasma profile predictions of Arlever[®] 20 mg (A) and Cinnarizine 30 mg tablets (B) by implementing biorelevant solubility of cinnarizine into the Simcyp[®] gastrointestinal solubility mask. 158

Fig. 7.12: Fed state plasma profile predictions of Arlever[®] 20 mg (A) and Cinnarizine 30 mg tablets (B) using Simcyp[®] predictions of cinnarizine solubility based on its physicochemical properties. 159

Fig. 7.13: Fed state plasma profile predictions of Arlever[®] 20 mg (A) and Cinnarizine 30 mg tablets (B) by implementing cinnarizine solubility at different pH values into the Simcyp[®] mask. 161

Fig. 7.14: Sensitivity analysis of the gastric emptying (A), the permeability (B), the volume of distribution (C) and the clearance (D) on plasma profile predictions of Arlever[®] in the fed state by implementing dissolution profiles in FeSSGF pH 5.0 and FeSSIF-V2 into Simcyp[®] 162

Fig. 7.15: Sensitivity analysis of the gastric emptying (A), the permeability (B), the volume of distribution (C) and the clearance (D) on plasma profile predictions of Cinnarizine 30 mg tablets in the fed state by implementing dissolution profiles in FeSSGF pH 5.0 and FeSSIF-V2 into Simcyp[®] 163

Fig. 7.16: Sensitivity analysis of the intestinal solubility (A), the supersaturation (B), the precipitation (C), the gastric emptying (D), the permeability (E), the volume of distribution (F) and the clearance (G)

VIII



on plasma profile predictions of Arlevert[®] in the fasted state by implementing biorelevant solubility of cinnarizine into the Simcyp[®] gastrointestinal solubility mask. 164

Fig. 7.17: Sensitivity analysis of the intestinal solubility (A), the supersaturation (B), the precipitation (C), the gastric emptying (D), the permeability (E), the volume of distribution (F) and the clearance (G) on plasma profile predictions of Stugeron[®] in the fasted state by implementing biorelevant solubility of cinnarizine into the Simcyp[®] gastrointestinal solubility mask. 165

Fig. 7.18: Sensitivity analysis of the gastric solubility (A), the intestinal solubility (B), the gastric emptying (C), the permeability (D), the volume of distribution (E) and the clearance (F) on plasma profile predictions of Arlevert[®] in the fed state by implementing biorelevant solubility of cinnarizine into the Simcyp[®] gastrointestinal solubility mask. 167

Fig. 7.19: Sensitivity analysis of the gastric solubility (A), the intestinal solubility (B), the gastric emptying (C), the permeability (D), the volume of distribution (E) and the clearance (F) on plasma profile predictions of Cinnarizine 30 mg tablets in the fed state by implementing biorelevant solubility of cinnarizine into the Simcyp[®] gastrointestinal solubility mask. 168

Fig. 7.20: Sensitivity analysis of the supersaturation (A), the precipitation (B), the gastric emptying (C), the permeability (D), the volume of distribution (E) and the clearance (F) on plasma profile predictions of Arlevert[®] in the fasted state using Simcyp[®] predictions of cinnarizine solubility by based on its physicochemical properties. 169

Fig. 7.21: Sensitivity analysis of the supersaturation (A), the precipitation (B), the gastric emptying (C), the permeability (D), the volume of distribution (E) and the clearance (F) on plasma profile predictions of Stugeron[®] in the fasted state using Simcyp[®] predictions of cinnarizine solubility based on its physicochemical properties. 170

Fig. 7.22: Sensitivity analysis of the gastric emptying (A), the permeability (B), the volume of distribution (C) and the clearance (D) on plasma profile predictions of Arlevert[®] in the fed state using Simcyp[®] predictions of cinnarizine solubility based on its physicochemical properties. 171

Fig. 7.23: Sensitivity analysis of the gastric emptying (A), the permeability (B), the volume of distribution (C) and the clearance (D) on plasma profile predictions of Cinnarizine 30 mg tablets in the fed state using Simcyp[®] predictions of cinnarizine solubility based on its physicochemical properties. 172

Fig. 7.24: Fasted state plasma profile predictions of Arlevert[®] 20 mg (A) and Stugeron[®] 25 mg (B) by implementing biorelevant solubility of cinnarizine into the Simcyp[®] gastrointestinal solubility mask. The two profiles were simulated using the “old Vd” (–) and “new Vd” (–) values. 173

Fig. 7.25: Fed state plasma profile predictions of Arlevert[®] 20 mg (A) and Cinnarizine 30 mg tablets (B) by implementing biorelevant dissolution profiles into the Simcyp[®] mask. The two profiles were simulated using the “old Vd” (–) and “new Vd” (–) values. 175

Fig. 7.26: Fasted state plasma profile predictions of atazanavir sulfate 100 mg (A), 200 mg (B), 400 mg (C) and 1200 mg (D) capsules by implementing kinetic biorelevant solubility of atazanavir into the Simcyp[®] gastrointestinal solubility mask. 178

Fig. 7.27: Predicted pH solubility profile for atazanavir in Simcyp[®]. 180



Fig. 7.28: Fasted state plasma profile predictions of atazanavir sulfate 100 mg (A), 200 mg (B), 400 mg (C) and 1200 mg (D) capsules using Simcyp [®] predictions of atazanavir solubility based on its physicochemical properties.....	180
Fig. 7.29: Fasted state plasma profile predictions of atazanavir sulfate 100 mg (A), 200 mg (B), 400 mg (C) and 1200 mg (D) capsules by implementing equilibrium solubilities of atazanavir at different pH values into the Simcyp [®] mask.....	182
Fig. 7.30: Fed state plasma profile predictions of atazanavir sulfate 400 mg capsules (2 x 200 Reyataz [®]) by implementing biorelevant solubility data into the Simcyp [®] gastrointestinal solubility mask: “worst case” (--) (using FeSSGEm pH 2.75 data) and “best case” (– –) (using FeSSGF pH 2.75 data).	184
Fig. 7.31: Fed state plasma profile predictions of atazanavir sulfate 400 mg capsules (2 x 200 Reyataz [®]) by using Simcyp [®] predictions of atazanavir solubility based on its physicochemical properties: “worst case” (--) (using FeSSGEm pH 2.75 data) and “best case” (– –) (using FeSSGF pH 2.75 data).....	186
Fig. 7.32: Fed state plasma profile predictions of atazanavir sulfate 400 mg capsules (2 x 200 Reyataz [®]) by implementing equilibrium solubilities of atazanavir at different pH values into the Simcyp [®] mask: “worst case” (--) (using FeSSGEm pH 2.75 data) and “best case” (– –) (using FeSSGF pH 2.75 data).	187
Fig. 7.33: Sensitivity analysis of the intestinal solubility (A), the gastric emptying (B), the permeability (C), the volume of distribution (D) and the clearance (E) on plasma profile predictions of 100 mg atazanavir sulfate in the fasted state by implementing biorelevant solubility of atazanavir into the Simcyp [®] gastrointestinal solubility mask.....	189
Fig. 7.34: Sensitivity analysis of the intestinal solubility (A), the gastric emptying (B), the permeability (C), the volume of distribution (D) and the clearance (E) on plasma profile predictions of 200 mg atazanavir sulfate in the fasted state by implementing biorelevant solubility of atazanavir into the Simcyp [®] gastrointestinal solubility mask.....	190
Fig. 7.35: Sensitivity analysis of the intestinal solubility (A), the gastric emptying (B), the permeability (C), the volume of distribution (D) and the clearance (E) on plasma profile predictions of 400 mg atazanavir sulfate in the fasted state by implementing biorelevant solubility of atazanavir into the Simcyp [®] gastrointestinal solubility mask.....	191
Fig. 7.36: Sensitivity analysis of the intestinal solubility (A), the gastric emptying (B), the permeability (C), the volume of distribution (D) and the clearance (E) on plasma profile predictions of 1200 mg atazanavir sulfate in the fasted state by implementing biorelevant solubility of atazanavir into the Simcyp [®] gastrointestinal solubility mask.....	192
Fig. 7.37: “worst case” example - sensitivity analysis of the intestinal solubility (A), the supersaturation (B), the precipitation (C), the gastric emptying (D), the permeability (E), the volume of distribution (F) and the clearance (G) on plasma profile predictions of 400 mg atazanavir sulfate in the fed state by implementing biorelevant solubility of atazanavir into the Simcyp [®] gastrointestinal solubility mask...	193
Fig. 7.38: “best case” example - sensitivity analysis of the intestinal solubility (A), the gastric emptying (B), the permeability (C), the volume of distribution (D) and the clearance (E) on plasma profile	

X



predictions of 400 mg atazanavir sulfate in the fed state by implementing biorelevant solubility of atazanavir into the Simcyp[®] gastrointestinal solubility mask. 194

Fig. 7.39: Sensitivity analysis of the gastric emptying (A), the permeability (B), the volume of distribution (C) and the clearance (D) on plasma profile predictions of 100 mg atazanavir sulfate in the fasted state using predicted atazanavir solubility by Simcyp[®]. 195

Fig. 7.40: Sensitivity analysis of the gastric emptying (A), the permeability (B), the volume of distribution (C) and the clearance (D) on plasma profile predictions of 200 mg atazanavir sulfate in the fasted state using predicted atazanavir solubility by Simcyp[®]. 195

Fig. 7.41: Sensitivity analysis of the gastric emptying (A), the permeability (B), the volume of distribution (C) and the clearance (D) on plasma profile predictions of 400 mg atazanavir sulfate in the fasted state using predicted atazanavir solubility by Simcyp[®]. 196

Fig. 7.42: Sensitivity analysis of the gastric emptying (A), the permeability (B), the volume of distribution (C) and the clearance (D) on plasma profile predictions of 1200 mg atazanavir sulfate in the fasted state using predicted atazanavir solubility by Simcyp[®]. 196

Fig. 7.43: “worst case” example - sensitivity analysis of supersaturation (A), precipitation (B), the gastric emptying (C), the permeability (D), the volume of distribution (E) and the clearance (F) on plasma profile predictions of 400 mg atazanavir sulfate in the fed state using predicted atazanavir solubility by Simcyp[®]. 197

Fig. 7.44: “best case” example - sensitivity analysis of the gastric emptying (A), the permeability (B), the volume of distribution (C) and the clearance (D) on plasma profile predictions of 400 mg atazanavir sulfate in the fed state using predicted atazanavir solubility by Simcyp[®]. 198

Fig. 7.45: Sensitivity analysis of the gastric emptying (A), the permeability (B), the volume of distribution (C) and the clearance (D) on plasma profile predictions of 200 mg atazanavir sulfate in the fasted state by implementing equilibrium solubilities of atazanavir at different pH values into the Simcyp[®] mask. 199

Fig. 7.46: Sensitivity analysis of the gastric emptying (A), the permeability (B), the volume of distribution (C) and clearance (D) on plasma profile predictions of 200 mg atazanavir sulfate in the fasted state by implementing equilibrium solubilities of atazanavir at different pH values into the Simcyp[®] mask. 199

Fig. 7.47: Sensitivity analysis of the gastric emptying (A), the permeability (B), the volume of distribution (C) and the clearance (D) on plasma profile predictions of 400 mg atazanavir sulfate in the fasted state by implementing equilibrium solubilities of atazanavir at different pH values into the Simcyp[®] mask. 200

Fig. 7.48: Sensitivity analysis of the gastric emptying (A), the permeability (B), the volume of distribution (C) and the clearance (D) on plasma profile predictions of 1200 mg atazanavir sulfate in the fasted state by implementing equilibrium solubilities of atazanavir at different pH values into the Simcyp[®] mask. 200

Fig. 7.49: “worst case” example - sensitivity analysis of the supersaturation (A), the precipitation (B), the gastric emptying (C), the permeability (D), the volume of distribution (E) and the clearance (F) on



plasma profile predictions of 400 mg atazanavir sulfate in the fed state by implementing equilibrium solubilities of atazanavir at different pH values into the Simcyp[®] mask.....201

Fig. 7.50: “best case” example - sensitivity analysis of the gastric emptying (A), the permeability (B), the volume of distribution (C) and the clearance (D) on plasma profile predictions of 400 mg atazanavir sulfate in the fed state by implementing equilibrium solubilities of atazanavir at different pH values into the Simcyp[®] mask..... 202



List of Tablets

Table 2.1: HPLC setup for the analysis of cinnarizine and atazanavir	28
Table 2.2: Composition of the biorelevant media simulating gastric fasted state.....	30
Table 2.3: Composition of the biorelevant media simulating gastric fed state	30
Table 2.4: Composition of the biorelevant media simulating gastric fed state under light meal conditions with orange juice.....	31
Table 2.5: Composition of the biorelevant media simulating fasted and fed intestinal states	31
Table 2.6: Pre-absorptive parameters (fasted and fed state) used in STELLA® PBPK models.....	43
Table 2.7: Pre-absorptive parameters (fasted and fed state) used in the Simcyp® modeling mask	48
Table 3.1: Initial dissolution rates (z values) for the various biorelevant media and cinnarizine formulations	57
Table 3.2: Maximum supersaturation ratios (maximum concentration achieved in the acceptor compartment relative to the solubility) of different doses of cinnarizine at various transfer rates.....	60
Table 3.3 First order precipitation constants of different doses of cinnarizine at various transfer rates	60
Table 3.4: Maximum supersaturation ratios (maximum concentration achieved in the acceptor compartment relative to the solubility) of different presentations of 20 mg cinnarizine at various transfer rates.....	62
Table 3.5: First order precipitation constants of different presentations of 20 mg cinnarizine at various transfer rates.....	62
Table 3.6: Maximum supersaturation ratios, fraction dissolved (f_d) and precipitation constants (k_p) for Arlever® and Stugeron® for different transfer rates.	64
Table 3.7: Pre-absorptive and absorptive parameters needed for the plasma profile simulation of cinnarizine using STELLA®	67
Table 3.8: Distribution and elimination parameters of cinnarizine used for <i>in silico</i> simulations (STELLA® and Simcyp®).....	67
Table 3.9: Comparison of <i>in vivo</i> data with <i>in silico</i> predictions of different PBPK models for Arlever®, Cinnarizine 30 mg tablets and Stugeron® in the fasted and fed state.....	72
Table 3.10: Statistical comparison of <i>in silico</i> predictions to <i>in vivo</i> observations using the difference factor (f_t) and point estimate ratios of bioequivalence test parameters for different cinnarizine IR formulations and transfer experiments (best fits in boldface).	73
Table 3.11: pH values in the dissolution vessel after dissolution of different doses of atazanavir sulfate in FaSSIF-V2	85
Table 3.12: Initial dissolution rates (z values) for the various biorelevant media and Reyataz® doses	86
Table 3.13: Maximum supersaturation ratios, fraction dissolved (f_d) and precipitation (k_p) constants of different doses of atazanavir sulfate (Reyataz®) for different simulated gastrointestinal states	94
Table 3.14: Distribution and elimination parameters of atazanavir used for <i>in silico</i> simulations (STELLA® and Simcyp®).....	96



Table 3.15: Pre-absorptive and absorptive parameters needed for the plasma profile simulation of atazanavir using STELLA®.....	97
Table 3.16: <i>In vivo</i> and predicted pharmacokinetic parameters for different doses of atazanavir sulfate in the fasted state.....	101
Table 3.17: <i>In vivo</i> and predicted pharmacokinetic parameters for 400 mg atazanavir sulfate (2 x 200 mg Reyataz®) capsules in the fed state.....	104
Table 7.1: Standard physicochemical parameters of cinnarizine implemented into Simcyp®	148
Table 7.2: <i>In vivo</i> and predicted pharmacokinetic parameters for Arlevert® and Stugeron® tablets in the fasted state by implementing biorelevant solubility of cinnarizine into the Simcyp® gastrointestinal solubility mask.....	149
Table 7.3: Ratios of predicted (using the GI solubility approach) to observed plasma profile parameters of cinnarizine tablets in the fasted state.....	150
Table 7.4 <i>In vivo</i> and predicted pharmacokinetic parameters for Arlevert® and Stugeron® tablets in the fasted state using Simcyp® predictions of cinnarizine solubility based on its physicochemical properties.....	151
Table 7.5: <i>In vivo</i> and predicted pharmacokinetic parameters for Arlevert® and Stugeron® tablets in the fasted state by implementing cinnarizine solubility at different pH values into the Simcyp® mask.....	154
Table 7.6: <i>In vivo</i> and predicted pharmacokinetic parameters for Arlevert® and Cinnarizine 30 mg tablets in the fed state by implementing dissolution profiles in FeSSGF pH 5.0 and FeSSIF-V2 into Simcyp®	155
Table 7.7: Ratios of predicted (using dissolution profile data) to observed plasma profile parameters of cinnarizine tablets in the fed state.....	157
Table 7.8: <i>In vivo</i> and predicted pharmacokinetic parameters for Arlevert® and Cinnarizine 30 mg tablets in the fed state by implementing biorelevant solubility of cinnarizine into the Simcyp® gastrointestinal solubility mask	157
Table 7.9: <i>In vivo</i> and predicted pharmacokinetic parameters for Arlevert® and Cinnarizine 30 mg tablets in the fed state using Simcyp® predictions of cinnarizine solubility based on its physicochemical properties.....	159
Table 7.10: <i>In vivo</i> and predicted pharmacokinetic parameters for Arlevert® and Cinnarizine 30 mg tablets in the fed state by implementing cinnarizine solubility at different pH values into the Simcyp® mask	160
Table 7.11: <i>In vivo</i> and predicted (Vd new and Vd old) pharmacokinetic parameters for Arlevert® and Stugeron® tablets in the fasted state by implementing biorelevant solubility of cinnarizine into the Simcyp® gastrointestinal solubility mask.....	173
Table 7.12: <i>In vivo</i> and predicted (Vd new and Vd old) pharmacokinetic parameters for Arlevert® and Cinnarizine 30 mg tablets in the fed state by implementing dissolution profiles in FeSSGF pH 5.0 and FeSSIF-V2 into Simcyp®	174
Table 7.13: Absorption, distribution and elimination parameters of atazanavir implemented into Simcyp®	176



Table 7.14: Standard physicochemical parameters of atazanavir implemented into Simcyp®	177
Table 7.15: <i>In vivo</i> and predicted pharmacokinetic parameters for different doses of atazanavir sulfate in the fasted state by implementing kinetic biorelevant solubility of atazanavir into the Simcyp® gastrointestinal solubility mask	179
Table 7.16: <i>In vivo</i> and predicted pharmacokinetic parameters for different doses of atazanavir sulfate in the fasted state using Simcyp® predictions of atazanavir solubility based on its physicochemical properties	181
Table 7.17: <i>In vivo</i> and predicted pharmacokinetic parameters for different doses of atazanavir sulfate in the fasted state by implementing equilibrium solubilities of atazanavir at different pH values into the Simcyp® mask.	183
Table 7.18: <i>In vivo</i> and predicted pharmacokinetic parameters for 400 mg atazanavir sulfate capsules (2 x 200 Reyataz®) in the fed state by implementing biorelevant solubility data into the Simcyp® gastrointestinal solubility mask: “worst case” (using FeSSGEm pH 2.75 data) and “best case” (using FeSSGF pH 2.75 data)	185
Table 7.19: <i>In vivo</i> and predicted pharmacokinetic parameters for 400 mg atazanavir sulfate capsules (2 x 200 Reyataz®) in the fed state using Simcyp® predictions of atazanavir solubility based on its physicochemical properties: “worst case” (using FeSSGEm pH 2.75 data) and “best case” (using FeSSGF pH 2.75 data).	186
Table 7.20: <i>In vivo</i> and predicted pharmacokinetic parameters for 400 mg atazanavir sulfate capsules (2 x 200 Reyataz®) in the fed state by implementing equilibrium solubilities of atazanavir at different pH values into the Simcyp® mask: “worst case” (using FeSSGEm pH 2.75 data) and “best case” (using FeSSGF pH 2.75 data).	188



List of Abbreviations

A	surface area
ADAM	advanced dissolution absorption and metabolism
API	active pharmaceutical ingredient
ART	antiretroviral therapy
AUC	area under the curve
BCRP	breast cancer resistance protein
BCS	biopharmaceutics classification system
BDDCS	biopharmaceutics drug disposition classification system
BioRAM	Biopharmaceutics risk assessment roadmap
Caco-2	heterogeneous human epithelial colorectal adenocarcinoma cells
CAT	compartmental absorption and transit
Cl	clearance
Cl/F	apparent clearance
C_{max}	maximum concentration
CV	coefficient of variance
DCS	developability classification system
DDI	drug-drug interaction
DMSO	dimethyl sulfoxide
DoE	Development of Experiments
EMA	European Medicines Agency
f_a	fraction absorbed
FaHIF	Fasted Human Intestinal Fluid
FaSSCoF	Fasted State Simulated Colonic Fluid
FaSSGF	Fasted State Simulated Gastric Fluid
FaSSIF	Fasted State Simulated Intestinal Fluid
FaSSIF-V2	Fasted State Simulated Intestinal Fluid-Version 2
f_d	fraction dissolved
FDA	Food and Drug Administration
FeHIF	Fed Human Intestinal Fluid
FeSSCoF	Fed State Simulated Colonic Fluid
FeSSGEm	Fed State Simulated Gastric Emulsion
FeSSGF	Fed State Simulated Gastric Fluid

XVI



FeSSIF	Fed State Simulated Intestinal Fluid
FeSSIF-V2	Fed State Simulated Intestinal Fluid-Version 2
Fig.	figure
GER	gastric emptying rate
GI	gastrointestinal
GUI	graphical user interface
H ₂	histamine 2 receptor
HBA	hydrogen bond acceptor
HBD	hydrogen bond donor
HPLC	high performance liquid chromatography
HPMC	hydroxypropyl methylcellulose
HT-29	mucus producing human colon cells
HTS	high throughput screening
ICH	International Conference on Harmonisation
IR	immediate release
ISO	International Organization for Standardization
IUPAC	International Union of Pure and Applied Chemistry
IVIVC	<i>in vitro-in vivo</i> correlation
IVIVE	<i>in vitro-in vivo</i> exploration
kcal	kilocalorie
K _m	Michaelis-Menten constant
k _p	precipitation constant
(L)ADME	(liberation), absorption, distribution, metabolism and excretion
LLC-PK1	Lewis lung carcinoma - porcine kidney
MATLAB	Matrix Laboratory
MDCK II	Madin-Darby canine kidney
MDR	multidrug resistance
MMC	migrating motor complex
MRP	multidrug resistance protein
MW	molar weight
OATP	organic anion transporting polypeptides
PAMPA	parallel artificial membrane permeability assay
P _{app}	apparent permeability



PBPK	physiologically based pharmacokinetics
PD	pharmacodynamics
P_{eff}	effective permeability
PK	pharmacokinetics
PPI	proton pump inhibitor
PSA	polar surface area
PTFE	polytetrafluoroethylene
QbD	quality by design
QbR	question-based review
QTPP	quality target product profile
R&D	research and development
SAP	surface activity profiling
SAR	structure-activity relationship
SDS	sodium dodecyl sulfate
SGF	Simulated Gastric Fluid
SIF	Simulated Intestinal Fluid
SNEDDS	Self-nanoemulsifying Drug Delivery System
STELLA	systems thinking for education and research
t_{max}	time of maximum concentration
US-FDA	United States Food and Drug Administration
USP	United States Pharmacopeia
UV-VIS	ultraviolet-visible spectroscopy
UWL	unstirred water layer
V_d	volume of distribution
V_d/F	apparent volume of distribution
V_{max}	maximal rate



1 Introduction

In earlier times active pharmaceutical ingredients (APIs) were discovered incidentally and derived from nature. Typical examples of such compounds are salicylic acid and penicillin, which were initially extracted from plants (bark of white willow) and fungi (*penicillium rubens*) [1, 2]. In the early 20th century drug research and development was based on empirical knowledge and little was known about drug pharmacokinetics (PK) or pharmacodynamics (PD). One of the first researchers to use a rational approach to drug development and therapy was Paul Ehrlich, who synthesized one of the first antibacterial chemotherapeutics in 1907, arsphenamine, which was later marketed by Hoechst AG under the trade name Salvarsan. Ehrlich hypothesized that by screening a number of compounds a drug with antibacterial activity could be discovered and selected for therapy without risking patients' lives.

After the Second World War new ways of conducting drug discovery emerged. Rational drug design was guided with the help of structure-activity relationship (SAR) in the second half of the 20th century. SAR enabled the identification of structural molecular components inducing an effect on a biological target [3]. Paul Ehrlich's approach of screening drugs before investigating them in humans was fully implemented through introduction of combinatorial chemistry as an industrial standard in late 1980s [4, 5]. This method made it possible to develop and use large compound libraries. High throughput screening (HTS) methods facilitate investigation of large numbers of potential candidates on target receptors or enzymes within a short amount of time. Molecules identified to interact with a target are called "hits". After being characterized and optimized, the most promising hits are selected as lead candidates for preclinical development. Based on the preclinical results certain lead candidates are then chosen for clinical development. In successful clinical programs, one or more of the clinical candidates are often able to reach the market.

Oral medication is the most convenient route of drug administration. Most compounds administered orally are designed to have systemic mode of action. Thus, if a compound is taken over the oral route it has to be liberated (from a formulation) and dissolved before being absorbed, distributed in the human body, metabolized



Introduction

and excreted. The “Liberation” step in this so-called LADME scheme implies that poorly soluble compounds can have absorption issues: drug dissolution in the gastrointestinal (GI) tract has shown to be a key requirement for oral drug absorption [6]. Selection of drug candidates using HTS predestines many compounds for absorption issues related to solubility/dissolution, since it is an *in vitro* tool where compounds are pre-dissolved in organic solvents such as DMSO and then diluted in aqueous buffers to perform the screen [7]. For this reason most of the hit and lead molecules tend to exhibit high lipophilicity and thus poor aqueous solubility [8, 9].

Prediction of oral drug absorption has become one of the fundamental elements in clinical development. In the last few decades many methods have emerged for the investigation of factors involved in *in vivo* drug dissolution and absorption [10-12]. It is a topic which continues to be of major interest in the pharmaceutical sciences as well as in industrial research and development.

1.1 Drug transit through the upper GI tract

When a dosage form is taken orally it first enters the stomach and may subsequently be transferred through all segments of the GI tract. For immediate release dosage forms, disintegration and drug dissolution are intended to take place in the stomach and/or the upper small intestine. After being liberated, the API has to stay in solution in order to be absorbed through the intestinal epithelia. Figure 1.1 illustrates the passage of a dosage form through the proximal GI tract. Immediate release dosage forms are generally designed to disintegrate and liberate the API in the gastric fluid upon entering the stomach. The API (dissolved and non-dissolved) will then be emptied into the small intestine, where dissolution should be completed to make the entire dose available for absorption. By contrast, delayed release dosage forms have to remain intact until they reach the GI segment in which they are supposed to disintegrate and liberate the API, while a third category, extended release dosage forms, are intended to assure prolonged drug liberation over a large part of the GI tract.

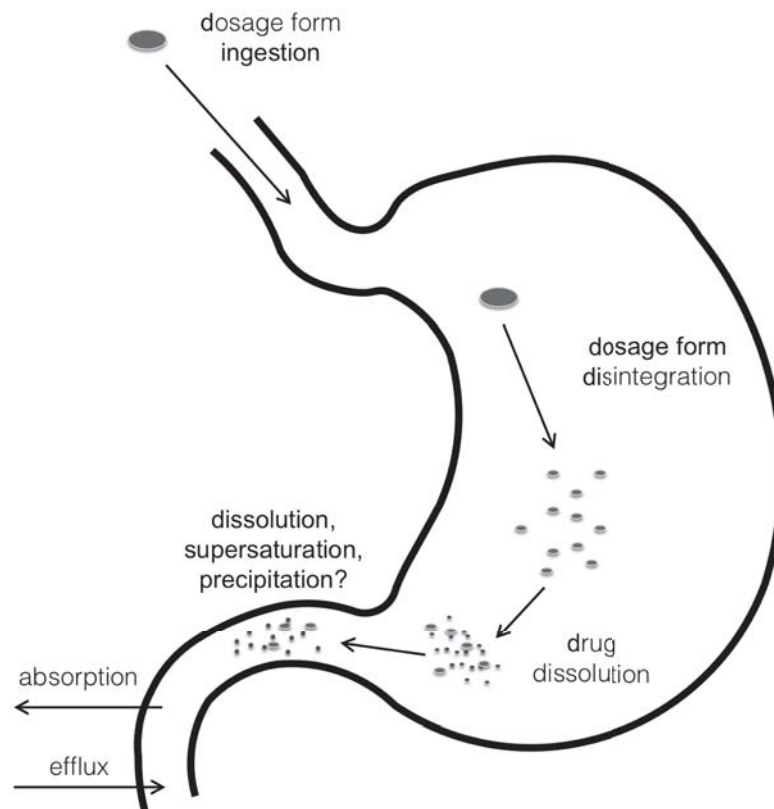


Fig. 1.1: Dosage form and drug transit in the upper GI tract

During the passage through the GI tract drug dissolution and absorption may be affected by a number of factors. After ingestion, dosage forms/APIs are exposed to drastic changes in environment. Shifts in pH and bile salt concentrations during the passage through the GI tract may significantly influence drug release, solubility and dissolution. If drugs are administered with food, they may additionally be subject to complexation with food components. Furthermore, food intake may significantly change GI motility and pH, and thus solubility and dissolution of certain compounds. Some drugs may even be subject to degradation. Moreover, poor permeability, site-specific absorption or drug efflux may restrict the extent of drug absorption. The next sections describe the interplay of factors which are crucial for prediction of drug absorption and the systems which attempt to describe them in more detail.



1.2 Determinants of drug absorption

1.2.1 The biopharmaceutics classification system

The biopharmaceutics classification system (BCS) was introduced in 1995 by Amidon and colleagues to describe factors involved in drug absorption [6]. The authors postulated that oral drug absorption is driven by two predominant parameters, drug solubility in the GI tract and *in vivo* drug permeability. According to the BCS framework, APIs are distinguished in four classes based on their solubility and permeability (Figure 1.2).

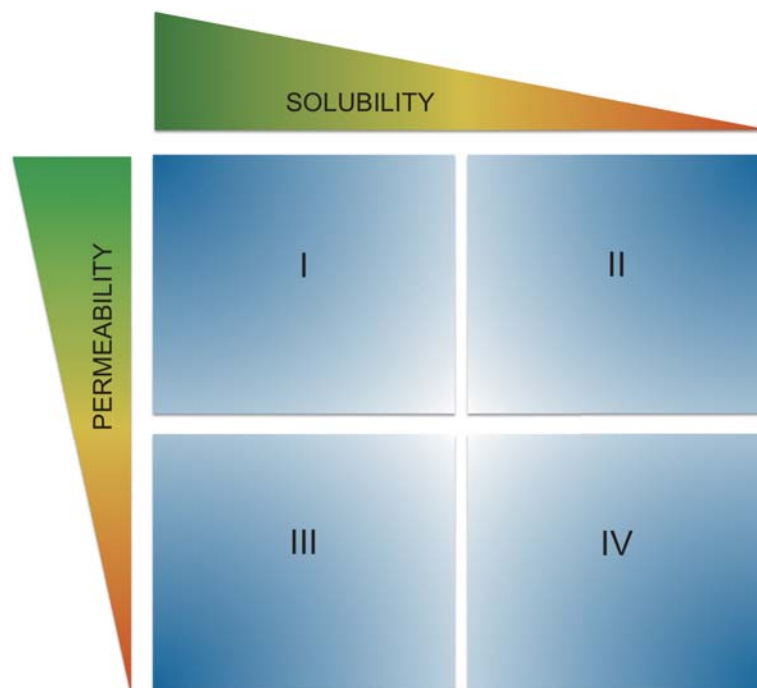


Fig. 1.2: Categorization of APIs based on the biopharmaceutics classification system

Poorly soluble weak bases, which are the focus of this work, are classified as BCS class II (highly permeable) and IV (poorly permeable) drugs. The BCS guidance established by the US-FDA suggests investigating drug solubility in aqueous media with pH values between 1 and 6.8. Drugs are regarded as highly soluble when the dose/solubility ratio is equal to or below 250 ml. Compounds are regarded as highly permeable when at least 85% of the administered dose is absorbed. Practically, permeability may be assessed through human bioavailability, mass balance studies and intestinal perfusion experiments [13, 14]. If human intestinal perfusion data are not available, drug permeability may be estimated through e.g. experiments in *in vitro* cell lines using a validated procedure [14-16].



1.2.2 The biopharmaceutics drug disposition classification system

The biopharmaceutics drug disposition classification system (BDDCS), which was published by Wu and Benet in 2005, modified the BCS scheme to describe drug disposition kinetics based on two factors, metabolism and solubility [17]. Based on the BCS the investigators were able to distinguish predominant routes of drug elimination. They found correlations of drug permeability with metabolism, whereby BCS class I and II drugs typically exhibit high metabolism, while BCS class III and IV compounds are mostly excreted in bile and urine as unchanged drug.

Moreover, the investigators came to a conclusion that the BCS classes can be linked with the possibility of transporter mechanisms in intestinal epithelia. Drug uptake mechanisms can be generally distinguished into two types, passive and active drug transport. The latter mechanism is mediated through carrier molecules, which may actively bind and transport APIs into cells by energy-requiring interactions. A typical group of such uptake transport molecules is the OATP (organic anion transporting polypeptides) family, which is responsible for active transport of a variety of compounds, such as antibiotics, chemotherapeutic agents, antihistaminic drugs, and diuretics [18]. By contrast, efflux carrier molecules are able to eliminate certain compounds from the enterocyte. The most studied of the efflux proteins is P-glycoprotein (P-gp). It belongs to the MDR (multidrug resistance protein) family and has a very wide substrate spectrum [18]. Class I drugs typically show minimal transporter effects. Because of their good solubility and permeability, saturation of both efflux and uptake transporters is probable. Due to the poor solubility of class II drugs, saturation of efflux transporters is considered improbable. Thus, efflux transporters are more likely to affect the net absorption of class II compounds. Class III drugs are highly soluble, however they often have to rely on uptake transporters, explaining their poor permeability. Alternatively, they may be absorbed by paracellular passive mechanisms. For class IV compounds both efflux and uptake mechanisms may be relevant. Based on their investigation Wu and Benet summarized the disposition kinetics of BCS drugs by introducing the BDDCS (Figure 1.3). This system facilitates the understanding drug characteristics and their absorption mechanisms on the basis of the BCS.

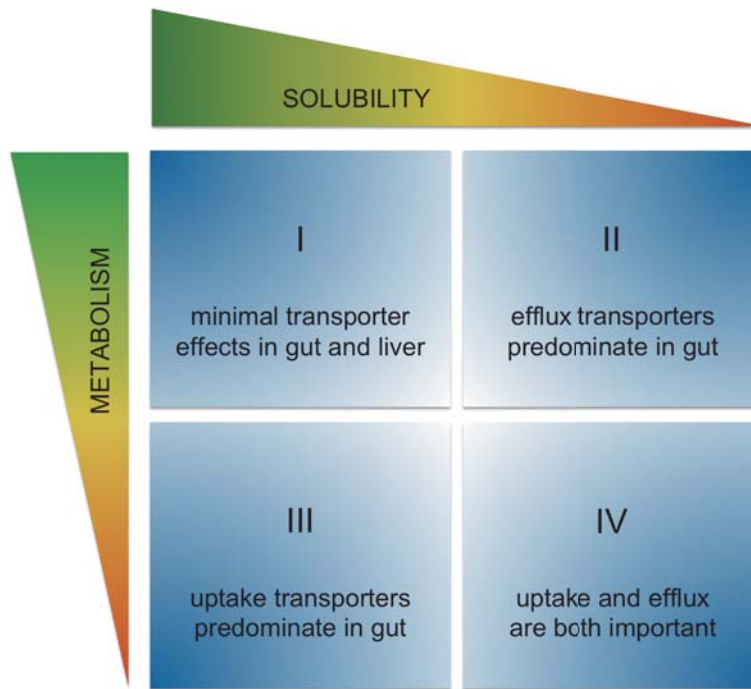


Fig. 1.3: Categorization of APIs based on biopharmaceutics drug disposition classification system

1.2.3 The developability classification system

Even though the BCS has shown to be a useful tool to assist drug development in the pharmaceutical industry, the boundaries for solubility and permeability are too strict to apply it as a screening tool for selection of lead compounds. In 2010 Butler and Dressman modified the BCS to better address candidate selection for drug development [19]. The developability classification system (DCS) utilizes a modified approach of classifying drugs (Figure 1.4). According to the DCS, *in vivo* drug solubility would optimally be assessed with the help of aspirated fasted state human intestinal fluids (FaHIF). If FaHIF is inaccessible, biorelevant media, which mimic the fluids of the GI tract, may be used for the estimation of *in vivo* drug solubility [20-22]. The comparator intestinal volume of liquids is set at 500 ml, indicating that solubility is not expected to constitute a major limitation to drug absorption at dose/solubility ratios ≤ 500 ml. The authors assumed compensatory effects of solubility and permeability for some class II compounds, distinguishing them into two groups. Class IIa compounds exhibit dissolution rate limited extent of absorption. For these APIs, the high permeability facilitates drug dissolution, which in turn enables absorption of the entire drug dose as long as the dissolution rate can be adequately improved via formulation. Class IIb drugs are solubility limited. For these, the compensatory

permeability effect is not sufficient enough to ensure dissolution and absorption of the entire drug dose and the formulation effect should be directed towards improving drug solubility.

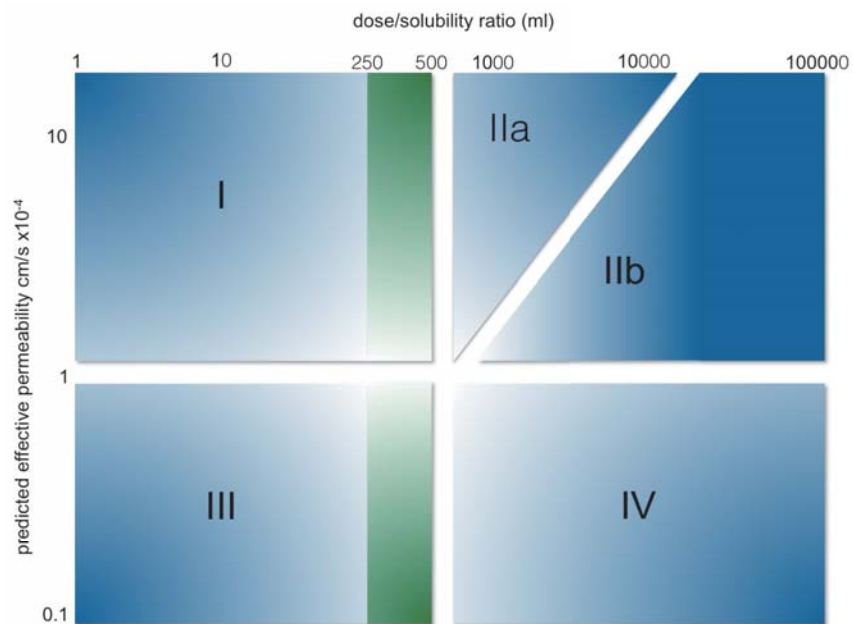


Fig. 1.4: Characterization of APIs based on developability classification system. Green bars describe the extension of the dose solubility ratio from 250 ml to 500 ml.

Interestingly, poorly soluble weakly basic drugs have a unique status according to the DCS, since they may undergo complex dissolution processes, which cannot easily be predicted by simple *in vitro* methods. The dissolution behavior of poorly soluble weak bases in the GI tract will be discussed in more detail in the following sections.

1.3 Weak bases and the GI tract

1.3.1 pH in the GI tract

Weakly basic and acidic drugs usually have pH dependent solubility and react sensitively to the pH changes that occur during GI transit. Figure 1.5 illustrates pH dependent solubility profiles of weak bases and acids, together with the pH values that predominate in the upper GI tract in the pre- and postprandial state.

The pH in the fasted stomach is estimated to generally lie between 1.4 and 2.1. When entering the upper small intestine compounds are exposed to significantly higher pH values of 4.4 to 6.6. After food ingestion the stomach pH increases to

Introduction

values between 4.3 and 5.4, whereas a slight decrease in pH is observed in the upper small intestine (pH 4.9 to 6.0) [23-25].

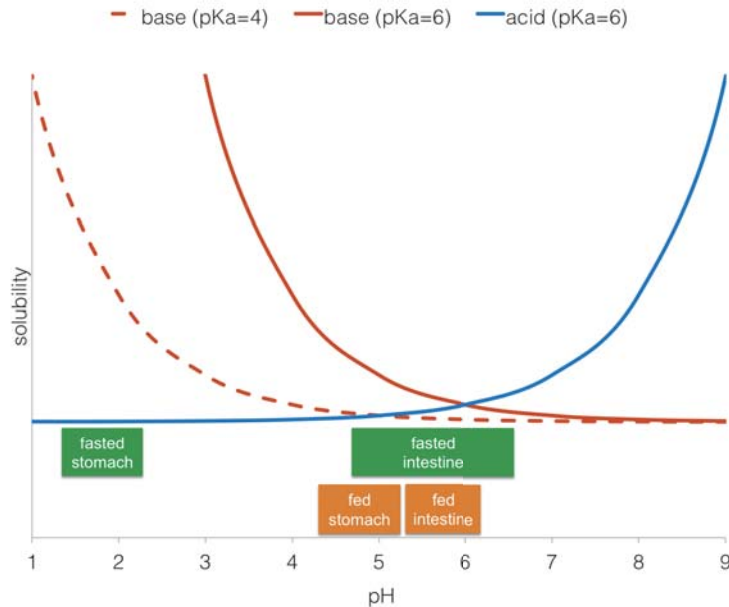


Fig. 1.5: pH solubility behavior of weak bases and acids in relation to the upper GI pH

Based on the pH/solubility profile, a large difference in solubility is expected for poorly soluble weak bases between the fasted stomach and intestine. A substantial drug amount is expected to dissolve in the fasted stomach. Upon entering the fasted intestine three general scenarios may be considered for poorly soluble weakly basic drugs (Figure 1.6):

1. Direct drug precipitation to the intestinal solubility
2. Drug supersaturation for extended period of time
3. Drug supersaturation and with subsequent precipitation towards the intestinal solubility.

Thus, supersaturation and precipitation may be important forces of the absorption of poorly soluble weakly basic drugs. It is therefore advisable to investigate factors which may influence drug supersaturation and precipitation following gastric emptying.

Additionally, this description evokes the assumption that bioavailability of poorly soluble weak bases may be vulnerable to gastric pH [26]. Indeed, absorption of weakly basic drugs is often negatively affected when H₂ receptor antagonists and proton pump inhibitors are co-administered, since these elevate the gastric pH [27, 28].

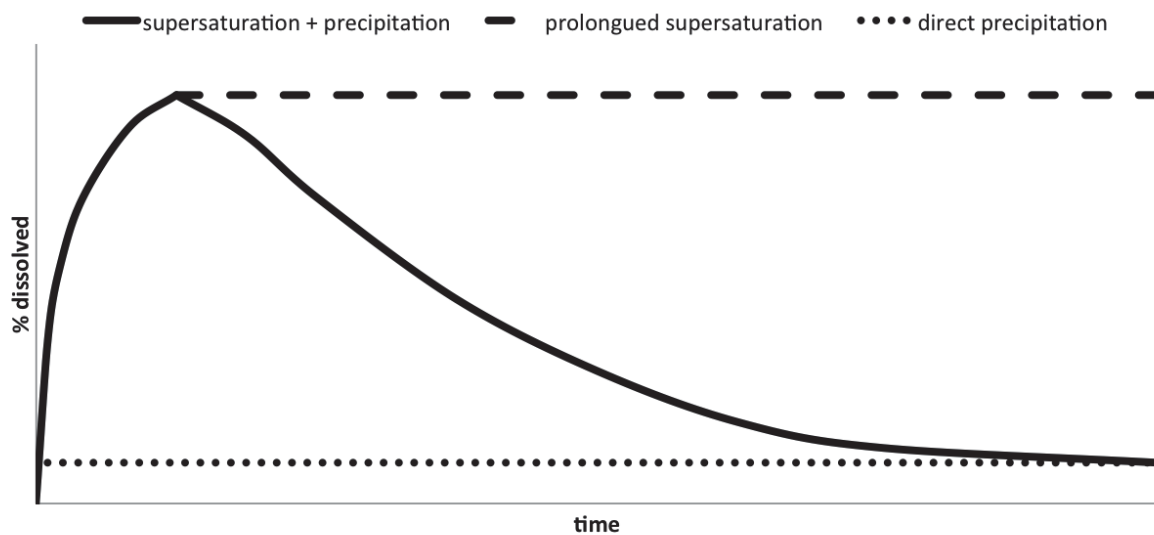


Fig. 1.6: Possible dissolution scenarios for weak bases upon entering the upper small intestine

1.3.2 Bile salts and food in the GI tract

Bile salts are secreted in the upper small intestine. Due to their formation of micellar structures they may enhance the solubility of lipophilic APIs in the GI tract via solubilization [29-31]. Hence, their presence may mitigate the pH mediated decrease in solubility of weakly basic compounds during gastric emptying and partly influence drug supersaturation and precipitation. Bile salt secretion depends on the prandial state. After food intake, luminal bile salt concentrations in humans are higher than in the fasted state [32]. Human intestinal aspirate data reveals bile salt concentrations of approximately 3 mM in the fasted state and of 10 mM in the fed state [33-35].

Another factor which may influence solubility of compounds is food. Food ingestion usually induces an increase in gastric pH and bile salt secretion, both of which can influence the solubility of weak bases. Food components or products of digestion may also influence solubilization of poorly soluble compounds and have to be



Introduction

considered when investigating drug dissolution [36]. Further, some food components can interact with gut epithelia and affect drug permeability. A typical representative of such food constituents is grapefruit juice, which exhibits inhibition of P-gp and can be therefore alter drug bioavailability [37].

1.3.3 Gastric emptying

In the fasted state, gastric motility is best characterized by cyclical fluctuations, which constitute the migrating motor complex (MMC). The MMC is divided into three phases: phase I is a quiescent period with almost no movement, phase II consists of intermittent and irregular contractions, which progressively increase in strength culminating in maximum frequency and strength of contractions in phase III. The mean cycle duration is estimated to be approximately 90-120 minutes, although it may range between 15 minutes to 3 hours [38-41]. Gastric emptying of liquids depends on the phase of the MMC and on the amount of liquids ingested [42, 43]. Whereas phase III includes an almost bolus gastric emptying, phases I and II motility patterns generally show first order emptying kinetics, with a high variability of 1 to 14 h⁻¹ [41-47]. Thus, dissolution, supersaturation, precipitation and absorption of weakly basic compounds could all depend on the MMC phase and on the volume of liquid taken with the drug. By contrast, the fed state gastric emptying follows linear kinetics (zero order) and depends mainly on the number of calories contained in the meal [48, 49]. With values between 1 and 4 kcal/min the gastric emptying rate is slower and less variable in the fed state than in fasted state [50, 51].

1.4 Simulation of *in vivo* drug dissolution

1.4.1 Dissolution media simulating GI fluids

Dissolution media have been developed and refined over the last two decades to mimic the *in vivo* gastric and intestinal conditions. Compendial dissolution media consist of simple aqueous solutions and buffers, and mimic solely the pH conditions of the GI environment. The US pharmacopeia (USP) introduced simulated gastric fluid (SGF) with a pH of 1.2 and simulated intestinal fluid (SIF) with a pH of 6.8 as standard dissolution media for oral dosage forms. SGF may contain pepsin to represent gastric conditions more physiologically. Sodium dodecyl sulfate (SDS) or



other surfactants may be added to SIF to increase solubility when investigating poorly soluble compounds [52]. The compendial media are especially useful for quality control assessment of solid oral dosage forms, however they have relatively little predictive power when it comes to *in vivo* dissolution behavior of poorly soluble compounds. In addition, use of synthetic detergents, such as SDS for the imitation of bile salts of human intestinal fluids is not necessarily satisfactory. In 1998 the simplistic pharmacopeial simulated gastric and intestinal fluids (SGF and SIF) were transformed into more biorelevant dissolution media FaSSGF (Fasted State Simulated Gastric Fluid), FaSSIF (Fasted State Simulated Intestinal Fluid) and FeSSIF (Fed State Simulated Intestinal Fluid) by adapting buffers and bile salt contents to human aspirate data [20, 21]. In 2008 Jantratid *et al.* further refined FaSSIF and FeSSIF to better represent the *in vivo* intestinal conditions by introducing new versions (version 2 – V2) of the two media, FaSSIF-V2 and FeSSIF-V2. To represent the higher bile salt secretion in the fed state, bile salt and lecithin concentrations are greater in FeSSIF-V2 than in FaSSIF-V2. Moreover, glycerol monooleate and sodium oleate were incorporated into FeSSIF-V2 to represent products of lipolysis of dietary fats of the fed intestine [22]. In addition, Jantratid and co-investigators introduced the fed state simulating gastric fluid (FeSSGF) to imitate the postprandial stomach. The introduction of biorelevant media of the ascending colon (FaSSCoF and FeSSCoF) in 2010 made it possible to simulate the dissolution behavior of extended release dosage forms or formulations with colon targeting [53]. Biorelevant media enable qualitative predictions of the *in vivo* dissolution performance of poorly soluble compounds. Today they are widely utilized for quantitative predictions of *in vivo* drug performance using *in vitro-in vitro* correlation (IVIVC) methods [54-57].

1.4.2 Simulation of GI dissolution conditions

The USP provides different apparatus for the investigation of dissolution behavior of solid oral dosage forms:

1. USP apparatus 1 (Basket apparatus) consists of a vessel filled with a defined volume of dissolution medium (usually 500 or 900 ml) and a perforated basket, which holds the dosage form. The rotary movement of the basket in the vessel



Introduction

is used to disperse the dosage form and release the API. The rotation speed is routinely set at 100 rotations per minute (rpm).

2. USP apparatus 2 (Paddle apparatus) is similar to the apparatus 1. The basket is exchanged for a paddle, which rotates inside the vessel. The rotation speed is usually set at 50 or 75 rpm. The dosage form initially resides at the bottom of the vessel in most cases. To prevent dosage forms like capsules from floating a sinker can be introduced.
3. USP apparatus 3 (reciprocating cylinder) is a tester consisting of six dissolution compartments in a row. Up to six rows, each with six vessels can be utilized in the apparatus. The vessels are smaller than in apparatus 1 and 2 and have maximal volume capacity of 250 ml. The dosage form is introduced into a holder, which is dipped into the medium at a predefined rate. This method enables the simulation of gastrointestinal transit of enteric coated or extended release dosage forms by sequentially transferring the dosage form holder from one vessel to the next. The core advantage of apparatus 3 is that dipping rates can be adjusted for each of the individual rows without stopping the apparatus.
4. USP apparatus 4 (flow-through tester) is commonly used for the analysis of extended release dosage forms. A glass cell is used to hold the formulation. The dissolution medium is pumped through the cell at a preset pumping rate.

The USP apparatus 1 to 4 have been widely used not only for quality control of oral dosage forms, but also for biorelevant dissolution testing. The apparatus 2 is the most typically utilized approach for the dissolution analysis of poorly soluble compounds in fasted and fed state simulated gastric and intestinal fluids. Additionally, a scaled down apparatus 2 (Mini Paddle apparatus) comprising a maximum volume of 500 ml was implemented to better represent volumes available for dissolution in the fasting stomach [58].

Individual dissolution testing has proven to be a useful tool to assess the *in vivo* behavior of poorly soluble drugs. However, it may have limited predictive power in the case of poorly soluble weak bases. In order to evaluate the behavior of weak bases during gastric emptying, Kostewicz *et al.* introduced the transfer model in 2004 (Figure 1.7) [59]. Unlike individual dissolution tests, the transfer model simulates changes in drug concentration induced by the sudden change in environment when the drug leaves the stomach and enters the small intestine.

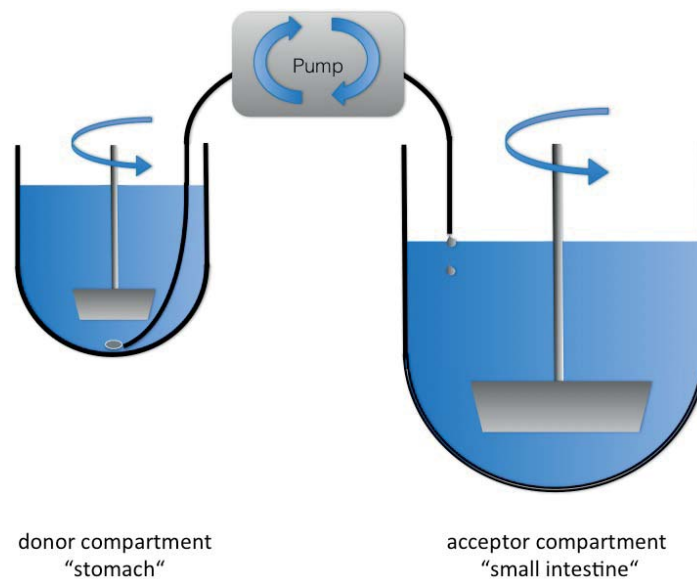


Fig. 1.7: Transfer model for the *in vitro* simulation of gastric emptying

The transfer model consists of a donor compartment (e.g. Mini Paddle apparatus) containing a medium simulating the stomach and an acceptor compartment (e.g. USP 2 apparatus), which represents the upper small intestine. Gastric emptying is mimicked with the help of a peristaltic pump. The pumping rate can be set up according to the desired simulation of the GI state. Contemporary pumps can be programmed to run nonlinear transfer kinetics, and thus enable the imitation of first order gastric emptying in the fasted state. Kostewicz and co-workers initially utilized the model by pre-dissolving weakly basic compounds (dipyridamol, BIBU 104 XX and BIMT 17 BS) in SGF and subsequently transferring the solutions into FaSSIF or FeSSIF [59]. Nowadays, sophisticated biorelevant media such as FaSSGF, FaSSIF-V2, FeSSGF and FeSSIF-V2 can be utilized in transfer experiments to simulate fasted and fed state gastric emptying conditions [60, 61]. The transfer model has proven to be an important tool not only for formulation development but also for the



Introduction

assessment of possible *in vivo* performance of several poorly soluble weak bases [60-65].

1.5 Drug permeability assessment

Human intestinal perfusion experiments enable a direct permeability assessment of compounds. Since experiments in volunteers need to be conducted to assess the effective permeability, such data are unfortunately not available for most APIs. Several alternative theoretical and practical tools are available today for the prediction of human intestinal permeability. The theoretical permeability assessment uses the chemical structure or physicochemical properties of the compound. Lipinski was one of the first to describe permeability of compounds with the help of their structural characteristics [66]. He introduced the “rules of five”, which postulates that poor absorption of a compound is more likely when there are more than 10 H-bond acceptors (HBA), 5 H-bond donors (HBD), the molecular weight (MW) is greater than 500 and the logP is greater than 5. More recently, different statistical methods have emerged to predict the permeability of compounds based on their molecular structure or physicochemical properties, e.g. MW, HBD and logP. Polar surface area (PSA) also provides information about API lipophilicity and thus may be used for permeability assessment. On the basis of these properties, several correlations have been proposed for the prediction of jejunal permeability [67-69].

However, the most commonly used methods for the investigation of intestinal permeation are *in vitro* tools. *In vitro* permeability studies can be distinguished into cell-based and non cell-based analyses. Surface activity profiling (SAP) and parallel artificial membrane permeability assay (PAMPA) represent non cell-based techniques.

SAP is an *in vitro* investigation of concentration dependent surface pressure profiles of compounds in aqueous buffers. The maximum surface pressure has been correlated with absorption (fraction absorbed) for a range of compounds. Therefore, it may be utilized as the predictive parameter for permeability of compounds. The



method has proven to be a practical tool to evaluate both oral absorption, and with some modifications, blood brain barrier penetration of drugs in humans [70, 71].

PAMPA uses an artificial semipermeable membrane, which separates a donor and an acceptor compartment, both filled with aqueous buffer. The compound is introduced into the donor solution and allowed to permeate the membrane. Time-concentration profiles are then generated to assess permeability of the compound. Like SAP, this method only allows the investigation of passive perfusion of compounds [72].

Cell-based permeability assessment may be performed using different kinds of cell systems, such as Caco-2, HT-29, MDCK II and LLC-PK₁. Alternatively, animal intestinal membranes, such as rat jejunum or ileum, may be used for this kind of investigation.

Caco-2 (heterogeneous human epithelial colorectal adenocarcinoma cells) and HT-29 (mucus producing human colon cells) cell lines are based on human derived intestinal cell systems. Caco-2 is the most commonly used assay for the investigation of permeation. The cell line was derived from heterogeneous human epithelial colorectal adenocarcinoma cells [73]. Interestingly, Caco-2 cells are morphologically similar to cells in the human upper intestinal epithelia. They express P-gp, metabolizing enzymes and several active uptake transporter proteins. The expression of those proteins may be inconsistent from batch to batch. Therefore, the permeability is optimally assessed on a relative basis using high and low permeability reference compounds. HT-29 cultures pose an alternative to Caco-2 cell lines. A fraction of the cells differentiate into goblet cells, which are capable of producing mucus [74]. HT-29 and Caco-2 cell assays may be combined by differentiating the HT-29 cells (into HT 29-H or HT29-MTX cells) and by co-culturing both cell lines [75]. MDCK-II (Madin-Darby canine kidney) and LLC-PK₁ (Lewis lung carcinoma - porcine kidney) are animal derived cell systems and pose alternatives to Caco-2 cultures. The main advantage of these cell lines is the shorter culture time. Each of the cell strains can be transfected with P-gp to mimic efflux kinetics. Since neither system is human derived, permeability values are expected to be significantly different to Caco-2 cultures [76, 77].



Introduction

Ex vivo rat intestine perfusion experiments pose a good alternative to cell based assays, since strong correlation of rat intestinal permeability with effective human intestinal permeability has been shown for a series of drugs [78].

1.6 Physiologically based pharmacokinetic modeling

Simulation of pharmacokinetics using multicompartment models was first described by Torsten Teorell in 1937 [79]. Physiologically based pharmacokinetic (PBPK) models are intended to mathematically describe the factors influencing pharmacokinetics on the basis of drug absorption, distribution, metabolism and excretion (ADME). In earlier times PBPK simulation was frustrated by limited computational capabilities. Increasing computational power over the last two decades has contributed to the development of functional PBPK modeling techniques, which can now be applied for complete description and investigation of drug pharmacokinetics. PBPK models can be constructed on a self-built basis using programming or statistical software such as MATLAB[®] and STELLA[®]. Specific PBPK programs such as Simcyp[®], GastroPlus[®], PK-Sim[®] and GI-Sim[®] have also been developed and the first three of these are commercially available, as of this writing.

PBPK modeling and simulation is now recognized as a useful tool in pharmaceutical research and development. For example, the US Food and Drug Administration and the European Medicines Agency (EMA) propose PBPK modeling in their guidance documents for the evaluation of drug – drug interactions (DDI) and studies on hepatic impairment [80, 81].

1.6.1 PBPK modeling approaches

PBPK modeling techniques can be generally distinguished into three groups, the top-down, bottom-up and middle-out approaches. The classical procedure for the investigation of factors influencing drug pharmacokinetics is represented by the top-down approach. This approach is typically used for the analysis of pharmacokinetic covariates with the help of clinical data. The modeling and simulation procedure is based on observed *in vivo* data (blood plasma concentration profiles), which is parameterized into various factors. By contrast, the bottom-up approach uses a



mechanistic *a priori* identification of relevant covariates which can be applied prior to conducting clinical studies [82]. This simulation technique can be distinguished into two stages, the “purist” and the “mixed” approach. In the “purist” approach, covariates of an API are described exclusively by algorithms, which are usually based on physicochemical parameters of the compound. The “mixed” approach additionally uses *in vitro* experimental data to describe the physiological covariates of a compound. This method applies statistical information gained from previous investigations on compounds with similar characteristics as well as *in vitro*, *in silico* and animal model data about the API. Development of standardized *in vitro* experiments facilitates the extrapolation of drug related data for the exploration of *in vivo* pharmacokinetics of APIs. Indeed, using these *in vitro-in vivo* exploration (IVIVE) techniques may lead to identification of covariates which cannot be easily assessed through clinical investigations [83, 84]. This approach is beneficial in the early stage of drug development when compound related data are limited. The middle-out approach combines elements of both the aforementioned methods. One should bear in mind that *in vitro* experimental data usually introduce some uncertainty, since the *in vitro* setup is very rarely a 1:1 copy of the *in vivo* situation. Uncertain or unknown parameters will thus be preferably determined from available *in vivo* studies, which enable more sophisticated estimations [85]. The middle-out approach to PBPK modeling may be advantageous for the full-scale investigation of API pharmacokinetics.

1.6.2 Software for PBPK modeling

1.6.2.1 MATLAB[®] and STELLA[®]

Programming and statistical software provide the possibility to develop PBPK models by setting up algorithms which can describe drug dissolution, absorption, metabolism, excretion kinetics, compartmental in- and outflows, or even virtual populations. MATLAB[®] (matrix laboratory) is a programming language which is typed in as a code in a command window. *In vitro* and *in vivo* observations can be parameterized through implementation of variables and development of vectors and matrices. In this language PBPK models are developed based on object-oriented programming, where pharmacokinetic elements can be defined as objects which can interact with each other. The program supports the development of applications with



Introduction

graphical user interface (GUI) features which enable the visualization of simulation results. MATLAB[®] is an abstract programming software which requires acquisition of considerable programming skills to implement algorithms and run simulations.

The STELLA[®] (systems thinking for education and research) software, in contrast to MATLAB[®], uses its GUI for the development of models. Hence, objects and object interactions are made visible for the user, without the need for writing codes. Simulations are run through conversion of these object-oriented models into a mathematical code. However, the user needs to implement properly defined *in vitro* and *in vivo* based algorithms (flows, step functions, etc.) into objects and object interactions for the development of an accurate PBPK model. The program is less abstract than MATLAB[®] and facilitates the identification and correction of errors without revising the entire simulation code. Simulation outputs can be displayed in tables and graphical profiles.

Both programs have been widely applied in pharmaceutical research and are well-accepted tools for PBPK modeling and simulation [60, 86-89].

1.6.2.2 Commercial software (Simcyp[®], GastroPlus[®], PK-Sim[®]) and GI-Sim[®]

Like the previously described models these PBPK software are based on object-oriented programming. In contrast to MATLAB[®] or STELLA[®] the development of user-tailored models and algorithms is not possible: these PBPK programs have pre-defined algorithms and are rigid in terms of model development. However, they provide a friendly GUI, where the user only has to input drug related data to run simulations. The fundamental advantage of these programs is that they offer a variety of simulation approaches. Simulations are possible even when little *in vitro* or *in vivo* data are available. According to the data available the user can customize the simulation procedure (e.g. bottom-up or middle-out approach). Moreover, data may be either implemented directly by the user or predicted by the program based on structural characteristics of the drug investigated (e.g. MW, logP, PSA) or other data provided (e.g. prediction of human intestinal permeability with Caco-2 data). Commercial programs generally try to reflect all aspects of physiology and therefore offer whole-body PBPK simulations in which calculation of drug distribution in organs and tissues is possible. Moreover, complex absorption, disposition and elimination mechanisms may be considered and simulated individually using these programs. Commercial PBPK software and GI-Sim[®] enable the simulation of compartmental



dissolution and absorption (e.g. stomach, duodenum, jejunum, ileum), drug supersaturation and precipitation, and efflux/uptake transporter kinetics. They offer simulations of pharmacokinetics in different human population groups such as healthy volunteers of different ages as a function of gender and/or weight, disease states and according to ethnicity. Additionally, investigations of pharmacokinetics are possible for different animal species such as dogs, pigs, rats and mice. These PBPK software thus offer a range of possibilities for the investigation of pharmacokinetic aspects during preclinical and clinical drug development and are widely used in pharmaceutical research.



1.7 Aims of this work

The first goal of this work was to explore the dissolution behavior of weakly basic drugs in the upper GI tract. Therefore, marketed oral dosage forms of two compounds, cinnarizine and atazanavir, were studied using different fasted and fed state biorelevant dissolution techniques, such as individual dissolution and transfer experiments. The various *in vitro* methods were compared and on the basis of the results a decision tree was proposed to facilitate *in vitro* investigation of drug dissolution for poorly soluble weakly basic APIs.

The second objective of this work was to investigate the influence of drug dissolution, supersaturation and precipitation on the pharmacokinetics of weakly basic drugs. To achieve this objective dissolution and transfer experiment results were coupled with PBPK models for the simulation of plasma profiles of the two compounds. Simulations were performed with two different programs, STELLA[®] and Simcyp[®]. To enable the implementation of drug supersaturation and precipitation kinetics during gastric emptying, the existing STELLA[®] model was modified and the value-added of the modifications was assessed. Similarly, simulations were run with Simcyp[®] using different simulation approaches in terms of dissolution, supersaturation and precipitation kinetics.

The final goal was to compare the simulation approaches offered by STELLA[®] and Simcyp[®] to identify the strengths and weaknesses of the two programs. On that basis implications for development of further of PBPK models were discussed.



2 Materials and Methods

2.1 Materials

2.1.1 Chemicals

Following chemicals were used in this study:

Chemical	Trade name / specification	Manufacturer	Lot number
Acetic acid (100%)	Analytical grade	VWR International	12B220509
Acetonitrile	Analytical grade	VWR International	I691330327
Ammonium acetate	Analytical grade	Merck KGaA	A0028716849
Ammonium dihydrogen phosphate	Analytical grade	VWR International	12A310046
Atazanavir sulfate powder (crystalline)	100% purity	Bristol-Myers Squibb Company	229975-97-7
Atazanavir sulfate capsules	Reyataz [®] 200 mg	Bristol-Myers Squibb Company	2H5117A
Cinnarizine powder	100% purity	Hennig Arzneimittel GmbH & Co KG	ZH001575PU521-MIC
Cinnarizine tablets	Stugeron [®] 25 mg	Janssen-Cilag AG	ACL1800
Cinnarizine/dimenhydrinate tablets	Arlevert [®] 20 mg/40 mg Tablets 30 mg/60 mg	Hennig Arzneimittel GmbH & Co KG	324011 11/228
Deionized water			
Egg phosphatidylcholine	99.1% purity	Lipoid GmbH	108015-1/42
Glycerol monooleate	99.5% purity	Rylo M19 Pharma	173403401989490
Hydrochloric acid (37%)	Analytical grade	VWR International	20L060526



Materials and Methods

Chemical	Trade name / specification	Manufacturer	Lot number
Lipofundin [®] MCT 20	Emulsion with 20% triglycerides	B. Braun Meisungen AG	132918084
Long-life milk	3.5% fat UTH and 1.5% fat UTH	AF Deutschland GmbH	
Maleic acid	Analytical grade	Sigma-Aldrich	A792767747
Methanol	Analytical grade	VWR International	I630607212
Ortho-phosphoric acid (85%)	Analytical grade	VWR International	12K210017
Pepsin	0.51 U/mg	Fluka Chemie AG	1241256
SIF Powder		Biorelevant.com	PHA S 1003 012/16
SIF Powder FaSSIF-V2		Biorelevant.com	02-1302-01
Sodium dihydrogen phosphate monohydrate	Analytical grade	Merck KGaA	A02140949112
Sodium acetate trihydrate	Analytical grade	Merck KGaA	A792767747
Sodium chloride	Analytical grade	VWR International	10J110040
Sodium hydroxide	Analytical grade	VWR International	09G300017
Sodium oleate	82.1% purity	Riedel-de Haën	51110
Sodium taurocholate	>97.1% purity	Prodotti Chimici E Alimentari S.P.A.	2011040152

2.1.2 Model substance cinnarizine

Cinnarizine (IUPAC name: (1-(diphenylmethyl)-4-(3-phenylprop-2-en-1-yl)piperazine) is a lipophilic weak base ($pK_{a1} = 1.95$ and $pK_{a2} = 7.47$ (both basic)) with a molecular weight of 368.514 g/mol and a logP of 5.6 [90, 91] (Figure 2.1). It exhibits a polar surface area (PSA) of 2.4 - 11.8 Å and low solubility at pH values greater than 4.5 [90, 92, 93]. A study on weak bases has shown cinnarizine to supersaturate and precipitate when being transferred from a highly acidic compartment (0.1 molar HCl)



into Fasted State Simulated Intestinal Fluid (FaSSIF) adjusted to a pH value of 5.5 [94]. Interestingly, no supersaturation was observed when the drug was moved from a compartment containing the McIlvaine buffer (pH 5.0) into FaSSIF (pH 6.5). This observation could partially explain the gastric acidity dependent bioavailability of cinnarizine, which has been observed in humans and dogs [95, 96]. A permeability investigation of cinnarizine in the Caco-2 cell culture model has shown a moderate P_{app} value of 4.2×10^{-6} cm/s (apical to basolateral (A→B) and basolateral to apical (B→A)) in comparison to mannitol (1.1×10^{-6} cm/s), a poorly permeable reference compound [97]. Because A→B and B→A permeability experiments revealed comparable values, it is most likely that cinnarizine undergoes passive intestinal absorption and is not a substrate for P-gp. Pharmacokinetic investigation of cinnarizine in beagle dogs revealed an oral bioavailability of 55-60%. The authors concluded that the modest oral bioavailability values are attributed to presystemic metabolism rather than to permeability constraints [90]. Cinnarizine demonstrated a positive food effect in pharmacokinetic studies on Arlevert[®] in healthy human volunteers. The administration of Arlevert[®] after a high fat meal resulted in a moderate increase of C_{max} and AUC values, by 8% and 44%, respectively. One possible explanation for the food effect is that there is precipitation of cinnarizine in the small intestine in the fasted state, but not in the fed state.

Cinnarizine was chosen as a model compound because it is a poorly soluble weak base and has an interesting *in vitro* dissolution behavior, i.e. supersaturation and precipitation. It shows a moderate positive food effect, which may be attributed to drug precipitation in the fasted, but not fed, upper small intestine. It is therefore an appropriate compound for *in vitro* dissolution investigation and for *in silico* modeling and simulation.

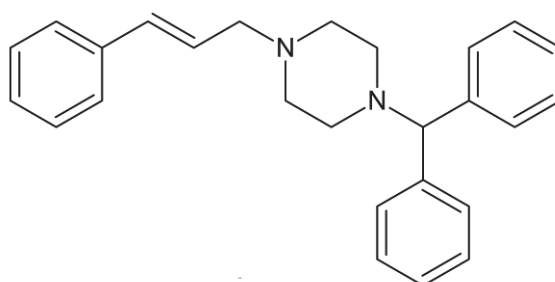


Fig. 2.1: Structure of cinnarizine



Materials and Methods

Cinnarizine formulations available in the market

Two marketed formulations were investigated in this work:

Arlevert[®] tablets comprised, besides the APIs (20 mg cinnarizine, 40 mg dimenhydrinate), talc, magnesium stearate, maize starch, microcrystalline cellulose, croscarmellose sodium, hypromellose and fumed silica.

Stugeron[®] tablets comprised, besides 25 mg cinnarizine, lactose monohydrate, maize starch, sucrose, talc, hydrogenated cottonseed oil and povidone K90.

The investigational formulation “Cinnarizine 30 mg tablets” comprised, besides the APIs (30 mg cinnarizine, 60 mg dimenhydrinate), the same ingredients as Arlevert[®] tablets: talc, magnesium stearate, maize starch, microcrystalline cellulose, croscarmellose sodium, hypromellose and fumed silica.

Pharmacokinetic studies on cinnarizine

One fed state and two fasted state PK studies were considered for this investigation. The fed state study comprised two different treatments. 28 healthy males were enrolled in a dose proportionality study in which Arlevert[®] 20 mg cinnarizine tablets were compared with Cinnarizine 30 mg tablets. In each treatment the subjects received a cinnarizine tablet (Arlevert[®] 20 mg or Cinnarizine 30 mg) after a standardized breakfast (high fat meal). Plasma samples were collected at 0, 0.25, 0.5, 0.75, 1, 1.25, 1.5, 1.75, 2.00, 2.5, 3, 4, 5, 6, 8, 12, 16 and 24 hours [98].

The first fasted state study was conducted in 16 healthy subjects who were treated with one Arlevert[®] tablet after an overnight fast. Blood samples were taken at 1.5 hours prior, and 0.5, 1, 1.5, 2, 2.5, 3, 3.5, 4, 4.5, 5, 6, 7, 8, 9, 10, 12, 14, 16, 18, 20 and 24 hours after oral administration [98]. In the second fasted state study 24 healthy male volunteers received one Stugeron[®] 25 mg tablet orally. Plasma concentrations were determined for the time points of 0, 0.5, 1, 1.5, 2, 2.5, 3, 3.5, 4, 6, 8, 12, 16, 24, 36, 48, and 72 hours [99].

2.1.3 Model substance atazanavir

Atazanavir (Figure 2.2) is an azapeptide HIV-1 protease inhibitor for the combination antiretroviral therapy (ART) of HIV-1 infected patients [100-104]. The marketed



product is Reyataz[®] by Bristol-Myers Squibb. Atazanavir (IUPAC name: methyl N-[(1S)-1-[[[(2S,3S)-3-hydroxy-4-[(2S)-2-[(methoxycarbonyl)amino]-3,3-dimethyl-N'-{[4-(pyridin-2-yl)phenyl]methyl}butanehydrazido]-1-phenylbutan-2-yl]carbamoyl]-2,2-dimethylpropyl]carbamate) is available on the market as a hydrosulfate salt and has a molecular weight of 704.86 g/mol referred to the free base. It has a basic pKa value of 4.7, a calculated octanol-water partition coefficient (logP) of 5.92 and a calculated polar surface area of 186.2 Å [105, 106]. The drug has a highly pH dependent solubility. In acidic environment it shows high solubility (5.2 mg/ml at pH 1.9) which decreases rapidly with increasing pH (0.002 mg/ml at pH 4.3) [106].

The absolute bioavailability of atazanavir is not known. However, a mass balance study was performed in three volunteers with 400 mg radioactively marked atazanavir sulfate under fed conditions. The investigation revealed that 79% (15 % as unchanged drug) of the dose administered was found in feces [106]. This suggests that the bioavailability is compound to be somewhat permeability restricted.

Atazanavir sulfate exhibits nonlinear pharmacokinetics over the dose range from 100 mg to 1200 mg. Since the compound is assumed to be CYP3A4 and CYP3A5 substrate and a CYP3A4 and UGT1A1 inhibitor, it is likely that atazanavir can undergo microsomal biotransformation saturation [106-108]. Elimination of the compound is assumed to take place predominantly via the biliary pathway [106]. A positive food effect for atazanavir was observed under light meal conditions containing orange juice. Interestingly, under high fat meal conditions both slight positive and negative food effects have been reported [106, 109-111]. A solubility study on atazanavir in fasted and fed state simulated fluids (FaSSIF and FeSSIF) resulted in similar values to its solubility in human intestinal fluids and little effect of prandial state was revealed: the solubility of 15.1 µM in FaHIF (Fasted human intestinal fluid) was similar to the solubility of 14.9 µM in FeHIF (Fed human intestinal fluid) [112]. However, atazanavir dissolution behavior under fasted and fed state conditions has not been thoroughly explored, nor have supersaturation/precipitation effects upon entry into the small intestine been investigated. The permeability of the compound in Caco-2 cell cultures was revealed to be concentration dependent (A to B at 1 µM ~ 1.5 x 10⁻⁶ cm/s and at 100 µM ~ 8 x 10⁻⁶ cm/s), indicating a possible

Materials and Methods

involvement of P-gp mediated efflux in atazanavir absorption [113]. Interestingly, a Caco-2 study which was conducted to assess the permeability of atazanavir using biorelevant media (FaSSIF or FeSSIF) in the apical compartment, revealed significantly higher permeability values in FeSSIF (1.25×10^{-5} cm/s) than in FaSSIF (1.5×10^{-6} cm/s). An analogous permeability behavior was observed during drug perfusion experiments using rat intestine [114].

When atazanavir was administered with H_2 antagonists or PPIs, the compound exhibited lower pharmacokinetic profiles than without co-medication [115, 116]. Since these agents reduce gastric acidity, they consequently decrease the solubility of the weak base atazanavir in the stomach. Lower gastric solubility in turn is expected to have a negative impact on intestinal dissolution and thus on absorption of atazanavir.

Atazanavir sulfate was chosen as a model substance since it is a poorly soluble weak base with as yet unknown biorelevant dissolution behavior. Another reason for choosing atazanavir was its nonlinear pharmacokinetics and the contradictory food effect observed for atazanavir sulfate in PK studies. Possible pre-absorptive efflux transporter interactions and post absorptive variability make the compound attractive not only for *in vitro* investigations but in particular for plasma profile predictions using *in silico* modeling and simulation.

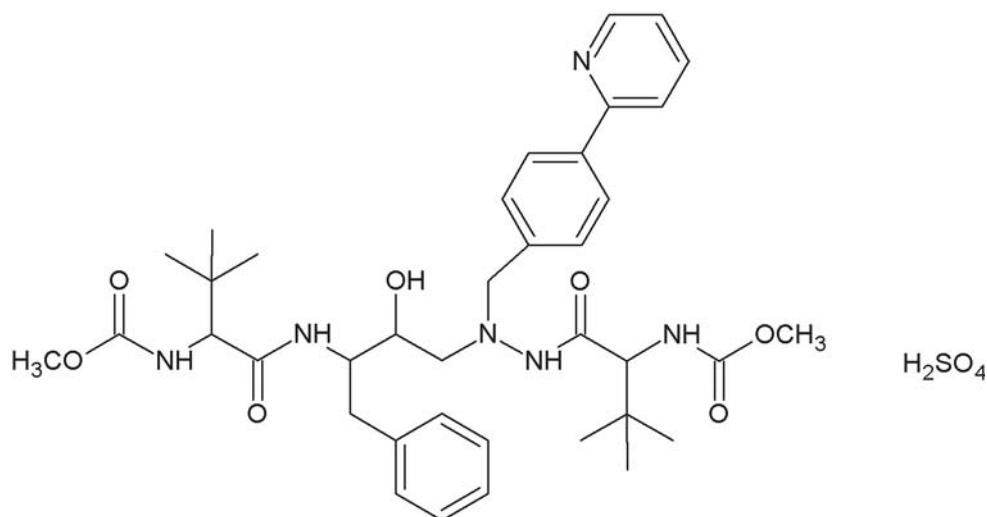


Fig. 2.2: Structure of atazanavir sulfate



Atazanavir formulations available on the market

Atazanavir is available as an amorphous sulfate salt in dose strengths of 100, 150, 200 and 300 mg as capsule formulation (Reyataz[®]). Other components of the formulation are the gelatin capsule shell colored with FD&C Blue No. 2 and titanium dioxide as well as crospovidone, lactose and magnesium stearate. Excipients for formulation enhancement are not present in Reyataz[®].

Pharmacokinetic studies on atazanavir sulfate

One fed state and three fasted state pharmacokinetic studies were considered for this investigation. In the fed state PK study 15 healthy young males (18-40 years) were enrolled. The subjects received atazanavir sulfate capsules (2 x 200 mg) after a light meal (~370 kcal), which consisted of 2 slices of toasted white bread, 1 teaspoon of low fat margarine, 1 tablespoon of jelly, 5 oz of orange juice and 5 oz of skim milk. Plasma samples were collected at 0.5, 1, 1.5, 2, 2.5, 3, 4, 5, 6, 8, 12, 16, 20 and 24 hours [106].

The first fasted state PK study consisted of two dose levels, namely 100 mg (2x50 mg) or 1200 mg (6x200 mg) atazanavir sulfate capsules. The study was completed in six healthy male subjects. Blood samples were collected prior to dosing and at 0.25, 0.5, 0.75, 1, 1.5, 2, 3, 4, 5, 6, 8, 12, 18, 24, 30 and 36 hours after oral administration [106]. The second fasted state study investigated the pharmacokinetics of six healthy males who received 200 mg atazanavir capsules after an overnight fast. Plasma samples were taken prior to dosing and at 0.25, 0.5, 0.75, 1, 1.5, 2, 3, 4, 6, 8, 12, 18 and 24 hours after dosing [106]. In the third fasted state study (four arm drug-drug interaction study) 32 healthy male subjects received 400 mg (2 x 200 mg) atazanavir sulfate capsules either as single oral administration or in combination with stavudine or didanosine after an overnight fast. Only the single dose mono-treatment study arm was considered in this investigation. Plasma samples were taken prior to dosing and at 0.25, 0.5, 0.75, 1, 1.5, 2, 3, 4, 5, 6, 8, 10, 12, 18 and 24 hours after administration [106].



Materials and Methods

2.2 Methods

2.2.1 HPLC-UV setup

The analytical HPLC setups for atazanavir and cinnarizine are summarized in Table 2.1

Table 2.1: HPLC setup for the analysis of cinnarizine and atazanavir

Equipment	Specification for atazanavir	Specification for cinnarizine
Detector	L-4250 UV-VIS: 288 nm	L-4250 UV-VIS: 254 nm
Precolumn	Merck LiChrospher® 100 RP-18 5 µm	Merck LiChrospher® 100 RP-18 5 µm
Column	Merck Purospher® STAR RP-18 endcapped (5 µm)	Merck LiChroCART 125-4 RP-18 (5 µm)
Interface		D-7000
Autosampler		L-7200
Pump		L-7100: 1.5 ml/min
Software	EZChrom Elite v2.8 software (Hitachi, Tokyo, Japan)	

Mobile phase for cinnarizine

The mobile phase comprised a 1% ammonium acetate/0.2% acetic acid aqueous buffer and acetonitrile in a ratio of 1:4. The flow rate was set at 1.5 ml/min while the injection volume was adjusted to 20 µl. The measurements were performed at a detection wavelength of 254 nm. Using this method the retention time was approximately 3.5 minutes and the cinnarizine limit of quantification was 50 ng/ml.

Mobile phase for atazanavir

The mobile phase comprised a 0.2% ammonium phosphate aqueous buffer adjusted to pH 2.5 with phosphoric acid and acetonitrile (1:1). The flow rate was set at 1.5 ml/min while the injection volume was adjusted to 20 µl. The measurements were performed at a detection wavelength of 288 nm. Using this method the retention time was approximately 3.5 minutes and the limit of quantification of atazanavir was 250 ng/ml.



2.2.2 Biorelevant media

Biorelevant media were used for solubility studies as well as for dissolution tests and transfer experiments. Media characterizing the pre- and postprandial conditions of the stomach were Fasted State Simulated Gastric Fluid, FaSSGF, and Fed State Simulated Gastric Fluid, FeSSGF pH 5.0 [21, 22]. FaSSGF has a pH of 1.6 representing the gastric acidity in the preprandial stomach. Moreover it has a small concentration of bile components to achieve a lower surface tension, which is assumed to originate from duodenal reflux of bile. Additionally, pepsin is added to the medium to mimic the *in vivo* conditions, since it was reported to be part of the fasted state gastric content [21].

As an alternative to FeSSGF, Fed State Simulated Gastric Emulsion (FeSSGEm pH 5.0) was developed. It contains the same amount of lipids as FeSSGF, which are in this case supplied from Lipofundin[®] MCT 20% infusion emulsion, but does not contain any proteins (which are contributed by milk in FeSSGF). To simulate special fed state conditions, two additional media were developed: FeSSGF pH 2.75 and FeSSGEm pH 2.75. The pH of the media was adjusted to a value of 2.75 to represent the gastric conditions after ingestion of a meal containing orange juice in PK studies on atazanavir sulfate (the fed state study described in 2.1.3). Orange juice has a pH value of approximately 3. A physical mixture of one part of 0.1N HCl, representing the gastric secretion in response to food intake, and two parts of orange juice, representing the fluid given with the meal, results in a pH value of 2.75.

Conditions of the pre- and postprandial intestine were simulated by Fasted State Simulated Intestinal Fluid, FaSSIF-V2, and Fed State Simulated Intestinal Fluid, FeSSIF-V2 [22].

When FaSSGF is emptied into FaSSIF-V2 during transfer experiments a pH change in the acceptor phase is inevitable. To avoid drastic pH shifts in the preprandial intestinal compartment during transfer experiments, the pH of FaSSGF was adjusted to a value of pH 2.0 [61]. To further comply with the transfer experiment requirements, the buffer capacity of FaSSIF-V2 was increased by exchanging the maleate buffer with a phosphate buffer (FaSSIF-V2(PO₄)) [59, 64].



Materials and Methods

The compositions of simulated fasted and fed state gastric and intestinal media used in this work are summarized in Tables 2.2 to 2.5.

Table 2.2: Composition of the biorelevant media simulating gastric fasted state

	FaSSGF pH 1.6	FaSSGF pH 2.0
<i>Composition</i>		
Sodium taurocholate (mM)	0.08	0.08
Lecithin (mM)	0.02	0.02
Pepsin (mg/mL)	0.1	0.1
Sodium chloride (mM)	34.2	34.2
Hydrochloric acid (mM)	25.1	12.6
<i>Characteristic parameters</i>		
pH	1.6	2.0
Osmolality (mOsm/kg)	120 ± 2.5	120 ± 2.5

Table 2.3: Composition of the biorelevant media simulating gastric fed state

	FeSSGF pH 5.0	FeSSGEm pH 5.0
<i>Composition</i>		
Sodium chloride (mM)	237.0	181.7
Acetic acid (mM)	17.1	18.3
Sodium acetate (mM)	29.8	33.0
Milk/buffer ratio	1/1	-
Lipofundin [®] /buffer ratio	-	27/250
<i>Characteristic parameters</i>		
pH	5.0	5.0
Osmolality (mOsm/kg)	400 ± 10	-
Buffer capacity (mM/ΔpH)	25	-



Table 2.4: Composition of the biorelevant media simulating gastric fed state under light meal conditions with orange juice

	FeSSGF pH 2.75	FeSSGEm pH 2.75
<i>Composition</i>		
Sodium chloride (mM)	122.6	122.6
Monobasic sodium phosphate (mM)	32.0	32.0
Orthophosphoric acid (mM)	7	7
Milk/buffer ratio	1/1	-
Lipofundin®/buffer ratio	-	27/250
<i>Characteristic parameters</i>		
pH	2.75	2.75

Table 2.5: Composition of the biorelevant media simulating fasted and fed intestinal states

	FaSSIF-V2	*FaSSIF-V2(PO ₄)	FeSSIF-V2
<i>Composition</i>			
Sodium taurocholate (mM)	3	3	10
Lecithin (mM)	0.2	0.2	2
Glycerol monooleate (mM)	-	-	5
Sodium oleate (mM)	-	-	0.8
Sodium chloride (mM)	68.62	62.60	125.5
Maleic acid (mM)	19.12	-	55.02
Monobasic sodium phosphate (mM)	-	28.6	-
Sodium hydroxide (mM)	34.8	8.7	81.65
<i>Characteristic parameters</i>			
pH	6.5	6.5	5.8
Osmolality (mOsm/kg)	180 ± 10	180 ± 10	390 ± 10
Buffer capacity (mM/ΔpH)	10	12	25

* used in transfer experiments

2.2.3 Solubility assessment

Equilibrium solubility

Drug solubility in FaSSGF pH 1.6, FaSSGF pH 2.0, FeSSGEm (pH 2.75 and 5.0), FaSSIF-V2, FaSSIF-V2(PO₄) and FeSSIF-V2 were measured utilizing the Uniprep® (Whatman Inc., Sanford, ME, USA) method. A combination of FaSSGF pH 2.0 and FaSSIF-V2(PO₄) in a ratio of 1:2 was used to additionally evaluate the solubilities of the compounds in the acceptor medium after completion of transfer experiments. To assess the bile salt dependence of drug solubility, measurements were also performed in blank buffers of FaSSIF-V2 and FeSSIF-V2.



Materials and Methods

Briefly, solubilities were determined by introducing an excess amount of drug into a Uniprep® vial, filled with 3 ml of biorelevant medium, locked with the Uniprep® cap, slightly shaken to remove bubbles and placed on an orbital shaker at 37° C for 24 hours. Subsequently, the dispersions were filtered through the integrated Uniprep® 0.45 µm PTFE filter. 500 µl of the filtrate was diluted with 500 µl of methanol and analyzed by HPLC. In the case of FeSSGEm, 500 µl of the filtrate was diluted with 1000 µl of acetonitrile to separate the fat content of the medium. The mixture was then centrifuged at 7500 rpm for 3 minutes and the supernatant was analyzed by HPLC.

For the determination of the solubility of the compounds in FeSSGF the standard shake flask method was utilized. An excess amount of drug was introduced into a 20 ml scintillation glass vial, 15 ml of the medium was added, mixed and the vial was incubated in an orbital shaker at 37° C for 24 hours. Due to insoluble milk proteins in the medium a filtration through a 0.45 µm filter was not possible. Thus, the dispersions were filtered through Whatman 2.7 µm glass microfiber syringe filters (25 mm GD/X, GE Healthcare UK Ltd., Buckinghamshire, UK). Subsequently, soluble proteins were precipitated by adding 2 ml of acetonitrile to 1 ml of filtrate. The mixtures were centrifuged at 7500 rpm for 3 minutes and the supernatant was analyzed by HPLC.

For each medium the measurements were performed in triplicate.

Kinetic solubility

The shake flask method was additionally used to investigate the time dependent drug concentration change in FaSSIF-V2, FeSSIF-V2 and combination of FaSSGF pH 2.0 and FaSSIF-V2(PO₄) in a ratio of 1:2. An excess amount of drug was introduced into a 20 ml glass vial, dispersed with 15 ml of the corresponding medium, mixed and the vial was incubated on an orbital shaker at 37° C. Samples were taken at 1, 2, 6 and 24 hours. The vials were then shaken using a vortex shaker, filtered using PTFE 0.45 µm filters, and the resulting filtrate diluted with methanol and analyzed by HPLC. For each medium the measurements were performed in triplicate.



2.2.4 Dissolution experiments

To mimic the fasted state gastric dissolution conditions the Mini Paddle assembly (Erweka DT 80, Heusenstamm, Germany), a scaled down USP 2 apparatus, was utilized. The volume of FaSSGF pH 1.6 was adjusted to 250 ml. The conditions in the fed state stomach and the fasted and fed intestine were mimicked using the USP 2 dissolution test apparatus with 500 ml of the corresponding medium (FeSSGF/FeSSGEm, FaSSIF-V2 and FeSSIF-V2). All dissolution tests were carried out at $37 \pm 0.5^\circ \text{C}$ and a revolution speed of 75 rpm. Sampling for all dissolution tests was performed at 0, 5, 10, 15, 20, 30, 45, 60, 90, 120, 180 and 240 minutes. The samples were taken manually via a 5 ml glass syringe, which was connected to a stainless steel sampling cannula and a 10 μm polyethylene cannula filter (Erweka GmbH, Heusenstamm, Germany). At each sampling point 5 ml of biorelevant medium were aspirated into the glass syringe and filtered through a 0.45 μm PTFE filter (Rezist 30, GE Healthcare UK Ltd., Buckinghamshire, UK) whereby 4 ml was returned to the dissolution vessel. For each medium, samples were prepared for analysis according to procedures described in the solubility measurement Section 2.2.3. All dissolution tests were performed in triplicate.

2.2.5 “Dumping” experiments

“Dumping” experiments were performed to screen for possible supersaturation and precipitation of cinnarizine and atazanavir during gastric emptying prior to conducting more sophisticated transfer experiments.

Briefly, a specified amount of the weak base was pre-dissolved in 250 mg FaSSGF pH 2.0 at $37 \pm 0.5^\circ \text{C}$ and the resulting solution was “dumped” (i.e. bolus transfer) into a USP apparatus 2 containing 500 ml FaSSIF-V2(PO_4). The rotation speed was set at 75 rpm. Sampling was performed at 0, 3, 6, 10, 30, 60, 90, 120, 180 and 240 minutes. The samples were prepared for analysis according to Section 2.2.3.

2.2.6 Transfer experiments

Previous work by Kostewicz *et al.* investigated supersaturation and precipitation of weak bases during gastric emptying using the transfer model [59]. Those studies were conducted by pre-dissolving the drugs in a donor compartment with simulated



Materials and Methods

gastric fluid (SGF) and transferring the solution into an acceptor compartment filled with FaSSIF or FeSSIF. In the current work the setup of the original transfer model was modified to better reflect conditions in a PK study. Usually, when an immediate release (IR) solid dosage form (e.g. tablet or capsule) is taken with a glass of water it starts to disintegrate and to release the drug in the stomach, during which the gastric content is simultaneously emptied into the intestine.

To summarize, the influence of different factors on dissolution behavior of weakly basic compounds and their dosage forms was investigated using three different types of transfer experiments:

1. Pre-dissolution of the pure compound in the donor compartment and subsequent transfer of the solution into the acceptor compartment
2. Pre-dissolution of the dosage form in the donor compartment and subsequent transfer of the solution/dispersion into the acceptor compartment
3. Simultaneous disintegration/dissolution of the dosage form in the donor compartment and transfer of the donor content into the acceptor compartment.

All of the three transfer setups were performed under simulated fasted state conditions, since supersaturation and precipitation of poorly soluble weak bases are expected to most likely occur in the fasted state. The Mini Paddle apparatus with 250 ml FaSSGF pH 2.0 was used as the donor compartment and the USP 2 Paddle apparatus with 500 ml FaSSIF-V2(PO_4) was used as the acceptor compartment. The paddle rotation speed was set at 75 rpm in each compartment and the temperature was adjusted to $37 \pm 0.5^\circ \text{C}$. The dose (pure compound or dosage form) was introduced into the donor compartment and one of the previously described options (1-3) was chosen for the transfer experiment. The transfer of the donor content into the acceptor compartment was performed with the help of a peristaltic pump (Ismatec Type IPC-8 V3.01, Glattbrugg-Zürich, Switzerland (cinnarizine) or Ismatec Type IP 65, Glattbrugg-Zürich, Switzerland (atazanavir)). Gastric emptying was mimicked through implementation of different transfer rates. Kostewicz *et al.* had utilized zero



order transfer rates of 9, 4, 2 and 0.5 ml/min [59]. However, population studies have shown that the gastric emptying proceeds on average according to first order kinetics in the fasted state and according to zero order kinetics in the fed state [117]. To comply with average human physiology in the fasted state a first order transfer with a rate constant of 3 h^{-1} (4 h^{-1} for atazanavir) was implemented and results were compared with zero order rates of 9, 4 (or 2), and 0.5 (optional) ml/min, representing faster than usual gastric emptying, approximately average, and slower than usual gastric emptying rates, respectively.

Additionally, some fed-state transfer experiments were conducted to investigate atazanavir behavior under light and standard meal conditions of administration. To simulate fed state gastric emptying the USP 2 Paddle apparatus was utilized with 500 ml of FeSSGF pH 5.0 or FeSSGEM pH 5.0 as a donor compartment and 500 ml FeSSIF-V2 as an acceptor compartment. In this case (1000 kcal and 4 kcal/min) the gastric emptying time was estimated to be 250 minutes. To simulate the light meal conditions, 250 ml FeSSGEM pH 2.75 (Mini Paddle apparatus) representing the gastric compartment and 500 ml FeSSIF-V2 (USP 2 apparatus) representing the upper intestinal compartment. The simulated gastric emptying rate had to be adapted to the volume present in the donor compartment and to the meal conditions used in PK studies. For the standard meal conditions the transfer rate was calculated to be 2 ml/min. For the light meal the transfer rate was estimated to be 4 ml/min.

The sampling times were adapted to the transfer rate. Samples were removed from the acceptor compartment and prepared for analysis using the procedures described in Section 2.2.3. All transfer experiments were performed in triplicate.

Calculation of fraction dissolved and precipitation values

When drug is emptied into the acceptor compartment it could be in one of two states, dissolved or solid state. Dissolved and solid states together represent the total drug amount emptied at a given time. Total drug transferred is represented by the theoretical curve whereas the amount of dissolved drug in the acceptor compartment is described by the observed concentration profile (Figure 2.3). The fraction dissolved (f_d) was calculated with the assistance of equation 1:



Materials and Methods

Equation 1

$$f_d = \frac{D_{t+1} - D_t}{T_{t+1} - T_t}$$

where $D_{t+1} - D_t$ is the mass difference of drug dissolved between the time points t and $t+1$ in the acceptor compartment and $T_{t+1} - T_t$ is the mass difference of total drug between the time points t and $t+1$ in the acceptor compartment. Simply put, this term represents the quotient of the slopes of mass of drug dissolved and total mass of drug transferred over a time interval t to $t+1$. The f_d value is thus a dynamic parameter and can be calculated individually for each time interval. However, if the f_d values do not vary significantly in between the time intervals, one f_d value can be utilized for the supersaturation parameterization.

The precipitation constant was calculated from the downslope of the observed profile (Figure 2.3). The decrease in concentration was fitted to an exponential function. The first order precipitation constant was obtained from the exponent of the function described in equation 2:

Equation 2:

$$\frac{dP_t}{dt} = D_{t'} \cdot e^{-k_p \cdot t}, t \geq t'$$

where P_t is the amount of precipitated drug at a given time, $D_{t'}$ is the amount of drug which is available for precipitation, e is Euler's number, k_p is the first order precipitation constant and t is time. The precipitation kinetics were calculated starting at time point t' , at which the drug concentration started to decrease in the transfer experiment profile.

Figure 2.3 illustrates the evaluation of supersaturation and precipitation kinetics with the aid of "theoretical" and "observed" concentration curves in the intestine during and after simulated gastric emptying.

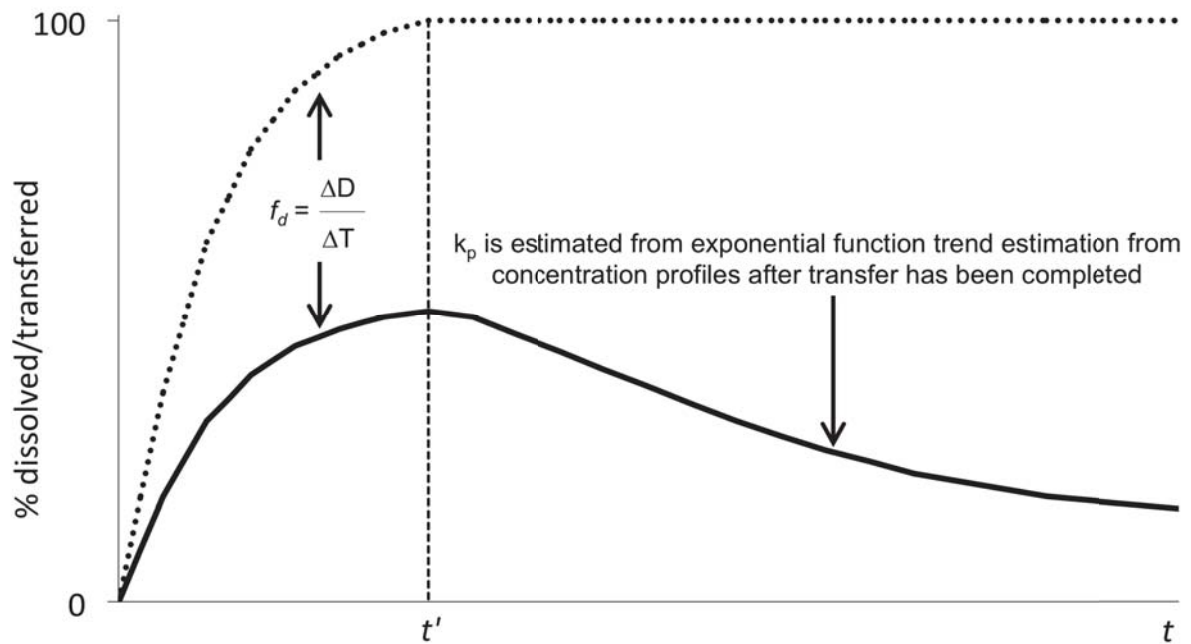


Fig. 2.3: Evaluation of fraction of drug dissolved (f_d) and precipitation kinetics during and after gastric emptying (k_p). Total mass of drug emptied into intestine at time t is shown as a theoretical concentration curve (\cdots). The observed percentage (mass) of drug dissolved in the intestine at time t and drug precipitation at times after gastric emptying is complete, t' , are presented in the continuous curve ($-$). The vertical line ($--$) represents the time at which gastric emptying is complete, t' .

Materials and Methods

2.2.7 WinNonLin[®] - assessment of pharmacokinetics of API formulations

For the evaluation of the distribution and elimination kinetics of cinnarizine and atazanavir, the WinNonLin[®] v. 4.1 pharmacokinetic software (Pharsight Corporation, Mountain View, CA, USA) was utilized. *In vivo* plasma concentration time data, dose and type of administration (per oral) were introduced into the software mask and the type of the compartment model (one or two compartment model) was selected. The following relevant data were taken from the calculation output sheet: absorption constant, k_{01} , elimination constant, k_{10} , apparent volume of distribution, V_d/F and apparent clearance, CL/F . For APIs exhibiting distribution into deep compartments two additional values have to be calculated: deep compartment inflow: k_{12} and deep compartment outflow: k_{21} . Figure 2.4 illustrates the model which was utilized in WinNonLin[®] to derive the absorption, distribution and elimination kinetics.

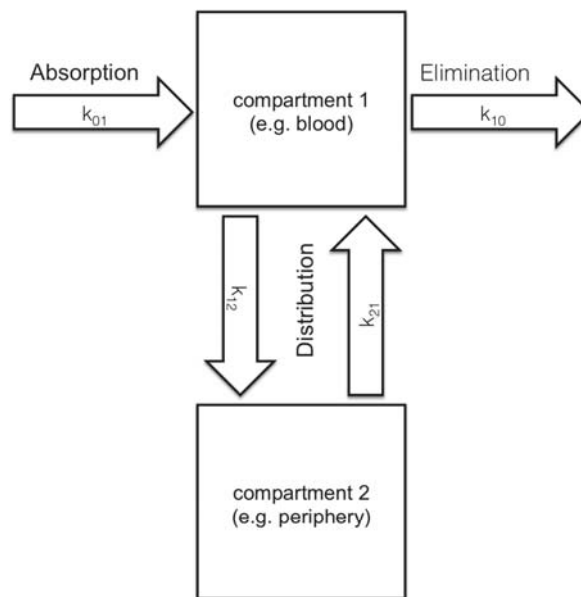


Fig. 2.4: Pharmacokinetic model used in WinNonLin[®]: k_{01} : absorption kinetics constant, k_{10} : elimination kinetics constant, k_{12} : deep compartment inflow constant (optional), k_{21} : deep compartment outflow constant (optional).



2.2.8 STELLA[®]

For the simulation of plasma profiles the STELLA[®] simulation software (v. 9.1.3, Isee Systems, Inc., Lebanon, NH, USA) was utilized. Solubility, dissolution and transfer experiment results as well as absorption, distribution and elimination kinetics (from WinNonLin[®]) were implemented into two different models, the “dissolution-only”, and the “supersaturation and precipitation” model. Figures 2.5 and 2.6 outline the two different STELLA[®] approaches for the prediction of plasma profiles of weak bases. The dissolution-only PBPK model, which has been previously described in several publications [60, 87-89], was employed to predict the fasted and fed state profiles of APIs. It utilizes dissolution kinetics and solubility of poorly soluble APIs in simulated gastric and intestinal media without considering drug supersaturation and precipitation.

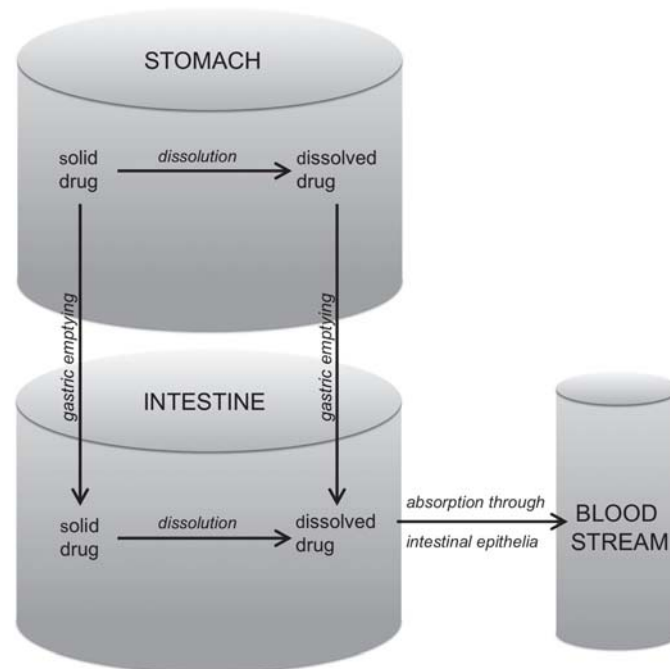


Fig. 2.5: PBPK model for *in vivo* API formulation behavior, in which only dissolution is accounted for (dissolution-only PBPK model).

The supersaturation and precipitation PBPK model incorporates supersaturation and precipitation kinetics during gastric emptying and therefore can be utilized if drug supersaturation and precipitation is observed *in vitro*.

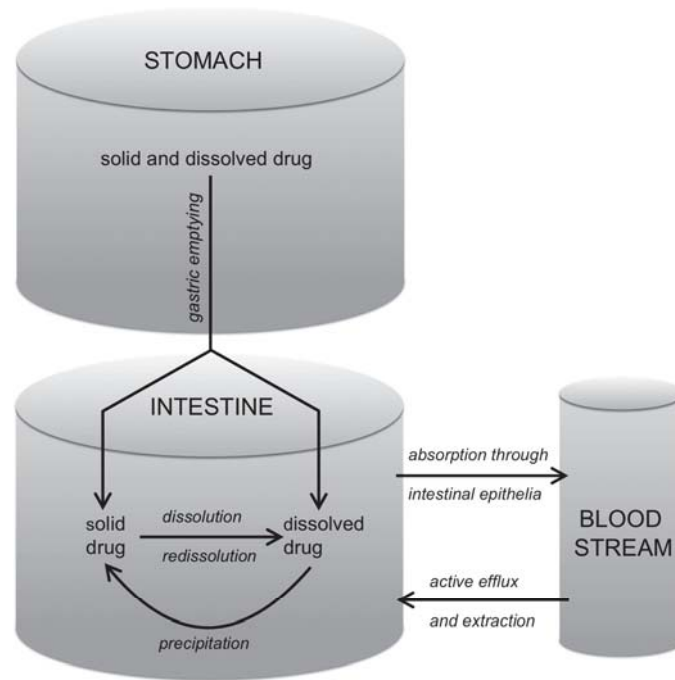


Fig. 2.6: PBPK model for *in vivo* API formulation behavior, in which dissolution, supersaturation, subsequent precipitation and efflux/extraction kinetics can be accounted for (supersaturation and precipitation PBPK model).

Dissolution-only PBPK model

The dissolution-only PBPK model assumes a gastric volume of 250 ml and a zero order gastric emptying rate of 2.8 h^{-1} for the fasted state. Simulations of the fed state consider a gastric volume of 750 ml (400 ml under light meal conditions) and a first order gastric emptying rate of 4 kcal/min [117]. Dissolution kinetics are described by the Noyes-Whitney dissolution model, which is presented in the following equation:

Equation 3

$$\frac{dW_t}{dt} = \frac{D\Gamma N^{1/3}}{V\delta\rho^{2/3}} W^{2/3} (X_s - W_t) = zW_t^{2/3} (C_s - C_t)$$

where W_t is the mass of drug dissolved in time t , D is the diffusion coefficient, Γ is the shape factor, N is the number of particles to be dissolved, W is the mass of drug remaining to be dissolved, X_s is the mass of drug that saturates the volume V , δ is the thickness of the diffusion layer, ρ is the particle density, C_s is the solubility of the drug and C_t is the concentration of the drug at time t . The expression $D\Gamma N/V\delta\rho^{2/3}$ can be merged into the initial dissolution rate constant z , which was obtained from



dissolution test results in simulated gastric and intestinal media for each drug dose and formulation. The model based on the Noyes-Whitney theory has been demonstrated to be reliable for the investigation of dissolution kinetics of drug compounds in several studies [56, 60, 87-89, 117, 118]. The dissolution-only model can be implemented with or without permeability restrictions. Figure 2.7 shows the STELLA[®] dissolution-only model without permeability restrictions, where pre-absorptive (green) and post-absorptive (orange) parameters are distinguished. The pre-absorptive parameters are the gastric and intestinal volumes, the gastric emptying rate (GER), the initial dissolution constants obtained from biorelevant dissolution tests (shown as z FeSSGF and z FeSSIF) and solubility values in biorelevant media.

The post-absorptive parameters (k_{10} , k_{12} , k_{21} and V_d/F), which were either obtained from WinNonLin[®] or from the literature, were introduced into the model. Note that k_{12} and k_{21} kinetics are only relevant for compounds which exhibit accumulation in deep compartments. This model was used for cinnarizine in the fed state as a comparator with the model shown in Fig. 2.8.

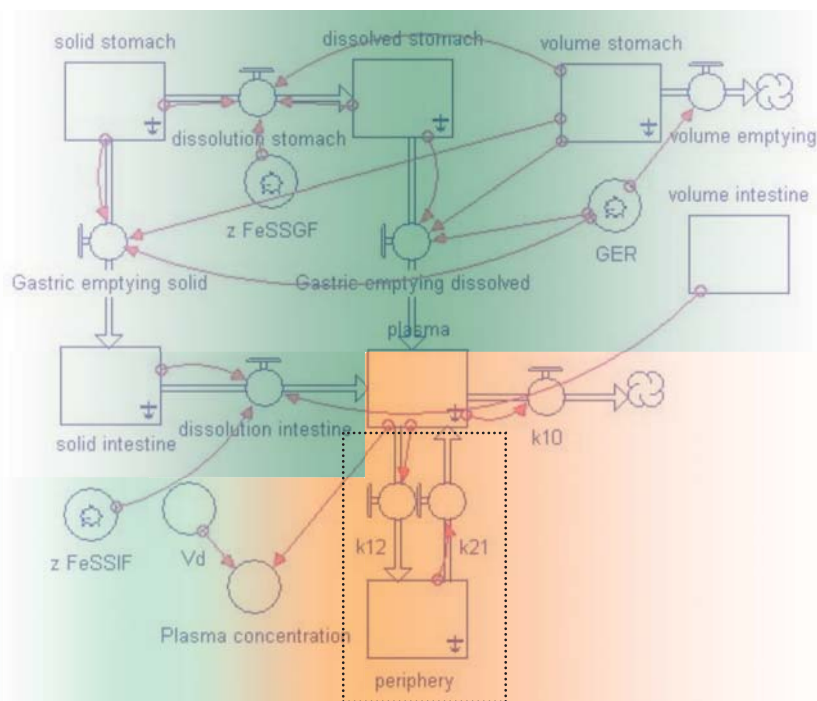


Fig. 2.7: STELLA[®] dissolution-only PBPK model without permeability restrictions; green: pre-absorptive kinetics (gastric and intestinal dissolution, gastric emptying), orange: post-absorptive kinetics (distribution and elimination), dotted square: (optional) deep compartment kinetics.



Materials and Methods

In Figure 2.8 an absorption restriction (red) is introduced in the dissolution-only STELLA[®] model. The absorption constant (k_{01}) can be obtained from WinNonLin[®]. However, drug absorption is dynamic and may depend on several factors:

- fluid volume in the intestine
- dissolution and precipitation (concentration) of the API in the intestine
- permeability of the API through the gut mucosa
- effective surface area of the gut mucosa at the absorption site

Since these pre-absorptive factors are already accounted for in the STELLA[®] model, it is not reasonable to use the hybrid k_{01} constant from WinNonLin[®] for *in vivo* predictions. Instead, drug flux from the intestinal lumen through the gut wall into the venous blood stream was calculated using following equation:

Equation 4

$$\frac{dY_t}{dt} = P_{app}A_{eff}C$$

where dY_t/dt is the rate of uptake of dissolved drug through the intestinal wall at time t , P_{app} is the permeability coefficient of the API (e.g. apparent permeability obtained from cell cultures), A_{eff} is the effective surface area in the intestine and C is the drug concentration in the intestine. The intestinal fluid volumes and effective surface area were obtained from the literature. The effective surface area was assumed to be 3.6 m², while the intestinal fluid volume was set at 320 ml in the fed state and at 212 ml in the fasted state [119, 120]. Permeability values for cinnarizine and atazanavir were obtained from Caco-2 culture experiments published in the literature [97, 113, 114]. All pre-absorptive parameters used in STELLA[®] models are presented in Table 2.6.

Table 2.6: Pre-absorptive parameters (fasted and fed state) used in STELLA® PBPK models

Parameter	Fed state (high fat meal)	Fed state (light meal)	Fasted state
Gastric volume	750 ml	400 ml	250 ml
Intestinal volume [119, 120]	320 ml	320 ml	212 ml
Gastric emptying rate [117]	4 kcal/min	4 kcal/min	2.8 h ⁻¹
A_{eff} [119]	3.6 m ²	3.6 m ²	3.6 m ²

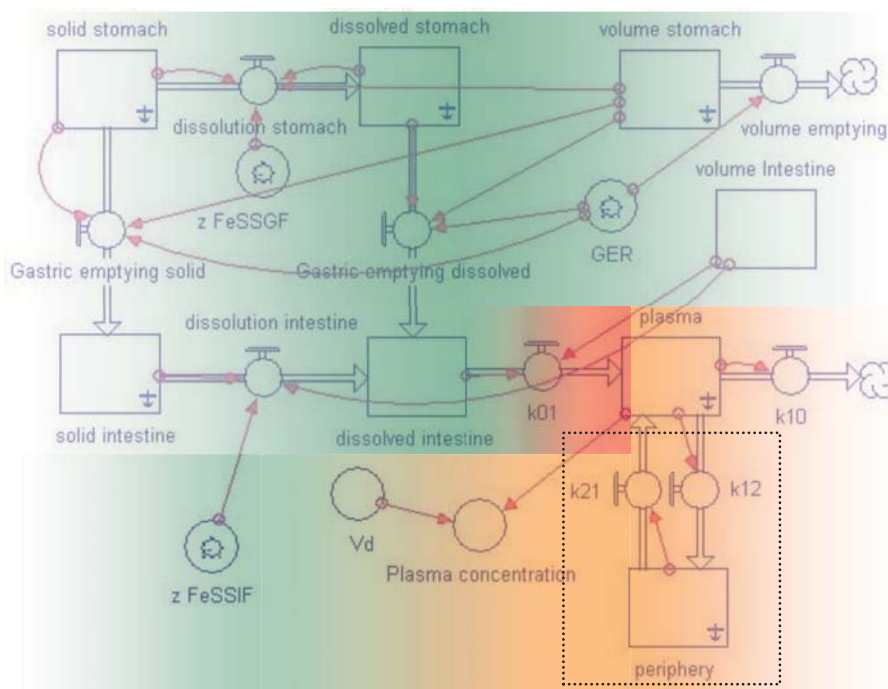


Fig. 2.8: STELLA® dissolution-only PBPK model with permeability restrictions; green: pre-absorptive kinetics (gastric and intestinal dissolution, gastric emptying), orange: post-absorptive kinetics (distribution and elimination), red: absorption kinetics, dotted square: (optional) deep compartment kinetics.

Supersaturation and precipitation PBPK model

Figure 2.9 demonstrates the modified STELLA® model, which considers supersaturation and precipitation. The initial gastric volume was assumed to be 250 ml for the fasted state and 750 ml for the fed state (400 ml for light meal conditions). The fasted state gastric emptying rate was assumed to follow first order kinetics (2.8 h⁻¹) and for the fed state the gastric emptying was considered to follow first order kinetics (4 kcal/min) [117]. The total drug emptied from the stomach into the intestinal compartment at a given time is described in the following equation:



Materials and Methods

Equation 5

$$\frac{dM}{dt} = k_e M$$

M is the total mass of drug that can be emptied into the intestine ($M = \text{dose}$) and k_e is the gastric emptying constant. During transfer the amount of dissolved drug in the intestine at a given time point can be described by the kinetics shown in equation 6

Equation 6

$$W_t = M_t f_d$$

where W_t is the amount of dissolved drug at time t , M_t is the total mass that has been transferred at time t and f_d is the fraction of drug in the intestine which is dissolved between the transfer time points t and $t+1$.

After the drug is emptied into the intestine it is assumed to be in a metastable supersaturated state. Precipitation kinetics of the supersaturated drug were previously described by Kambayashi *et al.* [121] and are presented in the following equation:

Equation 7

$$\frac{dP_t}{dt} = k_p (W_t - X_s), t \geq t'$$

where P_t is the amount of precipitated drug at a given time after the transfer from the stomach to the small intestine is complete (t'), k_p is the first order precipitation constant, W_t is the amount of dissolved drug at time t and X_s is the amount of the free base that saturates the volume V in the intestine (based on the API solubility in the intestinal fluids).

Dissolution of solid and re-dissolution of precipitated weak base in the intestine are described by the Noyes-Whitney based dissolution kinetics presented in equation 1. As for the dissolution model drug flux from the intestinal lumen through the gut wall into the venous blood stream was calculated using equation 4.



An optional compartment was added into the model to include efflux and/or first pass active extraction of the compound from the intestinal mucosa and/or liver. It enables incorporation of a first order efflux/extraction constant into the model and was used as a simplistic approach to investigate possible efflux/extraction mechanisms that had been reported for atazanavir. The mechanism is described by first order kinetics:

Equation 8

$$\frac{dX_t}{dt} = X_t k_{ex}$$

where dX_t/dt is the efflux/extraction rate of absorbed drug out of the intestinal mucosa and/or liver, X_t is the amount of drug which is available for efflux/extraction out of the intestinal mucosa and/or liver and k_{ex} is the first order efflux/extraction constant.

The absorptive and post-absorptive parameters of cinnarizine and atazanavir were introduced into the model according to the dissolution-only PBPK model.

Materials and Methods

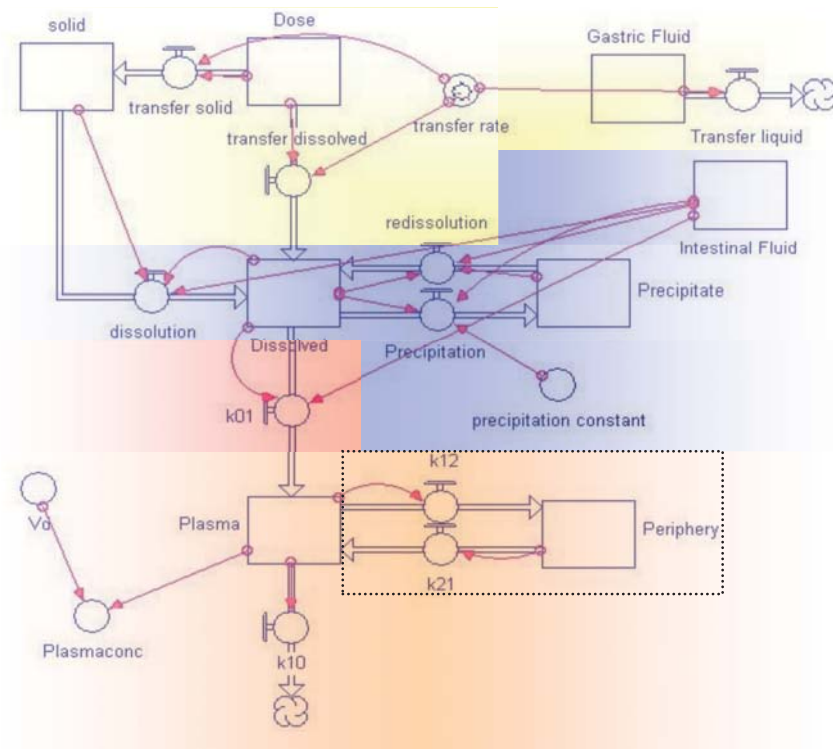


Fig. 2.9: STELLA[®] supersaturation and precipitation PBPK model with permeability restrictions; yellow: fractioning of dissolved and solid drug during gastric emptying, blue: precipitation, dissolution and re-dissolution of drug after gastric emptying, red: absorption kinetics, orange: post-absorptive kinetics (distribution and elimination), dotted square: (optional) deep compartment kinetics.



2.2.9 Simcyp®

Simcyp® simulations on both compounds were performed using the advanced dissolution, absorption and metabolism (ADAM) model. In contrast to other modeling approaches (First order absorption and compartmental absorption and transit (CAT) models) the ADAM model makes it possible to implement *in vitro* results obtained from solubility, dissolution and transfer experiments into the program. Within the ADAM model different “sub-models” can be chosen, where dosage forms and types of data involved with drug dissolution (solubilities, dissolution profiles, supersaturation and precipitation values) and absorption (*in vivo* and *in vitro* permeability) can be selected. Additionally the user can choose the way in which distribution and elimination data are implemented into the model. If distribution and elimination data are available from *in vivo* studies, these parameters can be introduced manually. Alternatively the user can choose internal program models to predict these parameters.

Setup of human gastrointestinal parameters

The Simcyp® software allows the selection of a virtual patient population for the simulations. The healthy volunteer population was chosen for both cinnarizine and atazanavir. GI parameters had to be adjusted to comply with *in vivo* studies performed for the two compounds. Parameters used for the simulation of fasted and fed state plasma profiles of cinnarizine and atazanavir in Simcyp® are presented in Table 2.7. The fed state gastric emptying times had to be changed, since the preset value is just 1 hour. The mean gastric emptying rate in the fed state is approximately 4 kcal/min. A high fat meal contains approximately 1000 kcal. Thus the gastric emptying time would result in 250 minutes, which is approximately 4 hours. The light meal administered to subjects in PK studies contained approximately 370 kcal. With a gastric emptying rate of 4 kcal/min the gastric emptying time would result in 1.5 hours. Additionally, the initial gastric volume was changed from 1000 ml to 400 ml corresponding to the composition of the light meal. The fasted state parameters were not altered, since the standard values are plausible for simulation of the PK studies that had been conducted. The initial gastric volume of 50 ml was not changed, because a co-administration of 200 ml of water can be selected as a trial design option of the program.



Materials and Methods

Table 2.7: Pre-absorptive parameters (fasted and fed state) used in the Simcyp® modeling mask

Parameter	Fed state (high fat meal)	Fed state (light meal)	Fasted state
Initial gastric volume	1000 ml (preset)	400 ml (altered)	50 ml (preset)
Gastric emptying time	4 h (altered)	1.56 h (altered)	0.4 h (preset)

Selection of trial design options

The trial design options describe the setup of the simulation study. It is similar to the general setup of clinical or PK trials. Amongst other settings one can choose the size of the population, the dose and time of administration, the volume of water co-administered and the trial length. For all simulations the trial length of 24 hours was chosen. A single dose oral administration was selected for both compounds. The volume of water co-administered in the fasted state was set at 200 ml.

Implementation of *in vitro* dissolution, supersaturation and precipitation results

Using the ADAM model the selection of the type of dosage form is possible. Since the dosage forms of the compounds investigated in *in vivo* studies were either capsules or tablets, the “solid” dosage form was chosen for the simulations. For different *in vitro* observations (dissolution, supersaturation and precipitation) different *in silico* simulation designs were applied:

1. For drugs exhibiting dissolution without supersaturation and precipitation the program offers a direct input of *in vitro* dissolution profiles (time - percent drug dissolved) into the program mask. Thus, biorelevant dissolution results under simulated gastric and intestinal conditions can be implemented using this approach.
2. In the case of a drug exhibiting supersaturation and precipitation the implementation of dissolution results is inappropriate. Instead, solubility results simulating gastric (FaSSGF in the fasted state or FeSSGF in the fed state) and intestinal (FaSSIF-V2 in the fasted state or FeSSIF-V2 in the fed state) conditions can be introduced into the program mask. Additionally, a maximum supersaturation ratio and a first order precipitation constant have to be entered into the mask.



Maximum supersaturation ratios and precipitation constants were calculated from *in vitro* transfer experiment results. The maximum supersaturation ratio is the quotient of the maximal concentration achieved and the solubility value in the simulated intestinal compartment (e.g. if the maximum concentration achieved during the transfer experiment is 100 µg/ml and the equilibrium solubility value is 10 µg/ml, then the maximum supersaturation ratio is calculated to be 10).

If supersaturation but no precipitation is observed, the maximum concentration during the transfer experiment should be used to represent the (kinetic) solubility in the intestinal compartment. In this case the precipitation constant has to be set to the value of 0 (the supersaturation value is then automatically set at 1).

This model can alternatively be used for drug dissolution without supersaturation and precipitation. Instead of time-concentration profiles, the GI solubility values from biorelevant solubility results are introduced.

3. Alternatively, simulations can be performed using predicted solubility. Intrinsic drug solubility can be predicted by Simcyp[®] using the physicochemical parameters of the compound, such as MW, logP and melting point. The program calculates a pH/solubility profile of the compound on the basis of its pKa values. Additionally, bile salt solubility enhancement can be chosen to make the simulation more biorelevant. Supersaturation and precipitation values are implemented using the same procedure as described in point 2.
4. Another alternative is the introduction of drug solubility concentrations at different physiological pH values. As described in point 3, bile salt solubility enhancement can be selected. Supersaturation and precipitation values can be applied according to point 2.

Implementation of permeability data (absorption)

The program mask gives several different options for implementing permeability data, e.g. effective permeability, cell culture data (Caco-2, MDCK-II, LLC-PK₁), PAMPA or compound related data (PSA and HBD). In the case of cinnarizine and atazanavir no effective human permeability data were available. However, Caco-2 cell culture data



Materials and Methods

were obtained from literature and were implemented into the program for both compounds. Simcyp[®] enables the selection of passive or active transport when using Caco-2 data. In the case of cinnarizine passive absorption is assumed and the setting was chosen accordingly. Since P-gp efflux is probable for atazanavir the setting “active transport” was chosen.

Implementation of distribution and elimination parameters

In Simcyp[®] distribution and elimination data can be implemented from external sources. It may also be predicted through algorithms implemented in the program. Consequently, three options can be chosen for parameterizing distribution and elimination data:

1. As in the case of simulations in STELLA[®], k_{12} , k_{21} and Vd/F values (obtained from WinNonLin[®]) can be implemented directly into the model. In contrast to STELLA[®] the implementation of the k_{10} value in Simcyp[®] is not possible. An apparent clearance value CL/F (predicted by WinNonLin[®]) was used instead.
2. Literature distribution and elimination data pose an alternative of attaining *in vivo* pharmacokinetic parameters on cinnarizine and atazanavir. If any data were obtainable from publications, they were used to evaluate and, if reasonable, to supplement or even replace results obtained from WinNonLin[®].
3. Alternatively the user can opt to predict the elimination and distribution data using Simcyp[®]. For the predictions of the k_{12} , k_{21} and Vd/F values, the program uses physicochemical data of the compound data (e.g. MW, pKa, logP, plasma protein bonding). This option should only be chosen when no data are available from external sources.



2.2.10 Statistical comparison of predicted plasma profiles using different transfer experiment approaches

To evaluate the influence of the experimental setup of the transfer model on the fasted state plasma profile predictions, results of different zero order transfer rates were implemented into the supersaturation and precipitation PBPK model and compared with data obtained from first order transfer results. All predictions were compared with *in vivo* data using point estimates ratios of the bioequivalence test parameters AUC and C_{\max} and the difference factor (f_1), which is a model independent comparator of plasma concentration time profiles. The calculation of the f_1 value was performed using equation 9:

Equation 9

$$f_1 = \frac{\sum_{t=1}^n |R_t - T_t|}{\sum_{t=1}^n R_t}$$

where n is the number of time points, R_t is the plasma concentration of the *in vivo* profile at time point t , T_t is the plasma concentration of the simulated plasma profile at time point t [122]. The comparison was performed for plasma concentrations at time points obtained from the *in vivo* studies (up to 24 hours). A f_1 cut-off limit of 20% was used in this study.



3 Results

3.1 Cinnarizine – investigation of *in vitro* behavior

3.1.1 Solubility results

Solubility results of cinnarizine in biorelevant media are presented in Figure 3.1. Earlier studies indicated that the solubility of cinnarizine is highly pH dependent [95], which is confirmed by this investigation. The solubility in FaSSGF pH 1.6 and FaSSGF pH 2.0, which represent the fasted stomach, is high (1077 µg/ml and 540 µg/ml respectively). In less acidic media such as FaSSIF-V2 pH 6.5, which characterizes the fasted state upper intestinal environment, cinnarizine solubility is much lower. The compound exhibits high bile salt and lecithin dependent solubility. If comparing FaSSIF-V2 with the corresponding blank buffer, a 17-fold increase in solubility is observed for the biorelevant medium (2.82 µg/ml versus 0.16 µg/ml). A previous solubility study of cinnarizine in the older version of FaSSIF (V1) confirms this observation [123]. FaSSIF contains a 3.75 times higher concentration of lecithin than FaSSIF-V2 and exhibits a 3.4 times higher solubilization of cinnarizine (9.47 µg/ml). Since FaSSIF-V2 and FaSSIF-V2(PO₄) have similar compositions, apart from the buffer, cinnarizine solubility between these media is similar (Student's t-test, $p > 0.05$).

Conditions in the fed state stomach are represented by FeSSGF pH 5.0, which contains fats and proteins due to the presence of 50% milk in the composition of the medium. Since cinnarizine is very lipophilic in its unionized form ($\log P \sim 5.6$) [91, 124], its interactions with lipids lead to a significant increase of cinnarizine solubility [95, 97, 124]. Thus, solubility of cinnarizine is considerably higher in FeSSGEm pH 5.0 and FeSSGF pH 5.0 (60.09 µg/ml and 43 µg/ml respectively) than in the corresponding aqueous buffer (6.45 µg/ml).

Cinnarizine exhibits relatively high solubility in the medium simulating the fed state intestinal milieu (73 µg/ml). In comparison with FaSSIF-V2, the higher solubility in FeSSIF-V2 can be explained by three factors. First, the pH in FeSSIF-V2 is considerably lower than in FaSSIF-V2, resulting in a higher extent of cinnarizine



ionization. Second, the concentration of bile salts and lecithin is significantly higher in FeSSIF-V2. And third, the fed state medium contains monoglycerides and fatty acids, which may additionally contribute to cinnarizine solubilization.

The solubility of cinnarizine in the medium representing the fasted state intestinal conditions after “gastric emptying” (mixture of FaSSGF pH 2.0 and FaSSIF-V2(PO₄) in the ratio 1 to 2) is higher than in pure FaSSIF-V2(PO₄). Since bile salt and lecithin concentrations are lower in the mixture, one might expect a lower solubility of cinnarizine. However, the combination of FaSSGF pH 2.0 and FaSSIF-V2(PO₄) results in a lower pH (5.95) than that of FaSSIF-V2(PO₄) (pH 6.5) leading to a higher degree of drug ionization and thus to a higher solubility.

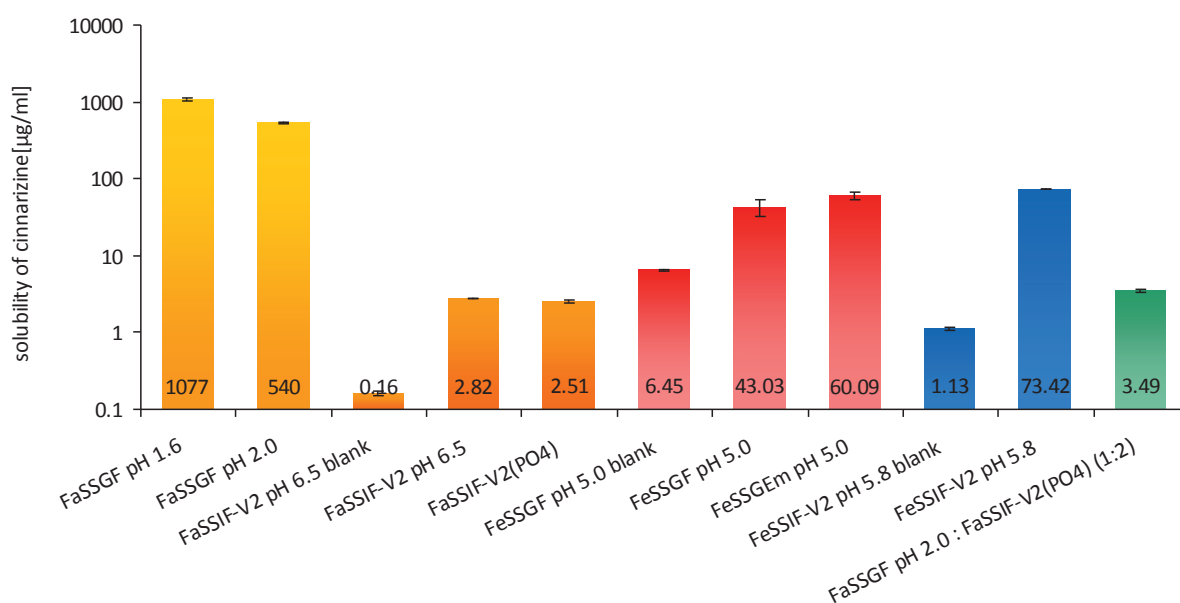


Fig. 3.1: Solubilities of cinnarizine in biorelevant media (logarithmic scaling). Solubility values in µg/ml along with the standard errors are shown on the bar for each medium.

3.1.2 Dissolution of cinnarizine tablets in biorelevant media

Dissolution profiles of 20 mg, 25 mg pure cinnarizine, Arlevert[®] (20 mg) and Stugeron[®] (25 mg) tablets in fasted state gastric and intestinal media, FaSSGF pH 1.6 and FaSSIF-V2, are presented in Figure 3.2. For clarity the theoretical percentage dissolved for 20 mg cinnarizine in FaSSIF-V2, based on the API solubility in this medium, is also shown. The results are consistent with the solubility data in Figure 3.1. As expected, the pure compound exhibited 100% dissolution for both 20 and 25 mg cinnarizine. However, for the first 5 minutes a lag time was observed, which was followed by rapid dissolution. Both formulations (described in Section



Results

2.1.2) exhibited rapid drug release and complete dissolution in FaSSGF pH 1.6 (Arlevert[®] tablets within 15 minutes and Stugeron[®] tablets within 30 minutes). Interestingly, Stugeron[®] exhibited a lower dissolution rate than Arlevert[®].

In FaSSIF-V2 the dissolution was slow, releasing only ~6% cinnarizine from both formulations. Similar behavior was observed for the pure compound. For both doses and formulations the profiles were still increasing towards the solubility values after 180 minutes. The different dissolution behavior of the two formulations in FaSSGF pH 1.6 and FaSSIF-V2 are reflected by the initial dissolution rates, which are characterized by z values in Table 3.1. A z value represents the initial dissolution velocity (within 10 to 60 minutes of the initial dissolution curve) of a drug dose in a volume of dissolution medium. High initial dissolution rates are represented by high z values (e.g. z value Arlevert[®] in FaSSGF: 5.16 mL/mg^{2/3}/h) whereas slow initial dissolution rates are described by low z values (e.g. z value Arlevert[®] in FaSSIF-V2: 0.2 mL/mg^{2/3}/h). Interestingly, Arlevert[®] (20 mg) exhibits comparable plasma profiles to Stugeron[®] (25 mg) *in vivo* despite the dose difference (see Figure 3.10). This observation is qualitatively in accordance with the comparatively higher z values of Arlevert[®] in FaSSGF pH 1.6 and FaSSIF-V2.

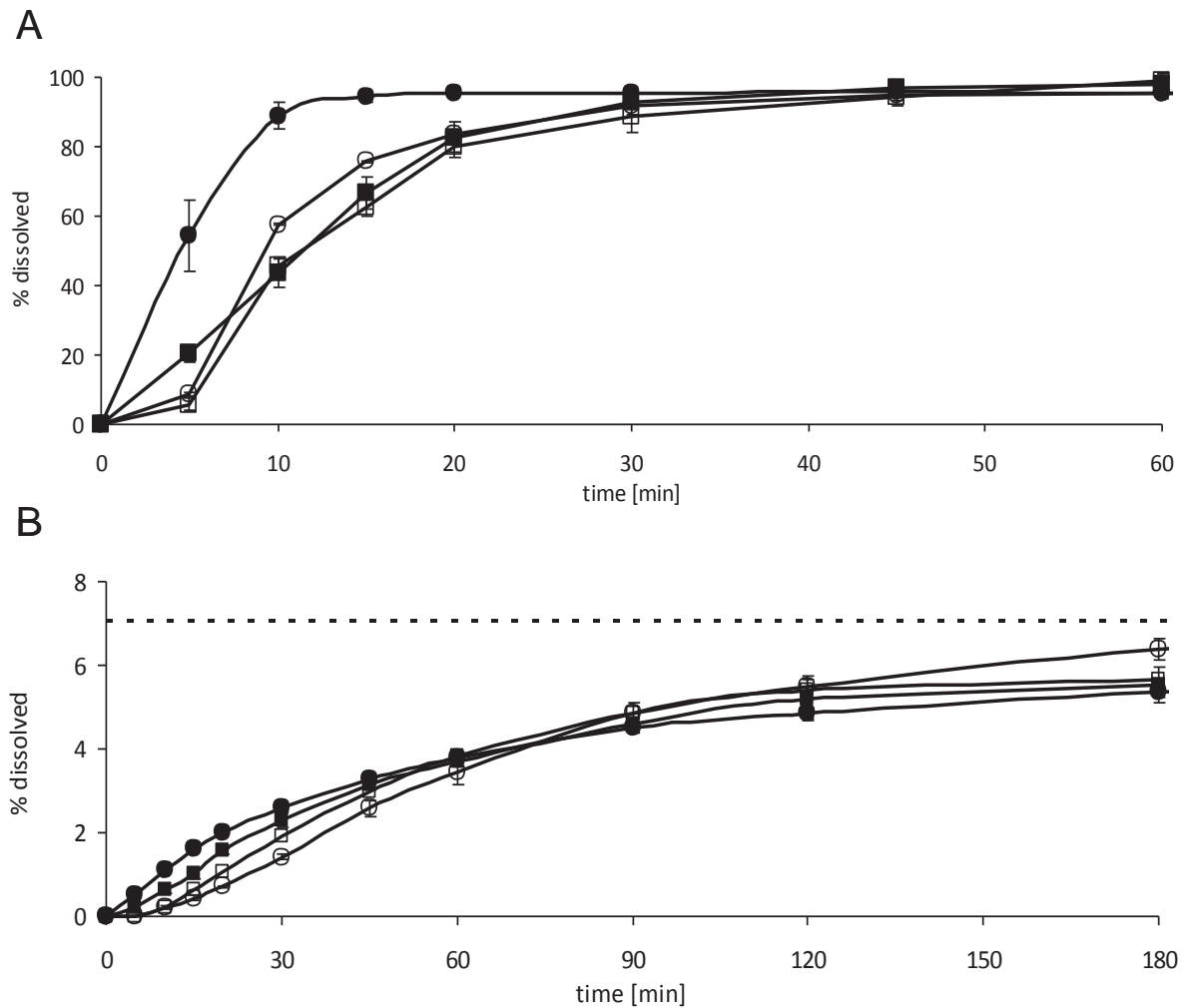


Fig. 3.2: Dissolution of pure cinnarizine and cinnarizine tablets in fasted state gastric (A) and intestinal (B) media (some symbols are bigger than the standard deviation bars): Arlevert[®] (●) and Stugeron[®] (■), cinnarizine 20 mg (○) and 25 mg (□) (curves are overlapping) along with the theoretical % dissolved for 20 mg cinnarizine in FaSSIF-V2, based on its solubility (- -).

Figure 3.3 shows dissolution results of 20 mg and 30 mg pure cinnarizine and of Arlevert[®] 20 mg and Cinnarizine 30 mg tablets in the fed state media, FeSSGF pH 5.0 and FeSSIF-V2. In FeSSGF pH 5.0, the fed gastric medium, 47% of the Arlevert[®] 20 mg dose was released after 240 minutes. With a solubility of 43 µg/ml of cinnarizine in FeSSGF (see Figure 3.1), 100% dissolution of this dose would be possible in 500 ml FeSSGF pH 5.0 if sufficient time was available. The dissolution rate of Cinnarizine 30 mg tablets was significantly slower (Student's t-test, $p < 0.01$), releasing only 27% of the dose in 240 minutes. This might be partially attributed to the higher dose (30 mg), which precludes more than 71% dissolution in 500 ml of FeSSGF pH 5.0. Interestingly, the dissolution of the pure compound in FeSSGF pH 5.0 was almost identical with that of the tablet formulations.



Results

In FeSSIF-V2, the fed intestinal medium, both formulations exhibited faster and more extensive dissolution than in FeSSGF pH 5.0. The higher dosed Cinnarizine 30 mg tablets exhibited lower dissolution values than Arlevert[®] (55% vs. 74%). Comparing the pure compound with the formulated tablets, the dissolution profiles were similar for both doses, 20 and 30 mg cinnarizine. In contrast to tablets, the pure compound profiles exhibited lag times of approximately 5 minutes. However, based on the solubility of cinnarizine in FeSSIF-V2 both dose strengths (20 mg and 30 mg cinnarizine) are expected to dissolve eventually. The initial dissolution rates of both marketed formulations in FeSSGF pH 5.0 and FeSSIF-V2 are shown in Table 3.1.

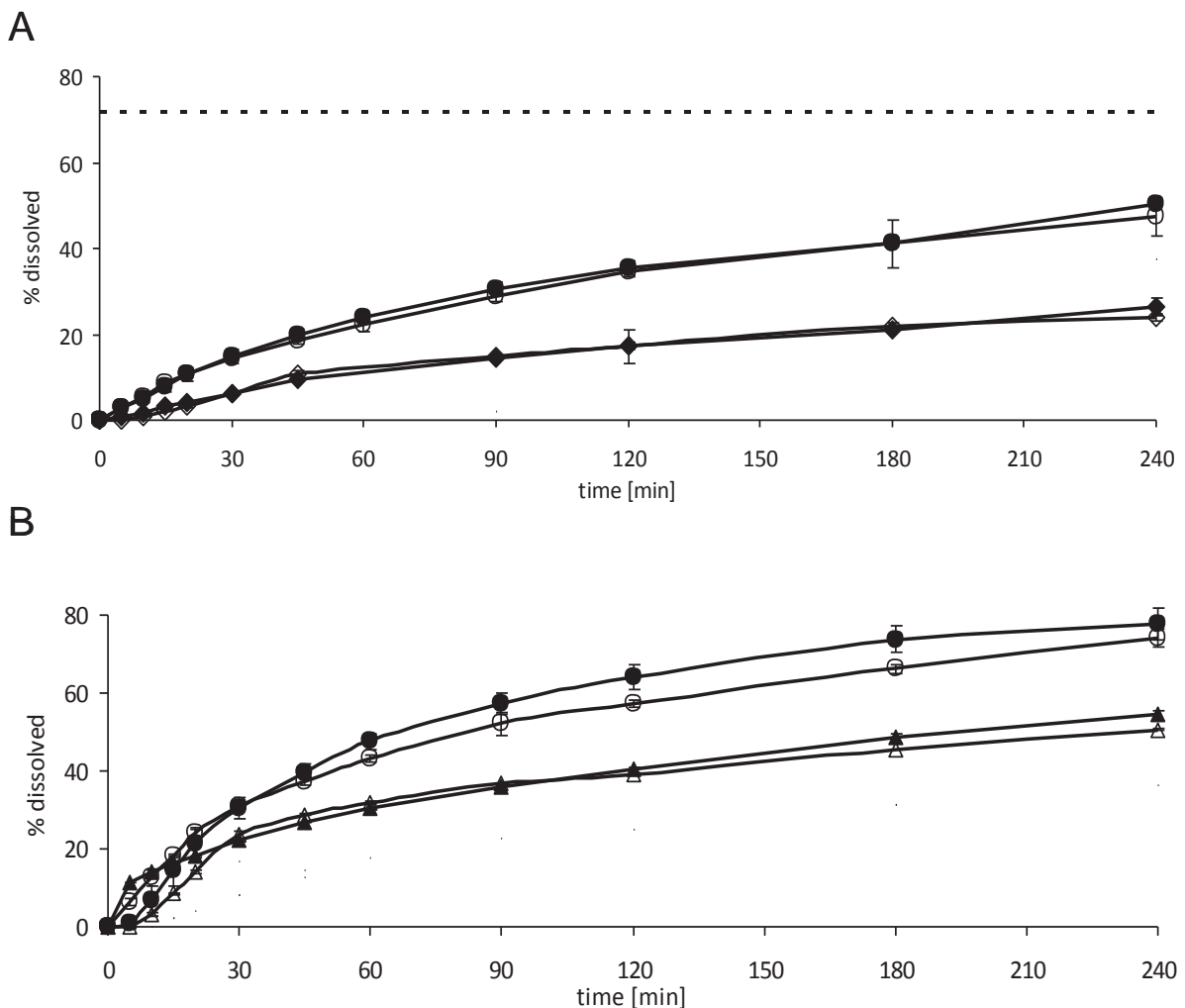


Fig. 3.3: Dissolution of pure cinnarizine and cinnarizine tablets in the fed gastric (A) and intestinal (B) biorelevant media (some symbols are bigger than the standard deviation bars): Arlevert[®] (●) and Cinnarizine 30 mg tablets (▲), pure cinnarizine 20 mg (○) and 30 mg (△) along with the maximum theoretical % dissolved for 30 mg cinnarizine in FeSSGF pH 5.0, based on its solubility (- -).



Table 3.1: Initial dissolution rates (z values) for the various biorelevant media and cinnarizine formulations

Dissolution medium	Formulation	z value \pm SE (mL/mg ^{2/3} /h)
FaSSGF pH 1.6	Arlevert [®]	5.16 \pm 0.536
FaSSIF-V2	Arlevert [®]	0.200 \pm 0.016
FeSSGF pH 5.0	Arlevert [®]	0.110 \pm 0.01
FeSSIF-V2	Arlevert [®]	0.173 \pm 0.004
FaSSGF pH 1.6	Stugeron [®]	2.28 \pm 0.324
FaSSIF-V2	Stugeron [®]	0.136 \pm 0.003
FeSSGF pH 5.0	Cinnarizine 30 mg	0.062 \pm 0.003
FeSSIF-V2	Cinnarizine 30 mg	0.081 \pm 0.001

3.1.3 Dumping of pure cinnarizine

Dumping tests can be performed to screen the supersaturation and precipitation behavior of compounds. Figure 3.4 shows the concentration change of cinnarizine after dumping 20 mg of the compound, which had been pre-dissolved in 250 ml of FaSSGF pH 2.0, into 500 ml of FaSSIF-V2(PO₄). The result shows that cinnarizine initially achieves a supersaturated state, dissolving almost entirely, after which it starts to precipitate towards the equilibrium solubility. The question remains as to whether supersaturation and precipitation of the compound are influenced by the transfer rate, viz. the gastric emptying rate. Thus, transfer experiments using different transfer rates were utilized to further characterize the supersaturation and precipitation behavior of cinnarizine.

Results

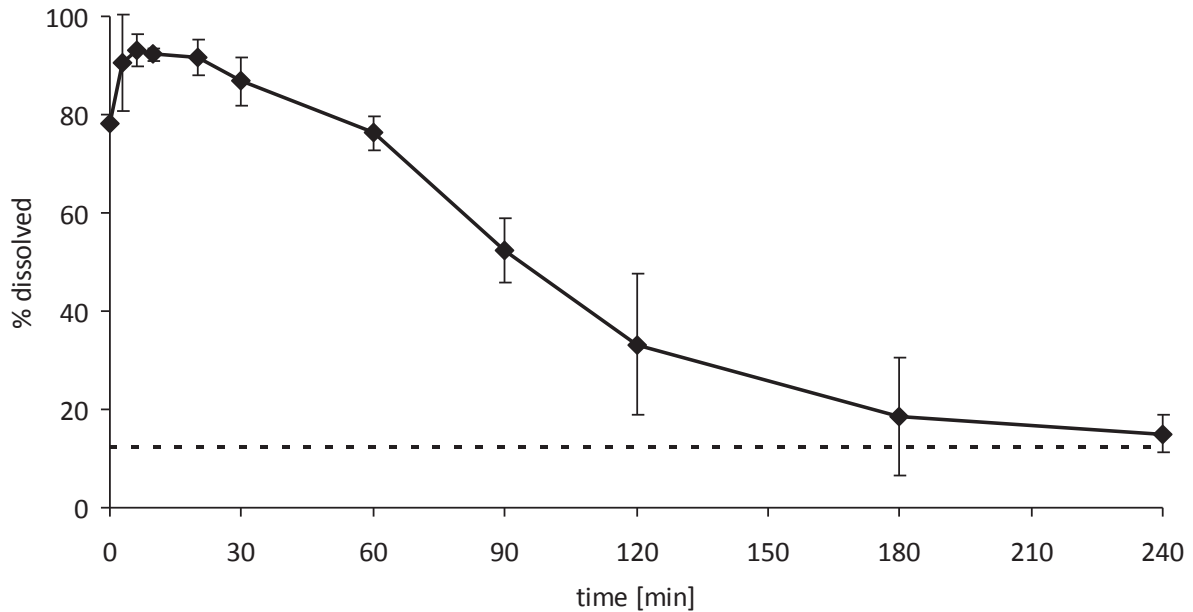


Fig. 3.4: Concentration profile of cinnarizine after dumping a solution of 20 mg cinnarizine in 250 ml FaSSGF pH 2.0 into 500 ml FaSSIF-V2(PO₄) along with the maximum theoretical % dissolved for 20 mg cinnarizine based on its solubility in the combination of FaSSGF pH 2.0 and FaSSIF-V2(PO₄) in the ratio of 1:2 (- -).

3.1.4 Investigation of supersaturation and precipitation of cinnarizine during transfer experiments

Figure 3.5 presents transfer experiment results for different doses (20, 40 and 80 mg) of pre-dissolved cinnarizine using first order and various zero transfer rates. In each diagram, the theoretical cumulative concentration curve of cinnarizine in the acceptor compartment is also shown. This represents the case in which the whole dose of cinnarizine dissolves and stays in solution during transfer. The profiles reveal that supersaturation and precipitation of the compound are dose dependent. Higher doses of cinnarizine result in faster achievement of the critical supersaturation concentration, but earlier onset of precipitation with a higher precipitation rate. Maximum supersaturation ratios and precipitation constants from transfer experiments using pre-dissolved cinnarizine are presented in Tables 3.2 and 3.3. Interestingly, the maximum supersaturation ratio was reached at a transfer rate of 4 ml/min for all doses of cinnarizine leading in turn to higher precipitation rate constants. This observation indicates that both supersaturation and precipitation of cinnarizine crucially depend on the transfer rate.

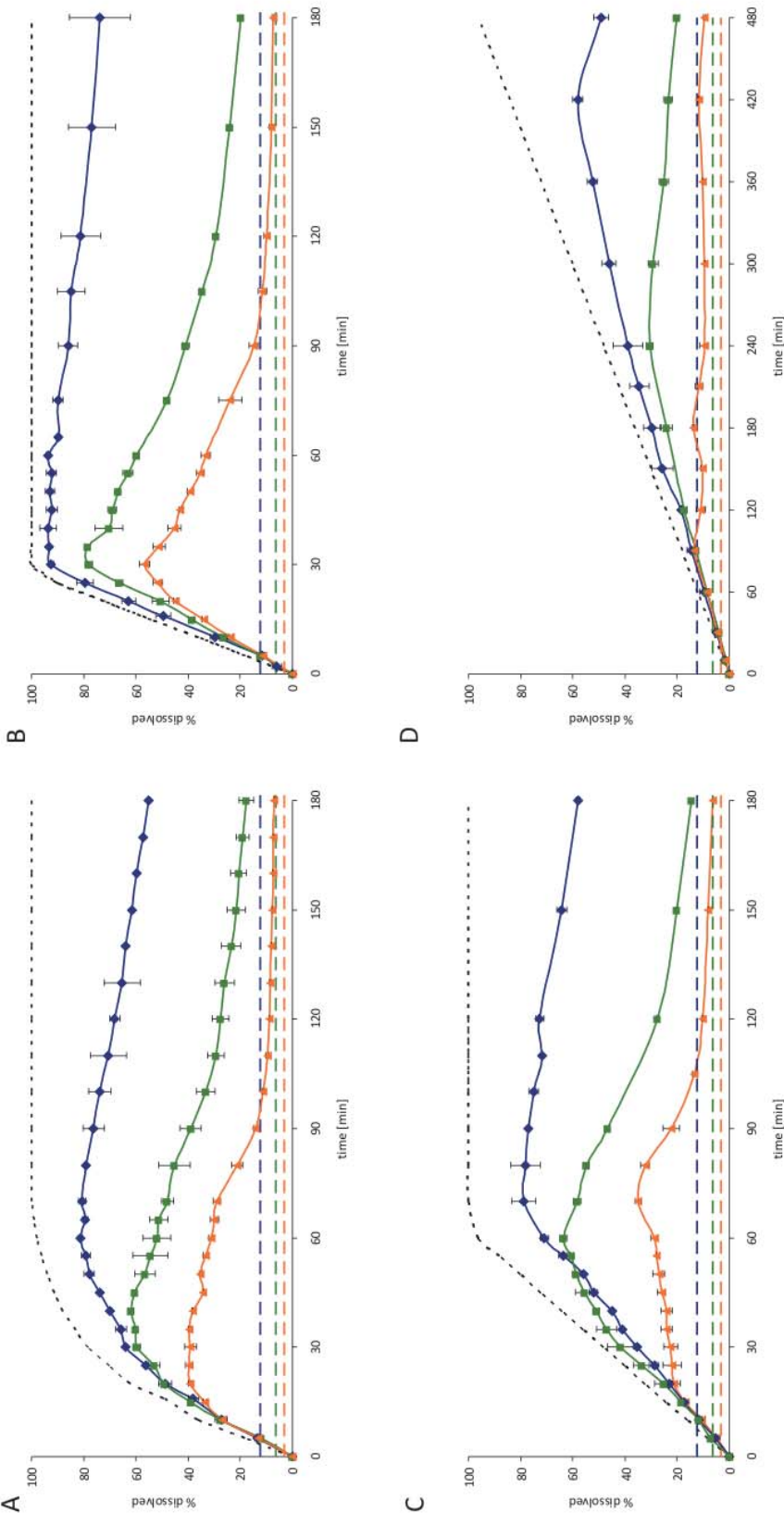


Fig. 3.5: Fasted state transfer of a solution of 20 (◆), 40 (■) and 80 mg (▲) cinnarizine in FaSSGF pH 2.0 into FaSSIF-V2(PO₄) using transfer rates of 3 h⁻¹ (A), 9 ml/min (B), 4 ml/min (C) and 0.5 ml/min (D). The theoretical transfer curve (- -) is displayed along with the maximum theoretical % dissolved for 20 mg cinnarizine based on its solubility in the combination of FaSSGF pH 2.0 and FaSSIF-V2(PO₄) in the ratio of 1:2 (- -).



Results

Table 3.2: Maximum supersaturation ratios (maximum concentration achieved in the acceptor compartment relative to the solubility) of different doses of cinnarizine at various transfer rates

Dose	first order (3 h^{-1}) \pm SD	9 ml/min \pm SD	4 ml/min \pm SD	0.5 ml/min \pm SD
20 mg	6.60 ± 0.16	5.80 ± 0.02	6.89 ± 0.27	4.67 ± 0.16
40 mg	10.39 ± 0.003	10.31 ± 0.06	12.74 ± 0.14	5.94 ± 0.23
80 mg	14.50 ± 0.09	11.22 ± 0.66	18.37 ± 0.40	5.94 ± 0.22

Table 3.3 First order precipitation constants of different doses of cinnarizine at various transfer rates

Dose	first order (3 h^{-1}) \pm SD	9 ml/min \pm SD	4 ml/min \pm SD	0.5 ml/min \pm SD
20 mg	0.20 ± 0.03	0.10 ± 0.04	0.17 ± 0.02	0.17 ± 0.03
40 mg	0.55 ± 0.04	0.59 ± 0.02	0.82 ± 0.01	0.15 ± 0.001
80 mg	1.16 ± 0.02	1.07 ± 0.07	1.20 ± 0.06	0.24 ± 0.04

A comparison of simultaneous dissolution and transfer of Arlevert[®] tablets with transfers of either pre-dissolved Arlevert[®] or pre-dissolved 20 mg pure cinnarizine using different transfer rates is presented in Figure 3.6, and Tables 3.4 and 3.5. Pre-dissolved tablets exhibited considerably lower maximum supersaturation ratios than the pure drug for all transfer rates. The reason for the inferior supersaturation behavior of pre-dissolved Arlevert[®] can most likely be attributed to insoluble components in the formulation, which are transferred with the dissolved drug and could act as nucleation enhancers in the acceptor medium. Not only is the supersaturation lower, but higher precipitation constants than for the pure drug are also observed.

Simultaneous dissolution and transfer of Arlevert[®] tablets exhibited lower supersaturation values, but similar precipitation kinetics compared to pre-dissolved Arlevert[®]. In contrast to the pre-dissolved cinnarizine tablet, Arlevert[®] has to disintegrate and release the drug in the donor compartment, which leads to lower amounts of drug in solution and thus lower concentration values in the acceptor compartment.

Generally, the concentration profiles in the “intestinal” compartment at different doses of cinnarizine during the transfer experiments imply that there is room for formulation

enhancement of the compound. Precipitation inhibition may be one approach to increase the concentration of the compound in the intestine over a larger time-frame and thus enhance its absorption and bioavailability.

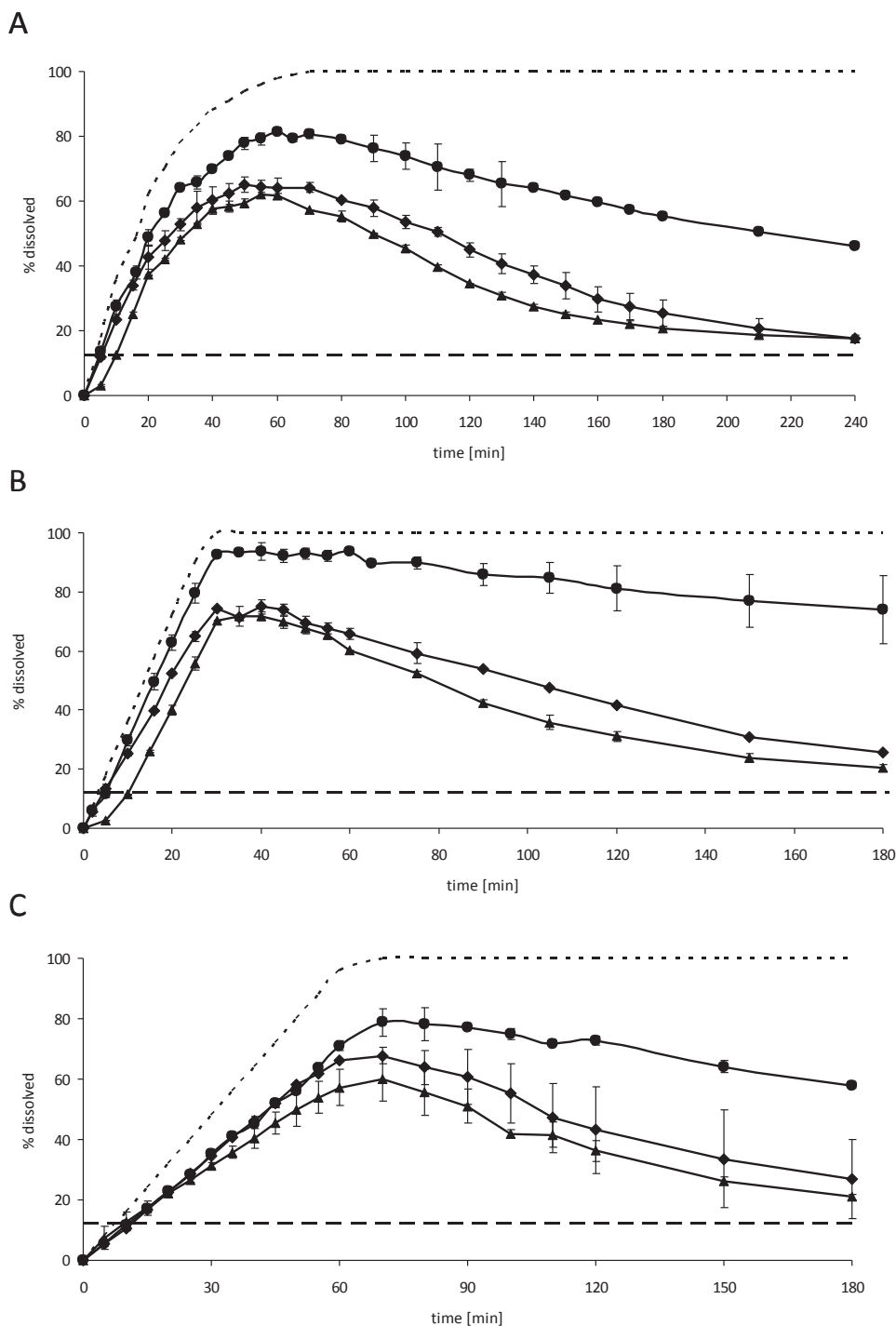


Fig. 3.6: Fasted state transfer of 20 mg cinnarizine as a solution (●), dissolved Arlevert[®] tablets (◆) and intact Arlevert[®] tablets (▲) in FaSSGF pH 2.0 into FaSSIF-V2(PO₄) using transfer rates of 3 h^{-1} (A), 9 ml/min (B) and 4 ml/min (C). The theoretical transfer curve (- -) is displayed along with the maximum theoretical % dissolved for 20 mg cinnarizine based on its solubility in the combination of FaSSGF pH 2.0 and FaSSIF-V2(PO₄) in the ratio of 1:2 (- · -).



Results

Table 3.4: Maximum supersaturation ratios (maximum concentration achieved in the acceptor compartment relative to the solubility) of different presentations of 20 mg cinnarizine at various transfer rates

Formulation	first order (3 h^{-1}) \pm SD	9 ml/min \pm SD	4 ml/min \pm SD
Cinnarizine 20 mg (pre-dissolved)	6.60 ± 0.16	5.80 ± 0.02	6.89 ± 0.27
Arlevert [®] 20 mg (pre-dissolved)	5.40 ± 0.20	6.10 ± 0.13	5.54 ± 0.17
Arlevert [®] 20 mg	5.14 ± 0.03	5.83 ± 0.20	4.91 ± 0.59

Table 3.5: First order precipitation constants of different presentations of 20 mg cinnarizine at various transfer rates

Formulation	first order (3 h^{-1}) \pm SD	9 ml/min \pm SD	4 ml/min \pm SD
Cinnarizine 20 mg (pre-dissolved)	0.20 ± 0.03	0.10 ± 0.04	0.17 ± 0.02
Arlevert [®] 20 mg (pre-dissolved)	0.48 ± 0.09	0.47 ± 0.06	0.53 ± 0.28
Arlevert [®] 20 mg	0.50 ± 0.04	0.67 ± 0.15	0.46 ± 0.05

Cinnarizine dissolution behavior in the transfer model exhibited different drug behavior than when the compound was dissolved in the individual gastric and intestinal media. A comparison of the dissolution behavior of Arlevert[®] in FaSSIF-V2 and FeSSIF-V2 reveals disparate maximum concentrations in these two media (compare Figures 3.2 and 3.3). Even though the results are in agreement with the positive food effect which was observed for Arlevert[®], the *in vitro* behavior only qualitatively reflects the *in vivo* observations. The solubility ratio of cinnarizine in FeSSIF-V2/FaSSIF-V2 (26.04) and the quotient of maximum concentrations measured during dissolution in FeSSIF-V2 and FaSSIF-V2 (5.05) would both suggest a much higher food effect than observed *in vivo* ($AUC_{\text{fed}}/AUC_{\text{fasted}} = 1.44$) [98]. This overestimation of the food effect is based on the assumption that dissolution in the stomach does not count towards availability of drug for absorption. However, the transfer experiments indicate that drug dissolution in the stomach leads to supersaturation in the small intestine under fasted conditions, resulting in a lower estimation of the food effect. The two models (only intestinal dissolution and solubility vs. transfer model) are compared using the *in silico* PBPK simulations in Section 3.2.3.



Figure 3.7 shows cinnarizine concentrations of the marketed Arlevert[®] 20 mg and Stugeron[®] 25 tablets in the acceptor phase during fasted state transfer experiments at 3 h⁻¹ (A), 9 ml/min (B), 4 ml/min (C) and 0.5 ml/min (D) transfer rates. For all transfer rates high supersaturation values were observed *in vitro*, reaching up to six times the solubility values. During transfer the discrepancy between the theoretical and observed concentrations is partly due to continuing dissolution (since part of the drug will be transferred as solid material) and partly due to precipitation of drug from solution. However, after transfer is completed, it can be assumed that any decrease in concentration is due solely to precipitation. Thus, the kinetics of this part of the curve can be fitted to describe the precipitation (Figure 2.3). The ability of Arlevert[®] to achieve higher concentrations in solution than Stugeron[®] (Section 3.1.2) is supported by most of the fasted state transfer experiment results. Supersaturation and precipitation kinetics for each formulation and transfer rate are presented as maximum supersaturation ratio, fraction dissolved (f_d) and first order precipitation (k_p) constants in Table 3.6. The maximum supersaturation ratio is higher for Arlevert[®] than for Stugeron[®] at fast transfer rates. However, Arlevert[®] exhibits faster precipitation than Stugeron[®] after transfer is completed (i.e. after time t') at most transfer rates.

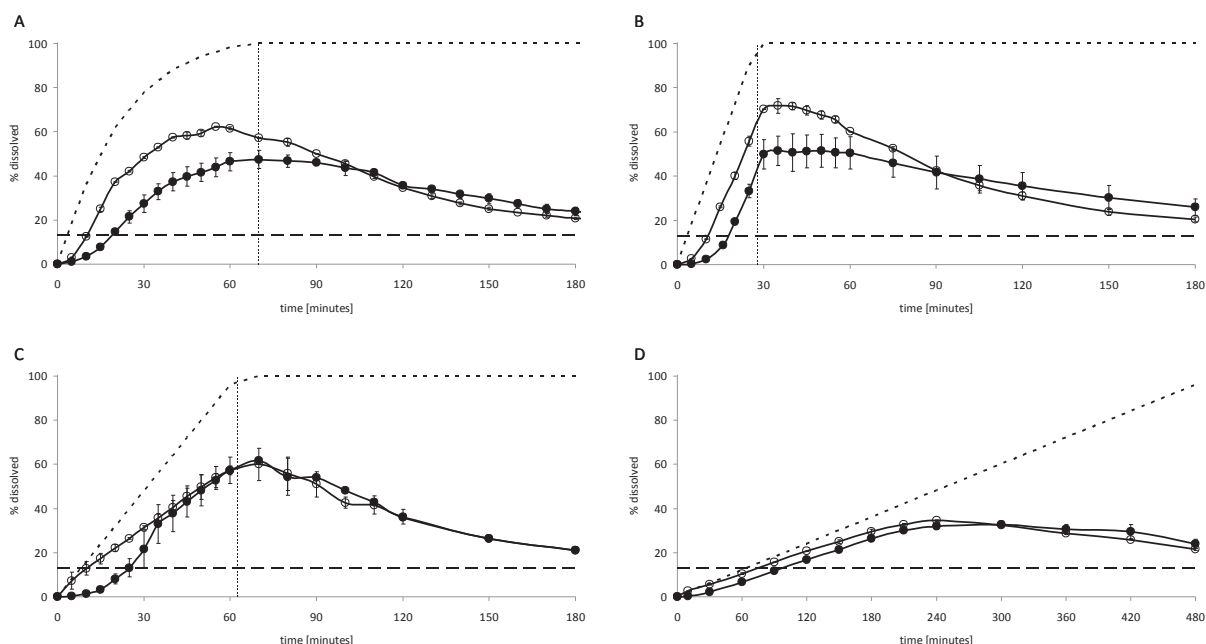


Fig. 3.7: Fasted state transfer of Arlevert[®] (○) and Stugeron[®] (●) cinnarizine tablets at 3 h⁻¹ (A), 9 ml/min (B), 4 ml/min (C) and 0.5 ml/min (D) transfer rates. The theoretical transfer curve (---) is displayed along with the solubility (—) of 25 mg cinnarizine in the combination of FaSSGF pH 2.0 and FaSSIF-V2(PO₄) in the ratio 1:2.



Results

Table 3.6: Maximum supersaturation ratios, fraction dissolved (f_d) and precipitation constants (k_p) for Arlevert[®] and Stugeron[®] for different transfer rates.

Transfer rate	Formulation	Supersaturation ratio	f_d	k_p (h ⁻¹)
First order (3 h ⁻¹)	Arlevert [®]	5.14	0.769	0.500 (> 60 min)
First order (3 h ⁻¹)	Stugeron [®]	4.61	0.519	0.198 (> 70 min)
9 ml/min	Arlevert [®]	5.40	0.748	0.674 (> 30 min)
9 ml/min	Stugeron [®]	4.98	0.520	0.189 (> 30 min)
4 ml/min	Arlevert [®]	5.14	0.582	0.464 (> 70 min)
4 ml/min	Stugeron [®]	6.00	0.610	0.473 (> 70 min)
0.5 ml/min	Arlevert [®]	3.23	0.788	0.415 (> 240 min)
0.5 ml/min	Stugeron [®]	3.73	0.746	0.354 (> 300 min)

Since the solubility of cinnarizine was revealed to be higher in FeSSIF-V2 than in FeSSGF pH 5.0, the entire cinnarizine dose is expected to dissolve in the simulated fed intestine. To test this assumption a fed state transfer experiment with highest dose of cinnarizine (Cinnarizine 30 mg tablets) was performed using 500 ml of FeSSGEm pH 5.0 as the donor compartment and 500 ml of FeSSIF-V2 as the acceptor compartment shown in Figure 3.8. The entire dose of Cinnarizine 30 mg tablets dissolved and stayed in solution during and after transfer. The difference between the theoretical and observed curves is minimal and is most likely attributable to sample handling and analytical issues.

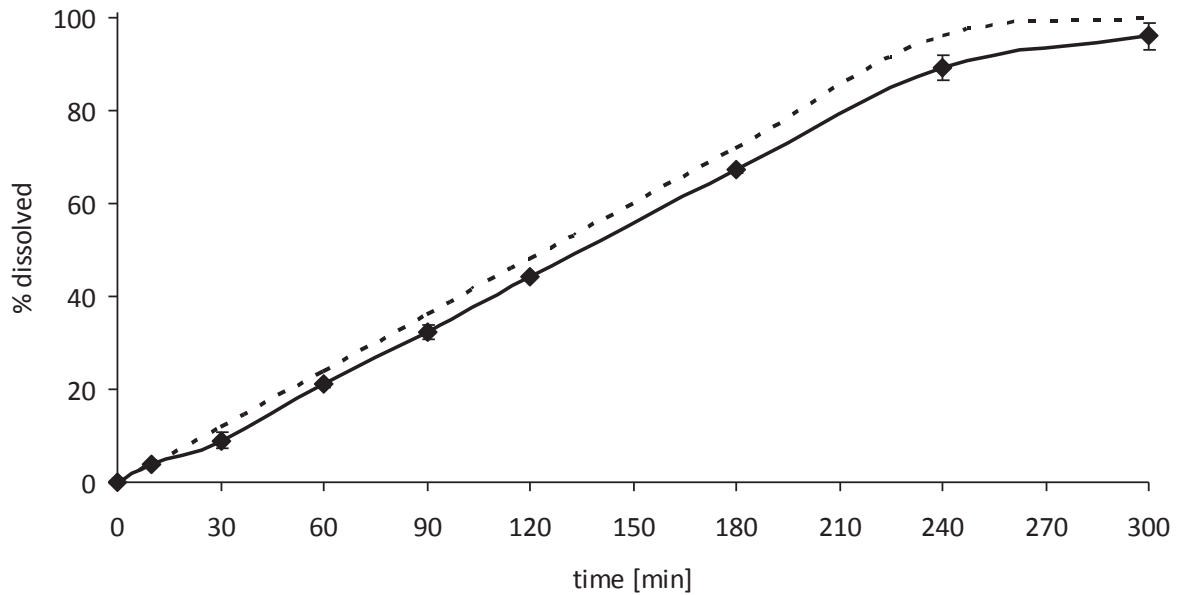


Fig. 3.8: Fed state transfer of Cinnarizine 30 mg tablets using the zero order transfer rate of 2 ml/min along with the theoretical transfer curve (- -).

These results show that it is advantageous to investigate the overall dissolution, supersaturation and precipitation behavior of cinnarizine formulations under fasted gastric and intestinal conditions by implementing the transfer model. Previous observations from *in vitro* transfer experiments also indicated that the smaller than expected food effect may be attributable to supersaturation of cinnarizine in the fasted state intestinal compartment [94]. The transfer results were therefore applied in the *in silico* simulations.



Results

3.2 Cinnarizine - *in silico* plasma profile simulation

3.2.1 Evaluation of distribution and elimination kinetics of various cinnarizine tablets using WinNonLin[®]

Intravenous plasma profiles are considered optimal for the investigation of the post-absorptive disposition kinetics of compounds. Since only oral data were available for cinnarizine, the distribution and elimination kinetics were evaluated using observed oral plasma profiles of cinnarizine formulations in the fasted and fed state with the help of a commercial pharmacokinetic software (WinNonlin[®] Professional v. 4.1, Pharsight Corporation, Mountain View, CA, USA). Pharmacokinetic studies of Arlevert[®] demonstrated a positive food effect for cinnarizine. It is assumed that food effects do not influence the disposition kinetics of drugs. Therefore it could be assumed that drug exposure was maximal under fed state conditions. The apparent volume of distribution V_d/F (i.e. V_d adjusted for bioavailability factor F) for the fed state was estimated to be 225.6 +/- 35.6 L. For the fasted state studies the V_d/F was estimated to be higher, 336.6 +/- 74.7L for Arlevert[®] and 352 +/- 199L for Stugeron[®]. However the standard error for the fasted state estimations is high and seems less reliable. As the F value in the fed state is assumed to be closer to 1, the apparent volume of distribution V_d/F should be closer to the “real” volume of distribution, V_d . Consequently, the fed state V_d/F was implemented into the simulation software for the prediction of both preprandial and postprandial plasma profiles. The distribution parameters k_{12} , k_{21} and the elimination constant k_{10} used for the fasted and the fed state were implemented specific to the conditions of administration. The pre-absorptive and post-absorptive parameters used for the simulation of cinnarizine plasma profiles under different gastric states are summarized in Tables 3.7 and 3.8.



Table 3.7: Pre-absorptive and absorptive parameters needed for the plasma profile simulation of cinnarizine using STELLA[®]

Parameter	Fasted state	Fed state
Gastric volume	250 ml	750 ml
Intestinal volume [119, 120]	212 ml	320 ml
Gastric emptying rate [117]	2.8 h ⁻¹	4 kcal/min
Permeability [113, 114]	4.2 x 10 ⁻⁶ cm/s	4.2 x 10 ⁻⁶ cm/s
A _{eff} [119]	3.6 m ²	3.6 m ²

Table 3.8: Distribution and elimination parameters of cinnarizine used for *in silico* simulations (STELLA[®] and Simcyp[®])

Parameter	Fed state	Fasted state
Vd/F	225.6 L *	
k ₁₂	0.218	0.145
k ₂₁	0.020	0.056
k ₁₀	0.116	0.148
Cl	18.8 L/h	71.46 L/h

*Value obtained for fed state PK data fitted to WinNonLin[®]

3.2.2 STELLA[®] model - investigation of permeability restrictions of cinnarizine using fed state simulations

Due to the good solubility of cinnarizine in both FeSSGF pH 5.0 (or FeSSGEm pH 5.0) and FeSSIF-V2 and a slow gastric emptying rate in the fed state, complete drug release of cinnarizine tablets (Arlevert[®] and Cinnarizine 30 mg) in the upper GI tract is expected. Precipitation is not likely to occur in the fed state since solubility in FeSSIF-V2 is higher than the solubility in FeSSGF pH 5.0 or FeSSGEm pH 5.0. The transfer experiment where 30 mg Cinnarizine tablets were introduced into 500 ml of FeSSGEm pH 5.0 and the content was emptied into 500 ml of FeSSIF-V2 also suggests that precipitation is not expected to occur *in vivo*. For these reasons, the dissolution-only PBPK model was used to evaluate the influence of drug permeability on the plasma profile predictions in the fed state.

The permeability of BCS class II drugs in STELLA[®] models is usually assumed not to be limited [117]. However, Markopoulos *et al.* have recently suggested that drug



Results

association into micelles in the biorelevant media effectively reduce the permeability [125]. Moreover, Shono *et al.* had to implement an unstirred water layer (UWL) permeability restriction into STELLA[®] for aprepitant, which has been described as a BCS class II compound (Caco-2 permeability of 7.8×10^{-6} cm/s), to achieve a good fit of the plasma profiles [89, 126, 127].

Wagner *et al.* were able to predict the oral absorption of Compound A, a BCS class IV drug with a Caco-2 permeability of 0.8×10^{-6} cm/s, by implementing this data as a permeability restriction in the STELLA[®] model [60]. Cinnarizine, which is assumed to be a borderline BCS class II/IV drug, shows a Caco-2 permeability of 4.2×10^{-6} cm/s. As for Compound A, effective human permeability was calculated by directly introducing the Caco-2 data along with the A_{eff} value from Table 3.7 (conducted in buffer solution) into equation 4 [60]. Although the Caco-2 methodology may have varied among these compounds, it is likely that the permeability of cinnarizine lies in between the values of aprepitant and Compound A.

Initial dissolution rates (z values) in FeSSGF and FeSSIF-V2 as well as the corresponding cinnarizine solubility values in both media were implemented into one version of the model, in which it was assumed that there are no permeability limitations to cinnarizine absorption (Figure 2.7). In a second version the permeability was restricted (Figure 2.8). The calculated effective permeability based on Caco-2 data in the dissolution-only PBPK model exhibited good fits with respect to AUC, C_{max} and t_{max} as shown in Figure 3.9 and Table 3.9. By contrast, a lack of permeability restriction resulted in substantial overestimation of the C_{max} and an earlier appearance of t_{max} at both dosages of cinnarizine. Following on from these simulations the Caco-2-based permeability was applied in all further simulations.

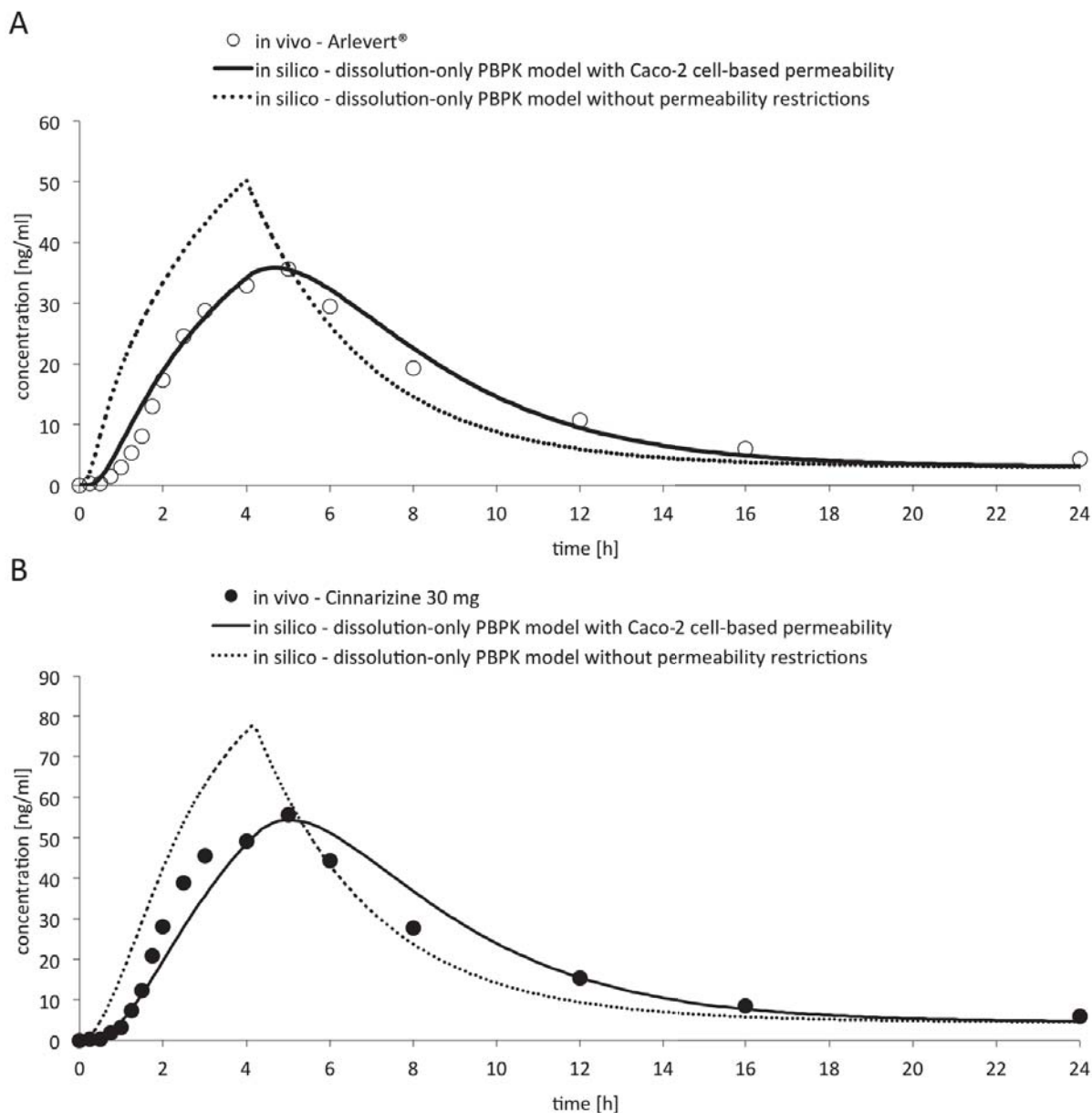


Fig. 3.9: Fed state plasma profile predictions of Arlevert® (A) and Cinnarizine 30 mg (B) tablets using the dissolution-only PBPK models with and without permeability restrictions based on Caco-2 data.

3.2.3 STELLA® “dissolution-only” vs. “supersaturation and precipitation” PBPK model in cinnarizine fasted state simulations

Initially, the dissolution-only PBPK model was used in order to simulate the fasted state plasma profiles of Arlevert® and Stugeron®. In this model, the Caco-2-based permeability was implemented, since permeability constraints were necessary to accurately simulate the pharmacokinetics in the fed state (see Section 3.2.2). Analogous to the fed state simulations, the model uses dissolution and solubility



Results

data, but does not consider supersaturation and precipitation of cinnarizine in the intestine.

Simulations of the fasted state were additionally conducted using the supersaturation and precipitation PBPK model. The model developed in this work introduces fraction dissolved (f_d) and first order precipitation (k_p) constants to predict the supersaturation and precipitation of cinnarizine in the intestine. For Arlevert[®], plasma profile predictions were conducted utilizing f_d (0.769) and k_p (0.50 h^{-1}) values obtained from first order transfer experiments together with a “gastric emptying rate” of 2.8 h^{-1} in the PBPK model. Dissolution and re-dissolution of non-dissolved and precipitated API was simulated using cinnarizine solubility ($2.82 \text{ } \mu\text{g/ml}$) as well as the z value of Arlevert[®] ($0.2 \text{ mg/ml}^{2/3}/\text{h}$) in FaSSIF-V2.

Figure 3.10 presents the predictions of fasted state plasma profiles of Arlevert[®] and Stugeron[®] comparing the two models. It demonstrates the significance of supersaturation and precipitation during and following gastric emptying (transfer rate = 3 h^{-1}) in the fasted state. The dissolution-only PBPK model underestimates the C_{max} and overestimates the AUC of both formulations, while the predictions using the supersaturation and precipitation PBPK model result in a good representation of their *in vivo* performance (Table 3.9).

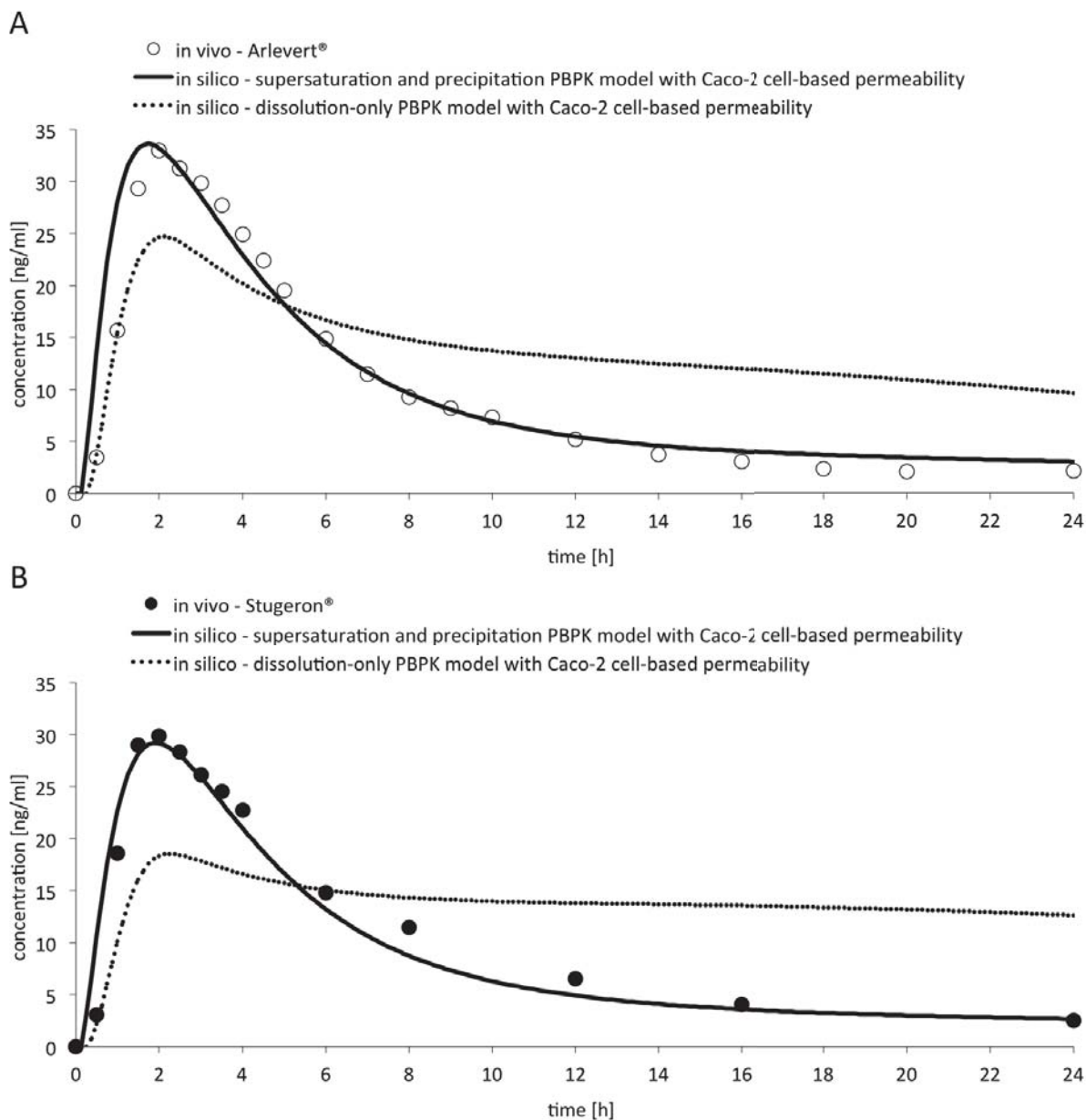


Fig. 3.10: Fasted state plasma profile predictions of Arlevert® (A) and Stugeron® (B) tablets using the dissolution-only and supersaturation and precipitation (obtained from transfer experiments at a rate of 3 h^{-1}) PBPK model.



Results

Table 3.9: Comparison of *in vivo* data with *in silico* predictions of different PBPK models for Arlever[®], Cinnarizine 30 mg tablets and Stugeron[®] in the fasted and fed state

Fasted state			
Arlever [®]	AUC ₀₋₂₄ (ng x h/ml)	C _{max} (ng/ml)	t _{max} (h)
<i>in vivo</i>	219	33	2.0
<i>predicted (dissolution-only)</i>	332	25	2.13
<i>predicted (supersaturation and precipitation)</i>	238	34	1.75
Stugeron [®]			
<i>in vivo</i>	233	30	2.0
<i>predicted (dissolution-only)</i>	331	19	2.25
<i>predicted (supersaturation and precipitation)</i>	215	29	1.88
Fed state			
Arlever [®]	AUC ₀₋₂₄ (ng x h/ml)	C _{max} (ng/ml)	t _{max} (h)
<i>in vivo</i>	315	36	5.0
<i>predicted (restricted permeability)</i>	315	36	4.63
<i>predicted (unrestricted permeability)</i>	324	50	4.0
Cinnarizine 30 mg			
<i>in vivo</i>	467	56	5.0
<i>predicted (restricted permeability)</i>	477	55	5.0
<i>predicted (unrestricted permeability)</i>	485	78	4.13

The simulation outcome demonstrates that dissolution experiments and solubility values deliver useful data for quantitative predictions of the plasma profiles of cinnarizine when supersaturation and precipitation of the drug is not expected i.e. in the fed state. By contrast, when supersaturation and precipitation are expected to occur i.e. in the fasted state, the use of transfer experiment data is essential to quantitatively assess oral absorption of this weak base.



3.2.4 STELLA[®] statistical comparison analysis of different transfer rates

Table 3.10 shows the comparison of fasted state *in vivo* data with *in silico* predictions using the results of various transfer experiments. Plasma predictions of Arlevert[®] and Stugeron[®] at each transfer rate (3 h⁻¹, 9, 4, and 0.5 ml/min) are presented in Figure 3.11. Results of the first order transfer rate lead to good plasma profile predictions for both Arlevert[®] and Stugeron[®]. Interestingly, plasma profiles of Arlevert[®] matched well with the predictions using the supersaturation and precipitation values from transfer experiments with the rate of 4 ml/min. A comparison of the first order and 4 ml/min transfer profiles of Arlevert[®] reveals several matching factors which may have lead to similar predictions i.e. a) the transfer time for both transfer rates lasted for about one hour, b) after one hour approximately the same amount of cinnarizine was released (60%) and c) the precipitation constants were similar for both transfer rates. However, in the case of Stugeron[®] the use of the transfer rate of 4 ml/min led to relatively poor *in vivo* predictions. The transfer rate of 9 ml/min overestimated the AUC and C_{max} of both formulations. Very poor predictions of the *in vivo* performance were demonstrated with the slowest transfer rate (0.5 ml/min). Overall, the first order transfer rate (3 h⁻¹) revealed best predictions of oral absorption of immediate release (IR) cinnarizine formulations in the fasted state.

Table 3.10: Statistical comparison of *in silico* predictions to *in vivo* observations using the difference factor (f_1) and point estimate ratios of bioequivalence test parameters for different cinnarizine IR formulations and transfer experiments (best fits in boldface).

Dosage/Transfer rate	Ratio AUC ₀₋₂₄	Ratio C _{max}	f_1
Arlevert [®] (20 mg, 3 h ⁻¹)	1.095	1.019	13.84
Arlevert [®] (20 mg, 9 ml/min)	1.207	1.179	21.80
Arlevert [®] (20 mg, 4 ml/min)	1.019	0.953	12.14
Arlevert [®] (20 mg, 0.5 ml/min)	1.493	0.757	46.00
Stugeron [®] (25 mg, 3 h ⁻¹)	0.922	0.977	10.31
Stugeron [®] (25 mg, 9 ml/min)	1.095	1.170	21.78
Stugeron [®] (25 mg, 4 ml/min)	1.221	1.327	30.30
Stugeron [®] (25 mg, 0.5 ml/min)	1.783	0.971	60.27

Results

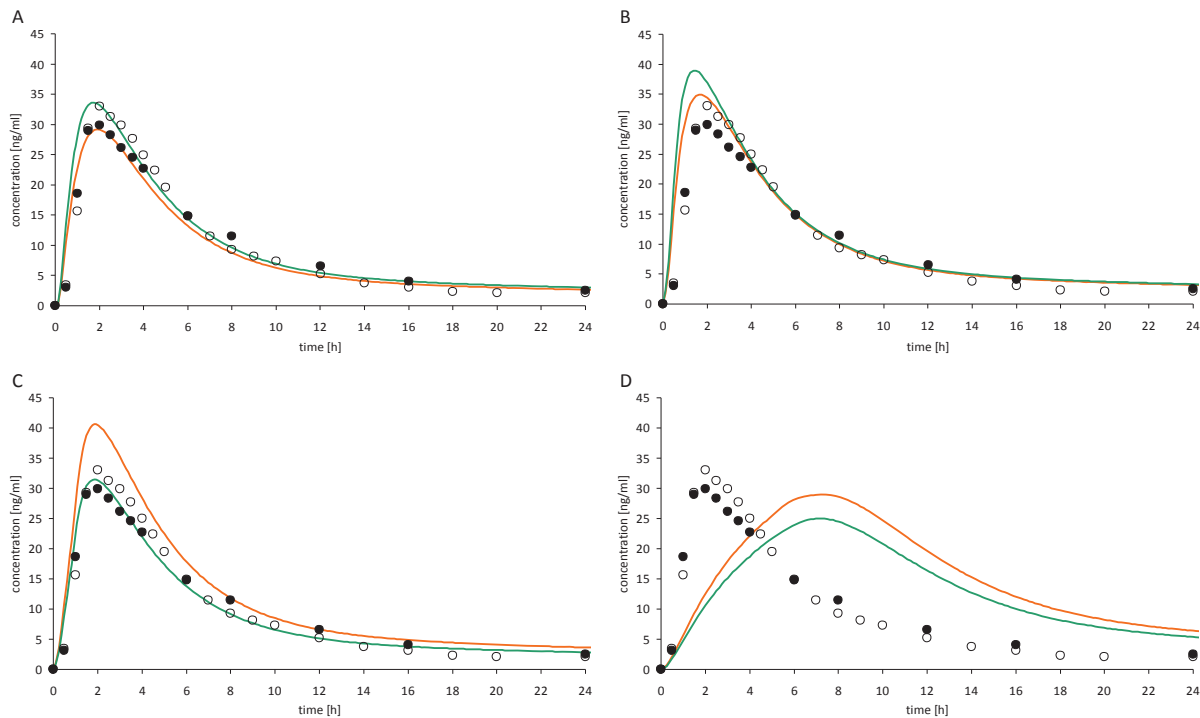


Fig. 3.11: Fasted state plasma profile predictions of Arlevert® (–) and Stugeron® (–) tablets using the supersaturation and precipitation PBPK model after implementing results of different transfer rates. The *in vivo* plasma profiles of Arlevert® (○) and Stugeron® (●) are displayed against profile predictions for each transfer rate, i.e. 3 h⁻¹ (A), 9 ml/min (B), 4 ml/min (C) and 0.5 ml/min (D).

3.2.5 STELLA® sensitivity analysis of cinnarizine plasma profile predictions

A sensitivity analysis was performed to identify the pre-systemic parameters which are most important for the simulation of cinnarizine plasma profiles. For this purpose the fasted and fed state gastric emptying rate (GER) and effective permeability (P_{eff}) values were varied in the range of 0.25-5 times GER and P_{eff} . In the fasted state it appears that the fraction dissolved (f_d) and precipitation constant (k_p) play a crucial role in the accurate prediction of plasma profiles (see Section 3.3). Thus, f_d values were varied between 0.25 and 1, and the k_p values were varied from 0.25 to 5 fold. To investigate the impact of dissolution on plasma profile predictions in the fed state, initial dissolution rates (z values) in FeSSGF and FeSSIF-V2 were varied from 0.25 to 5 fold.

The sensitivity analyses are shown illustratively for the fasted and fed state profiles of Arlevert® in Figures 3.12 and 3.13. The analysis of Stugeron® in the fasted state and



of Cinnarizine 30 mg in the fed state revealed similar behavior to Arlevert[®] and are presented in the Appendix section.

For the fasted state (Figure 3.12) the plasma profile predictions are highly dependent on the effective permeability (P_{eff}) as shown in Panel D. Additionally, plasma profile forecasts of cinnarizine are significantly dependent on the fraction dissolved (f_d) (Panel A). Variations of the constant f_d represent changes in the amount of drug dissolved/supersaturated during gastric emptying, and thus in the concentration of API available for absorption from the intestinal lumen into the blood stream. By contrast, the precipitation constant (k_p) represents the reduction in dissolved API in the intestine. Although changes in the precipitation rate constant influence the simulations (Panel B), they have less influence on the plasma profile predictions of cinnarizine than variations of the f_d value. Panel C demonstrates that plasma profile predictions are somewhat sensitive to the gastric emptying rate (GER).

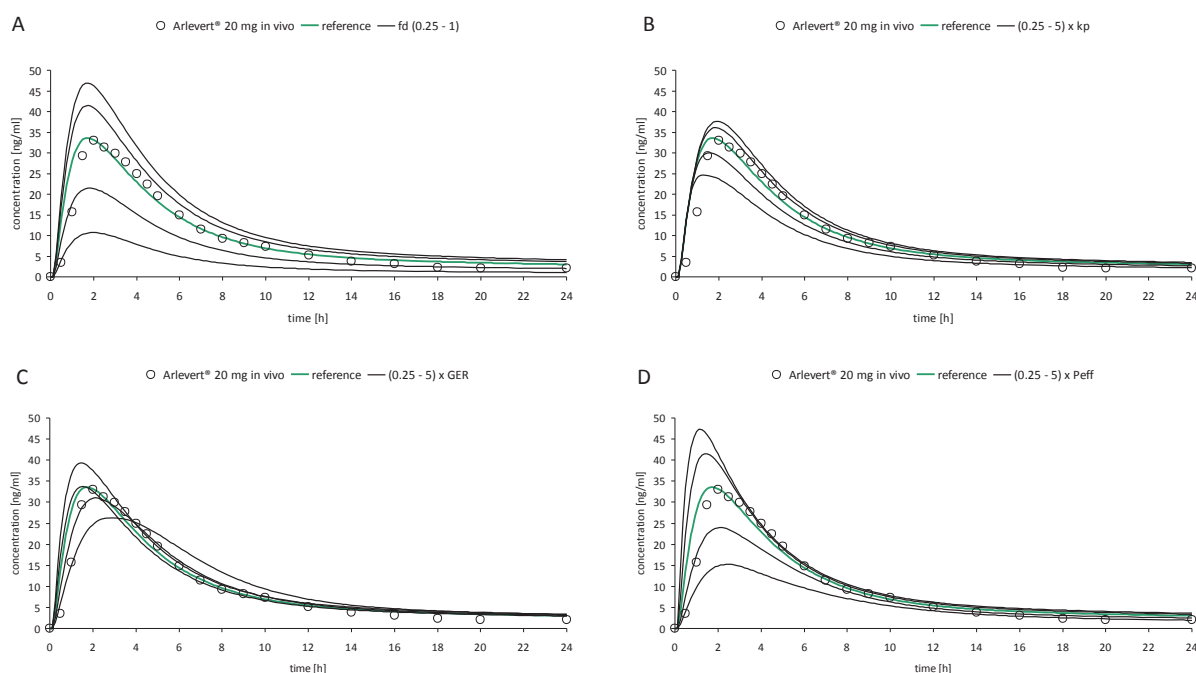


Fig. 3.12: Arlevert[®] in the fasted state - sensitivity analysis of the fraction dissolved constant (A), precipitation constant (B), the gastric emptying rate (C) and the effective permeability (D) on cinnarizine plasma profiles

In the fed state variations in GER and P_{eff} show most significant effects on plasma profile predictions (Figures 3.13, Panels C and D). Variation in initial dissolution rates (z values) in FeSSGF and FeSSIF-V2 had very little to no impact on pharmacokinetic predictions (Panel A and B). The negligible role of the z values on the *in vivo*

Results

pharmacokinetic predictions of cinnarizine is explained by the high solubility of the drug in the fed state media. The sensitivity analysis further demonstrates that the plasma predictions of cinnarizine highly depend on permeability, in accordance with its borderline BCS class II/IV drug status (according to DCS it is most likely to be considered a class IIb compound). It also confirms that supersaturation and precipitation play a crucial role for the bioavailability of cinnarizine the fasted state. Variations of the GER tend to have a bigger influence the plasma profiles in the fed state than in the fasted state.

Generally speaking, the sensitivity analysis reveals that the variability in plasma profiles under fasted conditions is expected to be higher than in the fed state. This is also in accordance with the *in vivo* observations. While the coefficient of variation for AUC in the fasted state was high (50%), in the fed state it was significantly lower (27%) [98].

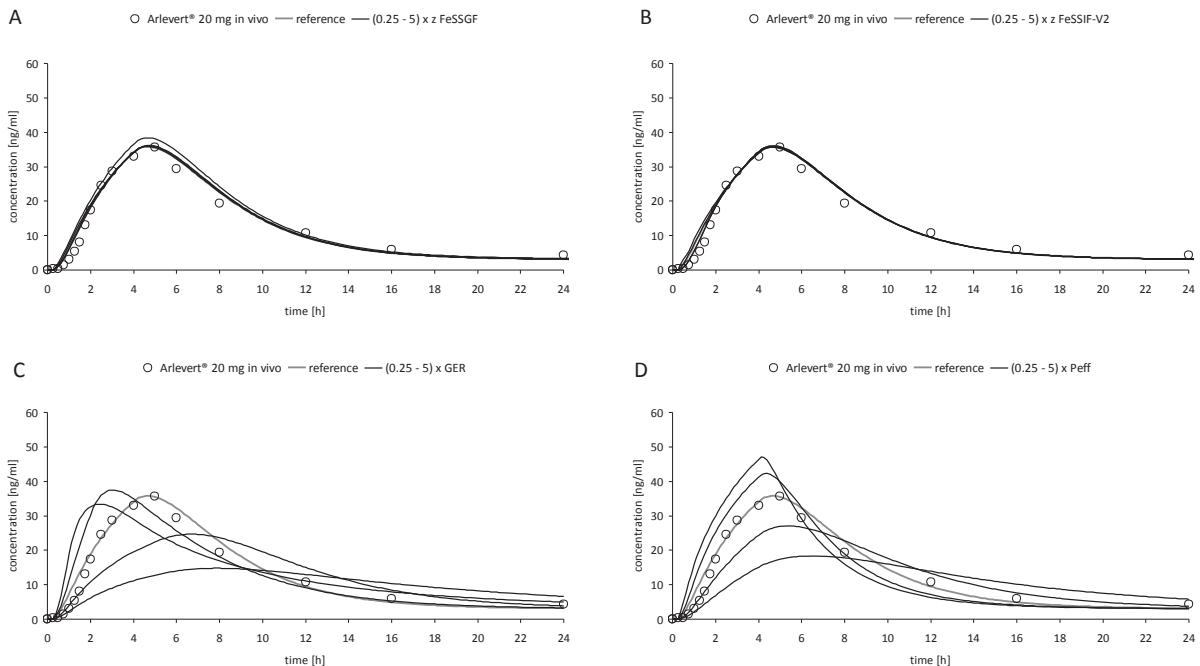


Fig. 3.13: Arlevert® in the fed state - sensitivity analysis of the z value in FeSSGF (A), the z value in FeSSIF-V2 (B) the gastric emptying rate (C) and the effective permeability (D) on cinnarizine plasma profiles



3.2.6 Summary of cinnarizine plasma profile simulations using Simcyp®

A detailed description of cinnarizine plasma profile simulations using Simcyp® can be found in the Appendix section. Four different approaches were utilized to simulate the plasma profiles of cinnarizine tablets in pre- and postprandial states (approaches described in Section 2.2.9). Reasonable fasted state simulations in terms of cinnarizine absorption (55% for Arlevert® and 32% for Stugeron®) were achieved when biorelevant solubility data were implemented into the GI solubility mask and supersaturation and precipitation data were utilized from transfer experiments. However, the plasma profiles were significantly underestimated when using this method. By contrast, cinnarizine plasma profile predictions using calculated (with predicted bile salt solubility enhancement) solubility by Simcyp® or equilibrium pH dependent solubility values (with bile salt solubility enhancement) from *in vitro* investigations demonstrated a good fit of the *in vivo* performance. However, these simulation approaches exhibited 100% drug absorption in the fasted state. Absorption of entire cinnarizine dose in the fasted state is not realistic, since cinnarizine exhibits a greater bioavailability in the fed state. “A good fit for the wrong reason” was achieved through compensatory effects, resulting from overestimations of the volume of distribution value (Vd). This assumption was consolidated when fed state plasma profiles were simulated using different simulation approaches. In most cases 100% drug absorption was calculated in the fed state simulations, however the *in vivo* performance was underestimated in all approaches. On that basis the volume of distribution was fitted (reduced) to represent the fed state *in vivo* profiles. The estimated “new” Vd value was then utilized in the fasted state simulation approach, where the GI solubility data and supersaturation and precipitation values were utilized. The simulation results were reasonable for the fed state, however the plasma profiles were still underestimated in the fasted state. The reason for the plasma profile underestimation in the fasted state using this method is assumed to originate from an inaccurate algorithm simulating supersaturation and precipitation in Simcyp®.

In summary, Simcyp® simulations of cinnarizine plasma profiles were most reasonable when biorelevant *in vitro* data (solubility, dissolution, transfer experiments) were utilized. Predictions of cinnarizine solubility on the basis of



Results

physicochemical parameters of the compound were inaccurate, resulting in false “good fits” of the *in vivo* performance. Still, the parameterization of *in vitro* supersaturation and precipitation is not sufficient enough to achieve realistic plasma profile predictions.

3.3 Summary of the cinnarizine investigation and formulation suggestions

The *in vitro* and *in silico* investigation of cinnarizine tablets revealed several important conclusions for formulation development of weak bases with similar behavior to cinnarizine. With respect to *in vivo* investigations, these can be summarized as follows:

1. Dissolution experiments are useful tools for compounds undergoing simple dissolution behavior, but they are limited in terms of supersaturation and precipitation investigation.
2. Dumping tests are a good screening method for supersaturation and precipitation of such compounds. Nevertheless they are incapable of reflecting some of the factors involved in supersaturation and precipitation variability. Thus, the results from dumping experiments are not optimal for plasma profile predictions using *in silico* models for compounds exhibiting this kind of behavior.
3. Transfer experiments were confirmed to be a powerful tool for the investigation of supersaturation and precipitation. The transfer results on cinnarizine revealed that its dissolution behavior depends on a multitude of physiological factors, such as bile salt concentrations, the pH and meal components in the GI tract as well as the gastric emptying rate. Moreover, it may depend on external parameters such as formulation ingredients and parameters during the manufacturing process. In case of cinnarizine, insoluble particles in Arlevert[®] tablets lead to an increase of the precipitation of the compound during transfer experiments. Moreover, the dissolution,



supersaturation, precipitation and thus the *in vivo* behavior of Stugeron[®] were inferior to Arlevert[®], even though the tablet contained a higher dose of cinnarizine.

In silico modeling of cinnarizine confirmed that the supersaturation and precipitation of the compound is a crucial factor for drug bioavailability in the fasted state. A reasonable parameterization of these two key factors is essential to simulate the *in vivo* behavior of cinnarizine. Kinetic factors appear to be critical to a correct simulation of pre-absorptive behavior of supersaturating drugs. The time to reach the maximum supersaturation concentration as well as the time of onset of precipitation are needed to characterize this behavior accurately. The STELLA[®] supersaturation and precipitation model uses all of the aforementioned factors for simulations. The time factor cannot currently be implemented into the Simcyp[®] supersaturation and precipitation model. This may have led to underestimations of the *in vivo* behavior of cinnarizine tablets in the fasted state.

Since supersaturation and precipitation appear to directly influence cinnarizine absorption, numerous strategies could be implemented to enhance the bioavailability of the compound. Several articles have been published on bioavailability improvement of cinnarizine using two principles, the enhancement of supersaturation and/or prevention of precipitation [90, 97, 128-134]. The common approach to improve bioavailability of cinnarizine was to incorporate the drug into colloidal systems, which enhance the solubility in the upper small intestine and inhibit precipitation of the API during gastric emptying. Earlier studies on cinnarizine formulation improvement revealed that oleic acid could increase the bioavailability of cinnarizine in dogs [130]. Another way of bioavailability enhancement was the incorporation of cinnarizine in cyclodextrins [90, 131]. Recently SNEDDS (Self-nanoemulsifying Drug Delivery Systems) exhibited an enhancement of drug supersaturation and inhibition of precipitation of cinnarizine leading to significant reduction of food effects in dogs [97, 132-134]. Alternative ways of improving bioavailability of cinnarizine by enhancing its solubility in the fasted state are micronization/nanonization of the API and its incorporation into solid vehicle systems as silicates (e.g. Aeroperl[®]) or polymers (e.g. Poloxamer 188). These so called solid



Results

solutions and dispersions enhance the supersaturation behavior of the API. Polymers, such as Poloxamer 188 and hydroxypropyl methylcellulose (HPMC) may additionally inhibit precipitation of cinnarizine upon its entering into the upper small intestine. All of these studies confirm that formulation effects on cinnarizine supersaturation and precipitation in the intestine have a crucial impact on the bioavailability of the compound in the fasted state.

3.4 Atazanavir sulfate – investigation of *in vitro* behavior

3.4.1 Solubility results

3.4.1.1 Equilibrium solubility

Equilibrium solubility results of atazanavir sulfate in biorelevant media are presented in Figure 3.14. As described in Section 2.1.3 the solubility of atazanavir is highly pH dependent. At lower pH values the solubility of the compound is high (7.488 and 4.443 mg/ml for FaSSGF pH 1.6 and FaSSGF pH 2.0, respectively). With increasing pH the solubility of the compound decreases significantly (3.82 µg/ml at pH 5.8 and 1.92 µg/ml at pH 6.5) (Student's t-test; $p < 0.001$). The solubility of atazanavir sulfate does not seem to depend on bile salts. Comparing solubilities in the blank buffers with complete biorelevant media, FaSSIF-V2 and FeSSIF-V2, modest “micellar solubilization” values of between just 1.43 and 1.08 were achieved. Interestingly, the solubility difference between FaSSIF-V2 (2.74 µg/ml) and FeSSIF-V2 (4.13 µg/ml) is also very modest, supporting the lack of bile salt effect on solubility. A study on solubility of HIV protease inhibitors in simulated and human intestinal fluids further underlines these observations [112]. In that investigation atazanavir solubility between FaSSIF and FeSSIF was also found to be not significantly different. Furthermore, even between human intestinal fluids, FaHIF (fasted) and FeHIF (fed) no significant difference in solubility was observed [112]. On the one hand, the relatively high logP value would support a bile salt mediated solubility enhancement of the API. On the other hand, its high molecular weight (705 g/mol) and high polar surface area (186.2 Å) may sterically hinder the binding of bile salt to the atazanavir molecule, which might explain the lack of bile salt effects.



The investigation of atazanavir solubility in FeSSGF pH 2.75 and FeSSGEm pH 2.75 revealed considerably different results between the two media. The solubility in FeSSGF pH 2.75 was observed to be more than 4.75 times higher than in its protein-free equivalent, FeSSGEm pH 2.75. It can be deduced from these results that the solubility of atazanavir is amplified through interaction with proteins of the milk in FeSSGF pH 2.75. Similar behavior was observed in the mixture of the simulated gastric fluids with FeSSIF-V2, where the solubility of atazanavir sulfate was almost 60 times higher for the mixture containing milk (FeSSGF pH 2.75/FeSSIF-V2) than in its albumin-free equivalent (FeSSGEm pH 2.75/FeSSIF-V2). PK studies have shown that atazanavir interacts with proteins, such as the α -1-acid glycoprotein and albumin [135, 136]. Additionally, atazanavir was observed to be excreted in breast milk which indicates a possible protein interaction [137, 138]. Although these findings support the hypothesis that milk proteins in FeSSGF contribute to the increase in atazanavir solubility, they are not confirmatory, since the proteins in plasma are not identical to the milk protein, casein.

Another possible explanation for the solubility disparities is the different analytical methodology used for the two media. A filter with a pore size of 0.45 μm was utilized for FeSSGEm pH 2.75, whereas the FeSSGF pH 2.75 samples were filtered through a filter with a bigger pore size of 2.7 μm . Hence, the probability that non-dissolved particles might have been able to pass through the filter is higher for the latter case. The filtered emulsions were subsequently diluted with organic solvents, which would have brought any non-dissolved atazanavir particles in the filtrate into solution. This may have resulted in the high “solubility” values measured in FeSSGF pH 2.75. Of course, it is possible that both of these phenomena contribute to the higher solubility observed in the milk-based media.

Results

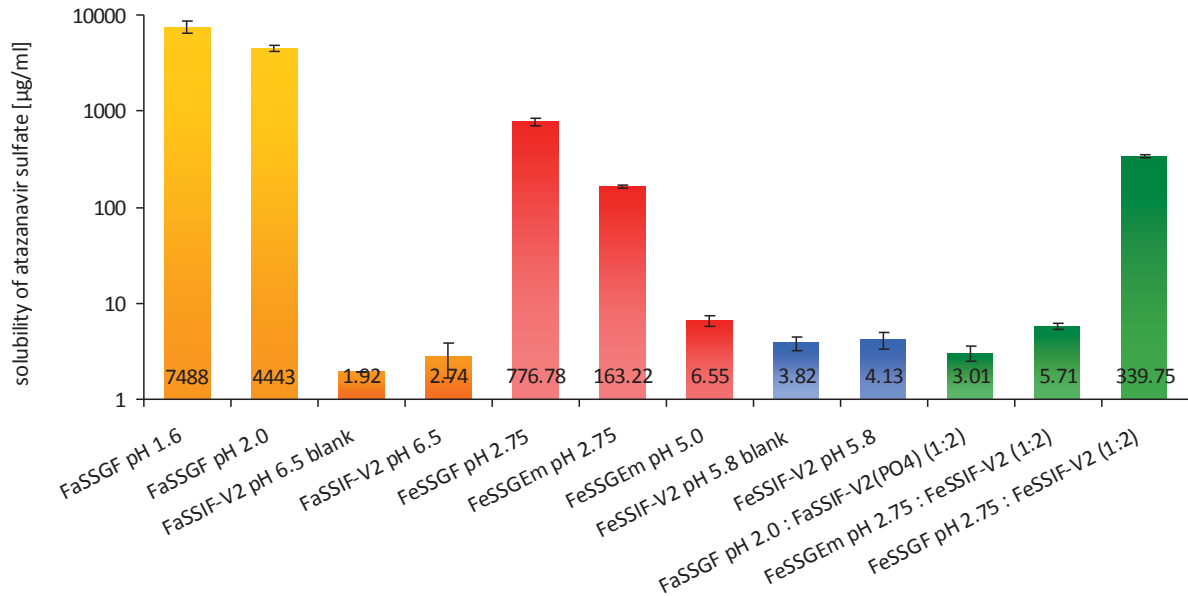


Fig. 3.14: Equilibrium solubilities of atazanavir in biorelevant media (logarithmic scaling). Solubility values in $\mu\text{g/ml}$ along with the standard deviations are shown on the bar for each medium ($n=3$).

3.4.1.2 Kinetic solubility

Kinetic (apparent) solubility results of atazanavir sulfate in biorelevant media are presented in Figure 3.15. The solubility of atazanavir sulfate revealed to be dynamic for all media used in this investigation (FaSSIF-V2, FaSSGF pH 2.0/FaSSIF-V2(PO4) 1:2 mixture and FeSSIF-V2). Since it was reported that the atazanavir sulfate transforms into an amorphous form while in contact with water, the initial concentration values (1 hour) may be assumed as apparent solubility or atazanavir in a supersaturated state. Over time, the solubility decreased rapidly in all media investigated. The final value (at 24 hours) is expected to reflect the solubility of the free atazanavir base. These results may help to explain the dissolution behavior of atazanavir sulfate in biorelevant media during dissolution and transfer experiments.

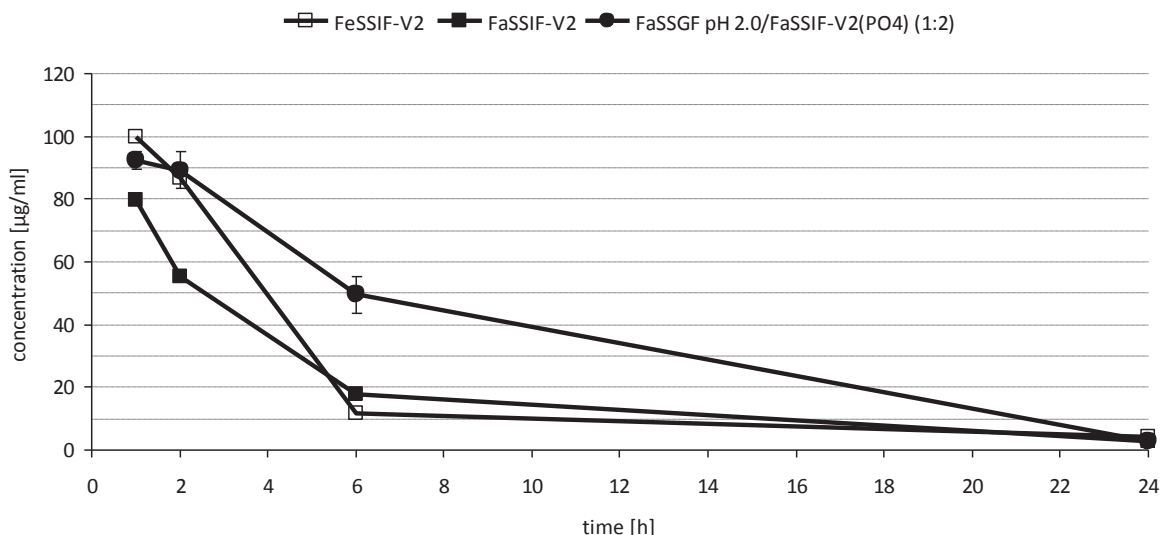


Fig. 3.15: Kinetic solubilities of atazanavir sulfate in biorelevant media over 24 hours (some symbols are bigger than the standard deviation bars) (n=3).

3.4.2 Dissolution results of atazanavir sulfate capsules in biorelevant media

Dissolution profiles of different doses (100, 200, 400 and 1200 mg) of atazanavir sulfate (Reyataz[®] capsules) in fasted state gastric and intestinal media, FaSSGF pH 1.6 and FaSSIF-V2, are presented in Figure 3.16. All doses dissolve entirely in FaSSGF pH 1.6, except for 1200 mg, which achieves 86% dissolution at 180 minutes. However, the entire dose of 1200 mg is expected to dissolve eventually since the solubility of the compound will not be exceeded in this medium.

The compound exhibits particular dissolution behavior for each dose in FaSSIF-V2. Interestingly, all doses reached “supersaturated state” concentrations, significantly exceeding the equilibrium solubility. However, generally low drug concentrations were observed for all doses of atazanavir sulfate (compare with gastric media). The highest % dissolved was achieved by the 100 mg dose (16.5%), followed by the 200 and 400 mg atazanavir sulfate (10.5% and 8.1%). The 1200 mg dose showed lowest release of just 4%. Interestingly, for the 1200 mg dose a decrease in drug concentration was observed after 60 minutes. A possible explanation for this observation may be that the drug first attains supersaturation and then starts to precipitate towards its equilibrium solubility. Unexpectedly, dissolution concentrations increased with higher doses, from 33 µg/ml (100 mg atazanavir sulfate) to 97 µg/ml (1200 mg atazanavir sulfate). This behavior can be explained by pH changes caused

Results

by the hydrosulfate salt of atazanavir. Table 3.11 shows the decrease in pH of FaSSIF-V2 by the end of the dissolution experiment. Clearly, with increasing amounts of atazanavir sulfate added, a stronger decrease in pH is observed.

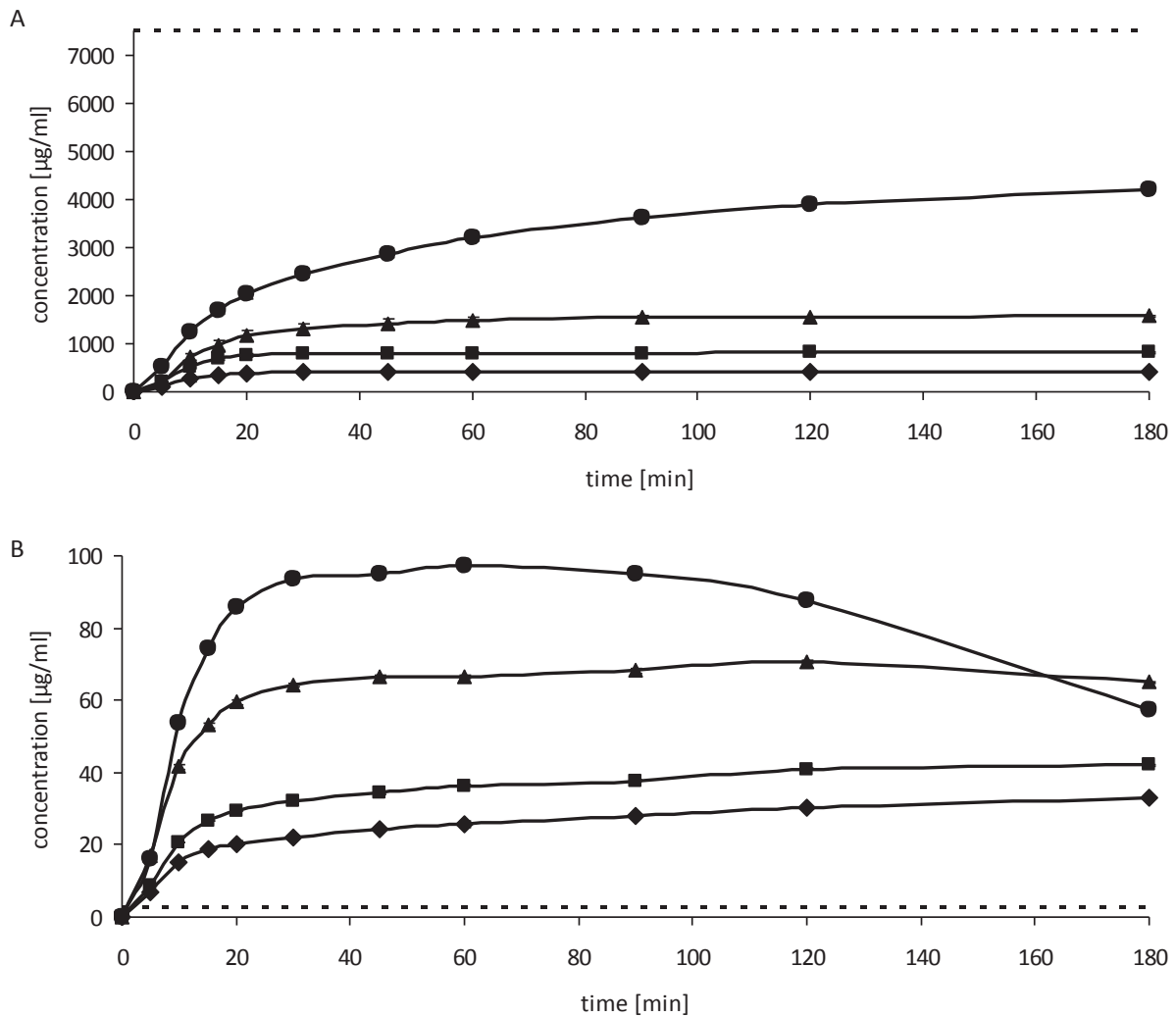


Fig. 3.16: Dissolution of different doses of atazanavir sulfate capsules (Reyataz[®]) in fasted state gastric (A) and intestinal (B) media (symbols are bigger than the standard deviation bars): 100 mg (♦), 200 mg (■), 400 mg (▲), 1200 mg (●) and solubility (- -).



Table 3.11: pH values in the dissolution vessel after dissolution of different doses of atazanavir sulfate in FaSSIF-V2

Dose atazanavir sulfate (mg)	pH after dissolution
100	6.45
200	6.41
400	6.35
1200	6.08

Dissolution testing of 400 mg atazanavir sulfate capsules under simulated fed state conditions (Figure 3.17) revealed qualitatively somewhat similar behavior to the fasted state (compare with Figure 3.16). Almost the entire dose (96%) was released at 60 minutes in FeSSGEM pH 2.75. At that point in time the compound reached a highly supersaturated state at 60 minutes, but then started to precipitate slowly with the rate of 0.334 h^{-1} . In FeSSGEM pH 5.0 the compound also exhibited supersaturation, but achieved lower concentrations than in FeSSGEM pH 2.75. In this case a precipitation rate constant of 0.724 h^{-1} was calculated for times after 120 minutes.

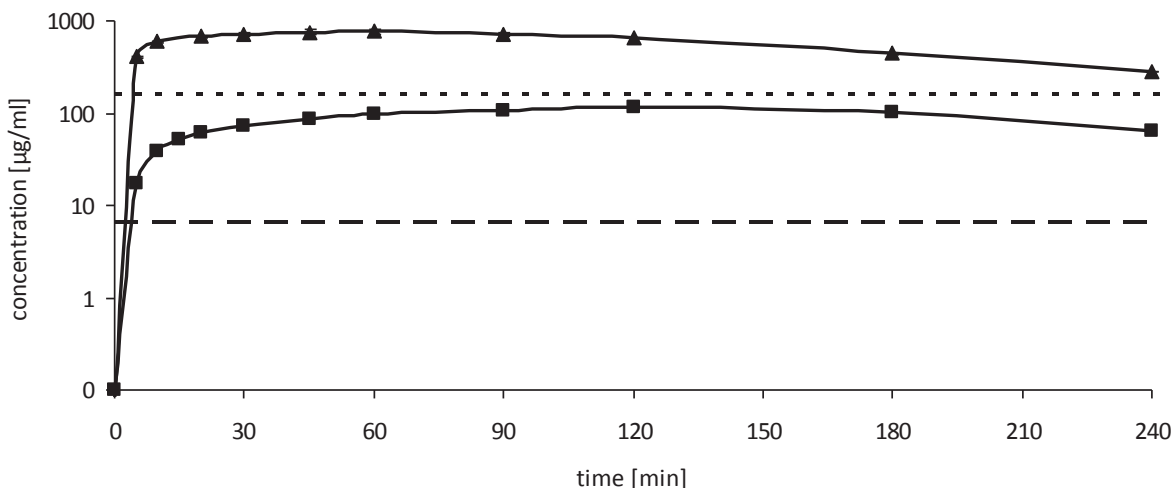


Fig. 3.17: Dissolution of 400 mg atazanavir sulfate capsules (Reyataz[®]) in the fed state biorelevant media (some symbols are bigger than the standard deviation bars): FeSSGEM pH 2.75 (\blacktriangle) and FeSSGEM pH 5.0 (\blacksquare) along with the equilibrium solubility in FeSSGEM pH 2.75 (—) and in FeSSGEM pH 5.0 (---). Concentrations are presented in a logarithmic scale.

In FeSSIF-V2 (Figure 3.18) the behavior followed a similar pattern, although much lower concentrations were achieved. In this case, 6.6% of the 400 mg dose was dissolved at 60 minutes (supersaturation), which was followed by a more rapid

Results

precipitation (1.14 h^{-1}), almost returning to the solubility at 240 minutes. The initial dissolution rates of the fasted and fed states were calculated for implementation into *in silico* models and are presented in Table 3.12.

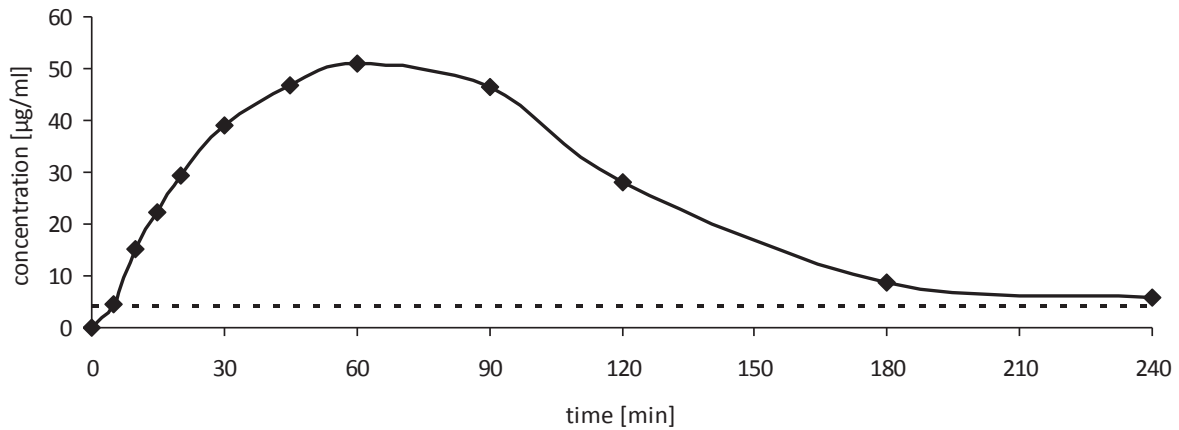


Fig. 3.18: Dissolution of 400 mg atazanavir sulfate capsules (Reyataz[®]) in FeSSIF-V2 (♦) (some symbols are bigger than the standard deviation bars) along with the equilibrium solubility (--). Symbols are bigger than the standard deviation bars.

Table 3.12: Initial dissolution rates (z values) for the various biorelevant media and Reyataz[®] doses

Dissolution medium	Dose	z value \pm SE ($\text{mL}/\text{mg}^{2/3}/\text{h}$)
FaSSGF	100 mg	2.173 ± 1.461
FaSSGF	200 mg	0.855 ± 0.134
FaSSGF	400 mg	0.142 ± 0.069
FaSSGF	1200 mg	0.040 ± 0.009
FaSSIF-V2	100 mg	0.141 ± 0.020
FaSSIF-V2	200 mg	0.138 ± 0.031
FaSSIF-V2	400 mg	0.130 ± 0.047
FaSSIF-V2	1200 mg	0.110 ± 0.021
FeSSGEm pH 2.75	400 mg	0.209 ± 0.047
FeSSGEm pH 5.0	400 mg	0.053 ± 0.017
FeSSIF-V2	400 mg	0.090 ± 0.049

Z values calculated from dissolution profiles in gastric media imply that pH in the fed state has a crucial impact on atazanavir dissolution. Comparing the 400 mg z values in FaSSGF and the two fed state gastric media (FeSSGEm 2.75 and FeSSGEm 5.0),



suggests a positive food effect to take place under light meal conditions and that a negative food effect is probable if atazanavir is taken with high fat meal.

Comparing the dissolution of 400 mg atazanavir sulfate in simulated fasted and fed state intestinal fluids, not even a qualitative prediction of the reported positive food effect is possible. Moreover, the quotient of maximal dissolution concentrations achieved in both media ($C_{\max}(\text{FeSSIF-V2}/\text{FaSSIF-V2}) = 0.722$) would lead to the conclusion that a negative food effect is to be expected. If taking the z values in FaSSIF-V2 and FeSSIF-V2 into account, one would also assume a negative food effect for the 400 mg dose.

Under both simulated fasted and fed state conditions, drug dissolution was higher for the simulated stomach (FaSSGF pH 1.6, FeSSGEm pH 2.75 and FeSSGEm pH 5.0) than for the simulated intestine (FaSSIF-V2 and FeSSIF-V2). However, dissolution tests may only partly reflect the *in vivo* behavior of atazanavir sulfate under fasted and fed state conditions. Since solubility and dissolution results revealed the compound to dissolve better in the simulated stomach media than in the simulated intestinal media, it may be important to identify the drug behavior during the passage from the stomach into the small intestine. This was achieved by applying transfer experiments as presented in the following chapters.

3.4.3 Dumping results of atazanavir sulfate

Figure 3.19 shows dumping of 200 mg atazanavir sulfate pre-dissolved in 250 ml of FaSSGF pH 2.0 into 500 ml of FaSSIF-V2(PO_4). Direct precipitation of the compound towards the apparent solubility value (supersaturation in the FaSSGF pH 2.0/FaSSIF-V2 mixture at a ratio of 1:2) was observed for the drug (91 $\mu\text{g}/\text{ml}$ corresponding to 33% of the 200 mg dose). The compound stays in the supersaturated state (kinetic solubility) for at least 120 minutes, and then tends to precipitate toward the equilibrium solubility value (3.01 $\mu\text{g}/\text{ml} \pm 1,1\%$). The result indicates that the transfer rate is unlikely to have an influence on atazanavir supersaturation and precipitation, since the compound directly achieved and retained the same concentration value over a timeframe comparable to the small intestine transit time (SITT).

Results

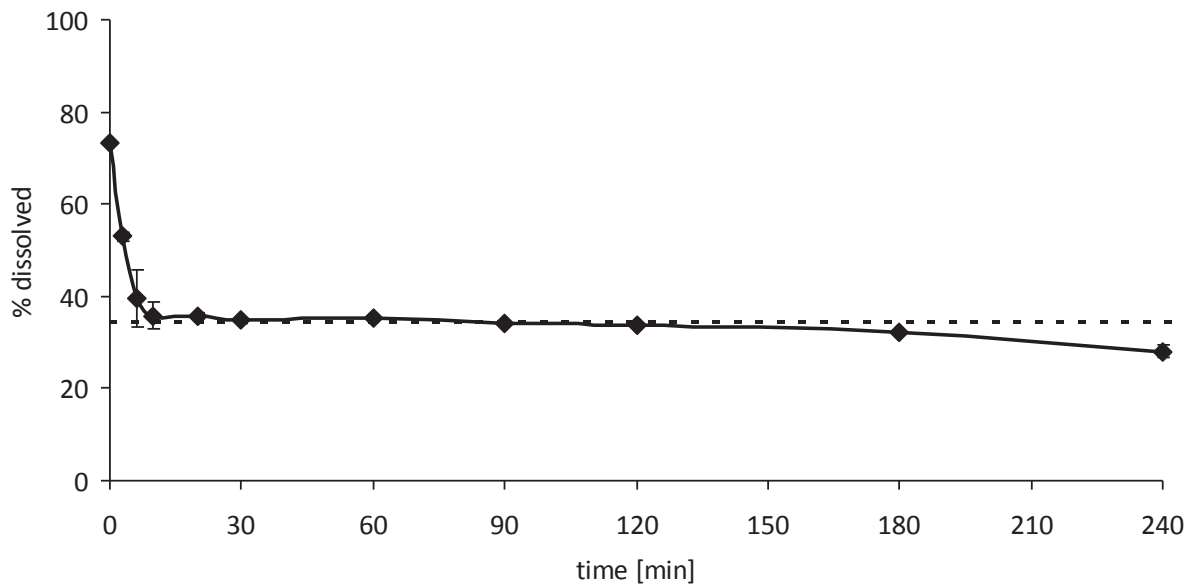


Fig. 3.19: Concentration profile of 200 mg atazanavir after the pre-dissolved compound in 250 ml FaSSGF pH 2.0 into 500 ml of FaSSIF-V2(PO₄) (some symbols are bigger than the standard deviation bars). The dotted line represents the kinetic solubility relative to the 200 mg atazanavir dose.

3.4.4 Investigation of the atazanavir sulfate concentration profile during simulated transfer from the stomach to the intestine

The fasted state transfer results of pre-dissolved 100 and 200 mg atazanavir sulfate at a transfer rate of 9ml/min are presented in Figure 3.20. Interestingly, the theoretical and practical curves overlap up to a certain time point, after which the compound precipitates to the apparent solubility value (supersaturation in the FaSSGF pH 2.0/FaSSIF-V2 mixture at a ratio of 1:2). Comparing the maximum dissolution concentrations (96 µg/ml) with the equilibrium solubility value (3.01 µg/ml) of the compound, a maximum supersaturation ratio of ~32 was achieved for both doses.

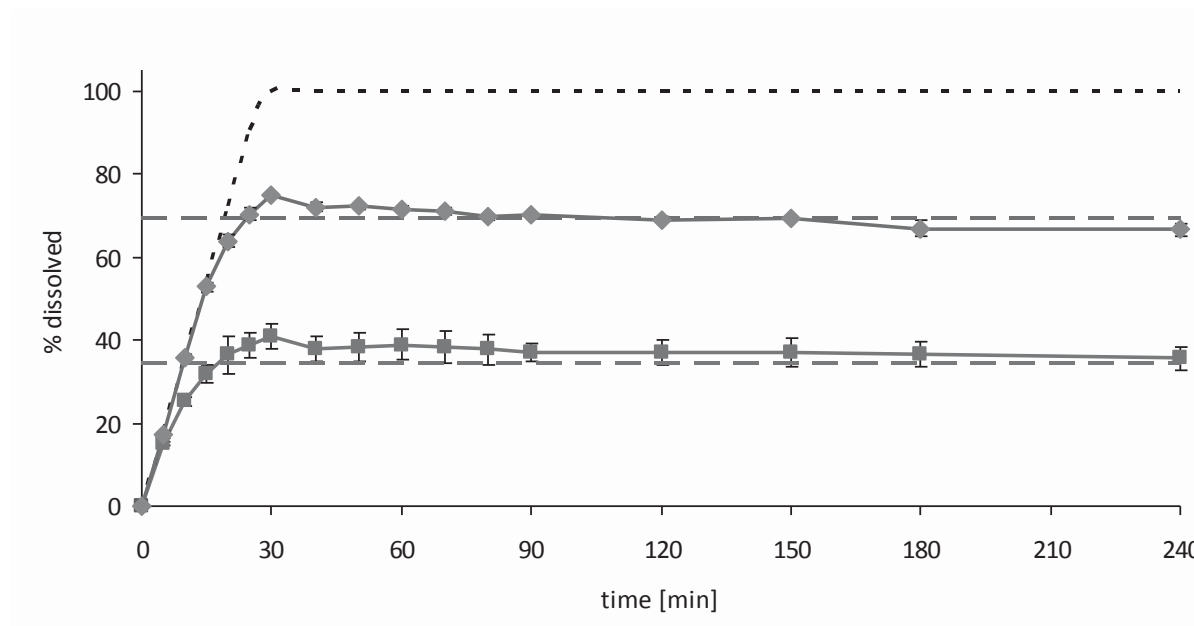


Fig. 3.20: Simulated fasted state transfer results of 100 mg (♦) and 200 mg (■) pre-dissolved atazanavir sulfate using the zero order transfer rate of 9 ml/min. The kinetic solubilities of atazanavir sulfate (solubility value at hour 1 in the 1:2 FaSSGF pH 2.0/FaSSIF-V2(PO₄) mixture) relative to the corresponding dose (—) are presented along with the theoretical transfer curve (- -). Some of the error bars are smaller than the symbols.

Figure 3.21 compares the transfer of pre-dissolved 200 mg atazanavir sulfate (crystalline) with simultaneous dissolution and transfer either of 200 mg pure atazanavir sulfate (crystalline) or Reyataz[®] 200 mg capsules at a transfer rate of 9 ml/in. Reyataz[®] comprises a predominantly amorphous form of atazanavir whereas bulk atazanavir sulfate is crystalline [139, 140]. The results reveal that the transfer profiles were similar for all of the three circumstances. All profiles reached the apparent solubility value within 30 minutes of the transfer experiment, leading to the conclusion that formulation effects do not significantly contribute to atazanavir behavior during gastric emptying. Indeed, a PK study which investigated the same dose of atazanavir sulfate in crystalline and amorphous forms, revealed that the pharmacokinetics of the two formulations were not significantly different *in vivo* [140].

Results

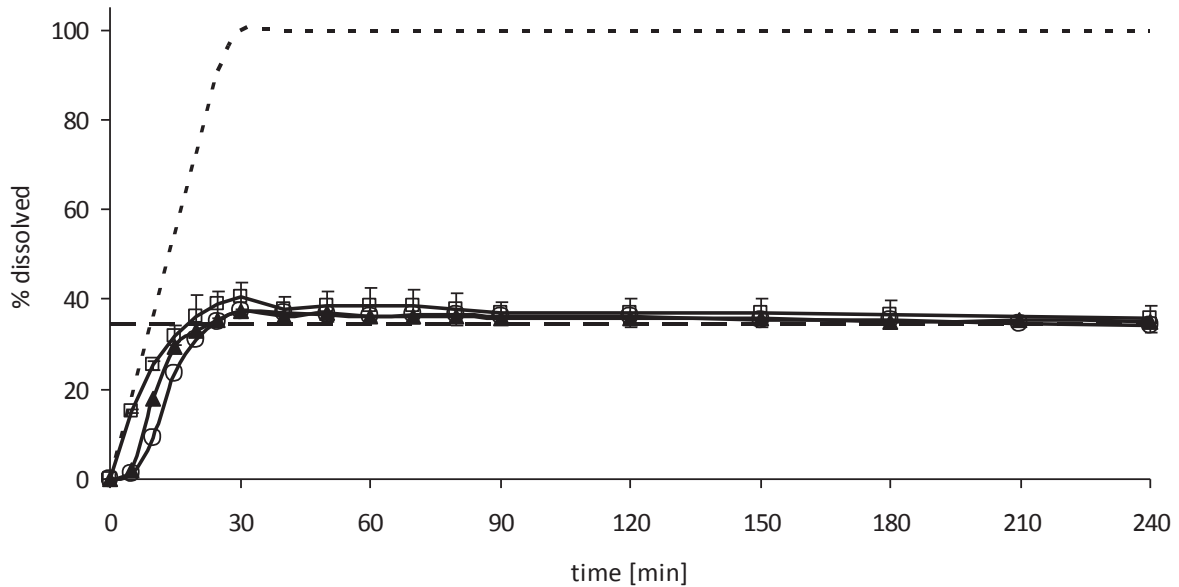


Fig. 3.21: Simulated fasted state transfer results of Reyataz[®] 200 mg (amorphous) (▲), 200 mg atazanavir sulfate compound (crystalline) (○) and pre-dissolved 200 mg atazanavir sulfate (crystalline) (□) using the zero order transfer rate of 9 ml/min. The kinetic solubility of atazanavir sulfate (solubility value at hour 1 in the 1:2 FaSSGF pH 2.0/FaSSIF-V2(PO₄) mixture) relative to the 200 mg dose (---) is presented along with the theoretical transfer curve (- -). Some of the error bars are smaller than the symbols.

When comparing the transfer of different doses of atazanavir sulfate capsules (Reyataz[®]) at different transfer rates, similar behavior is observed (Figure 3.22). All profiles reveal drug dissolution up to the kinetic solubility value. These “supersaturated” states of the API remain stable for all doses and transfer rates. Only at very high doses do the profiles show a tendency to drug precipitation towards the equilibrium solubility value, i.e. 1200 mg under first order transfer conditions. Additionally, the time of maximal dissolution/supersaturation generally depends on the transfer rate, i.e. the simulated gastric emptying rate. The maximum supersaturation ratio (maximal concentration achieved divided by equilibrium solubility), fraction dissolved (f_d) and the first order precipitation constant (k_p) (if precipitation was observed) are presented for each dose in Table 3.13. Fasted state transfer profiles revealed a lag time of about 5 minutes for all doses. Therefore two fraction dissolved values had to be calculated, i.e. $f_{d1} \leq 5$ minutes and $f_{d2} > 5$ minutes. Since gastric emptying under fasted conditions is reported to undergo first order kinetics, results of the first order transfer experiments were applied in the PBPK model [117].

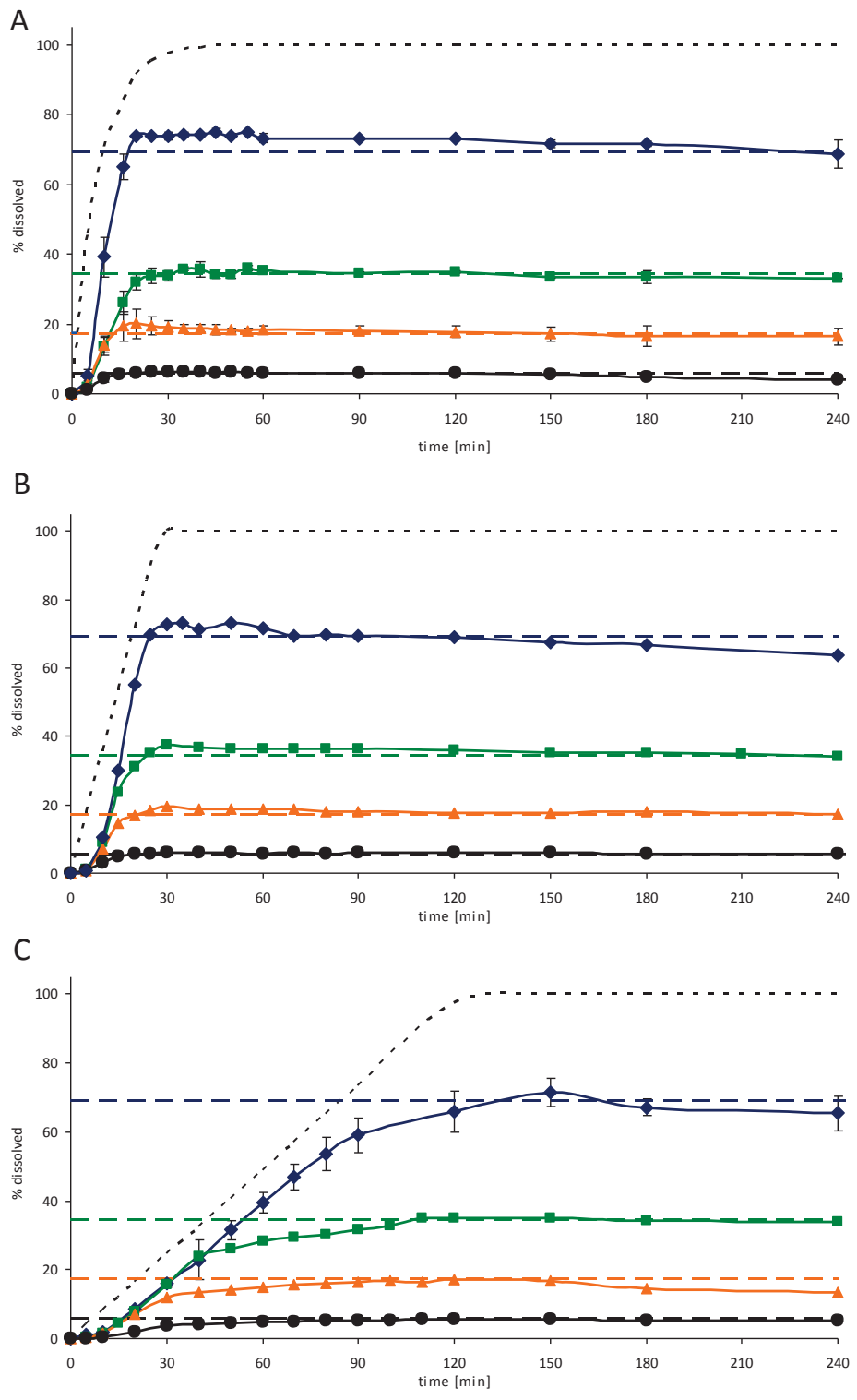


Fig. 3.22: Simulated fasted state transfer results of atazanavir sulfate capsules 100 mg (♦), 200 mg (■), 400 mg (▲), 1200 mg (●) using the first order transfer of 4 h^{-1} (A) and zero order transfer rates of 9 ml/min (B) and 2 ml/min (C). The kinetic solubilities of atazanavir sulfate (solubility value at hour 1 in the 1:2 FaSSGF pH 2.0/FaSSIF-V2(PO_4) mixture) relative to the corresponding dose (—) are presented along with the theoretical transfer curve (- -). Some of the error bars are smaller than the symbols.



Results

The fed state transfer results of 400 mg (2 x 200 mg) Reyataz[®] capsules are presented in Figures 3.23 and 3.24. The use of the milk and Lipofundin[®] based media in the donor compartment (FeSSGF and FeSSGEm at pH 2.75) resulted in completely different outcomes. When FeSSGEm pH 2.75 was used as the donor compartment, atazanavir sulfate achieved a maximum supersaturation value of ~ 26 at 30 minutes and subsequently started precipitating until reaching the equilibrium solubility (FeSSGEm pH 2.75/FeSSIF-V2 1:2 mixture) at 180 minutes. By contrast, when FeSSGF pH 2.75 was utilized the drug achieved the solubility value of the FeSSGF pH 2.75/FeSSIF-V2 1:2 mixture at 90 minutes. The remarkably better dissolution performance of the latter transfer experiment may be explained by solubilization of atazanavir by proteins in the milk of FeSSGF pH 2.75, which was also discussed in the solubility section (Section 3.4.1).

The transfer result simulating the high fat meal conditions (FeSSGEm pH 5.0 as donor compartment) is presented in Figure 3.24. It reveals that the compound achieved supersaturation to a significantly lower ratio (~11) than under simulated light meal conditions (~26). After 90 minutes the compound started to precipitate. The *in vitro* observation is qualitatively confirmed by *in vivo* studies, which reported lower AUC and C_{\max} for the high fat meal than for the light meal [106]. Unfortunately, comparison of *in silico* simulations with the fed state plasma profiles after a high fat meal are not possible, since single dose plasma profiles under these conditions were not reported (only descriptive PK data were available).

The transfer results were parameterized through the maximum supersaturation ratio, the fraction dissolved (f_d) and, if precipitation was observed, through the first order precipitation constant (k_p). Analogous to fasted state transfer results, the profiles exhibited a lag time. Thus, the f_d values were different for the initial (for FeSSGEm pH 2.75 \leq 10 minutes and for FeSSGF pH 2.75 \leq 20 minutes) and the subsequent ascending parts of the profiles. The fed state transfer results were parameterized (Table 3.13) for implementation in *in silico* models, along with the z values (Table 3.12) obtained from dissolution test.

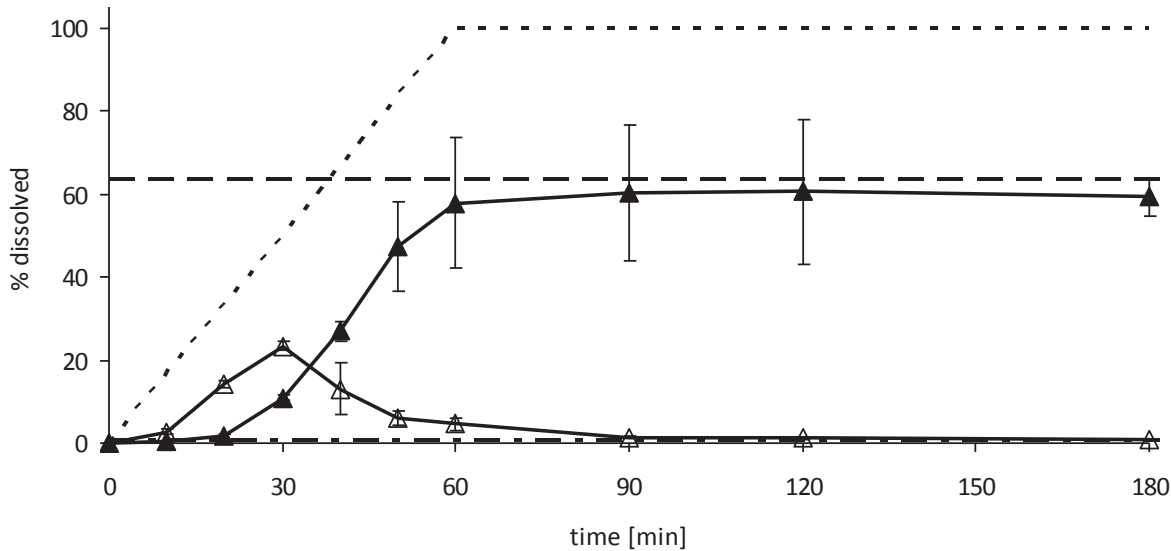


Fig. 3.23: Simulated fed state transfer results of 400 mg (2 x 200 mg) Reyataz[®] capsules using the 4 ml/min zero order transfer rate for 250 ml of FeSSGEm pH 2.75 (Δ) and FeSSGF pH 2.75 (\blacktriangle) as a donor compartment. The solubilities of atazanavir sulfate in mixtures of FeSSGEm pH 2.75/FeSSIF-V2 (1:2) (---) and FeSSGF pH 2.75/FeSSIF-V2 (1:2) (---) are presented along with the theoretical transfer curve (- -). Some of the error bars are smaller than the symbols.

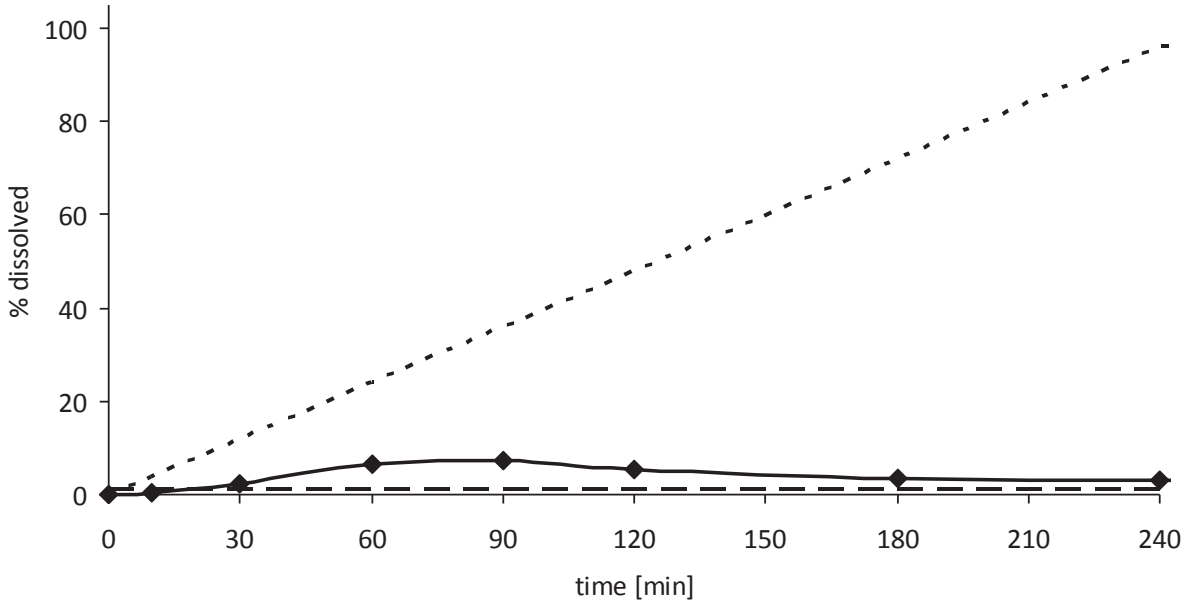


Fig. 3.24: Fed state transfer results (simulating the high fat meal) of 400 mg (2 x 200 mg) Reyataz[®] capsules using the 2 ml/min zero order transfer rate for 500 ml of FeSSGEm pH 5.0 (\blacklozenge) as a donor compartment. The solubility of atazanavir sulfate in FeSSIF-V2 (---) is presented along with the theoretical transfer curve (- -). Error bars are smaller than the symbols.



Results

Table 3.13: Maximum supersaturation ratios, fraction dissolved (f_d) and precipitation (k_p) constants of different doses of atazanavir sulfate (Reyataz[®]) for different simulated gastrointestinal states

Dose (mg)	Simulated GI state	Supersaturation ratio	f_{d1}	f_{d2}	k_p (h ⁻¹)
100	Fasted	33.77	0.114 (≤ 5 min)	0.7685 (> 5 min)	-
200	Fasted	32.34	0.040 (≤ 5 min)	0.6540 (> 5 min)	-
400	Fasted	36.67	0.058 (≤ 5 min)	0.4399 (> 5 min)	-
1200	Fasted	34.02	0.125 (≤ 30 min)	0 (> 30 min)	0.1642 (> 120 min)
400	Fed (light meal) (FeSSGEm pH 2.75)	26.32	0.230 (≤ 10 min)	0.6182 (> 10 min)	3.365 (> 30 min)
400	Fed (light meal) (FeSSGF pH 2.75)	-	0.040 (≤ 20 min)	1.000 (> 20 min)	-
400	Fed (high fat meal) (FeSSGF pH 5.0)	11.54	0.1026 (≤ 10 min)	0.3165 (> 10 min)	0.3527 (>90 min)



3.5 Atazanavir sulfate - *in silico* plasma profile simulation

3.5.1 Evaluation of distribution and elimination kinetics of atazanavir using WinNonLin[®] analysis of literature PK data

Generally, intravenous plasma profiles are considered necessary to investigate the post absorptive disposition kinetics of APIs. As in the case of cinnarizine, only oral data were available for atazanavir, so the distribution and elimination kinetics had to be estimated using observed oral plasma profiles of atazanavir sulfate formulations in the fasted and fed state with the help of a commercial pharmacokinetic software (Phoenix[®] WinNonLin[®] 6.3, Pharsight Corporation, Mountain View, CA, USA). Across fasted state studies the V_d/F value varied from $1636 \pm 150L$ (100 mg) to $266.9 \pm 244.7L$ (200 mg). Several further studies, which investigated the volume of distribution of atazanavir sulfate in patients (boosted and steady state, assuming maximal drug exposure) support a lower volume of distribution value of $\leq 103L$ [104, 141-144]. Pharmacokinetic studies on atazanavir sulfate demonstrated the compound to undergo a positive food effect under light meal conditions. Therefore it could be assumed that drug exposure was maximal (among the published pharmacokinetic studies) under light meal conditions. The apparent volume of distribution V_d/F (i.e. V_d adjusted for bioavailability factor F) for the fed state was estimated to be $82.9 \pm 7.4 L$, which is in accordance with published literature data. The apparent volume of distribution V_d/F in the light meal study should be closer to the “real” volume of distribution (V_d), since the F value in this fed state study was closer to 1.

Consequently, the lowest available V_d/F value from literature (400 mg atazanavir, boosted with ritonavir under fed state conditions) of 80.8L was implemented into the simulation software for the prediction of both pre- and postprandial plasma profiles [142]. The elimination constants k_{10} and clearance values were obtained from WinNonLin[®] specific to the administration conditions of each study. Distribution and elimination data for each dose of atazanavir are presented in Table 3.14.



Results

Table 3.14: Distribution and elimination parameters of atazanavir used for *in silico* simulations (STELLA[®] and Simcyp[®])

Parameter	Fasted state	Fed state (light meal)
Vd/F [142]	80.8 L	80.8 L
k ₁₀ (100 mg)	0.2269	-
k ₁₀ (200 mg)	0.2040	-
k ₁₀ (400 mg)	0.1595	0.1958
k ₁₀ (1200 mg)	0.1283	-
Cl (100 mg)	247.0 L/h	-
Cl (200 mg)	77.40 L/h	-
Cl (400 mg)	65.99 L/h	34.9 L/h
Cl (1200 mg)	63.00 L/h	-

3.5.2 Permeability evaluation of atazanavir

Atazanavir is generally assumed to be a BCS class II drug [105, 145]. Nevertheless a recent study supposed that the compound might belong to the BCS class IV due to its interplay with efflux proteins in the intestinal membrane [114]. Benet *et al.* reported that intestinal absorption of BCS class IV drugs is generally determined by uptake transporters and that drug elimination could be influenced by intestinal efflux transporters [146]. Atazanavir shows efflux transporter interactions in the intestine and excretion over the biliary pathway, which is in concordance with a class IV classification according to BDDCS. A Caco-2 study in the literature confirmed a concentration dependent atazanavir permeability ($1.5 - 8 \times 10^{-6}$ cm/s), which may be mediated via intestinal transporters [113]. Caco-2 and rat intestinal perfusion experiments have also been conducted using atazanavir solutions in FaSSIF and FeSSIF as donor phases. The investigation revealed that under simulated fed state conditions the permeability was significantly higher in both Caco-2 monolayers (FaSSIF: 1.75×10^{-6} cm/s v. FeSSIF: 1.25×10^{-5} cm/s) and rat intestine [114]. Since the BCS classification of atazanavir cannot be clearly defined from human studies, it was assumed that absorption of the compound is permeability restricted, whereby the permeability was measured to be higher under fed state conditions [114]. Thus, Caco-2 permeability values from the literature were integrated into STELLA[®] and Simcyp[®], implementing different values for the fasted state (for STELLA[®] variable values depending on the luminal concentration) and for the fed state [113]. The



permeability data used for simulations of atazanavir plasma profiles are presented along with other pre-absorptive parameters in Table 3.15.

Table 3.15: Pre-absorptive and absorptive parameters needed for the plasma profile simulation of atazanavir using STELLA®

Parameter	Fasted state	Fed state (light meal)
Gastric volume	250 ml	400 ml
Intestinal volume [119, 120]	212 ml	320 ml
Gastric emptying rate [117]	2.8 h ⁻¹	4 kcal/min
Permeability [113, 114]	1.5-8 x 10 ⁻⁶ cm/s	1.25 x 10 ⁻⁵ cm/s
A_{eff} [119]	3.6 m ²	3.6 m ²

3.5.3 STELLA® plasma profile predictions of atazanavir capsules in the fasted state

Simulations were performed by implementing the pre-absorptive and absorptive data from Table 3.15, distribution parameters (V_d/F and k_{10}) from Table 3.14 and the *in vitro* data (z values, f_d , k_p and precipitation time) from Tables 3.12 and 3.13 into the STELLA® supersaturation and precipitation model.

Atazanavir exhibits nonlinear pharmacokinetics. When the dose is increased from 100 mg to 200 mg atazanavir sulfate, the C_{max} increases more than 14-fold and the AUC more than 9-fold [106]. This observation can neither be explained by the dissolution results nor by the transfer experiments, both of which exhibited lower percentage of drug release at higher doses. By contrast, at doses between 400 and 1200 mg, proportionality of the AUC was observed [106].

It is therefore probable that factors other than drug dissolution are responsible for the nonlinear *in vivo* behavior between 100 and 200 mg doses. *In vitro* studies have shown atazanavir sulfate to be a substrate of P-gp [113, 147, 148]. Interactions with other efflux and influx proteins are also possible, since the compound was also found to be a substrate for multidrug resistance protein (MRP) and breast cancer resistance protein (BCRP) [149]. Kis *et al.* reported that the P-gp efflux of atazanavir might be saturable [113]. Yet other sources report that atazanavir may be an inhibitor of the P-



Results

gp [106, 145, 150, 151]. On the basis of the information, it seems likely that drug efflux is greater when lower doses of atazanavir sulfate are administered and that at higher doses the P-gp efflux becomes saturated, resulting in supra-proportional increases in C_{max} and AUC compared to the 100 mg dose.

Moreover, atazanavir may undergo saturable presystemic first pass extraction. Atazanavir is reported to be largely metabolized in the liver and excreted over the biliary pathway [106]. The drug is mainly metabolized by CYP3A and conjugated by UGT1A1. Atazanavir was revealed to be a moderate inhibitor of CYP3A4 and a competitive inhibitor of UGT1A1 [145]. Thus, a saturation of atazanavir first pass CYP3A4 biotransformation is also possible at higher doses. The hypothesis that atazanavir undergoes saturable presystemic drug efflux and extraction is supported by the fact that when it is co-administered with ritonavir, an inhibitor of P-gp and CYP3A4, a significantly higher pharmacokinetic profile is observed than when it is administered alone [137, 152, 153]. An investigation of the metabolism of atazanavir in the fed state revealed that almost 79% of the administered dose of 400 mg was eliminated in fecal matter, mainly as metabolites (85%). 13.1% of the API were found in urine [106]. This would suggest a fraction of atazanavir absorbed of 0.80 (= $0.79 \times 0.85 + 0.131$) at this dose.

Taking all the aforementioned factors into account, it was assumed that for the 100 mg dose high drug efflux or/and first pass extraction occurs. However, the rate and extent of these processes has not been reported in the literature *bis dato*. Thus, to fit the pharmacokinetic profile an extraction rate had to be estimated using equation 8. Caco-2 experiments on atazanavir exhibited concentration dependent permeability. The $B \rightarrow A/A \rightarrow B$ ratio, which indicates the extent of drug efflux (efflux possible at values >10), was 11 at 1 μM (0.704 $\mu\text{g/ml}$) and still about 10 at concentrations under 10 μM (7 $\mu\text{g/ml}$). It was assumed that, for the 100 mg dose lower atazanavir concentrations initially reach the intestine during gastric emptying resulting in P-gp efflux of the compound. Moreover, due to reports about atazanavir first pass metabolism and biliary excretion, which additionally significantly contributed to low bioavailability of the 100 mg dose, an efflux/extraction rate of 90% was assumed [106]. For doses higher than 100 mg a saturation of efflux/extraction was presumed,



resulting in exclusion of efflux/extraction kinetics in the simulations. The simulated profiles of the 100 mg dose, with and without efflux/extraction, are shown in Figure 3.25.

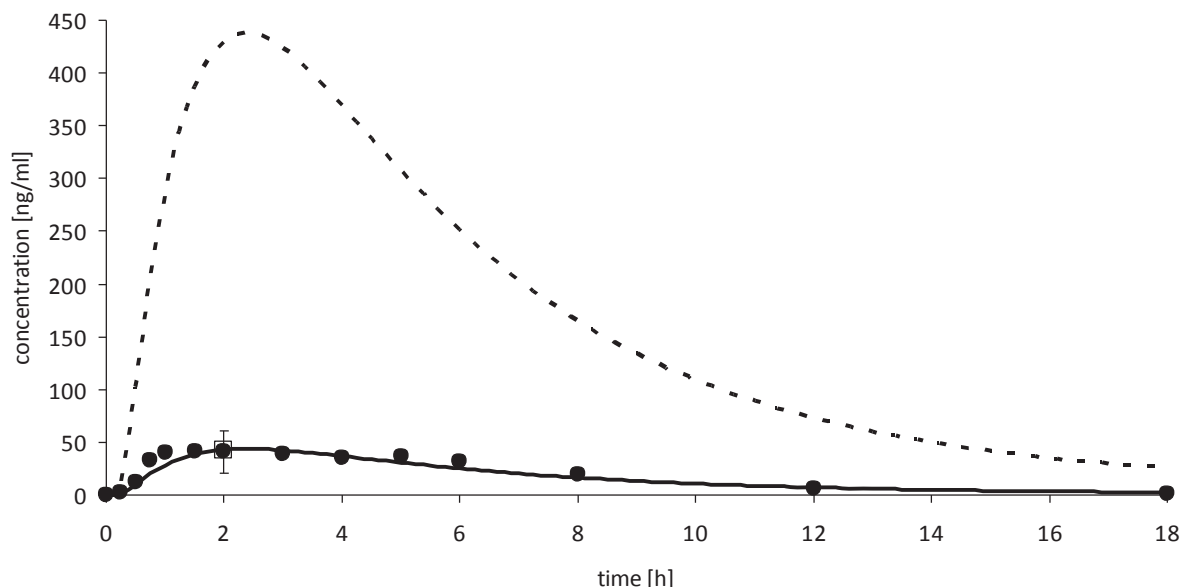


Fig. 3.25: Observed (●) and predicted fasted state plasma profiles of 100 mg atazanavir sulfate capsules with 90% (—) and without (---) efflux/extraction kinetics. Coefficient of variation is shown for the C_{max} value (reported as geometric mean (□)).

When efflux and first pass elimination were not considered in the PBPK model, the simulation vastly overestimated the pharmacokinetic profile of the 100 mg dose. Due to the combination of first pass elimination and P-gp-based efflux an extraction constant of 0.9 (90%) was taken into consideration, were the simulation results in agreement with the *in vivo* pharmacokinetic profile.

Predictions of the fasted state profiles of 200, 400 (2 x 200) and 1200 (6 x 200) mg capsules are presented in Figure 3.26. The simulations appear to increasingly underestimate the mean *in vivo* performance of the compound as the dose is increased. However, it must be noted that atazanavir exhibits highly variable pharmacokinetics. The coefficients of variation (CV) of the *in vivo* profiles were high and increased with higher doses (> 43% for AUC and > 52% for C_{max}) [106]. Standard deviation values were only reported for the C_{max} value, not for concentrations at other time points. Taking this variability into account, the predictions at all doses lie safely within the CV. The *in vivo* to *in silico* comparison of

Results

pharmacokinetic parameters AUC, C_{max} and t_{max} of all investigated doses is presented in Table 3.16.

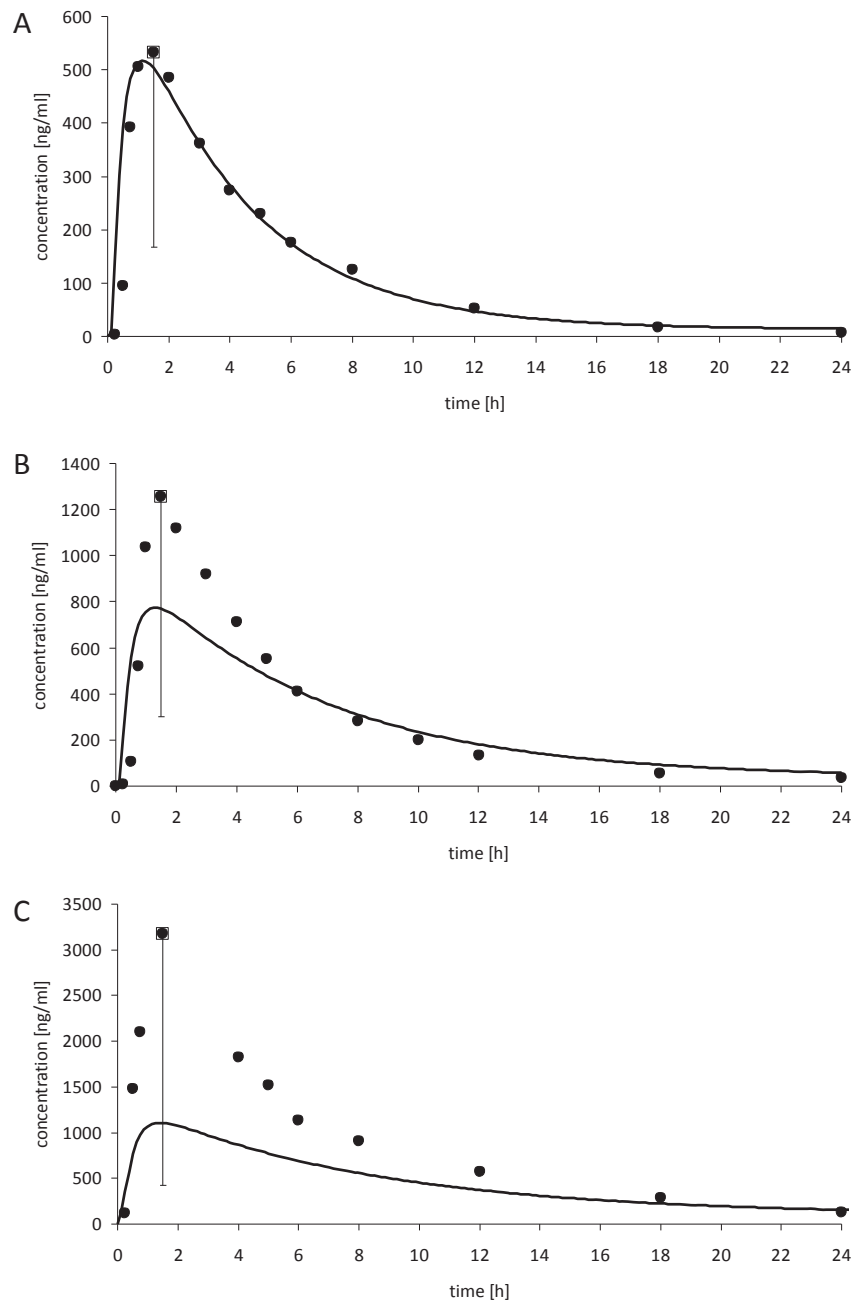


Fig. 3.26: Observed (●) and predicted fasted state plasma profiles of 200 mg (A), 400 mg (B) and 1200 mg (C) atazanavir sulfate capsules (—). Coefficients of variation are shown for the C_{max} values (reported as geometric means (□)).



Table 3.16: *In vivo* and predicted pharmacokinetic parameters for different doses of atazanavir sulfate in the fasted state.

Atazanavir sulfate 100 mg			
	AUC ₀₋₁₈ (ng x h/ml)	C _{max} (ng/ml)	t _{max} (h)
<i>in vivo</i>	311*	41*	2.0
<i>predicted (no efflux/extraction)</i>	3090	437	2.38
<i>predicted (90% efflux/extraction)</i>	333	44	2.38
Atazanavir sulfate 200 mg			
	AUC ₀₋₂₄ (ng x h/ml)	C _{max} (ng/ml)	t _{max} (h)
<i>in vivo</i>	2828*	533*	1.5
<i>predicted</i>	2864	518	1.25
Atazanavir sulfate 400 mg			
	AUC ₀₋₂₄ (ng x h/ml)	C _{max} (ng/ml)	t _{max} (h)
<i>in vivo</i>	6721*	1255*	1.5
<i>predicted</i>	6431	774	1.25
Atazanavir sulfate 1200 mg			
	AUC ₀₋₂₄ (ng x h/ml)	C _{max} (ng/ml)	t _{max} (h)
<i>in vivo</i>	20648*	3175*	1.5
<i>predicted</i>	11161	1107	1.5

*Since *in vivo* data were calculated from mean concentration/time plasma profiles variability of AUC and C_{max} is not available.

STELLA[®] plasma profile predictions of atazanavir capsules in the fed state (light meal)

Simulation results using the two different transfer experiments of atazanavir sulfate capsules (2 x 200 mg Reyataz[®]) in the fed state are presented in Figure 3.27 and Table 3.17. The *in silico* simulation which incorporated the results of the transfer experiment using FeSSGEm pH 2.75 as the donor medium was considered as the “worst case”. By contrast, the model utilizing transfer data, in which FeSSGF pH 2.75 was the donor compartment, was regarded as the “best case”. The results show that these two simulations made it possible to bracket the pharmacokinetic profile of atazanavir in the fed state. These simulation results imply that big interindividual differences in the intestinal dissolution, supersaturation and precipitation are possible, which would significantly influence the *in vivo* performance of the compound. Interestingly, creating a profile, which represents the average of the “best” and “worst” cases, came close to the *in vivo* data.



Results

Good simulation results could only be achieved when the Caco-2 permeability data obtained in FeSSIF was used. Low permeability values, such as those obtained from Caco-2 experiments in FaSSIF, resulted in underestimations of the *in vivo* profiles for most of the simulations (shown in Section 3.5.5). These results provide a kind of validation that the differences observed in the Caco-2 experiments are relevant for human pharmacokinetics.

Additionally, the light meal contained orange juice. Orange juice on the one hand is expected to result in an acidic pH in the fed state gastric fluid. On the other hand, it has been reported that orange juice might inhibit P-gp in the intestinal lumen [37, 106], noting that the effect is not considered to be as pronounced as demonstrated for grapefruit juice. These two factors could together be responsible for the better *in vivo* performance of atazanavir under light meal conditions than under a high fat meal. Indeed, in some studies the *in vivo* performance of atazanavir under high fat meal conditions was worse than in the fasted state [138]. It is postulated that the positive food effect under light meal conditions as compared to fasted state is driven by four major factors:

1. better solubilization of atazanavir sulfate in the fed state gastric fluids after a light meal due to the relatively low gastric pH (the high fat meal had an initial pH of 6.51 [154]),
2. possible solubility enhancement through interaction with the proteins in the meal,
3. better intestinal permeability due to higher bile salt concentration in the fed state and
4. better intestinal permeability due to possible P-gp efflux inhibition by orange juice.

Factors 1, 2 and 3 were taken into consideration by applying transfer model results and appropriate Caco-2 data for the simulations. Factor 3 was additionally confirmed by perfusion experiments through rat jejunum and ileum using FaSSIF and FeSSIF as apical media, where the permeability of atazanavir was higher when the latter solution was utilized. However, the extent of the P-gp inhibition by orange juice has

not been studied for atazanavir. A further reservation about the importance of this effect is provided by simulations of the fasted state, which assumed saturation of the P-gp efflux at the 400 mg dose of atazanavir sulfate used in the food effect PK study.

In general, the simulation results suggest that the modeling approach is appropriate. Since atazanavir is a compound with highly variable PK, exact predictions cannot be expected. The absorption of the API seems to be influenced by many factors, including drug efflux and first pass extraction, drug and bile salt concentration dependent permeability, gastric pH, and food components such as fruit juices and proteins. Additionally, it is also possible that some further factors influencing atazanavir absorption have not been identified yet.

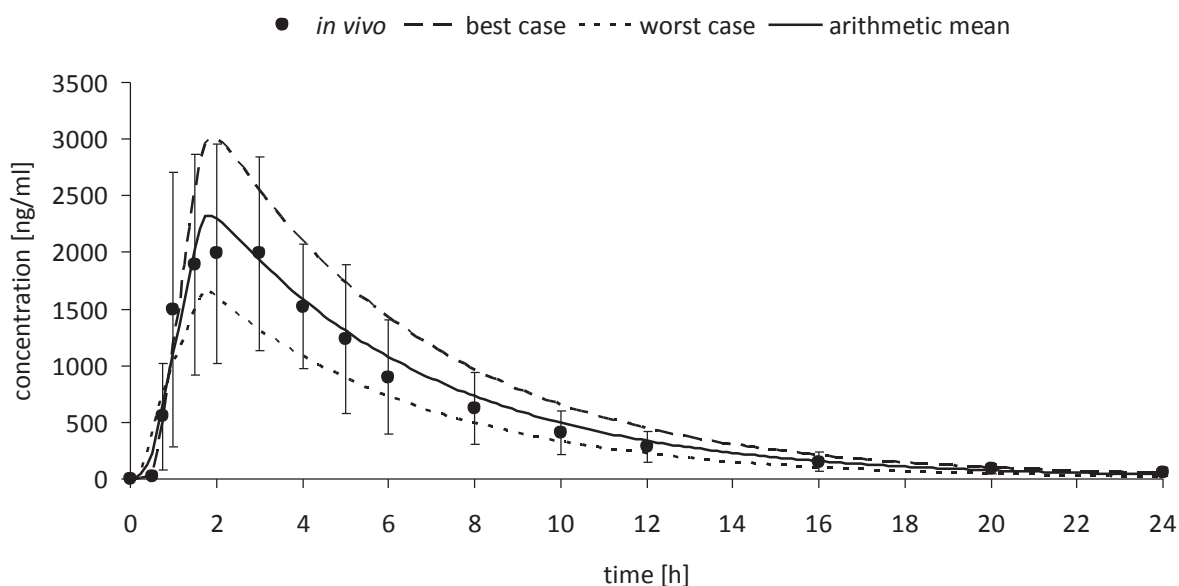


Fig. 3.27: Observed and predicted fed state plasma profiles of 400 mg atazanavir sulfate (2 x 200 mg Reyataz[®]) capsules. Predictions were made using different transfer experiments using either FeSSGF pH 2.75 (“best case”) or FeSSGEm pH 2.75 (“worst case”) as donor media. The solid line shows the average of the best and worst case scenarios.



Results

Table 3.17: *In vivo* and predicted pharmacokinetic parameters for 400 mg atazanavir sulfate (2 x 200 mg Reyataz[®]) capsules in the fed state

Atazanavir sulfate 400 mg	AUC ₀₋₂₄ (ng x h/ml)	C _{max} (ng/ml)	t _{max} (h)
<i>in vivo</i>	13232	1988	2
<i>best case</i>	18619	3009	1.88
<i>worst case</i>	10063	1680	1.88
<i>arithmetic mean</i>	14341	2324	1.88

3.5.4 STELLA[®] sensitivity analysis on atazanavir plasma profile predictions

In this section the sensitivity analysis is illustratively discussed for atazanavir sulfate 400 mg capsules in the fasted state as well as in the fed state (“worst case” and “best case”) in Figures 3.28 to 3.30. The fasted state sensitivity analyses of the 100, 200 and 1200 mg doses exhibited similar behavior to the 400 mg dose and therefore are presented in the Appendix section.

The sensitivity analysis was performed to identify the pre-systemic parameters which are most important for the simulation of atazanavir plasma profiles using the STELLA[®] model. For this purpose the fasted and fed state gastric emptying rate (GER) and effective permeability (P_{eff}) values were varied in the range of 0.25-5 times GER and P_{eff} . Fraction dissolved (f_d) values were varied between 0 and 1, and the precipitation constant (k_p) values were varied 0.25-5 fold. To investigate the impact of systemic factors such as elimination and volume of distribution on plasma profile predictions, k_{10} and Vd/F were varied 0.25-5 fold.

For the fasted state simulations (Figure 3.28), the plasma profile predictions at all doses appear to be sensitive to changes in almost all factors investigated. Vd , the parameter addressing distribution in the human body, proved to be the factor to which the simulated plasma profile is most sensitive at all doses and in all dosing conditions. Other factors to which the simulation is highly sensitive were the fraction dissolved (f_d at time > 5 min), and the GER. Variations in the constant f_d represent changes in the concentration of dissolved API available for absorption. For atazanavir sulfate, changes in the f_d value result in changes in the C_{max} and AUC, but

not in the t_{max} values. Elimination (k_{10}) also plays an important role in plasma profile predictions, especially at longer times after dosing. However, the large changes in the k_{10} value necessary to invoke the variation in the prediction do not reflect data observed *in vivo*, and were chosen only to illustrate their effects on the PK profile. Alterations of P_{eff} caused a large shift in t_{max} , but minor changes of C_{max} and AUC, while the dissolution at early times (f_d at time < 5 min) had some effect on C_{max} , but little on t_{max} or AUC.

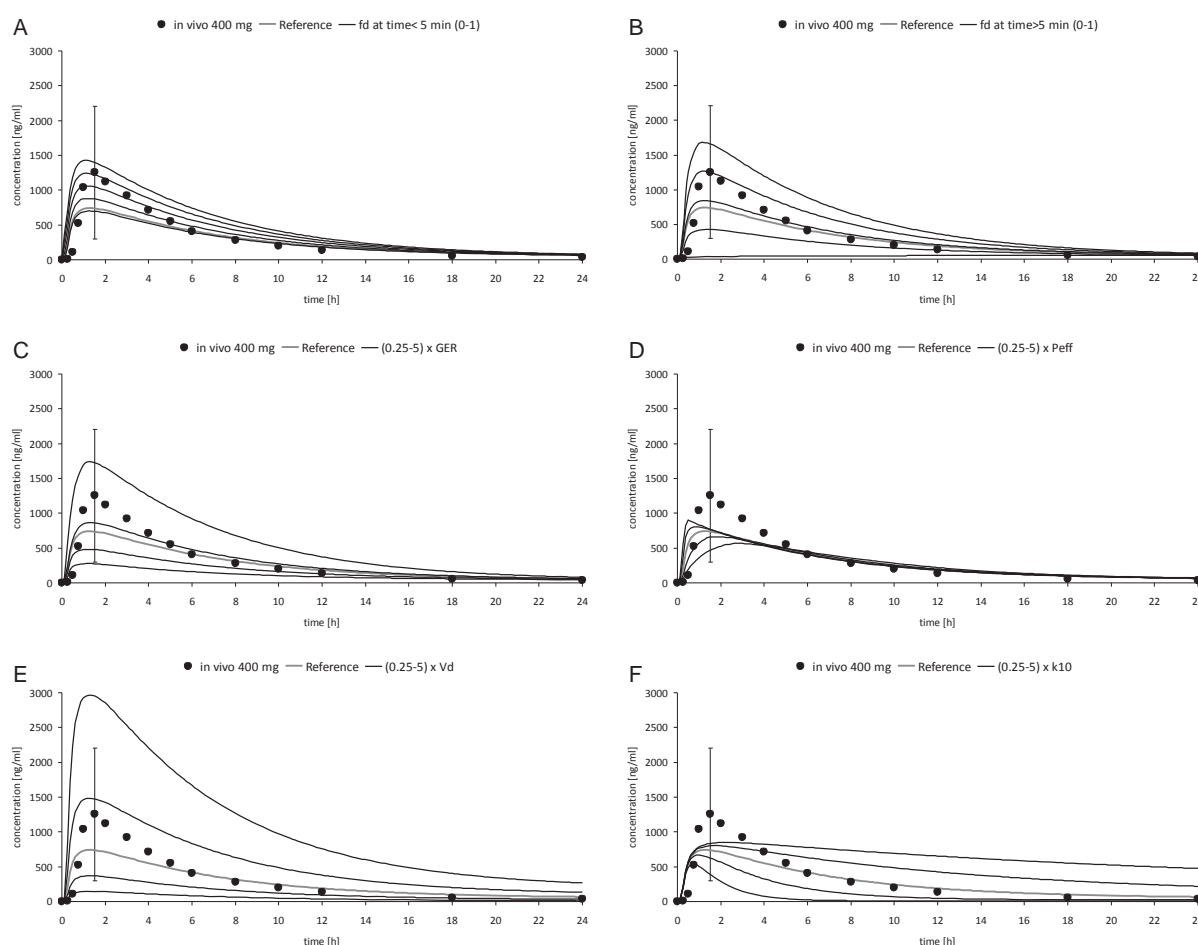


Fig. 3.28: Sensitivity analysis of the fraction dissolved constant < 5 min (A), the fraction dissolved constant > 5 min (B), the gastric emptying constant (C), the permeability (D) the volume of distribution (E), and the elimination constant (F) on plasma profile predictions of 400 mg (2 x 200 mg) atazanavir sulfate capsules in the fasted state. The observed *in vivo* profile is shown along with coefficient of variation for the C_{max} value (reported as geometric mean).

In the fed state (Figures 3.29 and 3.30), as in the fasted state, the predicted plasma profiles are sensitive to changes in most parameters.

In the “worst case” fed state example (FeSSGEm pH 2.75, light meal) drug precipitation was observed for the fed state, so precipitation effects (k_p) were also



Results

investigated and the plasma profile predictions of atazanavir proved to be sensitive to alterations in the k_p value. Gastric emptying was demonstrated to have an influence on the C_{max} and t_{max} values of the simulation. The C_{max} and AUC are mostly dependent on the P_{eff} value. Drug (re-)dissolution in the intestine as a result of higher permeability is assumed to be responsible for this phenomenon (as seen for DCS class 2a compounds). This behavior is not observed in the “best case” simulations, since most of the drug was calculated to be in solution in the upper intestinal compartment. Since availability of dissolved drug is dependent on the GER, alterations of the P_{eff} value have little influence on the t_{max} , as for the fasted state. Additionally the sensitivity analysis suggests that plasma profile variability is expected to be lower in the fed state, since the gastric emptying in the fed state (zero order kinetics) is likely to be less variable than in the fasted state. This is expected to have a knock-on effect on most of the factors which are dependent on the GER, such as the f_d and k_p . Indeed, the *in vivo* plasma profile variability of the 400 mg dose was observed to be lower for the fed state (31.08%) than for the fasted state (84.18%) [106].

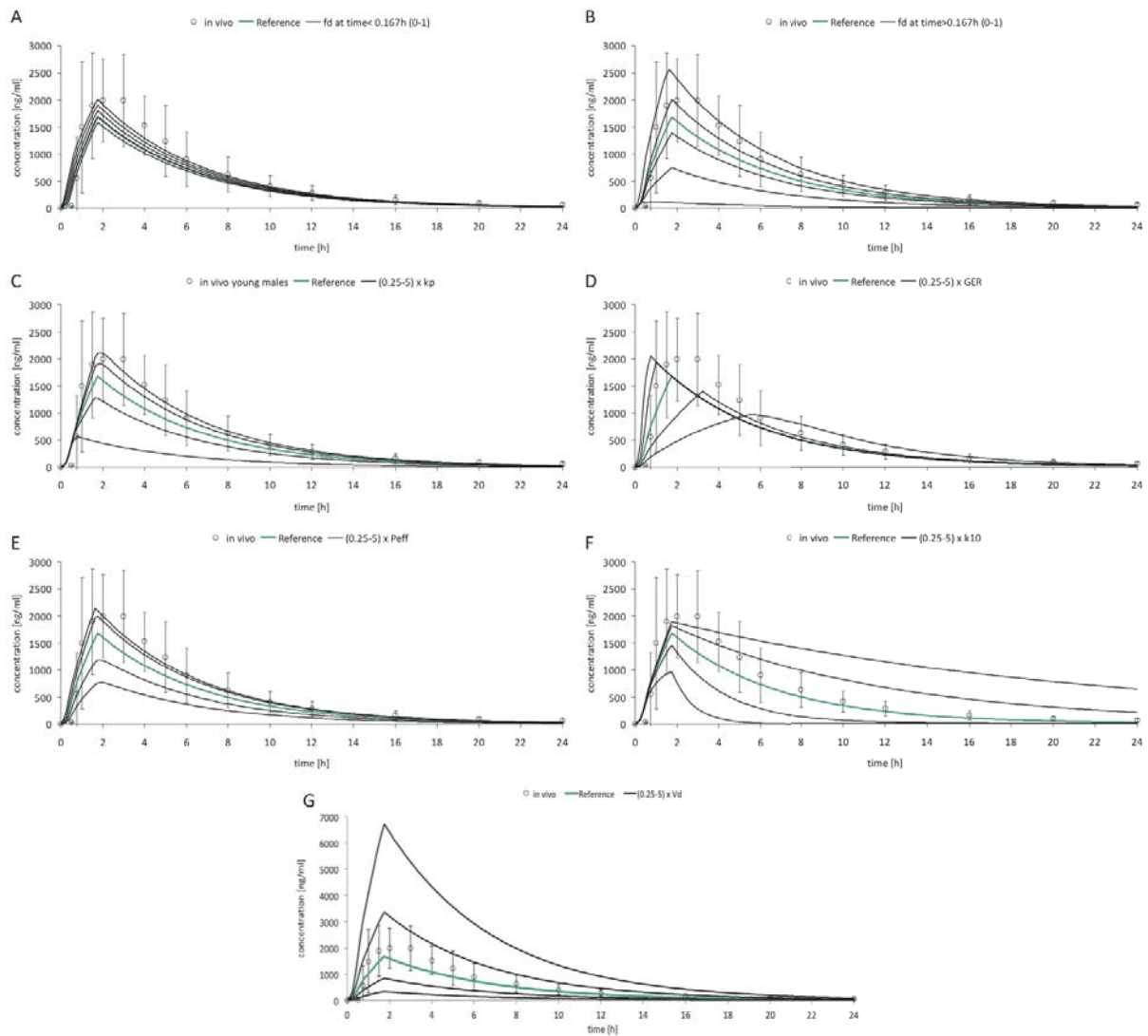


Fig. 3.29: Sensitivity analysis was performed for simulations using data obtained from transfer experiments with FeSSGE_m pH 2.75 as the donor compartment (“worst case”). Analysis of the fraction dissolved constant < 10 min (A), the fraction dissolved constant > 10 min (B), the precipitation constant (C), the gastric emptying constant (D), the permeability (E), the elimination constant (F), and the volume of distribution (G) on plasma profile predictions of 400 mg (2 x 200 mg) atazanavir sulfate in the fed state.

Results

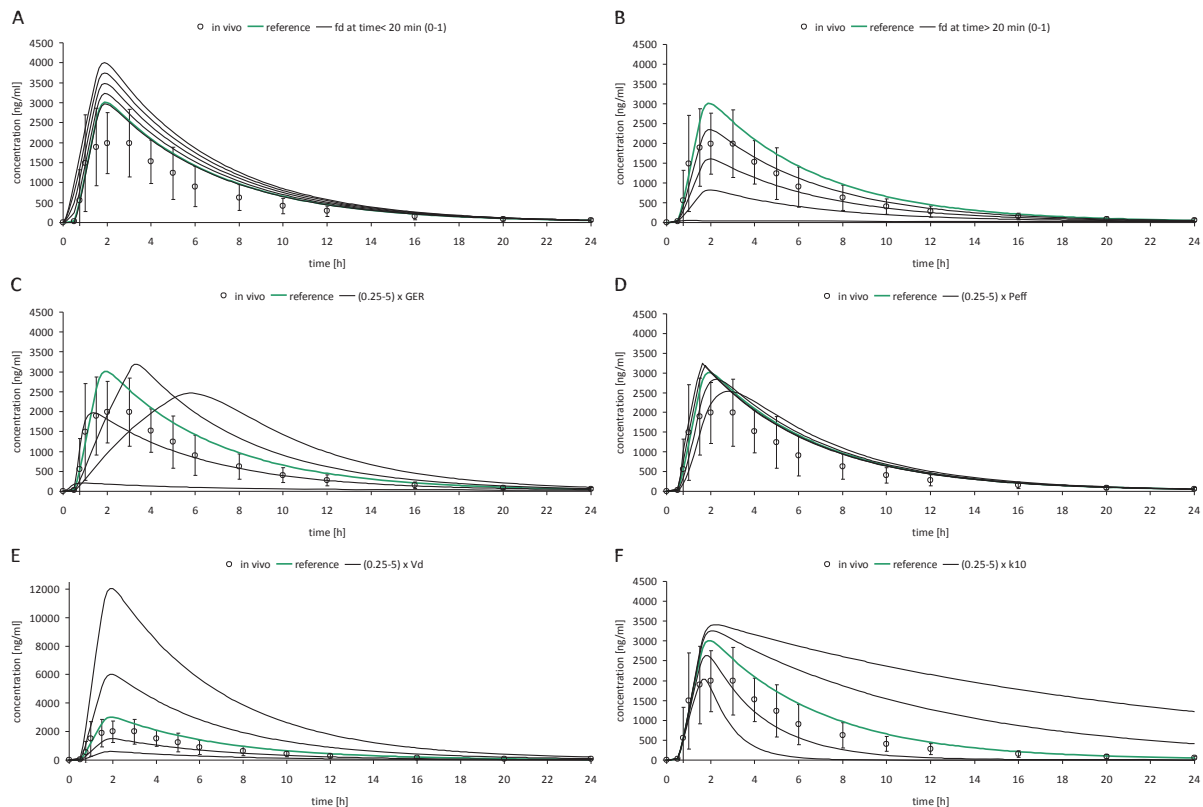


Fig. 3.30: Sensitivity analysis was performed for simulations using data obtained from transfer experiments with FeSSGF pH 2.75 as the donor compartment (“best case”). Analysis of the fraction dissolved constant < 20 min (A), the fraction dissolved constant > 20 min (B), the gastric emptying constant (C), the permeability (D), the volume of distribution (E) and the elimination constant (F) on plasma profile predictions of 400 mg (2 x 200 mg) atazanavir sulfate in the fed state.

The sensitivity analysis demonstrates that the plasma predictions of atazanavir depend on all parameters describing pre-absorptive, absorptive and post-absorptive behavior of the compound. The pre-absorptive factors, hence drug dissolution, supersaturation, precipitation and gastric emptying underscore the highly variable pharmacokinetic profile of this API and make it challenging to predict the *in vivo* performance of the compound in any given study. The absorptive factor is mostly described by the P_{eff} value, which proved to have a significant impact on the PK of atazanavir, especially in the fed state (“worst case”). However, the Vd value was demonstrated to have the largest effect on plasma profile predictions (Figure 3.30, panel E). Since the compound exhibited a highly variable PK profile (described by highly variable Vd in Section 3.5.1), factors related to post-absorptive behavior, seem to play the key role for drug bioavailability and outweigh the variability of pre-absorptive and absorptive parameters.



3.6 Summary of atazanavir plasma profile simulations using Simcyp[®]

A detailed description of atazanavir plasma profile simulations using Simcyp[®] can be found in the Appendix section. Simulations of atazanavir plasma profiles using Simcyp[®] demonstrated overall reasonable predictions, which were similar to the results calculated with STELLA[®]. Different simulation approaches (GI solubility, predicted solubility, pH/equilibrium solubility profile) demonstrated similar predictions of plasma profiles in the fasted state. All simulations overestimated the *in vivo* performance of 100 mg atazanavir sulfate capsules. Efflux/extraction could not be simulated for the 100 mg dose (as it was possible with STELLA[®]), since concrete Michaelis-Menten kinetic data were necessary, but not available for simulations. With increasing doses plasma profiles were increasingly underestimated. The sensitivity analysis demonstrated that post-absorptive factors had the most significant influence on the plasma profile predictions. The pre-absorptive and absorptive parameters had relatively little influence on the plasma profile variability of atazanavir. Simulations of postprandial (light meal) plasma profiles were realistic for the three simulation approaches applied. The implementation of biorelevant solubility into the GI solubility mask led to most representative simulations.

Similar to the investigation of cinnarizine, the volume of distribution (V_d) of atazanavir seemed to be overestimated in Simcyp[®]. When predicted solubility or pH dependent equilibrium solubility values were utilized for simulations of the light meal *in vivo* performance of 400 mg atazanavir sulfate capsules, 100% absorption was calculated. This prediction is at odds with an *in vivo* mass balance study which calculated a fraction absorbed of approximately 80% for the 400 mg dose in the fed state [106]. These considerations indicate that a smaller V_d value is probably more applicable for Simcyp[®] simulations.

Based on the simulations and sensitivity analysis, it is predicted that atazanavir clearance and volume of distribution is subject to high interindividual post-absorptive variability. Moreover, post-absorptive elements such as first-pass metabolism play a crucial role on atazanavir bioavailability, since they may be significantly influenced by



Results

the atazanavir sulfate dose, the prandial state and co-medication (e.g. boosting effect by ritonavir).

3.7 Summary of the atazanavir investigation and formulation suggestions

The *in vitro* investigation of atazanavir sulfate formulations using the transfer model exhibited unique supersaturation and precipitation behavior for both the simulated fasted and fed state. In the fasted state a stable supersaturation of the drug was observed for at least 2 hours. *Per contra* the supersaturation was not stable (FeSSGEm pH 2.75 or FeSSGEm pH 5.0) or nonexistent (FeSSGEm pH 2.75) under simulated light meal conditions with orange juice. The transfer investigations of atazanavir sulfate capsules under simulated fasted and fed state conditions were qualitatively in agreement with the pharmacokinetic studies. The food effect under light meal conditions could be qualitatively assessed with transfer experiments. Moreover, the results indicated a possible negative food effect under high fat meal conditions, which was also observed in literature.

The *in silico* simulations using the STELLA[®] supersaturation and precipitation model were mostly consistent with the *in vivo* data. Furthermore, implementation of efflux kinetics into the model demonstrated that saturable P-gp and first-pass hepatic extraction might be responsible for nonlinear pharmacokinetics of atazanavir in the fasted state. However, concrete data were not obtainable to simulate efflux/extraction kinetics appropriately. Simulations increasingly underestimated the *in vivo* performance for higher doses of atazanavir in the fasted state. It was concluded that underestimations most probably originated from higher variability of clearance and volume of distribution when high doses were administered. On the other hand simulations using *in vitro* transfer data could define the *in vivo* variations of the compound in the fed state under light meal conditions.

Simcyp[®] simulations of the fasted state *in vivo* performance produced qualitatively similar results to these obtained when using STELLA[®]. The use of compartmental GI solubility exhibited the best simulation performance. Simcyp[®] simulations of cinnarizine supersaturation and precipitation underestimated the *in vivo* performance



of the compound. Similar results were exhibited in simulations of atazanavir supersaturation and precipitation in the fed state. Even though Simcyp[®] simulations performed better for atazanavir than for cinnarizine, simulations with STELLA[®] gave more realistic estimates of *in vivo* performance in general.

Variation in atazanavir permeability had a relatively little effect on the bioavailability in both prandial states (except for the fed state “best case” example, where atazanavir dissolution is presumably overestimated). However, studies have shown that atazanavir permeability was higher under fed state conditions [114]. Thus, it is possible that the positive food effect under light meal conditions may be affected not only by pH of the gastric milieu, but also by bile salt mediated permeability enhancement.

In summary, the following conclusion can be drawn on atazanavir formulation development. A salt formation of atazanavir has shown to be the most promising approach to enhance (kinetic) drug solubility in the GI tract. The development of an amorphous atazanavir salt did not reveal a significant improvement of drug solubility or dissolution compared to crystalline atazanavir sulfate. For example the transfer study, which compared the dissolution behavior of the crystalline salt and the predominantly amorphous form of atazanavir sulfate, confirmed that the profiles were not significantly different *in vitro* (Figure 3.21). This observation is consolidated by reports in literature, where the administration a fixed dose of different solid states of atazanavir sulfate did not reveal significant differences *in vivo* [140].

The *in vitro* and *in silico* investigation of atazanavir supersaturation and precipitation implies that efforts to improve PK through further formulation enhancement of the compound may not be as productive as for cinnarizine. In the sensitivity analysis, pre-absorptive factors had relatively little impact on the PK of atazanavir. However, it was shown that supersaturation and precipitation may play a role in drug bioavailability in the fasted and fed state. This implies that there could be alternative ways of enhancing drug solubility and supersaturation, and reducing drug precipitation. Several optimized atazanavir formulations such as SNEDDS, nanoparticles and solid dispersions have been reported to date [155-157]. However,



Results

most studies compared the optimized formulation with the free atazanavir base and not with the hydrosulfate salt of the compound. Thus, a clear improvement to the marketed formulation could not yet be identified. Moreover, all of the *in vivo* studies of these formulations were conducted in homogeneous rat populations, whereby PK variability of the drug was automatically reduced. Hence, the studies on atazanavir formulation improvement do not clearly indicate that bioavailability enhancement may take place *in vivo*.



4 General discussion and conclusions

4.1 Choosing the right *in vitro* investigation approach

The design of biorelevant media and their application to *in vitro* solubility and dissolution testing have proven to be two important developments in the quest to predict the *in vivo* behavior of oral pharmaceutical products. These were accompanied by the introduction of the transfer model, which enabled the simulation of gastric emptying, and thus investigation of the supersaturation and precipitation behavior of poorly soluble compounds. A number of investigations have demonstrated successfully that advanced *in vitro* techniques, such as the transfer model, can be essential to simulation of the *in vivo* performance of poorly soluble weak bases [59, 60, 62-64, 94, 158, 159]. Moreover they can suggest approaches for formulation development of these drugs. In the current studies, cinnarizine and atazanavir exhibited quite distinct *in vitro* behavior in terms of dissolution, supersaturation and precipitation. The different behavior of the two compounds indicates that, even for drugs which have generally similar physicochemical properties, *in vivo* behavior may be quite different.

In 2005 the US Food and Drug Administration (FDA) introduced the Question-based review (QbR), which basically focused on assuring product quality through design and performance based specifications [160]. In the late 2000s the QbR was extended by the International Conference on Harmonisation (ICH) to the Quality by Design (QbD) approach, which has taken hold in the pharmaceutical industry [161]. QbD is involved in all aspects of pharmaceutical development, including designing, developing and testing of formulations. The key principles of QbD are described by the ICH in the following guidelines: Pharmaceutical Development (Q8), Quality Risk Management (Q9) and Pharmaceutical Quality System (Q10). The aim of the Q8 guideline is to apply knowledge from scientific approaches and quality risk management to development of a product and its manufacturing process. It is intended to provide a comprehensive understanding of the product and manufacturing process for reviewers and inspectors. Additionally, it can create a basis for flexible regulatory approaches through demonstration of greater understanding of pharmaceutical and manufacturing sciences. ICH Q9 provides the



General discussion and conclusions

key principles and instruments of quality risk management, which may be applied in all aspects of pharmaceutical development, manufacturing and distribution. Guideline Q10 defines a model of an effective pharmaceutical quality system based on International Organization for Standardization (ISO) guides and Good Manufacturing Practices (GMP) including the ICH Q8 and Q9 guidelines. The guideline supports efforts on the part of industry and regulatory authorities to enhance quality and availability of medicines around the world.

To improve efficiency of pharmaceutical development the design of experiments (DoE) approach can be implemented. Using these methods a quality target product profile (QTPP) can be set and validated.

Taking the QbD approach, an experimental outline was established to aid decision-making in the development of drug products containing weak bases. Figure 4.1 illustrates the proposed experimental framework.

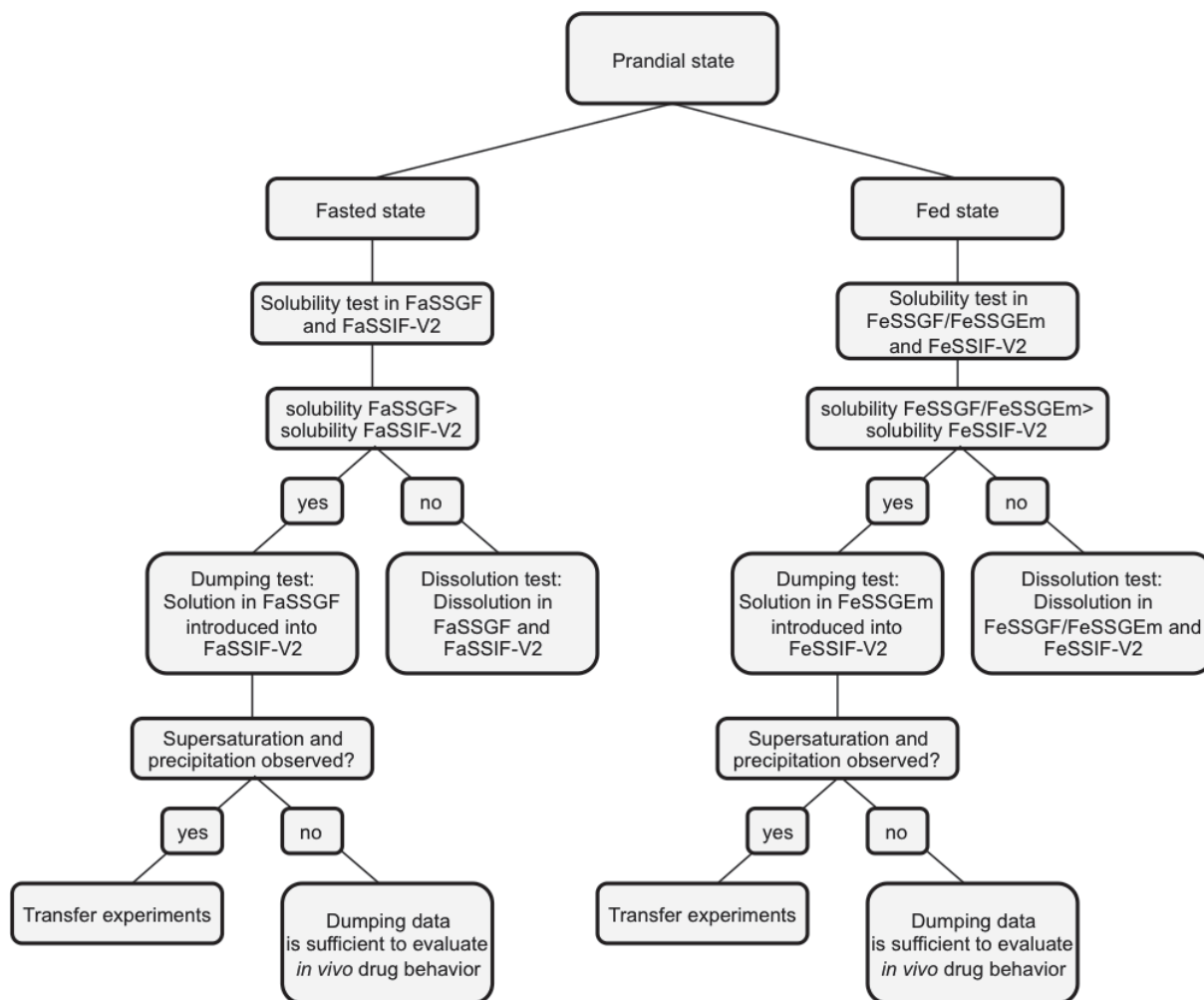


Fig. 4.1: Proposed outline of *in vitro* experiments for investigation and development of drug products containing weak bases.

Before embarking on laboratory work, a decision should be reached about which prandial state(s) need(s) to be examined. When both the fasted and the fed states are to be considered, studies should be run for both states in parallel. Solubility tests are first performed in the simulated gastric and intestinal media for each GI state. If the solubility is observed to be similar or higher in simulated intestinal media than in simulated gastric media, precipitation of the drug in the intestine will be improbable. In this case, it will be sufficient to run individual dissolution tests in both the simulated gastric and intestinal media to simulate the *in vivo* dissolution behavior of the drug product. On the other hand, if the solubility in the simulated intestinal media is lower than in gastric media (which is more usual for weak bases), supersaturation and precipitation of the compound may occur after gastric emptying and should be investigated. The simplest method to investigate the supersaturation and precipitation of compounds is the dumping test. The setup is utilized as a precursor



General discussion and conclusions

for transfer experiments and gives insight as to whether more specific transfer experiments have to be performed. If supersaturation is stable, or conversely if there is instant precipitation to the solubility value, the use of the dumping test may be sufficient for predicting *in vivo* behavior, since the supersaturation or precipitation behavior of the compound is not expected to be transfer rate dependent (e.g. as observed for atazanavir sulfate). But when supersaturation and precipitation are observed over time in the dumping experiment, the use of more specific transfer experiments is recommended for formulation development, since the kinetics of the two processes may change with different transfer rates (as observed for cinnarizine).

Fasted state transfer experiments should be performed with FaSSGF pH 2.0 as a donor medium to avoid drastic pH shifts in the acceptor medium, FaSSIF-V2. Additionally, FaSSIF-V2 should be constructed with phosphate buffer for this purpose. Alternatively, the older version of FaSSIF (V1) may be utilized to investigate the supersaturation and precipitation behavior of API and API products. However, if the *in vitro* data are to be coupled with *in silico* models to predict the *in vivo* drug performance, it is advisable to use the updated biorelevant medium, FaSSIF-V2.

Fed state transfer experiments should be performed using FeSSGEM as the donor medium. FeSSGEM was demonstrated to be discriminating in terms of the supersaturation and precipitation analysis of weakly basic drugs. Moreover, the analytical method seems to be more reliable when using FeSSGEM instead of FeSSGF. Since FeSSGF contains proteins from milk, it cannot be filtered using small pore size filters. Instead, filters with approximate pore size of 2.7 μm have to be utilized. This procedure does not assure separation of non-dissolved drug particles and thus may overestimate the concentration in solution of certain drugs. Additionally, specific gastric media may need to be developed to represent the gastric conditions of *in vivo* studies. In the case of atazanavir the pH of FeSSGEM and FeSSGF had to be reduced from 5 to 2.75 to simulate conditions after an ingestion of a light meal containing orange juice. Other factors such as the co-administration of H₂ antagonist and proton pump inhibitors (PPI) could also be considered, since they increase gastric pH and thus may limit the dissolution of weak bases in the stomach. The decision tree serves as a guide to decide which



experiments are most appropriate for the investigation of *in vivo* behavior of weakly basic drugs. *Prima facie*, for poorly soluble weakly basic drugs not all of the experiments are essential to assess drug dissolution behavior in the GI tract. In the case of the two compounds investigated only a fraction of the experimental outcomes was actually utilized for *in silico* simulations.

The selection of appropriate *in vitro* experiments is a crucial decision process in drug investigation and formulation development. It enables the assessment of the parameters which will be physiologically relevant to drug absorption. For weak bases these parameters can include the maximum supersaturation ratio, the critical (supersaturation) concentration, the precipitation kinetics and the onset of precipitation. *In vivo*, these processes may be additionally dependent on other parameters such as hydrodynamics, volume gastric and intestinal fluids, gastric emptying rates, bile salt concentrations and drug absorption. In the future, *in vitro* investigations should consider all of these parameters, taking into account the following issues:

- Reproducing GI hydrodynamics is complicated, since the movement of GI fluids is not uniform and varies depending on different MMC phase and prandial state. Variations in hydrodynamics, e.g. the rotation speed in the dissolution tester, could possibly be used for bracketing the hydrodynamic states of the GI tract and their influence on drug dissolution and precipitation.
- The influence of gastric emptying kinetics on supersaturation and precipitation of weak bases was partly investigated in this work (see cinnarizine example). Generally one would assume that the degree of supersaturation might be directly related with gastric emptying. For compounds exhibiting both supersaturation and precipitation, different phases of the MMC may have a crucial influence on drug absorption and can be simulated by applying different pumping rates during transfer experiments. However, for some compounds it does not play a significant role (e.g. atazanavir).



General discussion and conclusions

- Investigations on gastric and intestinal volumes in different prandial states indicate that the quantity of liquids in the GI tract may vary significantly [120, 162-166]. Since simulated gastric and intestinal volumes have a critical impact on drug dissolution and precipitation, volumes of simulated fluids could be varied and outcomes validated in future *in vitro* and *in vivo* experiments.
- Many drugs exhibit bile salt dependent solubility. In this work, cinnarizine was shown to be subject to extensive bile salt solubility enhancement. During classical transfer experiments bile salt dilution is unavoidable unless a third compartment is added to the setup. These dilution effects may have an influence on precipitation behavior of compounds and this aspect should be investigated in more detail in the future.
- Moreover, simulated gastric emptying in the fed state has to be investigated to a greater extent. Certain weak bases may exhibit supersaturation and precipitation in the fed state (especially if the co-administrative liquid is acidic), which may be relevant in drug absorption. When 400 mg atazanavir sulfate were investigated with the transfer method, lower drug concentration profiles were observed in the acceptor compartment under simulated fed state (high fat meal) than under simulated fasted state conditions. This qualitatively confirmed the negative food effect, which has been reported for atazanavir [109]. The fed state transfer model should be validated and extended for a range of weakly basic drugs.
- Another factor, which may influence drug supersaturation and precipitation, is permeability. *In vivo* drug absorption correlates directly with drug dissolution. As demonstrated in this work for cinnarizine (a borderline BCS II/IV drug), the precipitation rate positively correlates with the degree of supersaturation. If drug absorption is slow the degree of supersaturation is kept high, this in turn will result in drug precipitation. On the other hand, when investigating BCS class II compounds, one should bear in mind that high drug permeability may lead to reduction of drug supersaturation and/or precipitation. Rapid drug absorption leads to low luminal concentrations (and increased stability of the



drug solution), since the degree of supersaturation is kept low. Thus, the transfer model presented in this work may overestimate drug precipitation of BCS class II or DCS class IIa compounds.

To overcome the overestimated precipitation issue faced by highly permeable weakly basic drugs, two research groups modified the transfer model of Kostewicz *et al.* The three-compartment *in vitro* setup developed by Psachoulas *et al.* in 2012 introduced an additional reservoir compartment containing a concentrated bile salt solution (FaSSIF). The aim was to reduce the bile salt dilution effects during the transfer experiment [65]. This model was applied for the *in vitro* precipitation investigation of ketoconazole and dipyridamole, both highly permeable drugs. Even though the *in vitro* simulations of the compounds came close to *in vivo* observations, the precipitation behavior was still overestimated in the *in vitro* experiments.

In 2005 Gu and co-workers introduced a multicompartiment model simulating both gastric emptying and the absorption from the intestinal compartment [94]. Absorption was mimicked by transferring the content from the “intestinal” compartment into the “absorption” compartment. A filter was applied to exclude solid particles from entering the absorption compartment. Two poorly soluble weak bases, cinnarizine and dipyridamole were investigated using this method. The study exhibited little precipitation for dipyridamole (<10%), presumably a DCS class IIa compound, which was in agreement with *in vivo* observations [65]. For cinnarizine (assumed as borderline BCS class II/IV or DCS class IIb/IV) considerable precipitation (>36%) was observed even when absorption was taken into account in the *in vitro* experiments. Such modifications of the classical transfer model may be useful for the examination for weakly basic drugs with high permeability. However, the relationship between the transfer rate into the third compartment and the permeability needs to be better defined to make this approach generally applicable.



4.2 Formulation enhancement approaches for weakly basic drugs

The *in vitro* investigations on marketed formulations of atazanavir and cinnarizine performed in this work led to different outcomes. In the case of cinnarizine supersaturation and precipitation were demonstrated in fasted state transfer experiments. This kind of behavior could not be demonstrated by only applying individual dissolution experiments. By contrast, individual fed state dissolution test outcomes did not exhibit drug supersaturation and were in line with transfer experiment results for the formulations investigated. In the case of atazanavir sulfate individual dissolution test and transfer experiments exhibited somewhat similar results in both prandial states. “Stable” supersaturation the API was observed for at least 2 hours after completion of the fasted state transfer experiment. *Per contra*, simulations of the fed state gastric emptying (“worst case”) demonstrated supersaturation and precipitation of atazanavir and were similar to outcomes from individual dissolution tests.

When supersaturation and precipitation are observed for a weak base, the two factors are expected to interact with factors and processes, such as (pre-) dissolution in the simulated stomach, the presence of non-dissolved particles and transfer kinetics (as in the case of cinnarizine). There following conclusions can be drawn for development of poorly soluble weak base formulations from *in vitro* outcomes on cinnarizine. Drug supersaturation can be increased through disintegration and dissolution rate enhancement. Rapid formulation disintegration can be achieved by superdisintegrants, such as sodium starch glycolate or croscarmellose sodium. Weak base dissolution can be enhanced through acidifiers, such as citric or fumaric acid, which create an acidic environment for the compound. Moreover, insoluble components such as talc or starch should be avoided or reduced to decrease seed crystallization and thus drug precipitation after gastric emptying. Cinnarizine supersaturation can be retained through precipitation inhibitors such as hypromellose (HPMC). Interestingly, some of the components, such as croscarmellose sodium and HPMC are already utilized in the marketed cinnarizine formulation Arlevert[®]. By contrast, the composition of Stugeron[®] does not contain any supersaturation enhancers and precipitation inhibitors. This may be the reason for Arlevert[®] performing better than Stugeron[®] *in vivo*.



On the basis of the *in vitro* results on atazanavir sulfate, it was concluded that the formation of an amorphous salt could be a successful approach of enhancing drug bioavailability by inducing a stable drug supersaturation during gastric emptying. Due to the lack of supersaturation beyond the kinetic solubility of atazanavir, it does not appear that addition of precipitation inhibitors would be beneficial to the *in vivo* performance of the API.

There are several successful approaches to improve bioavailability of weak bases through solubility enhancement. Development of nanoformulations, such as SNEDDS and nanosuspensions, has shown to be a promising approach for several weakly basic compounds [97, 132-134, 167]. Moreover, some cyclodextrin formulations have been shown to be successful in enhancing bioavailability of weak bases [90, 131, 168-170]. A further approach of increasing bioavailability of weak bases is by developing gastroretentive systems. These formulations are designed to float in the stomach. An extended release and dissolution of low drug concentrations is achieved, by which precipitation is avoided when the compound enters the intestine. Floating of tablets and beads can be realized through introduction of gas forming agents such as sodium bicarbonate together with an acid (e.g. citric acid). Extended release can be realized by using coating polymers, such as Eudragit[®] RL and RS. Gastroretentive systems are aimed to increase patients' compliance through reduction of daily drug administrations. Several approaches to extend release and enhance bioavailability of cinnarizine using this formulation design have been reported in the literature [171-174]. In a recent *in vivo* study this approach increased the AUC of cinnarizine at a dose of 25 mg by a factor of 4 [175].



4.3 Choosing the right PBPK modeling approach

4.3.1 Development and evolution of the STELLA[®] model

In 2001 Nicolaidis and co-workers reported a STELLA[®] model, which incorporated algorithms simulating simple drug dissolution based on Noyes-Whitney, and drug distribution and elimination using the traditional pharmacokinetic model [117]. The model was initially designed for poorly soluble compounds with high permeability (BCS class II) and thus did not consider any permeability restrictions. Constraints on drug absorption were only based on drug solubility and dissolution. Using this model Shono *et al.* were able to accurately simulate *in vivo* PK data from *in vitro* biorelevant dissolution results of celecoxib formulations [88]. Next, Shono and co-workers developed an advanced STELLA[®] model incorporating hypothetical absorption restrictions on the basis of the unstirred water layer (UWL) method for aprepitant [89]. Jünemann and co-workers took a leap forward by investigating permeability restrictions of fenofibrate, introducing an absorption compartment into the STELLA[®] model [118]. The first employment of permeability restrictions based on a physiological model was in 2011 by Shono and colleagues who used the drug permeation method through an UWL in order to predict the absorption of nelfinavir [87, 176, 177]. The authors also developed a STELLA[®] model which considered possible supersaturation and precipitation of the weak base. The model assumed precipitation based on crystal growth theory rather than using experimental data to characterize precipitation of the drug. The first report of implementing experimental precipitation kinetics in STELLA[®] was published by Wagner *et al.*, who investigated the *in vivo* performance of a BCS class IV base which showed instant precipitation in the fasted state transfer model [60]. Wagner and colleagues also utilized an *a priori* approach to the absorptive step by incorporating Caco-2 permeability data and a calculation of the effective intestinal area to directly assess the uptake rate constant for the compound in the intestine. Following these efforts, a study of a dantrolene salt formulation using STELLA[®] was able to predict the plasma profile of the compound by implementing dissolution and precipitation data (in the stomach) obtained from fasted state biorelevant dissolution testing [121].



Throughout the development and enhancement of the STELLA[®] model its general structure has not changed. The model relies basically on Noyes-Whitney dissolution kinetics obtained from individual dissolution tests. Dissolution kinetics are parameterized through calculation of initial dissolution rates (z values) for each of the individual dissolution test. Precipitation and permeability kinetics are implemented by adding compartments into the basic STELLA[®] model (referred to in this work as the “dissolution-only” model). The first approach to parameterizing supersaturation and precipitation kinetics from transfer experiments and implementing these into an advanced STELLA[®] model is presented in this work. Since transfer experiments combine gastric emptying with drug dissolution and precipitation, Noyes-Whitney dissolution kinetics are not appropriate for application in the classical STELLA[®] model. The STELLA[®] supersaturation and precipitation model enables the investigation of drug dissolution during gastric emptying of compounds under different prandial conditions. Thus, it permits simulation of *in vivo* drug behavior under more “realistic” conditions than using data from individual dissolution tests. The model was applied to poorly soluble weak bases in this work. Nevertheless, it may be analogously utilized for other types of compounds such as weak acids and neutral compounds housed in enhanced formulas. Furthermore, the advanced STELLA[®] model allows the implementation of drug efflux and excretion as shown for atazanavir. However, the approach could only be tested empirically in this work and due to lack of appropriate data for atazanavir will have to be further evaluated with compounds where concrete efflux data is available.

4.3.2 Self-built versus commercial PBPK models (STELLA[®] versus Simcyp[®])

The STELLA[®] software has shown to be a useful program to simulate *in vivo* behavior for a variety of drugs. Because of its transparent nature, the user is able to review and to modify her/his models if necessary. Commercial PBPK models enable the incorporation of complex dissolution and absorption parameters for simulations. Nevertheless, the user is not able to view the calculation processes running in these models. Thus, these types of programs by and large are opaque for the operator.



General discussion and conclusions

4.3.2.1 Input of release and dissolution profiles

Initially specific STELLA[®] models were constructed to simulate *in vivo* behavior of immediate release drug products, where a fast onset of therapeutic action is desired. The simulations were run with limited numbers of compartments (gastric and intestinal) to simulate drug absorption in the upper GI tract. Within this paradigm, STELLA[®] models are highly flexible. They enable the user to develop and modify the input of dissolution kinetics according to the observed *in vitro* behavior. Even complex dissolution data with supersaturation and precipitation can be used for simulations.

Input of dissolution kinetics in commercial PBPK models is usually predefined and cannot be easily modified. In most of the programs the user can choose between different predefined dissolution kinetics offered by the platform (Noyes-Whitney, Weibull, first order). Alternatively, one can introduce dissolution profiles (time-percent dissolved) obtained from *in vitro* investigations into a mask. In some programs (PK-Sim[®], GastroPlus[®]) the data can be even easily imported from Microsoft[®] Excel spreadsheets. Alternatively, dissolution can be simulated based on solubility values of the compound. This facilitates running simulations when little or no *in vitro* data are available. Some commercial PBPK models allow the introduction bile salt mediated solubility enhancement (GastroPlus[®], Simcyp[®]), which can be estimated on physicochemical properties of the compound.

However, certain dissolution behavior cannot be represented well with commercial PBPK programs. Even though these programs do offer the incorporation of supersaturation and precipitation data into their models, this behavior is simulated in a rather simple, almost naïve manner. Hence, for supersaturation and precipitation only a limited data set can be introduced (maximum supersaturation ratio, precipitation constant, precipitation time). However, the duration of supersaturation and the onset of precipitation cannot be implemented, which may lead to incorrect simulations in some cases (as shown for cinnarizine).



4.3.2.2 Opportunities for simulating pharmacokinetics of modified release formulations

By introducing additional intestinal compartments STELLA[®] models could be extended, enabling a simulation of transit and dissolution of extended release dosage forms through the entire GI tract. However, the parameterization of dissolution and absorption for a number of GI compartments is challenging, since algorithms have to be developed for each of the additionally integrated segments.

Commercial PBPK programs have the advantage of featuring a segmentation of the GI tract. Thus, they enable the incorporation of segmental dissolution and absorption parameters into the model in order to simulate the *in vivo* behavior of modified release formulations (dosage forms with extended release and/or colon targeting) or of drugs exhibiting poor absorption (for local drug targeting). Recently, for example, Simcyp[®] was successfully utilized to simulate the GI transit of intraluminal concentrations of paromomycin, a highly soluble non-absorbable compound [178].

4.3.2.3 Input of permeability

Self-built models require specific algorithms to simulate drug permeability through gut epithelia based on data available. Using STELLA[®] two general approaches were developed, the unstirred water layer (UWL) method and the *a priori* estimation of permeability using Caco-2 data [60, 87]. When few data are available, a first order absorption constant (k_{01}) can be estimated or calculated from clinical data. Specific absorption and efflux mechanisms can be additionally implemented into self-built models. In this work, efflux mechanisms had to be estimated in the STELLA[®] model for atazanavir at the 100 mg dose level.

Commercial PBPK models offer a range of possibilities to incorporate permeability data. Simple absorption parameters as fraction absorbed (f_a), first order absorption constant ($k_a = k_{01}$) and lag time can be easily introduced from clinical data (calculated by WinNonLin[®]). Moreover, permeability values may be integrated from *in vivo* permeability investigations (P_{eff} = effective permeability), estimated using physicochemical parameters (PSA, HBD) or *in vitro* cell-based data (Caco-2,



General discussion and conclusions

PAMPA, MDCK II, LLC-PK₁). This makes it easier for the user to implement data available without developing complicated calculations as in self-built models. Interestingly, commercial PBPK models have the option of introducing efflux kinetics from *in vitro* experiments. However, efflux can only be estimated if the data are appropriate for using Michaelis-Menten kinetics (V_{\max} , K_m).

4.3.2.4 Middle-out and Bottom-up modeling approaches

STELLA[®] models are generally based on the middle-out modeling approach. Hence, pharmacokinetic distribution and elimination parameters have to be acquired from pharmacokinetic or clinical studies (preferably intravenous data) and determined by other statistical software (WinNonLin[®]). STELLA[®] models incorporating WinNonLin[®] analysis use the classical distribution and elimination kinetics approach (k_{12} , k_{21} , k_{10} , V_d) since *a priori* simulations of drug distribution through organs and tissues are not possible with STELLA[®] models available to date. With regard to metabolism, it is certainly possible to simulate complex metabolism kinetics with self-built models, however it could be very time consuming to develop algorithms to simulate this behavior accurately.

Commercial PBPK software can be used for either middle-out or bottom-up modeling. The advantage of the bottom-up approach is that drug pharmacokinetics can be estimated when few or even no *in vivo* data are available. The technique is particularly useful early in drug discovery and formulation development [179]. It enables the estimation of absorption, distribution, metabolism and elimination of a compound based on its physicochemical properties (logP, pKa, molecular weight). Simulations may be refined by additionally utilizing *in vitro* and/or *in vivo* data.

Although bottom-up PBPK modeling can give insights on the potential *in vivo* behavior of drugs candidates, even with little information available, these calculations are connected with a good deal of uncertainty, since calculated values for parameters such as solubility and dissolution can easily be an order of magnitude away from the actual value. *In silico* estimation of saturation of (first-pass) metabolism is also possible with the commercial PBPK programs, if *in vitro* microsomal activity profiles have been established. One limitation of the current software is the metabolism kinetics need to be implemented according to Michaelis-



Menten kinetics and even so, estimates may not reflect the actual metabolic behavior in humans accurately.

4.3.2.5 Virtual populations

Most commercial PBPK software contain statistical data on different population groups. Thus simulations may be performed on healthy populations groups of different age, ethnicity or state (pregnancy) [180-182], populations with medical conditions (diabetes, cancer, kidney impairment) [183] or populations with polymorphic enzyme disposition [184, 185]. On that basis, possible drug-drug interactions can be investigated with this type of program [186-188]. Apart from that, commercial PBPK models can be utilized to simulate pharmacokinetics of different species [189]. Due to their simple structures, self-built models are less conducive to the simulation of drug-drug interactions, enzyme polymorphisms, different species, age groups, ethnicities or medical conditions.

4.3.2.6 Summary

In summary, self-built models usually have a comparatively rudimentary character. Although they provide limitless possibilities for development of PBPK models simulating complicated pharmacokinetic behavior due to their flexible and transparent nature, it would be challenging to develop the algorithms necessary to correctly reflect complicated *in vivo* or *in vitro* observations. In any case the user needs to acquire sufficient programming skills to make proper use of self-built modeling.

By contrast, commercial PBPK programs do not require any special programming expertise. The most substantial disadvantage of these programs is their lack of transparency. Thus, the user can only guess whether *in silico* simulations correlate with *ex silico* observations (e.g. supersaturation and precipitation). To run reasonable simulations the user has choose the appropriate model and implement the data in a correct manner. Nonetheless, commercial programs provide a wide range of simulation possibilities, which are not practical to develop with self-built models.

Interestingly, self-built models may provide new insights for further development of commercial PBPK software. One should bear in mind that both models are based on object-oriented programming. Hence, self-built algorithms developed to characterize



General discussion and conclusions

specific aspects of *in vivo* behavior in a more physiological way could be incorporated into commercial PBPK programs. This work concludes that the self-built models available to date may provide a better representation of certain pre-absorptive drug behavior such as supersaturation and precipitation, whereas commercial PBPK models are preferable for simulation of post-absorptive aspects of pharmacokinetics, for running virtual clinical trials and for predicting DDI.

4.4 Outlook

This work investigated dissolution and absorption of poorly soluble weakly basic compounds and their influence on drug pharmacokinetics using *in vitro* experiments coupled with PBPK modeling. The final objective of every drug and formulation development is to achieve the desired pharmacological effect after drug administration.

Pharmacological effects are dependent on certain drug concentrations in specific organs and tissues. Hence, attaining the appropriate plasma profiles is a key requirement for optimizing the therapeutic effect. On that basis the pharmacodynamics (PD) can be directly or indirectly correlated with pharmacokinetics using *in silico* modeling. The first concept of coupling pharmacokinetics and pharmacodynamics with modeling techniques was established by Levy *et al.* in 1969 [190]. But until the early 1990s these relationships could only be simulated in a simplistic way. With increasing computational power in the turn of the millennium more complex pharmacokinetic/pharmacodynamic (PK/PD) relationships could be modeled. The development of commercial PBPK modeling programs offers the possibility of coupling simulations from physiologically based pharmacokinetics to pharmacodynamics (PBPK/PD) for early drug and formulation development. With that said, PBPK/PD modeling has opened new prospects for the investigation of clinical equivalence of formulations and therapeutic risk assessment.

In 2014 the biopharmaceutics risk assessment roadmap (BioRAM) was established with the objective of optimizing drug development and performance on a basis of clinical relevance. It is intended to couple drug development with drug targets and the desired therapeutic outcomes. BioRAM proposed a structured QbD approach, which

includes key steps from drug discovery to development of the final drug product. One of its essential items is identifying the pharmacokinetics and pharmacodynamics and, if possible, assessing a PK/PD relationship of APIs [191]. On that basis *ex ante* investigations may be carried out using appropriate PBPK/PD modeling tools. This can optimize and facilitate the development of pre-clinical and clinical studies [192]. On the other hand PK/PD investigation may be useful to investigate *ex post* clinical equivalence of drug products already on the market. Moreover, several studies have been published using PK/PD modeling for a variety of purposes including drug risk assessment and PD interactions [193-196]. As an illustration, PK/PD modeling was recently utilized to evaluate the therapeutic necessity for the treatment of dental pain and antipyresis with ibuprofen. Even though the ibuprofen doses investigated were not equivalent in terms of the PK, they were shown to be therapeutically equivalent using PBPK/PD modeling [197]. In conclusion, PBPK/PD modeling techniques are likely to become key tools for clinically-based drug development to improve formulation, drug therapy and patient safety.

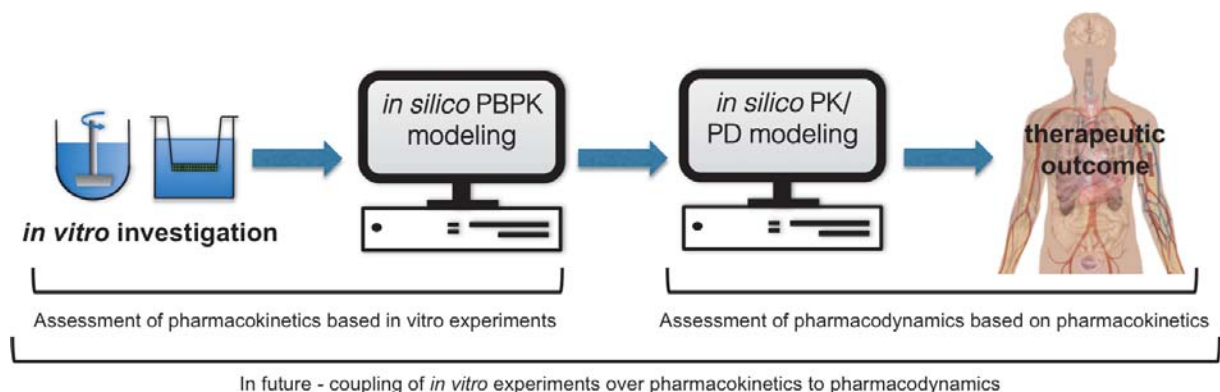


Fig. 4.2: Coupling of *in vitro* data to *in silico* PBPK/PD modeling in order to investigate a therapeutic outcome of an API.

In the future, therapeutic assessment of APIs is expected to be based on *in vitro* investigations coupled with *in silico* PBPK and PK/PD modeling (Figure 4.2). *In silico* analyses of *in vivo* drug dissolution, permeability, pharmacokinetics, pharmacodynamics and therapy will become key instruments in all aspects pharmaceutical research and development, and clinical drug safety and efficacy investigations. Finally, combining *in vitro* data with PBPK and PK/PD tools will reduce



General discussion and conclusions

the need for conducting time- and cost-intensive *in vivo* studies and accelerate patent access to breakthrough drugs [198, 199].



5 Summary

Oral drug absorption is principally dependent on two major factors, drug dissolution and intestinal drug permeability. Since new drug entities often exhibit poor solubility in aqueous environment, drug dissolution has become one of the key issues in early and clinical development. Therefore prediction of dissolution and absorption of active pharmaceutical ingredients (APIs) after oral administration is a topic which plays an essential role in pharmaceutical research and development (R&D). Several *in vitro* methods have been developed to facilitate the investigation of drug dissolution in the gastrointestinal (GI) tract as well as drug permeability in the intestine. The introduction of biorelevant media, which mimic the fluids of the GI tract, has enabled the assessment of the *in vivo* behavior of poorly soluble drugs. A variety of biorelevant dissolution test methodologies are available today enabling qualitative *in vitro-in vivo* correlations, especially of poorly soluble compounds. Further, *in vitro* data can be coupled with *in silico* programs, called physiologically based pharmacokinetic (PBPK) models, in order to quantitatively assess the *in vivo* performance of such APIs. Commercial *in silico* PBPK programs, such as GastroPlus[®], Simcyp[®] and PK-Sim[®], and in-house programs such as GI-Sim[®] have been developed over the last decades and are now widely used in pharmaceutical R&D. Moreover, PBPK models can be established using statistical and computational software, such as STELLA[®] or MATLAB[®], to mimic *in vivo* drug dissolution and absorption.

Poorly soluble weak bases have a particular status in terms of drug solubility and dissolution in the GI tract. Since weakly basic compounds usually demonstrate pH dependent solubility, this may become an issue when these drugs are taken orally. The human stomach comprises usually an acidic environment in the fasted state, with the pH lying around 1.5-2 in most healthy volunteers. By contrast, the pH in the fasting upper small intestine is considerably higher with usual values around 6-7. On this basis, a weak base is expected to be better soluble in the fasted stomach and less soluble in the fasted intestine. Thus, the compound may be subject to supersaturation/precipitation upon entering the intestine. Moreover, absorption of poorly soluble weak bases may be influenced by food, which changes gastric emptying kinetics and gastrointestinal pH (pH stomach: ~5, pH intestine 5-6). Food



Summary

components induce secretion of bile salt components and can inhibit intestinal enzymes (e.g. P-gp by grapefruit juice), or interact with the compound itself. Drug absorption can be additionally influenced by drug degradation in the GI tract, permeability restrictions and efflux through intestinal transporter proteins, such as P-glycoprotein (P-gp).

In this work, the oral availability of poorly soluble weak bases was addressed in terms of the pre-absorptive, absorptive and post-absorptive behavior of two model compounds, cinnarizine and atazanavir. Cinnarizine had shown supersaturation and precipitation behavior in previously published *in vitro* investigations of the 25 mg dose (Stugeron[®]). It was also known that the compound has a positive food effect at the 20 mg dose (Arlevert[®]). In the case of atazanavir, which is marketed as a sulfate salt formulation, no previous investigations of supersaturation/precipitation had been reported in the literature. It was known that a positive food effect is only observed when a 400 mg dose is taken after a light meal with orange juice, whereas under high fat meal conditions a negative or only slightly positive food effect has been reported for the same dose. Moreover, it was also known that over the dose range of 100 to 1200 mg atazanavir exhibited nonlinear pharmacokinetics when it was administered in the fasted state.

In vitro investigations of cinnarizine and atazanavir sulfate were performed using various solubility, dissolution, dumping and transfer experiment setups in biorelevant media simulating fasted and fed stage gastric (FaSSGF, FeSSGF (pH 5.0 and 2.75), FeSSGEm (pH 5.0 and 2.75)) and intestinal (FaSSIF-V2 and FeSSIF-V2) conditions. Dissolution experiments were performed using the USP 2 Paddle or the miniaturized Paddle apparatus (Mini Paddle) with the appropriate biorelevant medium. Dumping experiments, in which a drug solution in a simulated gastric medium is introduced as a bolus into a defined volume of simulated intestinal medium, were performed as indicative tests for drug supersaturation and precipitation. The transfer model was used to investigate the supersaturation and precipitation behavior of the two compounds during fasted and fed state gastric emptying. Therefore the Paddle or the Mini Paddle apparatus filled with simulated gastric fluid was used as the donor compartment. The Paddle apparatus filled with simulated intestinal fluid was used as



the acceptor compartment. The donor phase (including the drug or drug product) was transferred into the acceptor phase with the help of a peristaltic pump at a physiological transfer rate.

The *in vitro* results were introduced into PBPK models along with Caco-2 permeability and PK data from the literature. In this case, two fundamentally different modeling setups were applied. On the one hand, a STELLA[®] PBPK model was conducted. This is a self-built approach requires the development of algorithms simulating *in vitro* drug dissolution, supersaturation and precipitation as well as drug intestinal perfusion and efflux, and distribution and elimination kinetics. On the other hand, the commercial program Simcyp[®] was utilized for plasma profile predictions by introducing “pre-absorptive” *in vitro* results along with absorptive and post-absorptive parameters calculated from literature data. *In silico* simulation outcomes using STELLA[®] and Simcyp[®] were compared with *in vivo* observations. On that basis, the relative importance of factors which can influence oral drug absorption were investigated in detail (e.g. dissolution, precipitation, permeability restrictions, efflux mechanisms, volume of distribution, elimination) using sensitivity analysis.

The *in vitro* investigations demonstrated completely disparate dissolution behaviors for the two compounds. Cinnarizine exhibited supersaturation and precipitation in fasted state transfer experiments. Interestingly, both processes were dependent on the simulated gastric emptying rate. By contrast, simulated gastric emptying under high fat meal conditions exhibited dissolution of the entire cinnarizine dose.

Fasted state transfer experiments of atazanavir sulfate displayed supersaturation for extended period of time (at the kinetic solubility), which was unaffected by transfer kinetics or dose. Simulated gastric emptying of 400 mg atazanavir sulfate under light meal conditions exhibited two different *in vitro* behaviors. When FeSSGEm pH 2.75 was utilized as the (light meal) gastric medium, supersaturation and precipitation of the compound were observed. By contrast, the use of FeSSGF pH 2.75 as the donor medium exhibited good dissolution without supersaturation or precipitation. A transfer experiment using FeSSGEm pH 5.0 as the donor medium was also conducted to simulate the conditions after administration of a high fat meal. It demonstrated poor dissolution and precipitation of atazanavir in the acceptor compartment.



Summary

In contrast to simple biorelevant dissolution tests in individual media, food effects (positive and negative) were qualitatively illustrated for both compounds with the help of transfer experiments. Therefore transfer experiment results were preferred for use in *in silico* simulations.

The STELLA[®] model developed in this work was able to distinguish the *in vivo* behavior of two cinnarizine formulations (Arlevert[®] and Stugeron[®]) in the fasted state. Additionally, the positive food effect of Arlevert[®] could quantitatively be demonstrated with the help of STELLA[®] simulations.

Supersaturation and precipitation behavior of atazanavir in the fasted and fed state was parameterized and implemented into the STELLA[®] model. Simulations revealed reasonable predictions of the fasted *in vivo* performance for 200 to 1200 mg atazanavir sulfate capsules. When efflux/extraction kinetics were introduced into the STELLA[®] model, the nonlinear pharmacokinetics of the compound between 100 and 200 mg doses could also be simulated. Good fits were achieved through implementation of 90% efflux/extraction for the 100 mg atazanavir dose, although it must be noted that the fit was strictly empirical due to lack of any experimental data. Nevertheless, the result supports the hypothesis that nonlinear PK is probably attributed to saturation of P-gp efflux and first-pass metabolism. The positive food effect under light meal conditions with orange juice could also be successfully simulated with STELLA[®] for 400 mg atazanavir capsules.

Simulations in Simcyp[®] resulted in poorer predictions of the *in vivo* behavior of both compounds than in STELLA[®]. Simcyp[®] predictions underestimated the *in vivo* performance of both compounds in all prandial states. The program utilizes a more simplistic parameterization of supersaturation and precipitation than the STELLA[®] model developed in this work. The reasons for these outcomes were assumed to originate from inaccurate program calculations of dissolution, supersaturation and precipitation behavior and imprecise estimations of volume of distribution (Vd).

In summary, STELLA[®] demonstrated more accurate simulations of the pre-absorptive dissolution, supersaturation and precipitation behavior than Simcyp[®] simulations. By contrast, it is more reasonable to use Simcyp[®] when new drug candidates, for which only little information is available, are investigated.



Several conclusions can be drawn from this work for future investigations. First, the comparison of dissolution behavior during transfer experiments revealed different outcomes for cinnarizine and atazanavir. Cinnarizine is subject for supersaturation and subsequent precipitation. This opens the path to improving cinnarizine formulation by adding excipients which are able to enhance supersaturation or/and inhibit precipitation. Indeed, this pathway is supported by reports from the literature, which have shown several formulation approaches to be promising in terms of enhancing the bioavailability of cinnarizine.

Further optimization of the atazanavir sulfate formulation, which under most experimental conditions exhibited a supersaturation for extended period of time, was concluded to be limited. Here too, the conclusion was supported by the literature, where “enhanced” atazanavir formulations are not regarded advantageous to the marketed amorphous sulfate salt formulation.

Second, a decision tree was developed based on the results of *in vitro* investigations. The proposed experimental procedure was introduced to simplify the investigation of dissolution, supersaturation and precipitation of weakly basic drugs. An analogous decision tree could also be developed for neutral and acidic compounds.

Third, a critical evaluation of PBPK models was performed on the basis of *in silico* simulations. This work comes to the conclusion that the development of “self-built” *in silico* models using programming tools, such as STELLA[®], could be beneficial for the re-evaluation of simulation approaches utilized in commercial software, such as Simcyp[®], GastroPlus[®] and PK-Sim[®], or in GI-Sim[®].

Commercial programs enable a variety of investigations including drug-drug interactions, simulation of pharmacokinetics in different species, human ethnic groups and disease states. Moreover, they can be utilized to correlate pharmacokinetic data with pharmacodynamic (PD) effects to evaluate the quality and efficiency of formulations in drug therapy. Some of the aspects are already included in guidelines from European Medicines Agency and the US Food and Drug Administration. This work concludes that in the near future *in vitro* investigations will be routinely combined with PBPK models, which in turn will be coupled with PK/PD



Summary

simulation tools in order to improve the efficiency of formulation development, reduce the need of health and cost-intensive *in vivo* studies, identify options to optimize formulations from the clinical point of view and thereby improve drug therapy for the patient.



6 German Summary (Deutsche Zusammenfassung)

Die Aufnahme von Arzneistoffen über den Magen-Darm-Trakt (MD-Trakt) hängt hauptsächlich von zwei Faktoren ab: der Auflösung und der intestinalen Permeabilität des Arzneistoffes. Da neue Arzneistoffe oft eine schlechte Wasserlöslichkeit aufweisen, stellt deren Auflösung eine der wichtigsten Herausforderungen in der präklinischen und klinischen Entwicklung dar. Dies führte dazu, dass sich die Vorhersage der Auflösung und Aufnahme oral eingenommener Arzneistoffe zu einer der essentiellsten Disziplinen in der pharmazeutischen Forschung und Entwicklung (F&E) entfaltete. Die Entwicklung diverser *In-vitro*-Methoden in den letzten Jahrzehnten erleichterte die Vorhersage der Arzneistoffauflösung und -permeabilität im MD-Trakt. Zu diesem Fortschritt trugen insbesondere biorelevante Medien bei, welche die Zusammensetzung von Flüssigkeiten des MD-Traktes widerspiegeln und dazu eingesetzt werden Zustände, denen ein Arzneistoff oder Arzneimittel nach peroraler Einnahme ausgesetzt ist, nachzuahmen. Vielfältige Arten von biorelevanten Freisetzungsmethoden wurden im letzten Jahrzehnt entwickelt und werden heute in Forschungseinrichtungen und Industrie genutzt. Wenn Ergebnisse aus *In-vitro*-Untersuchungen mit *In-silico*-Modellen, auch physiologisch basierte pharmakokinetische (PBPK) Modelle genannt, verknüpft werden, kann das *In-vivo*-Verhalten von Arzneimitteln/Arzneistoffformulierungen quantitativ vorausgesagt werden. Zahlreiche Modelle wurden in Form von kommerziellen Software-Programmen wie GastroPlus[®], Simcyp[®] und PK-Sim[®] sowie „in-house“ Programmen wie GI-Sim[®] entwickelt und werden zunehmend in pharmazeutischer F&E eingesetzt. Zusätzlich können PBPK Modelle mit Hilfe von Statistik- und Entwicklungssoftware wie STELLA[®] und MATLAB[®] vom Anwender selbst entwickelt werden.

Schwerlösliche schwache Basen zeigen ein besonderes Löslichkeits- und Auflösungsverhalten im MD-Trakt. Schwach basische Arzneistoffe weisen normalerweise eine pH-abhängige Löslichkeit auf, was zu Lösungsproblemen bei oraler Applikation führen kann. Der pH-Wert im menschlichen nüchternen Magen liegt im sauren Bereich bei ca. 1,5-2. Im Gegensatz dazu ist der pH-Wert im nüchternen Darm mit einem pH von ca. 6-7 wesentlich höher. Folglich ist zu erwarten, dass sich schwach basische Arzneistoffe im nüchternen Magen gut und im



German Summary (Deutsche Zusammenfassung)

nüchternen Darm schlecht auflösen. Beim Eintritt der gelösten schwachen Base aus dem nüchternen Magen in den nüchternen Darm kann deshalb eine Übersättigung und Präzipitation des Arzneistoffes stattfinden. Zudem kann die Arzneistoffabsorption durch Nahrungsmittelaufnahme, die unter anderem den pH-Wert im oberen MD-Trakt erhöht (pH im Magen: ~5, pH im Darm: 5 - 6), beeinflusst werden. Chymusbestandteile induzieren die Ausschüttung von Gallensalzen und können Enzyme im MD-Trakt hemmen (z.B. Hemmung des P-gp durch Grapefruitsaft) oder auch mit dem Arzneistoff direkt interagieren. Die Arzneistoffaufnahme kann zusätzlich durch Degradation des Arzneistoffes im MD-Trakt sowie durch Permeabilitätseinschränkungen und Efflux-Mechanismen (z.B. P-gp) beeinträchtigt werden.

In dieser Arbeit wurde das *In-vivo*-Verhalten zweier schwerlöslicher schwach basischer Arzneistoffe, Cinnarizin und Atazanavir, untersucht. Dabei wurden diverse *In-vitro*- und *In-silico*-Methoden angewandt, um deren präabsorptives, absorptives und postabsorptives Verhalten näher zu erforschen.

Cinnarizin wies in früheren Untersuchungen eine Übersättigung und Präzipitation während der nüchternen Magenentleerung auf. Zusätzlich wurde ein positiver „Food-Effekt“ (höhere Bioverfügbarkeit unter postprandialen Bedingungen) in pharmakokinetischen (PK) Studien an Arlevert[®] (20 mg Cinnarizin) beobachtet. Bei Atazanavir ist das Auflösungsverhalten während der Magenentleerung nicht bekannt. Der Arzneistoff wird in Form einer amorphen Sulfatsalzformulierung (Reyataz[®]) vermarktet. *In-vivo*-Studien zeigten bei der Einnahme von 400 mg Atazanavirsulfat mit einer leichten Mahlzeit und Orangensaft einen positiven Food-Effekt. Bei der Einnahme der gleichen Dosis mit einer hochkalorischen Mahlzeit (ohne Orangensaft) wurde ein negativer bis leicht positiver Food-Effekt beobachtet. Außerdem wurde eine nicht-lineare Pharmakokinetik des Arzneistoffes für den Dosisbereich von 100 bis 1200 mg im nüchternen Zustand festgestellt.

Das *In-vitro*-Verhalten von Cinnarizin und Atazanavirsulfat wurde mit unterschiedlichen Löslichkeits-, Freisetzungs-, „Dumping“- und Transferexperimenten in biorelevanten Medien untersucht. Zur Simulation des nüchternen Magens und Dünndarmes wurden die Medien FaSSGF und FaSSIF-V2 verwendet. Der gesättigte



Magen wurde mit FeSSGF (pH 5,0 oder 2,75) oder FeSSGEm (pH 5,0 oder 2,75) und der gesättigte Darm mit FeSSIF-V2 nachgeahmt. Individuelle Freisetzungsforschungen wurden für die einzelnen zu simulierenden MD-Abschnitte (Magen und Dünndarm) mit der USP Apparatur 2 (Paddle) oder der miniaturisierten Paddle Apparatur („Mini Paddle“) durchgeführt. „Dumping“-Tests wurden als Vorstufe zu Transferexperimenten eingesetzt, um das generelle Übersättigungs- und Präzipitationsverhalten der beiden Arzneistoffe während der Magenentleerung zu ermitteln. Dabei wurde der zu untersuchende schwach basische Arzneistoff in simuliertem Magenmedium aufgelöst und die Lösung als Bolus in ein definiertes Volumen eines simulierten Darmmediums überführt. Das Transfer-Modell wurde eingesetzt, um das Freisetzungverhalten der beiden Substanzen während der simulierten Magenentleerung zu untersuchen. Dabei wurde ein Donorkompartiment, bestehend aus einer Paddle oder Mini Paddle Apparatur, die mit einem simulierten Magenmedium gefüllt wurde, eingesetzt. Das Akzeptorkompartiment bestand aus der Paddle Apparatur, in der sich ein simuliertes Darmmedium befand. Die „Donorphase“ inklusive Arzneistoff/Arzneiform wurde mit Hilfe einer peristaltischen Pumpe unter einer physiologischen Rate in die „Akzeptorphase“ übertragen.

Die *In-vitro*-Ergebnisse wurden in Kombination mit Caco-2 Permeabilitätsdaten und PK-Daten aus der Literatur in PBPK Modelle eingesetzt. Dabei wurden zwei grundlegend verschiedene Ansätze angewandt. Einerseits wurde ein PBPK Modell mit dem STELLA[®] Programm aufgebaut. Dieses selbsterstellte Modell erfordert die Entwicklung von mathematischen Algorithmen, die das beobachtete *In-vitro*- und *In-vivo*-Verhalten widerspiegeln. Alternativ wurde das kommerzielle Programm Simcyp[®] eingesetzt, um Plasmaprofile der beiden Arzneistoffe zu simulieren. Dabei wurden die *In-vitro*-Daten sowie absorptive und postabsorptive Parameter aus der Literatur in die Programmaske implementiert. Die simulierten Plasmaprofile der vermarkteten Arzneiformen von Cinnarizin und Atazanavir wurden anschließend mit reellen Beobachtungen aus *In-vivo*-Studien verglichen. Darauf basierend wurde der relative Einfluss von Faktoren (z.B. Freisetzung, Präzipitation, Permeabilität, Effluxmechanismen, Verteilungsvolumen, Elimination) auf das *In-vivo*-Verhalten der Arzneistoffe im Rahmen einer Sensitivitätsanalyse untersucht.



German Summary (Deutsche Zusammenfassung)

Die *In-vitro*-Untersuchungen zeigten grundlegend verschiedene Freisetzungs-, Überstättigungs- und Präzipitationsverhalten für Cinnarizin und Atazanavirsulfat auf. Cinnarizin wies während der Transferexperimente, die den nüchternen MD-Zustand simulierten, eine Übersättigung und Präzipitation auf. Die beiden Prozesse waren direkt von der Transferrate abhängig. Im gesättigten Zustand war die Auflösung der gesamten Cinnarizin-Dosis zu beobachten. Während der Simulation der „nüchternen“ Magenentleerung von Atazanavirsulfat (100, 200, 400 und 1200 mg Kapseln) wurde eine stabile Übersättigung des Arzneistoffes (im Zustand der kinetischen Löslichkeit des Sulfatsalzes) gezeigt. Das Übersättigungsverhalten war unabhängig von der Transferkinetik oder Arzneistoffdosis. Bei der Simulation der Magenentleerung unter einer leichten Mahlzeit mit Orangensaft wurden zwei verschiedene Transferexperimente für 400 mg Atazanavirsulfat angewandt. Beim Einsatz von FeSSGEM pH 2,75 als Donormedium war eine Übersättigung und Präzipitation des Arzneistoffes festzustellen. Bei der Verwendung von FeSSGF pH 2,75 als ein Donormedium wurde ein Großteil der Atazanavirsulfat-Dosis freigesetzt, jedoch war weder eine Übersättigung noch eine Präzipitation des Arzneistoffes zu beobachten. Im Gegensatz zu einfachen Freisetzungsuntersuchungen konnten mit Hilfe von Transferexperimenten (positive und negative) Food-Effekte für die beiden Substanzen qualitativ bestätigt werden. Aus diesem Grund war der Einsatz von Daten aus Transferexperimenten geeigneter für *In-silico*-Simulationen als Ergebnisse aus herkömmlichen Freisetzungsuntersuchungen.

Mit dem selbstentwickelten STELLA[®]-Modell konnte das Übersättigungs- und Präzipitationsverhalten der zwei Cinnarizin-Formulierungen nachgeahmt (Arlevert[®] und Stugeron[®]) und somit deren *In-vivo*-Verhalten im nüchternen Zustand erfolgreich simuliert werden. Zusätzlich konnte der positive Food-Effekt von Arlevert[®] quantitativ nachgewiesen werden.

Das Übersättigungs- (und Präzipitations-) Verhalten von Atazanavirsulfat konnte für den nüchternen sowie den gesättigten Zustand parametrisiert und in das STELLA[®]-Modell implementiert werden. Die Simulationen ergaben realistische Vorhersagen des nüchternen *In-vivo*-Verhaltens für den Dosisbereich von 200 bis 1200 mg Atazanavirsulfat (Reyataz[®] Kapseln). Die nicht-lineare Pharmakokinetik zwischen den 100 und 200 mg Atazanavirsulfat-Dosen konnte durch den Einbau einer



90%igen Efflux-/Exkretionskinetik in das STELLA[®]-Modell berücksichtigt werden. Jedoch muss hier angemerkt werden, dass diese Schätzung der Efflux-/Exkretionskinetik aufgrund nicht ausreichender Datenlage strikt empirisch war. Nichtsdestotrotz konnten P-gp-Efflux und First-Pass-Metabolismus als mögliche Gründe für die nicht-lineare PK von Atazanavir identifiziert werden. Des Weiteren konnte der positive Food-Effekt bei einer leichten Mahlzeit mit Orangensaft für die 400 mg Dosis erfolgreich simuliert werden.

Simulationen, die mit Simcyp[®] durchgeführt wurden, unterschätzten das *In-vivo*-Verhalten der beiden Arzneistoffe. Mögliche Gründe für die schlechteren Simulationsergebnisse mit Simcyp[®] sind einerseits die ungenaue Wiedergabe des Auflösungs-, Übersättigungs- und Präzipitationsverhaltens durch das Programm und andererseits die inexakte Einschätzung des Verteilungsvolumens der beiden Arzneistoffe.

Zusammenfassend ist zu sagen, dass das STELLA[®]-Modell das präabsorptive Freisetzungs-, Übersättigungs- und Präzipitationsverhalten genauer widerspiegelt als Simcyp[®]. Andererseits ist Simcyp[®] nützlicher, wenn neue Arzneistoffkandidaten mit begrenzter Datenlage erforscht werden sollen.

Folgende Schlussfolgerungen konnten aus dieser Arbeit für weitere Untersuchungen gezogen werden:

Erstens wurden zwei unterschiedliche Freisetzungsverhalten für Cinnarizin und Atazanavir während der Transferexperimente festgestellt. Da Cinnarizin eine Übersättigung und Präzipitation im nüchternen Zustand aufwies, erscheint der Einsatz von übersättigungsstabilisierenden oder präzipitationsinhibierenden Hilfsstoffen zur Verbesserung der Formulierung als sinnvoll. Tatsächlich wurden mehrere vielversprechende Formulierungskonzepte für Cinnarizin in der Literatur vorgestellt.

Atazanavirsulfat zeigte in den meisten Fällen eine stabile Übersättigung auf. Aus diesem Grund ist eine Verbesserung der Atazanavir-Formulierung weitgehend begrenzt. „Verbesserte“ Atazanavir-Formulierungen aus aktuellen Veröffentlichungen können keinen Vorteil gegenüber dem vermarkteten amorphen Sulfatsalz aufweisen.



German Summary (Deutsche Zusammenfassung)

Zweitens wurde ein Entscheidungsbaum anhand der *In-vitro*-Untersuchungsergebnisse erstellt, um das *In-vivo*-Freisetzungs-, Übersättigungs- und Präzipitationsverhalten von schwerlöslichen schwach basischen Arzneistoffen zu untersuchen. Zusätzlich kann ein analoger Entscheidungsbaum für neutrale und schwach saure Arzneistoffe entwickelt werden.

Und drittens wurde eine kritische Begutachtung der PBPK Modelle anhand der durchgeführten *In-silico*-Simulationen erstellt. Diese Untersuchung kam zu der Feststellung, dass selbsterstellte *In-silico*-Modelle (z.B. mit STELLA®) eine Neubewertung und Verbesserung der vorhandenen Simulationsansätze von kommerziellen Programmen ermöglichen. Andererseits bieten kommerzielle Programme diverse Untersuchungsmöglichkeiten an, die mit selbsterstellten Modellen kaum möglich sind (z.B. Arzneistoffwechselwirkungen, Bewertung der PK in unterschiedlichen Spezies, ethnischen Gruppen und Krankheitszuständen). Die kommerziellen Programme ermöglichen ebenfalls die Korrelation der Pharmakokinetik mit der Pharmakodynamik (PD) eines Arzneistoffes und damit eine Qualitäts- und Effizienzuntersuchung von Arzneiformen in der Arzneimitteltherapie. Einige dieser Aspekte wurden in Richtlinien der europäischen (EMA) und der US amerikanischen (US-FDA) Arzneimittelzulassungsbehörden aufgenommen.

Diese Arbeit soll verdeutlichen, dass eine routinemäßige Kombination von *In-vitro*-Untersuchungen mit PBPK Modellen und deren anschließende Kopplung mit PK/PD Simulationsinstrumenten sinnvoll ist, um die Formulierungsentwicklung effizienter zu gestalten, den Bedarf von gesundheits- und kostenintensiven *In-vivo*-Studien zu reduzieren, Formulierungen vom klinischen Standpunkt aus zu optimieren und demzufolge die Patiententherapie zu verbessern.

7 Appendix

7.1 STELLA[®] sensitivity analysis of cinnarizine plasma profile predictions

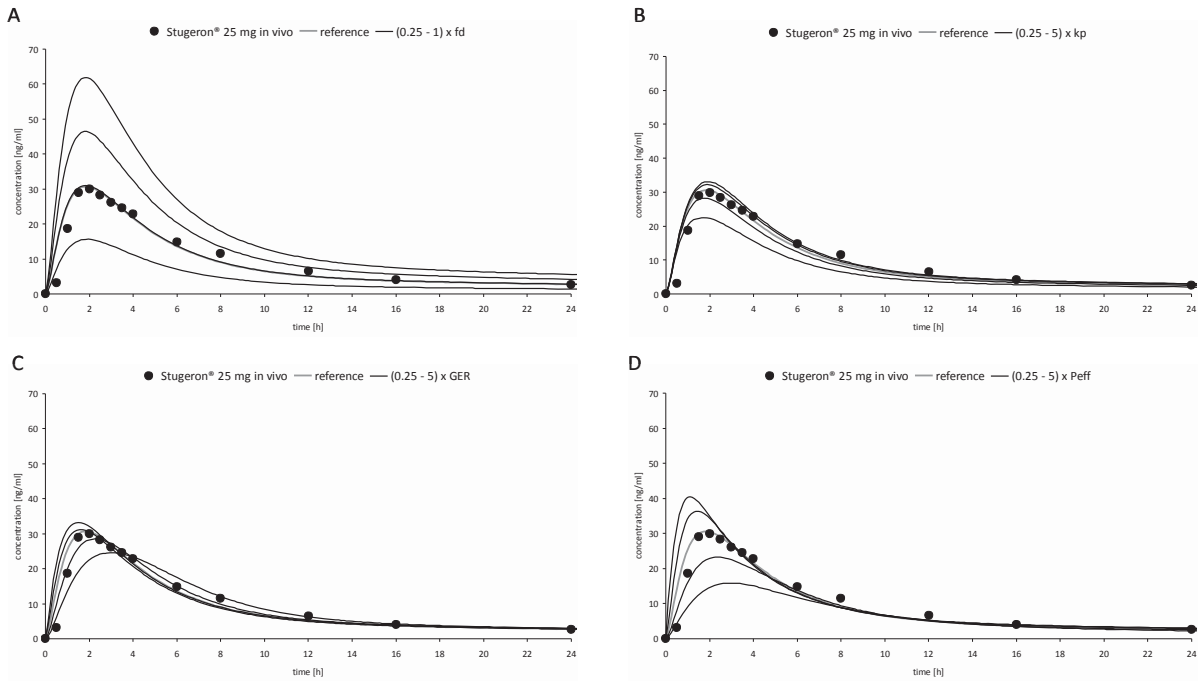


Fig. 7.1: Stugeron[®] in the fasted state - sensitivity analysis of the fraction dissolved constant (A), the precipitation constant (B), the gastric emptying rate (C) and the effective permeability (D) on cinnarizine plasma profiles.



Appendix

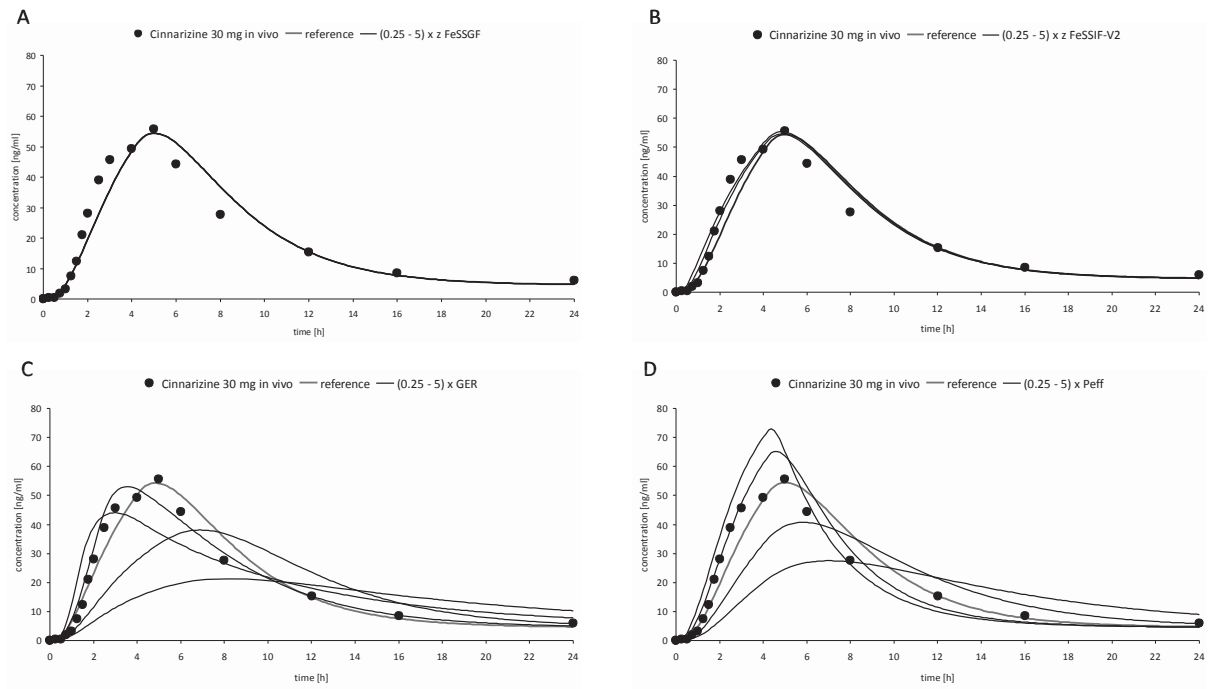


Fig. 7.2: Cinnarizine 30 mg tablets in the fed state - sensitivity analysis of the z value in FeSSGF (A), the z value in FeSSIF-V2 (B) the gastric emptying rate (C) and the effective permeability (D) on cinnarizine plasma profiles.

7.2 STELLA[®] sensitivity analysis of atazanavir sulfate plasma profile predictions

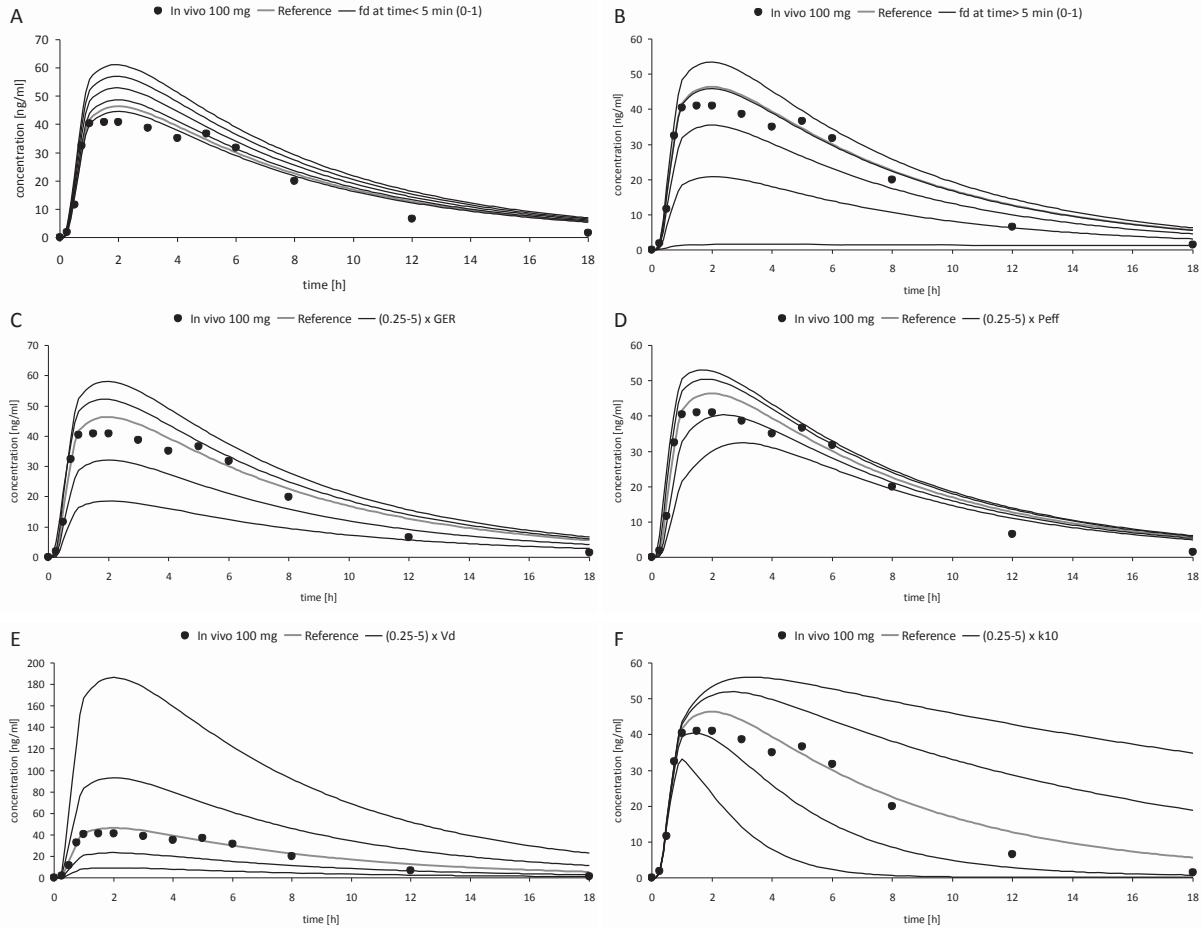


Fig. 7.3: Sensitivity analysis of the fraction dissolved constant < 5 min (A), the fraction dissolved constant > 5 min (B), the gastric emptying constant (C), the permeability (D), the volume of distribution (E), and the elimination constant (F) on plasma profile predictions of 100 mg atazanavir sulfate capsules in the fasted state.

Appendix

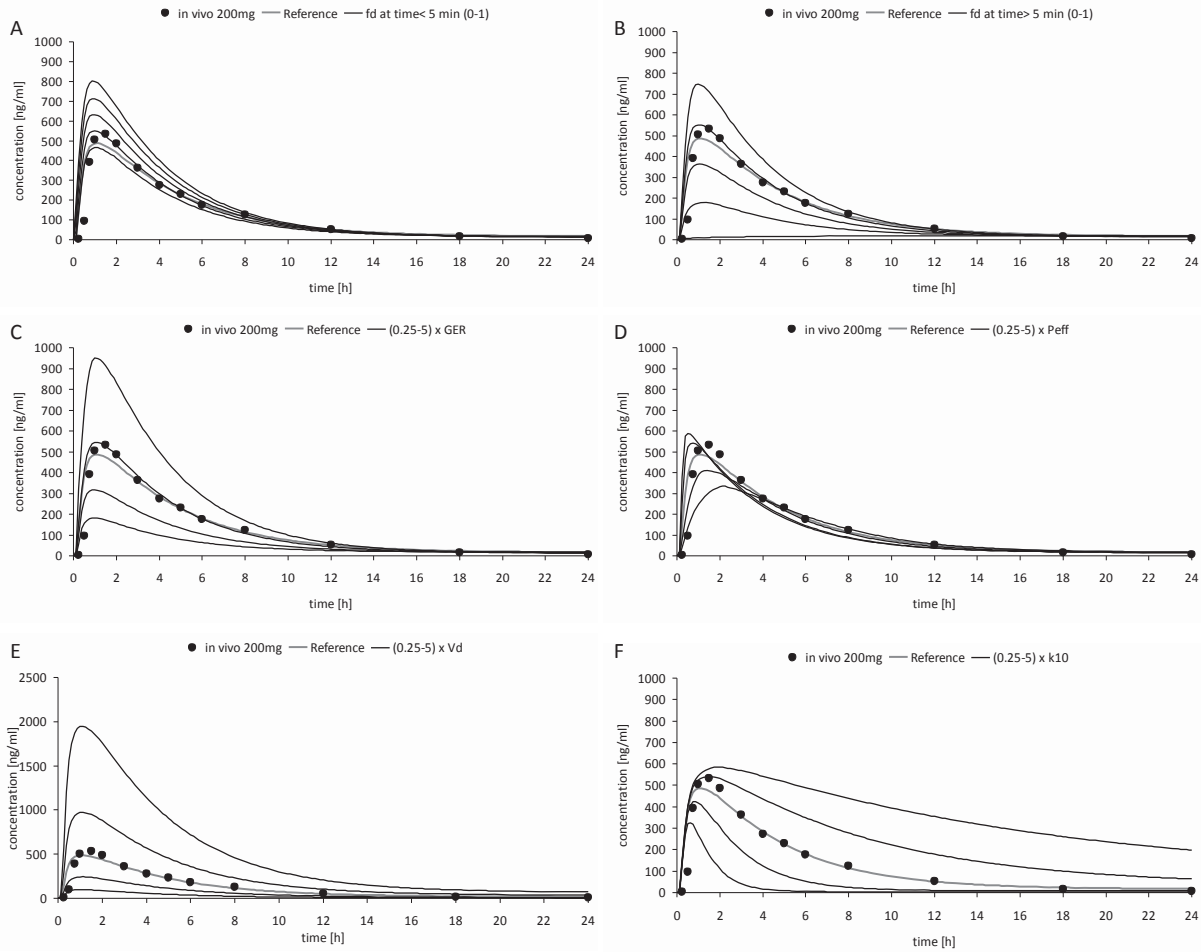


Fig. 7.4: Sensitivity analysis of the fraction dissolved constant < 5 min (A), the fraction dissolved constant > 5 min (B), the gastric emptying constant (C), the permeability (D), the volume of distribution (E), and the elimination constant (F) on plasma profile predictions of 200 mg atazanavir sulfate capsules in the fasted state.

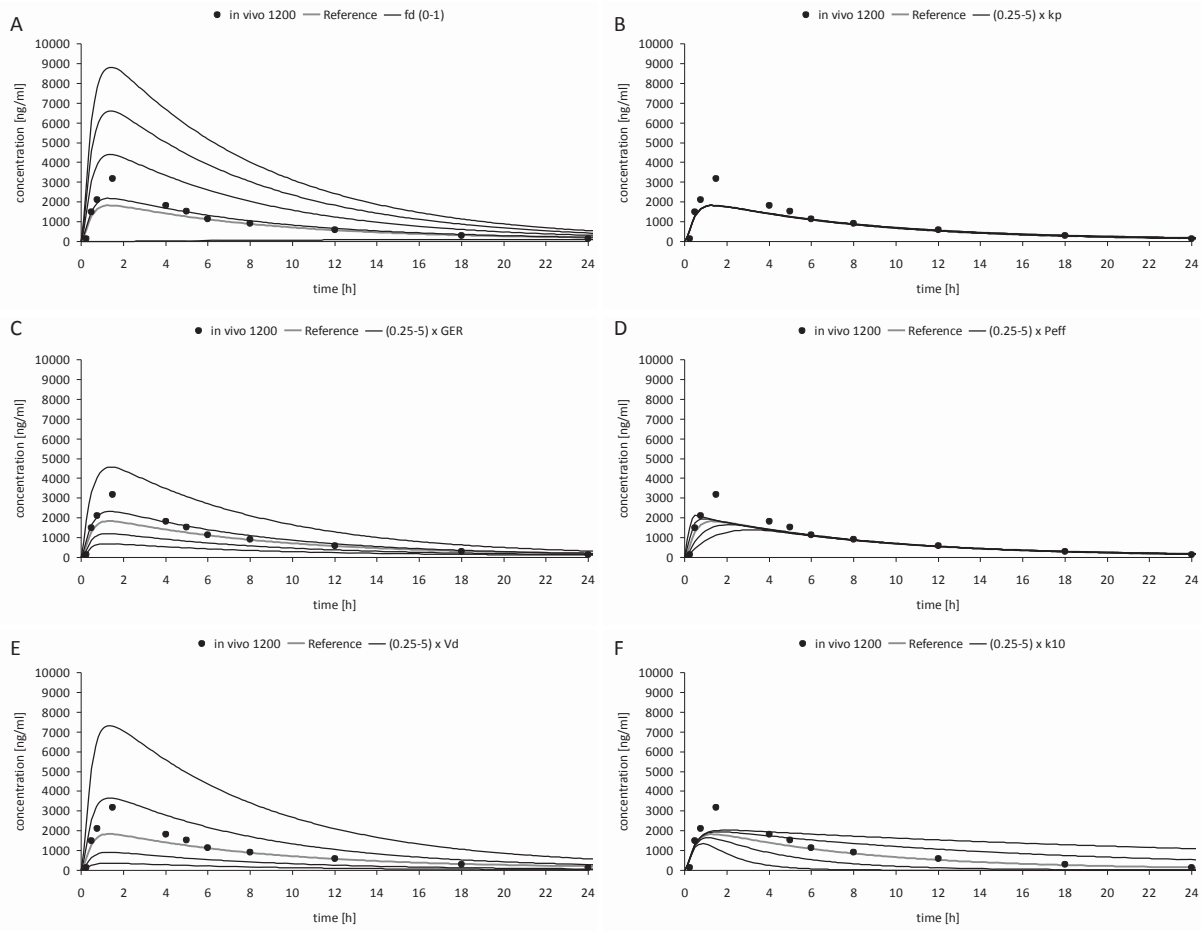


Fig. 7.5: Sensitivity analysis of the fraction dissolved constant (A), the first order precipitation constant (B), the gastric emptying constant (C), the permeability (D), the volume of distribution (E), and the elimination constant (F) on plasma profile predictions of 1200 mg atazanavir sulfate capsules in the fasted state.



7.3 Simcyp[®] plasma profile predictions of cinnarizine

7.3.1 Simcyp[®] plasma profile predictions of cinnarizine in the fasted state

Plasma profile predictions of cinnarizine tablets in the fasted state were prepared by introducing compound related input parameters into the program mask. These were the molecular weight, the pKa values, the logP value and the melting temperature (Table 7.1). Additionally, Caco-2 permeability of cinnarizine was introduced into the model by using the value of 4.2×10^{-6} cm/s from the literature [97]. The distribution parameters were obtained from WinNonLin[®] (Table 3.8) and implemented into the program mask.

Fasted state plasma profiles were simulated using three approaches: implementation of biorelevant solubility data into GI solubility program mask, utilization of predicted solubility and implementation of pH dependent solubility data. The maximum supersaturation ratio and the precipitation constant (k_p) were calculated from first order transfer experiments (Table 3.6) and used for all of the three approaches.

Table 7.1: Standard physicochemical parameters of cinnarizine implemented into Simcyp[®]

Parameter	Value
Molecular weight	368.514 g/mol
pKa	1: 1.95; 2: 7.47
logP	5.6
Melting temperature	120° C

Predictions obtained by implementing biorelevant solubility of cinnarizine into the Simcyp[®] gastrointestinal solubility mask

Cinnarizine solubility in biorelevant media was implemented into the program mask, representing different sections of the human gastrointestinal tract. Hence the solubility value of FaSSGF pH 1.6 was introduced into “gastric solubility” box and the value obtained in FaSSIF-V2 was implemented in the “intestinal solubility” box. Moreover, supersaturation and precipitation values obtained from transfer

experiments on Arlevert[®] and Stugeron[®] were used in the model. Simulation results for both formulations are shown in Table 7.2 and Figure 7.6.

Table 7.2: *In vivo* and predicted pharmacokinetic parameters for Arlevert[®] and Stugeron[®] tablets in the fasted state by implementing biorelevant solubility of cinnarizine into the Simcyp[®] gastrointestinal solubility mask

Formulation	AUC ₀₋₂₄ (ng x h/ml)	C _{max} (ng/ml)	t _{max} (h)
Arlevert[®]			
<i>in vivo</i>	218.72	33.0	2.0
<i>predicted</i>	108.00	13.68	1.681
Stugeron[®]			
<i>in vivo</i>	232.81	29.87	2.0
<i>predicted</i>	79.54	11.81	1.683

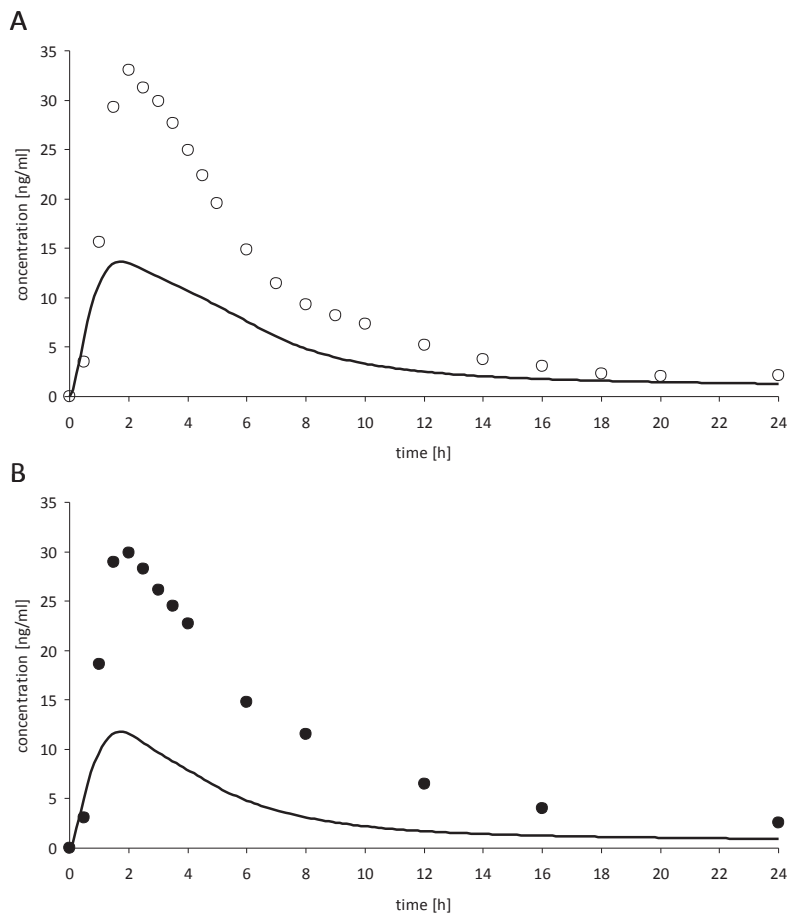


Fig. 7.6: Fasted state plasma profile predictions of Arlevert[®] 20 mg (A) and Stugeron[®] 25 mg (B) by implementing biorelevant solubility of cinnarizine into the Simcyp[®] gastrointestinal solubility mask.



Appendix

Simulations significantly underestimated the plasma profiles of both cinnarizine tablet formulations. Predictions were compared with the *in vivo* observations (shown in Table 7.3) by dividing predicted PK parameters (AUC, C_{max} and t_{max}) with the *in vivo* values. The comparison exhibited overall low ratios for AUC and C_{max} . Interestingly, the AUC ratios were similar to fraction of drug absorbed (f_a) values predicted by Simcyp[®] for both tablets. The predicted f_a values were 0.55 for Arlevert[®] and 0.32 for Stugeron[®]. Thus, one may assume that in case of entire dissolution and absorption of the cinnarizine dose (meaning $f_a = 1.0$) the predictions would be close to the *in vivo* observations of both tablet formulations. However, a fraction absorbed of 1.0 is unlikely to occur in the fasted state, since a positive food effect was observed in the fed state. If fraction absorbed would be assumed to be 1.0 in the fasted state, the value would consequently have to be greater than 1.0 in the fed state. This would only be possible if the compound was subject to enterohepatic circulation, which has not been reported for cinnarizine. Therefore, underestimations of cinnarizine plasma profiles are most likely to originate from inaccurate estimations of post-absorptive factors.

Table 7.3: Ratios of predicted (using the GI solubility approach) to observed plasma profile parameters of cinnarizine tablets in the fasted state

Formulation	AUC ₀₋₂₄ (ng x h/ml)	C_{max} (ng/ml)	t_{max} (h)
Arlevert [®]			
<i>predicted/observed</i>	0.494	0.415	0.841
Stugeron [®]			
<i>predicted/observed</i>	0.342	0.395	0.842

Predictions obtained by using predicted cinnarizine solubility by Simcyp[®]

Cinnarizine solubility was predicted by Simcyp[®] using the predicted intrinsic solubility value and bile salt solubility enhancement on the basis physicochemical properties of the compound. Figure 7.8 shows the predicted pH solubility profile of cinnarizine. The data were then applied for plasma profile simulations of Arlevert[®] and Stugeron[®] tablets. Results are presented in Table 7.4 and Figure 7.6.

The *in silico* predictions fitted well the *in vivo* behavior of Arlevert® and Stugeron®. However, on the basis of the calculations, the predictions do not seem to be realistic. Looking at the f_a , both simulations exhibited a value of 1.0. This would assume a 100% dissolution (no precipitation involved) and absorption of both cinnarizine doses. This result is not reasonable, since a positive food effect was observed for Arlevert®. Thus, if this simulation approach would be applied to predict the fed state plasma profiles of Arlevert®, the fraction absorbed value would have to be greater than 1.0, otherwise the fed state *in vivo* performance of Arlevert® would be underestimated. The overestimation of the f_a value originates from inaccurate predictions of cinnarizine solubility (as shown in Figure 7.8).

Table 7.4 *In vivo* and predicted pharmacokinetic parameters for Arlevert® and Stugeron® tablets in the fasted state using Simcyp® predictions of cinnarizine solubility based on its physicochemical properties.

Formulation	AUC ₀₋₂₄ (ng x h/ml)	C _{max} (ng/ml)	t _{max} (h)
Arlevert®			
<i>in vivo</i>	218.72	33.0	2.0
<i>predicted</i>	197.16	32.59	1.448
Stugeron®			
<i>in vivo</i>	232.81	29.87	2.0
<i>predicted</i>	246.38	40.73	1.453

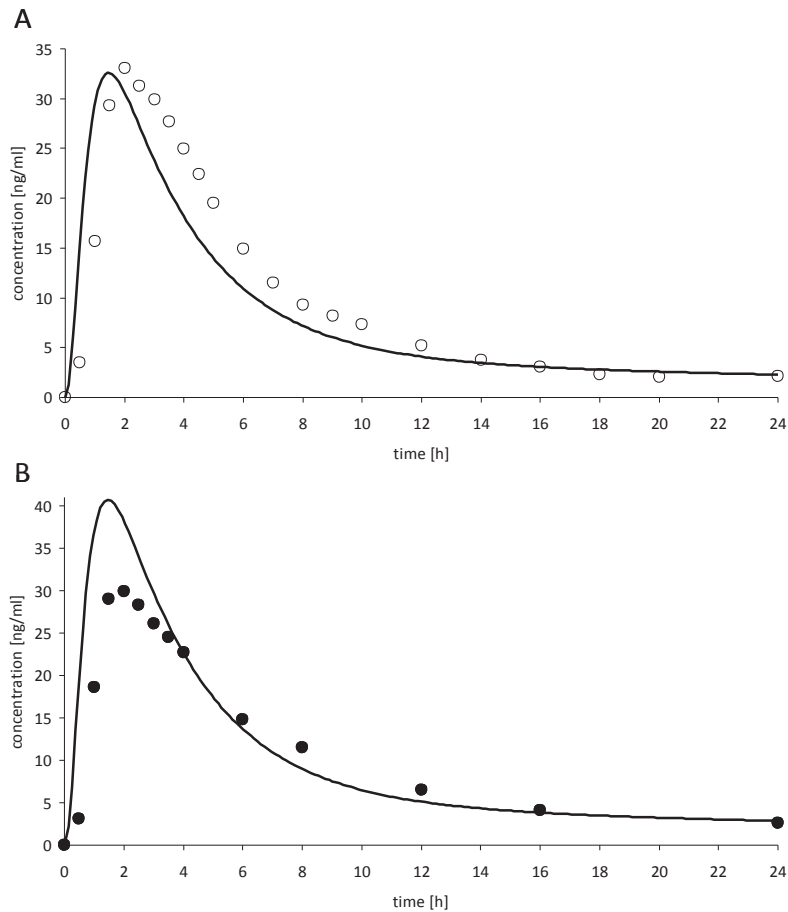


Fig. 7.7: Fasted state plasma profile predictions of Arlevert® 20 mg (A) and Stugeron® 25 mg (B) using Simcyp® predictions of cinnarizine solubility based on its physicochemical properties.

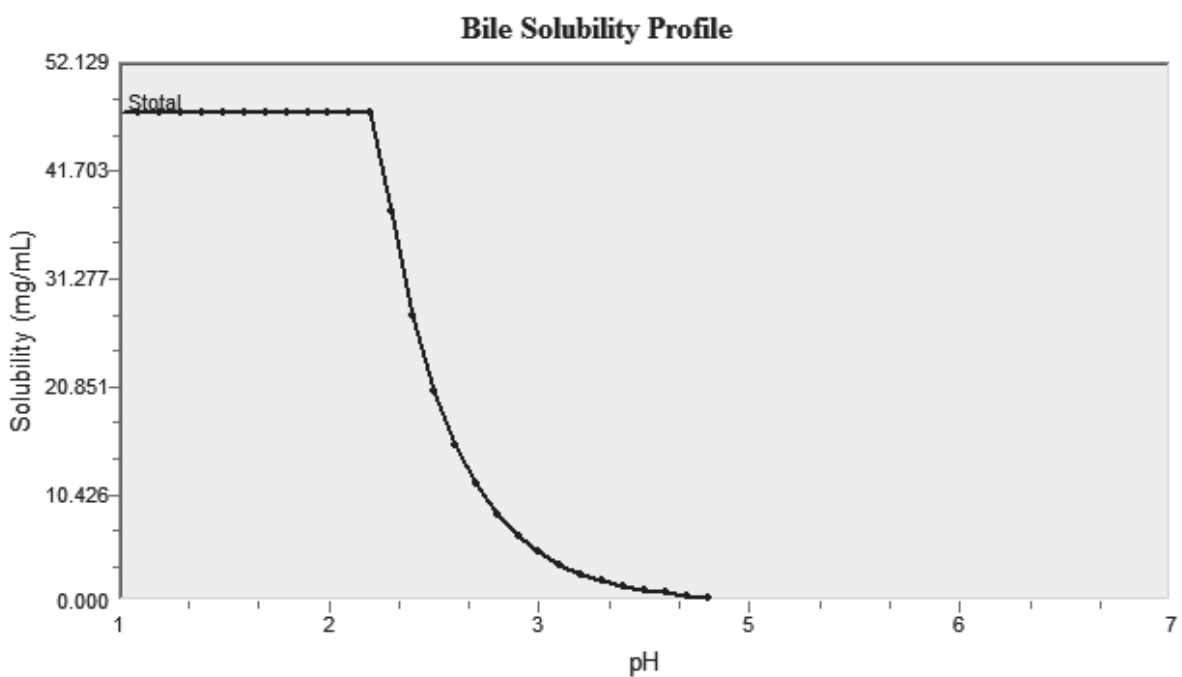


Fig. 7.8: pH solubility profile of cinnarizine predicted by Simcyp®.



Predictions obtained by introducing pH dependent solubility of cinnarizine into the Simcyp[®] mask

In this simulation approach cinnarizine solubilities in blank buffers at different pH values were implemented into the program. Bile salt mediated solubility enhancement was utilized for the simulations. The simulation results are presented in Table 7.5 and Figure 7.9.

The same results were obtained as in the investigation using predicted cinnarizine solubility. The simulations revealed f_a values of 1.0 for both Arlevert[®] and Stuger[®]. Thus, using this approach overestimated the solubility of cinnarizine and resulted in an inaccurate “good fits” to the *in vivo* behavior of both cinnarizine formulations.

Appendix

Table 7.5: *In vivo* and predicted pharmacokinetic parameters for Arlevert[®] and Stugeron[®] tablets in the fasted state by implementing cinnarizine solubility at different pH values into the Simcyp[®] mask

Formulation	AUC ₀₋₂₄ (ng x h/ml)	C _{max} (ng/ml)	t _{max} (h)
Arlevert[®]			
<i>in vivo</i>	218.72	33.0	2.0
<i>predicted</i>	197.10	32.58	1.457
Stugeron[®]			
<i>in vivo</i>	232.81	29.87	2.0
<i>predicted</i>	246.41	40.73	1.461

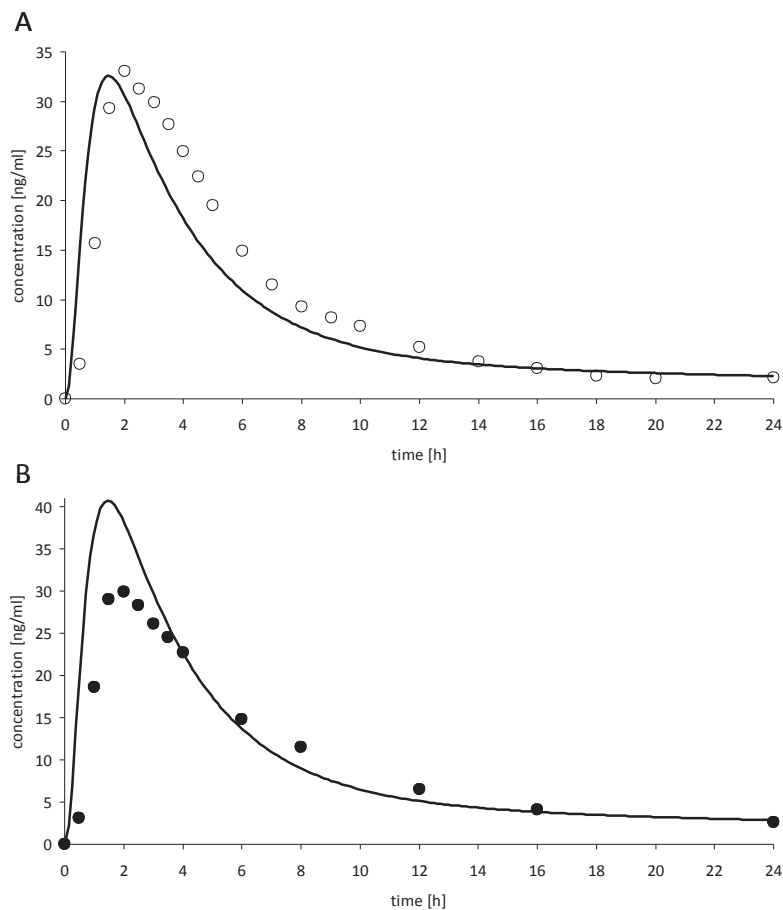


Fig. 7.9: Fasted state plasma profile predictions of Arlevert[®] 20 mg (A) and Stugeron[®] 25 mg (B) by implementing cinnarizine solubility at different pH values into the Simcyp[®] mask.

7.3.2 Simcyp[®] plasma profile predictions of cinnarizine in the fed state

Fed state simulations of Arlevert[®] and Cinnarizine 30 mg tablets were performed using four different approaches. The first approach was the implementation of dissolution profiles into the program. The further three simulation setups were identical to the ones used in the fasted state investigations of cinnarizine formulations. Neither supersaturation nor precipitation was observed in the fed state *in vitro* experiments on cinnarizine tablets. The same Caco-2 permeability was utilized as in the fasted state investigations. Distribution (Vd/F) and elimination data (Cl/F) were obtained from Table 3.8 (calculated by WinNonLin[®]) and implemented into the models.

Predictions by implementing dissolution profiles of cinnarizine tablets into the program mask

Dissolution profiles (time - percent dissolved) in FeSSGF pH 5.0 and FeSSIF-V2 were implemented into Simcyp[®] for both Arlevert[®] and Cinnarizine 30 mg tablets. Simulation results are presented in Table 7.6 and Figure 7.10.

Table 7.6: *In vivo* and predicted pharmacokinetic parameters for Arlevert[®] and Cinnarizine 30 mg tablets in the fed state by implementing dissolution profiles in FeSSGF pH 5.0 and FeSSIF-V2 into Simcyp[®]

Formulation	AUC ₀₋₂₄ (ng x h/ml)	C _{max} (ng/ml)	t _{max} (h)
Arlevert[®]			
<i>in vivo</i>	315.22	35.69	5.0
<i>predicted</i>	232.52	21.66	4.697
Cinnarizine 30 mg			
<i>in vivo</i>	466.50	55.68	5.0
<i>predicted</i>	321.34	31.20	5.296

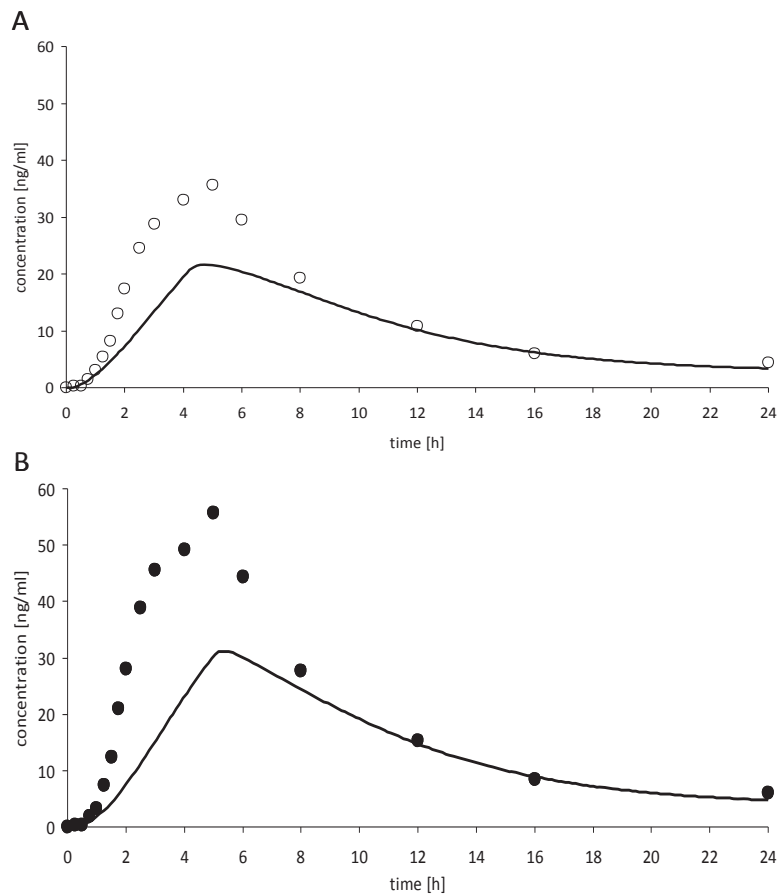


Fig. 7.10: Fed state plasma profile predictions of Arlevert[®] 20 mg (A) and Cinnarizine 30 mg tablets (B) by implementing dissolution profiles in FeSSGF pH 5.0 and FeSSIF-V2 into Simcyp[®].

When using this simulation approach the *in vivo* behavior of both tablet formulations was significantly underestimated. The comparison of predicted to observed AUC, C_{max} and t_{max} is shown in Table 7.7. The fraction absorbed values obtained from Simcyp[®] were 0.84 for Arlevert[®] and 0.77 for Cinnarizine 30 mg tablets. The fraction of drug absorbed values seem to be reasonable if they are compared to values obtained from fasted state simulations using the GI solubility approach (Section 7.3.1). However, even if a fraction of drug absorbed of 1.0 was considered using this simulation method, the *in vivo* profiles would still be underestimated for both tablet formulations.

Table 7.7: Ratios of predicted (using dissolution profile data) to observed plasma profile parameters of cinnarizine tablets in the fed state

Formulation	AUC ₀₋₂₄ (ng x h/ml)	C _{max} (ng/ml)	t _{max} (h)
Arlevert[®]			
<i>predicted/observed</i>	0.738	0.607	0.939
Cinnarizine 30 mg			
<i>predicted/observed</i>	0.689	0.560	1.060

Predictions obtained by implementing biorelevant solubility of cinnarizine into the Simcyp[®] gastrointestinal solubility mask

Simulations of plasma profiles of Arlevert[®] and Cinnarizine 30 mg tablets were performed using the GI solubility approach (implementation of cinnarizine solubility in FeSSGF pH 5.0 and FeSSIF-V2 into the gastric and intestinal solubility boxes in Simcyp[®]). Results (Table 7.8 and Figure 7.11) show underestimations of both *in vivo* profiles. However, the results are somewhat better than the ones observed in the simulations using dissolution profile data. This is justified by the higher fraction absorbed value of 0.91 for both formulations. Still, a fraction absorbed of 1.00 would underestimate plasma profiles of Arlevert[®] and Cinnarizine 30 mg tablets in the simulations.

Table 7.8: *In vivo* and predicted pharmacokinetic parameters for Arlevert[®] and Cinnarizine 30 mg tablets in the fed state by implementing biorelevant solubility of cinnarizine into the Simcyp[®] gastrointestinal solubility mask

Formulation	AUC ₀₋₂₄ (ng x h/ml)	C _{max} (ng/ml)	t _{max} (h)
Arlevert[®]			
<i>in vivo</i>	315.22	35.69	5.0
<i>predicted</i>	255.62	21.48	4.200
Cinnarizine 30 mg			
<i>in vivo</i>	466.50	55.68	5.0
<i>predicted</i>	383.42	32.22	4.202

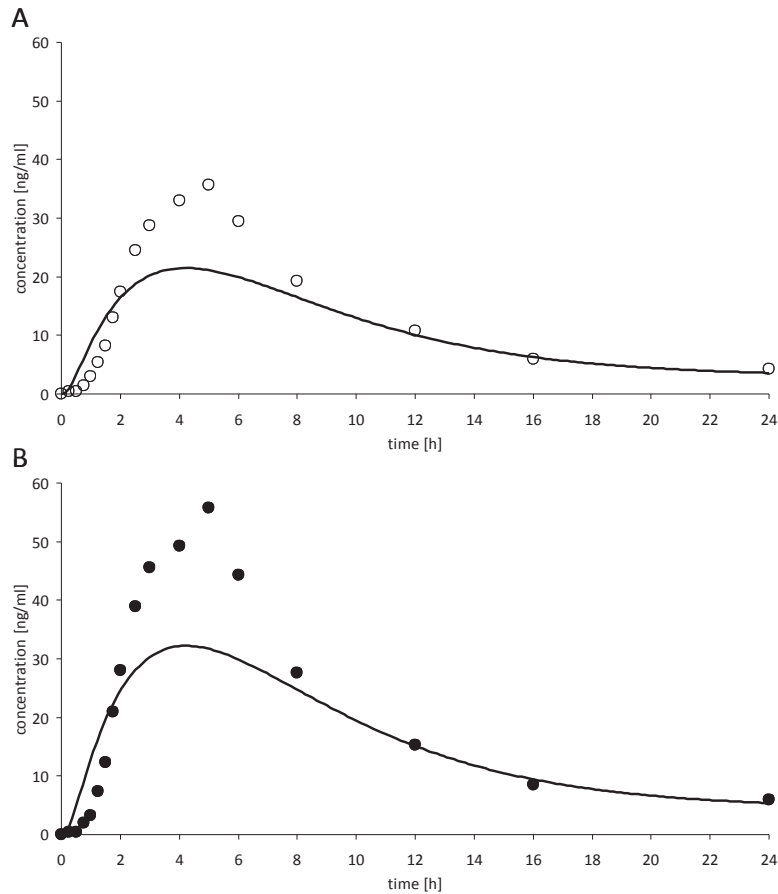


Fig. 7.11: Fed state plasma profile predictions of Arlevert[®] 20 mg (A) and Cinnarizine 30 mg tablets (B) by implementing biorelevant solubility of cinnarizine into the Simcyp[®] gastrointestinal solubility mask.

Predictions obtained by using predicted cinnarizine solubility by Simcyp[®]

As it was observed in the fasted state predictions, simulations using the predicted solubility method exhibited a f_a value of 1.0 the fed state (Table 7.9 and Figure 7.12). However, the AUC and C_{max} for both Arlevert[®] and Cinnarizine 30 mg tablets were significantly underestimated. This confirms the assumption that possible overestimations post-absorptive parameters by Simcyp[®] are responsible for this simulation output.

Table 7.9: *In vivo* and predicted pharmacokinetic parameters for Arlevert® and Cinnarizine 30 mg tablets in the fed state using Simcyp® predictions of cinnarizine solubility based on its physicochemical properties

Formulation	AUC ₀₋₂₄ (ng x h/ml)	C _{max} (ng/ml)	t _{max} (h)
Arlevert®			
<i>in vivo</i>	315.22	35.69	5.0
<i>predicted</i>	280.18	23.53	4.328
Cinnarizine 30 mg			
<i>in vivo</i>	466.50	55.68	5.0
<i>predicted</i>	420.31	35.30	4.348

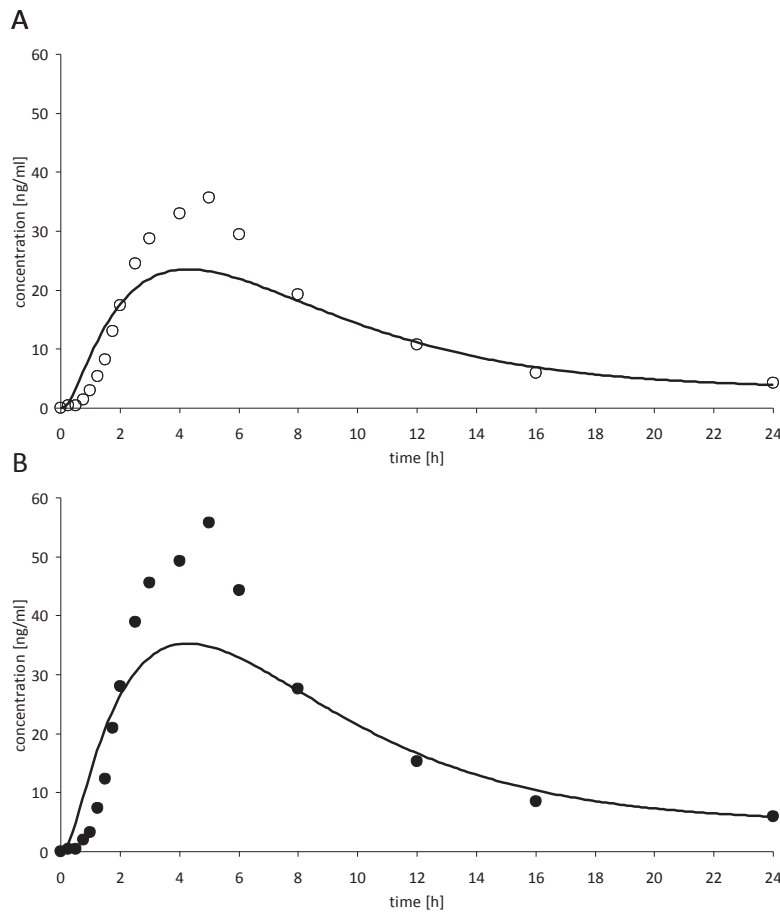


Fig. 7.12: Fed state plasma profile predictions of Arlevert® 20 mg (A) and Cinnarizine 30 mg tablets (B) using Simcyp® predictions of cinnarizine solubility based on its physicochemical properties.



Appendix

Predictions obtained by introducing pH dependent solubility of cinnarizine into the Simcyp[®] mask

When using the pH dependent solubility approach the same simulation results were achieved as when using the predicted cinnarizine solubility method (Table 7.10 and Figure 7.13). Again, Simcyp[®] calculated a fraction absorbed of 1.0 and underestimated the plasma profiles for both formulations. Reasons for these underestimations were further investigated with the sensitivity analysis of cinnarizine plasma profile predictions (Section 7.3.3).

Table 7.10: *In vivo* and predicted pharmacokinetic parameters for Arlevert[®] and Cinnarizine 30 mg tablets in the fed state by implementing cinnarizine solubility at different pH values into the Simcyp[®] mask

Formulation	AUC ₀₋₂₄ (ng x h/ml)	C _{max} (ng/ml)	t _{max} (h)
Arlevert [®]			
<i>in vivo</i>	315.22	35.69	5.0
<i>predicted</i>	280.18	23.53	4.234
Cinnarizine 30 mg			
<i>in vivo</i>	466.50	55.68	5.0
<i>predicted</i>	420.17	35.27	4.327

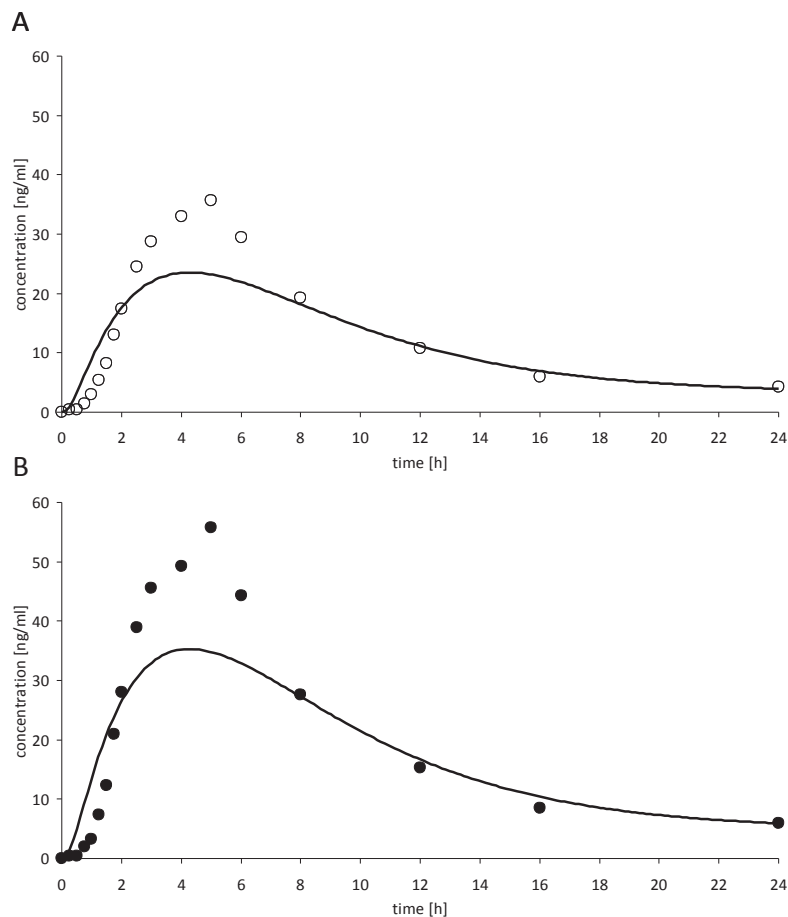


Fig. 7.13: Fed state plasma profile predictions of Arlevert[®] 20 mg (A) and Cinnarizine 30 mg tablets (B) by implementing cinnarizine solubility at different pH values into the Simcyp[®] mask.

7.3.3 Simcyp[®] sensitivity analysis of cinnarizine plasma profile predictions

The sensitivity analysis was performed for all doses, gastric states and simulation approaches. Variations were executed for the gastric solubility (fed state), intestinal solubility, intestinal permeability, the gastric emptying rate (GER), the effective permeability (P_{eff}), the volume of distribution (Vd) and the clearance (Cl). When the maximum supersaturation ratio and precipitation (k_p) were used in simulations, variations of both parameters were additionally performed. When predicted solubility, pH dependent solubility and dissolution profile data were used for simulations only the GER, P_{eff} , Vd and Cl values were altered. All factors were varied 0.5 to 2 fold, except for the GER value, which was altered 0.5-5 fold in the fasted state and 0.2-1 fold in the fed state. Simcyp[®] does not allow the gastric emptying time to exceed the value of 4 hours for fed state. Therefore the value could not be varied beyond this

Appendix

limit. The sensitivity analysis of the fasted and fed state simulations is shown for Arlevert[®], Stugeron[®] and Cinnarizine 30 mg tablets in Figures 7.14 to 7.23.

Sensitivity analysis by implementing biorelevant dissolution profiles of cinnarizine into Simcyp[®]

The factorial analysis of the biorelevant dissolution model (fed state) exhibits that only two factors may have a significant influence on the fed state plasma profile predictions, namely the GER and Vd (Figures 7.14 and 7.15). The most significant effect on the simulations was observed through variations of the Vd value. Alterations of the P_{eff} and CI values did not have a remarkable influence on the plasma profiles. This analysis indicates that the underestimations of the cinnarizine plasma profiles in the fed state may originate from overestimated volume of distribution value used in the simulations.

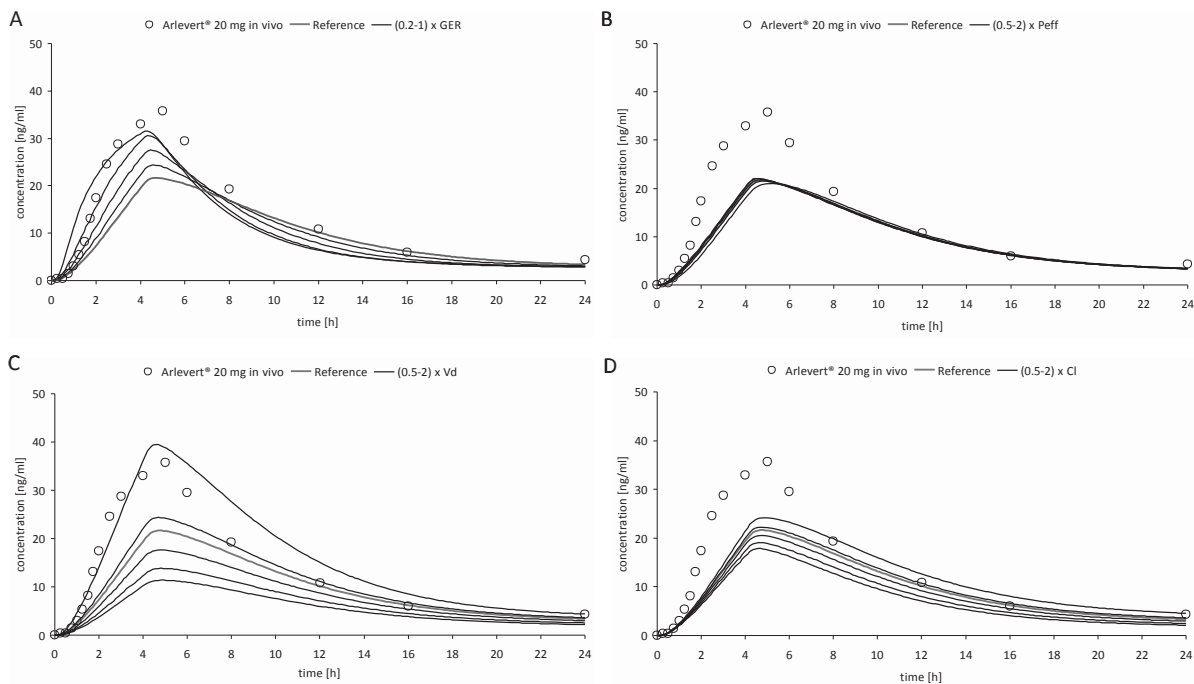


Fig. 7.14: Sensitivity analysis of the gastric emptying (A), the permeability (B), the volume of distribution (C) and the clearance (D) on plasma profile predictions of Arlevert[®] in the fed state by implementing dissolution profiles in FeSSGF pH 5.0 and FeSSIF-V2 into Simcyp[®].

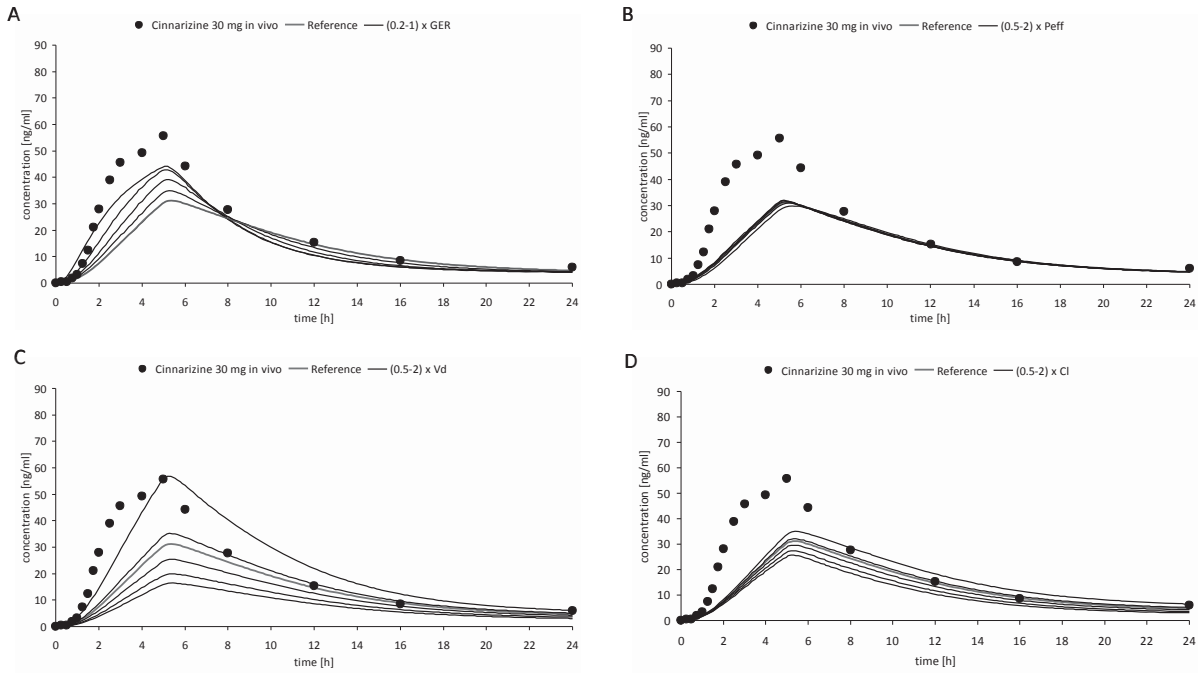


Fig. 7.15: Sensitivity analysis of the gastric emptying (A), the permeability (B), the volume of distribution (C) and the clearance (D) on plasma profile predictions of Cinnarizine 30 mg tablets in the fed state by implementing dissolution profiles in FeSSGF pH 5.0 and FeSSIF-V2 into Simcyp®.



Appendix

Sensitivity analysis by implementing biorelevant solubility of cinnarizine into the Simcyp[®] gastrointestinal solubility mask

The sensitivity analysis of the fasted state simulations using the GI solubility method revealed that almost all parameters have an influence on plasma profile predictions (Figures 7.16 and 7.17).

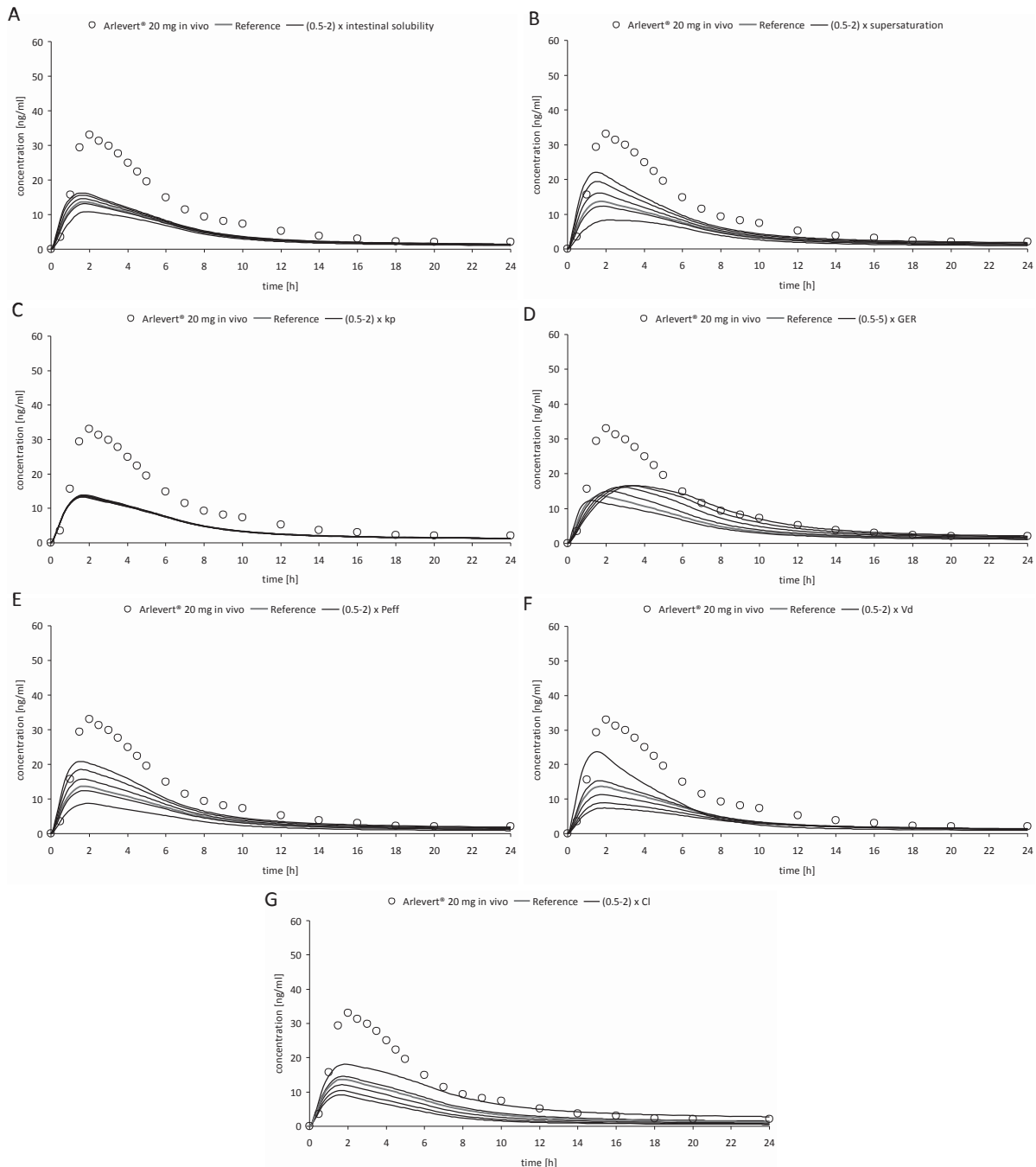


Fig. 7.16: Sensitivity analysis of the intestinal solubility (A), the supersaturation (B), the precipitation (C), the gastric emptying (D), the permeability (E), the volume of distribution (F) and the clearance (G) on plasma profile predictions of Arlevert[®] in the fasted state by implementing biorelevant solubility of cinnarizine into the Simcyp[®] gastrointestinal solubility mask.

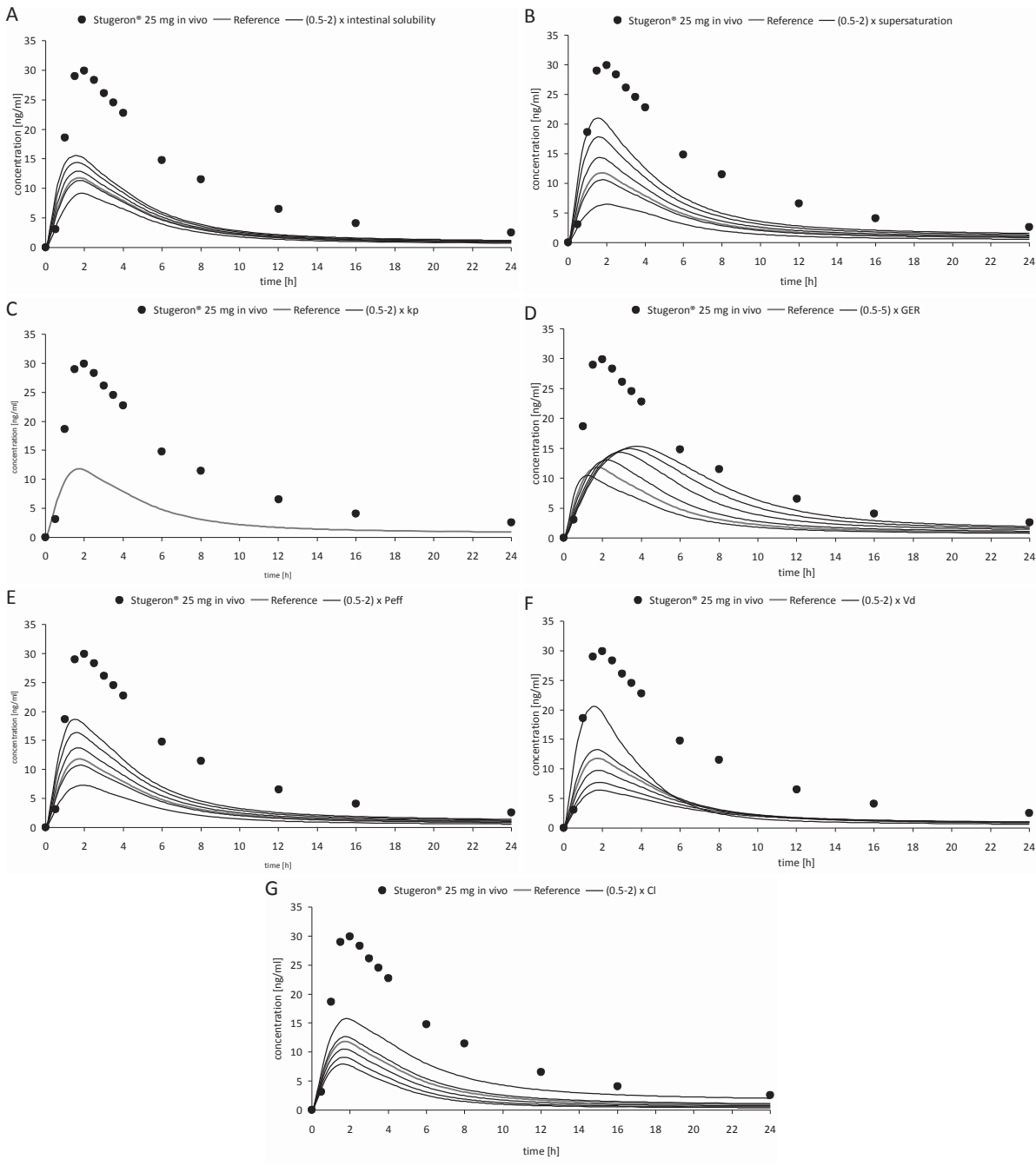


Fig. 7.17: Sensitivity analysis of the intestinal solubility (A), the supersaturation (B), the precipitation (C), the gastric emptying (D), the permeability (E), the volume of distribution (F) and the clearance (G) on plasma profile predictions of Stugeron® in the fasted state by implementing biorelevant solubility of cinnarizine into the Simcyp® gastrointestinal solubility mask.

The biggest effects on AUC and C_{max} were observed when the volume of distribution was altered. Significant changes of the predictions (AUC and C_{max}) were exhibited by variations of the supersaturation and P_{eff} values. Less significant effects were seen when the GER and intestinal solubility were varied. Alterations of the GER value



Appendix

affected the C_{\max} and the t_{\max} value. Almost no effect was observed when the precipitation value was modified.

The sensitivity analysis of the fed state shows similar results as for the fasted state (Figures 7.18 and 7.19). The most influential factors on the profile predictions were the V_d and GER. Changes of the V_d revealed the most significant effect on the C_{\max} and AUC. Alterations of the GER showed a big effect on the t_{\max} value. Changes of clearance (Cl) and permeability (P_{eff}) had only little influence on the AUC and C_{\max} variability. Gastric and intestinal solubility values did not have any influence on the plasma profile predictions.

The sensitivity analysis leads to the same assumption posed in the sensitivity investigation utilizing the dissolution profile model. The V_d value seems to be overestimated in the plasma profile simulations of cinnarizine in Simcyp[®]. The next sensitivity analysis should verify this assumption.

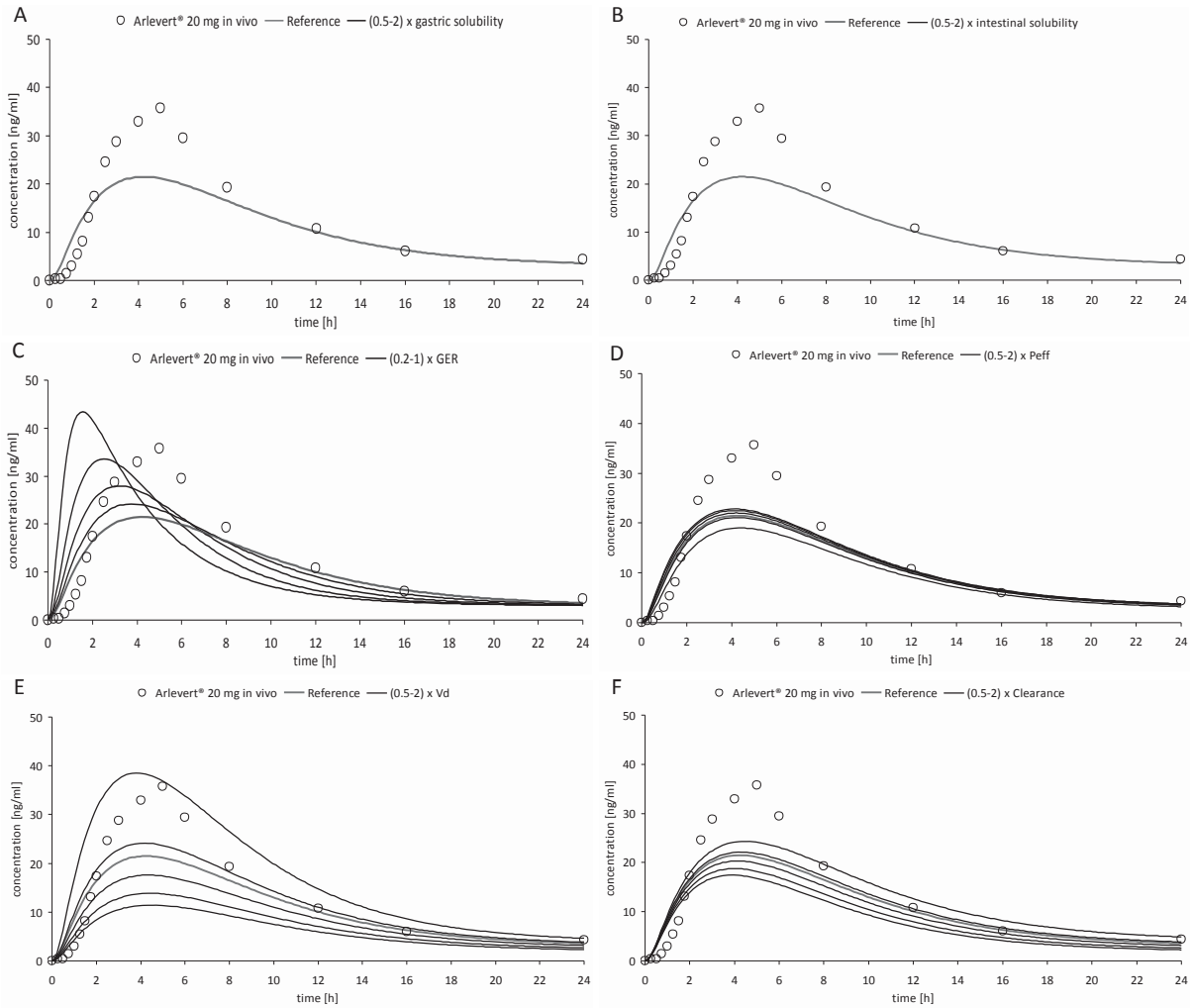


Fig. 7.18: Sensitivity analysis of the gastric solubility (A), the intestinal solubility (B), the gastric emptying (C), the permeability (D), the volume of distribution (E) and the clearance (F) on plasma profile predictions of Arlevert® in the fed state by implementing biorelevant solubility of cinnarizine into the Simcyp® gastrointestinal solubility mask.

Appendix

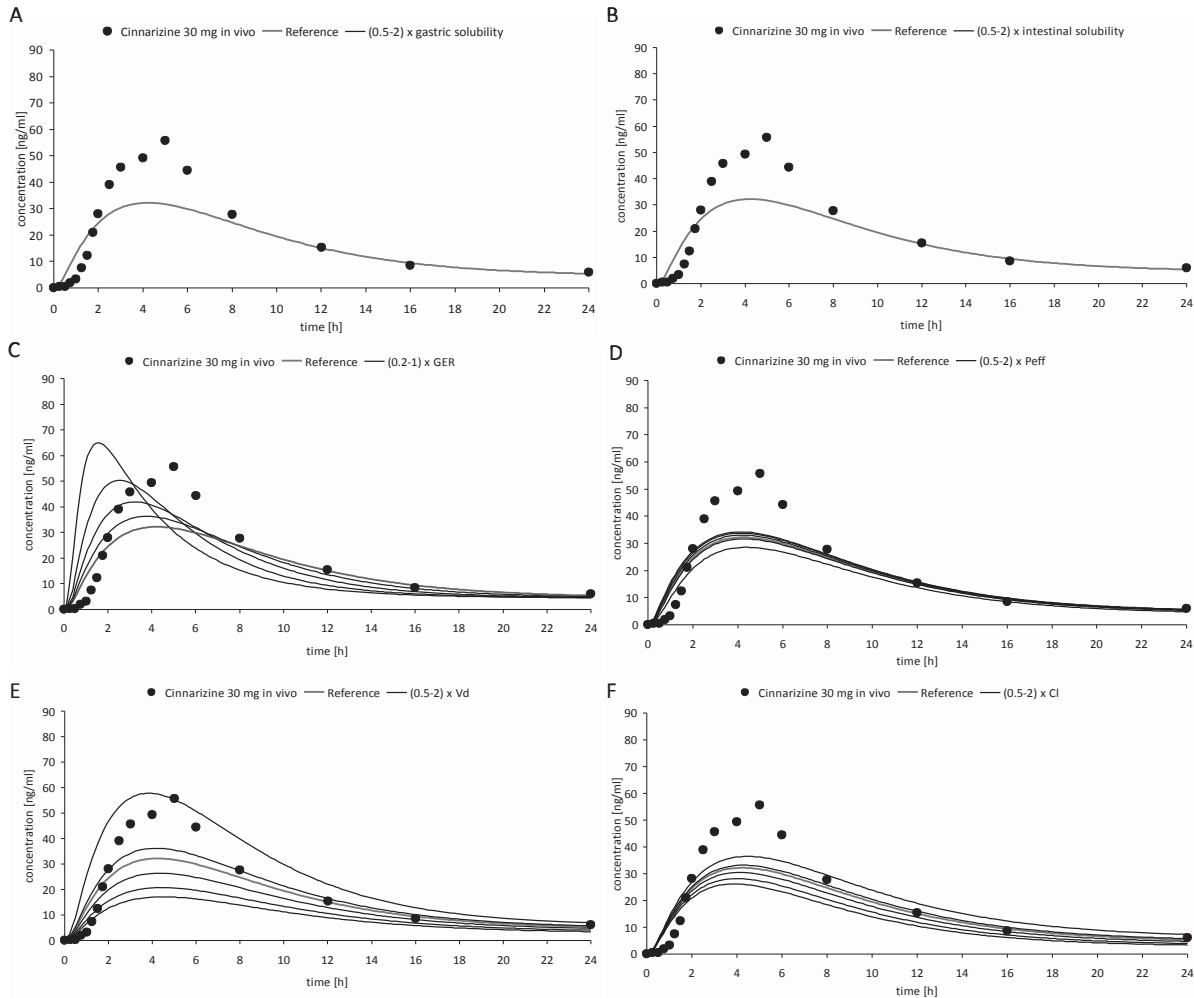


Fig. 7.19: Sensitivity analysis of the gastric solubility (A), the intestinal solubility (B), the gastric emptying (C), the permeability (D), the volume of distribution (E) and the clearance (F) on plasma profile predictions of Cinnarizine 30 mg tablets in the fed state by implementing biorelevant solubility of cinnarizine into the Simcyp® gastrointestinal solubility mask.

Sensitivity analysis using predicted and pH dependent solubility of cinnarizine

Since the plasma profile predictions and the sensitivity analysis using predicted solubility and pH dependent solubility methods were almost identical, only one of those methods (using predicted cinnarizine solubility) is presented in Figures 7.20 to 7.23.

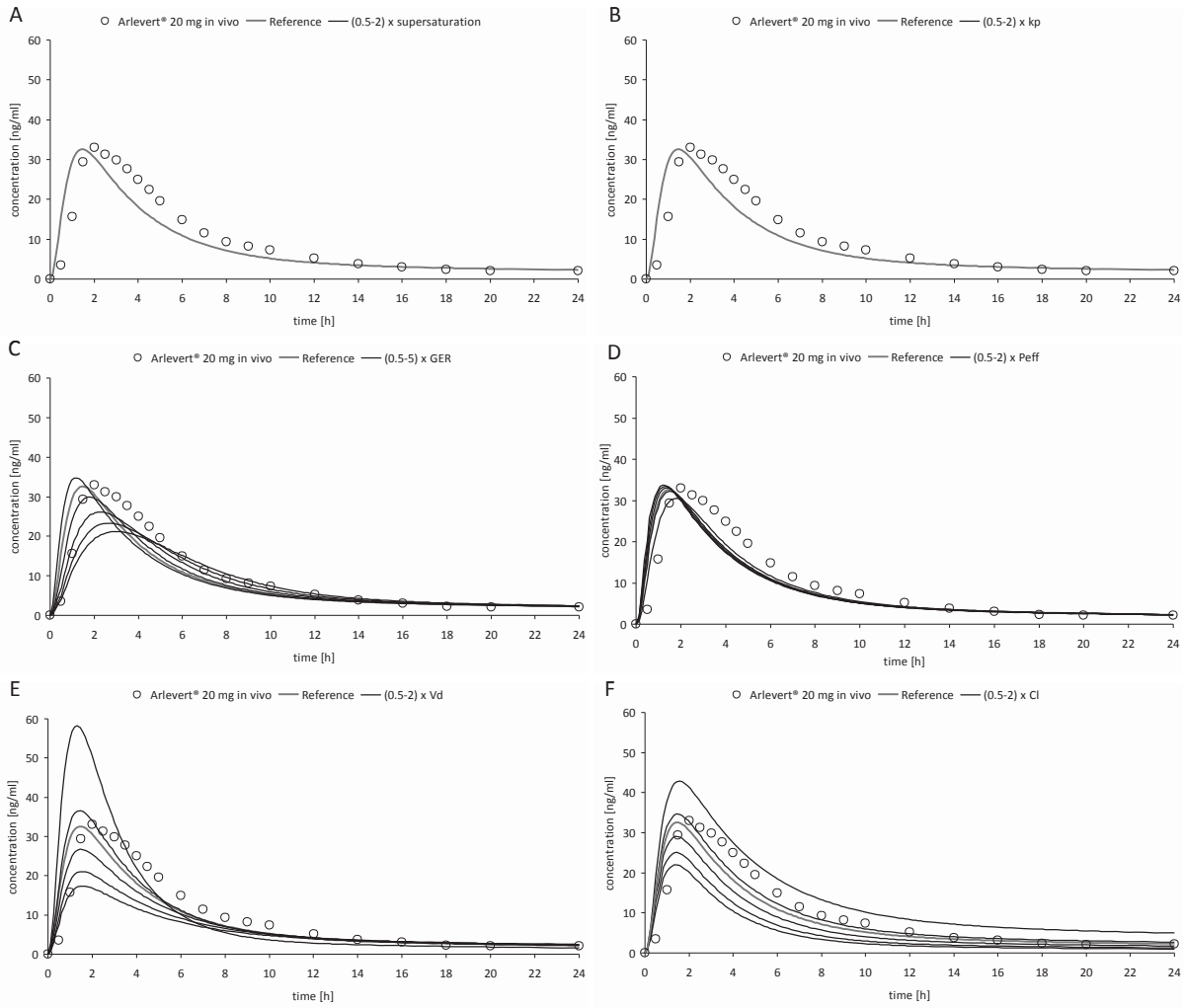


Fig. 7.20: Sensitivity analysis of the supersaturation (A), the precipitation (B), the gastric emptying (C), the permeability (D), the volume of distribution (E) and the clearance (F) on plasma profile predictions of Arlevert® in the fasted state using Simcyp® predictions of cinnarizine solubility by based on its physicochemical properties.

Appendix

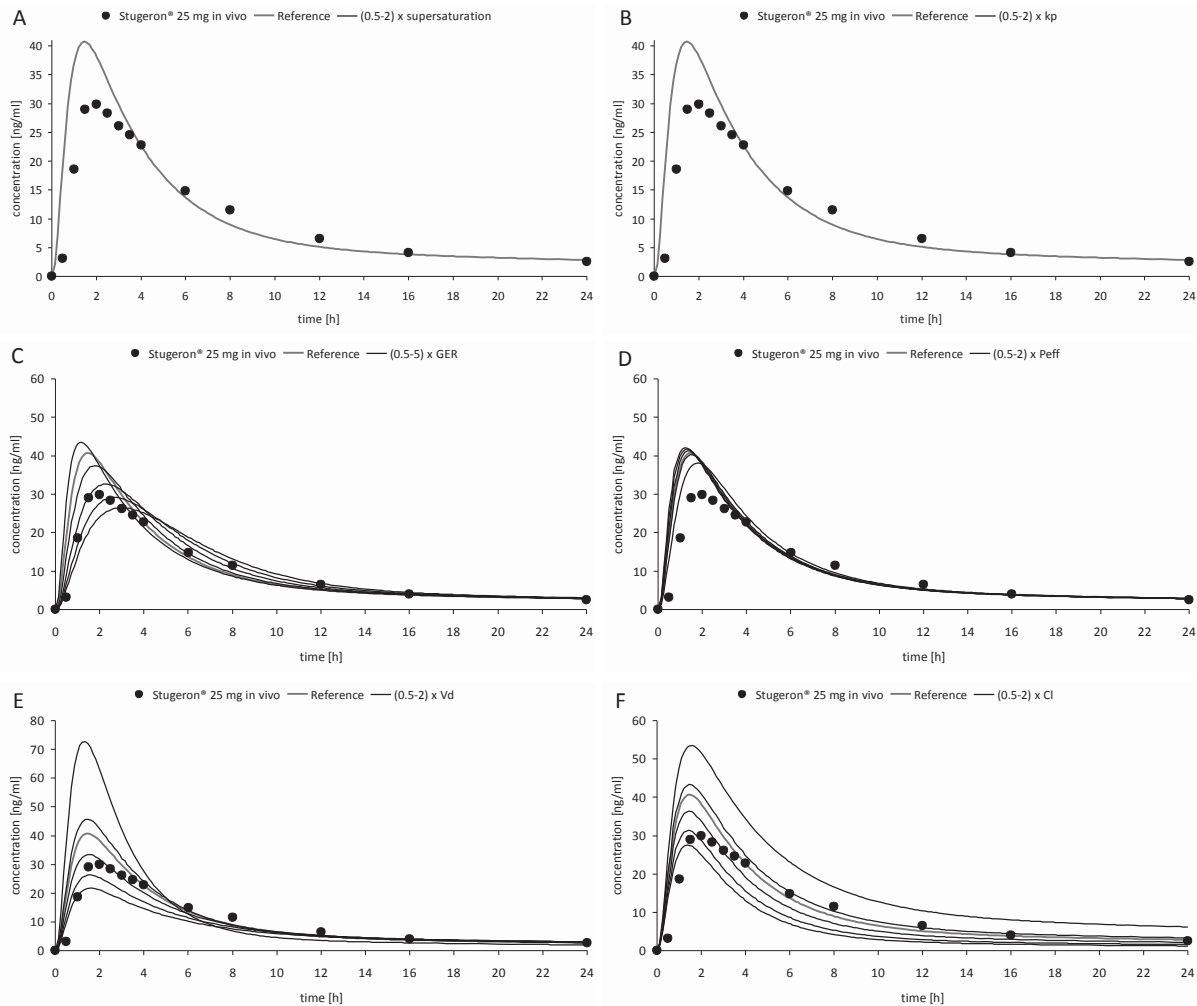


Fig. 7.21: Sensitivity analysis of the supersaturation (A), the precipitation (B), the gastric emptying (C), the permeability (D), the volume of distribution (E) and the clearance (F) on plasma profile predictions of Stugeron® in the fasted state using Simcyp® predictions of cinnarizine solubility based on its physicochemical properties.

Simcyp® simulations revealed a fraction absorbed value of 1.0 for all formulations and gastric states due to overestimated solubility values of cinnarizine. This is reflected in the sensitivity analysis of these simulation methods. Biggest influences on the plasma profile predictions in the fasted state were exhibited by changes of the Vd and clearance values. Changes of the GER and permeability values had also an effect on the predictions. Supersaturation and precipitation did not influence the plasma profiles, since the predicted solubility value of cinnarizine was overestimated.

The sensitivity analysis of the fed state demonstrated similar results as observed in the fasted state investigations. Despite the fact that the entire dose of the compound was absorbed in the simulations, plasma profiles of the fed state were generally

underestimated (Figures 7.22 and 7.23). Moreover, only the V_d and clearance values had an effect on the AUC value of the compound. Thus, the V_d of cinnarizine was most likely overestimated in the plasma profile simulations using Simcyp[®]. Since the value was calculated using fed state *in vivo* plasma with the help of WinNonLin[®], the estimation of the V_d value may not be exact. However, alternative V_d values for cinnarizine could not be found in the literature and WinNonLin[®] estimations had to be utilized for the simulations. Simcyp[®] allows internal predictions of the V_d value based on the physicochemical and blood protein binding properties of the compound. Simcyp[®] estimations of the V_d value (using the data from Table 7.1) proved to be even higher than the ones obtained from WinNonLin[®]. Thus, to simulate the plasma profiles of cinnarizine accurately the V_d value had to be fitted. The following section shows an approach of simulating cinnarizine plasma profiles using a fitted V_d value.

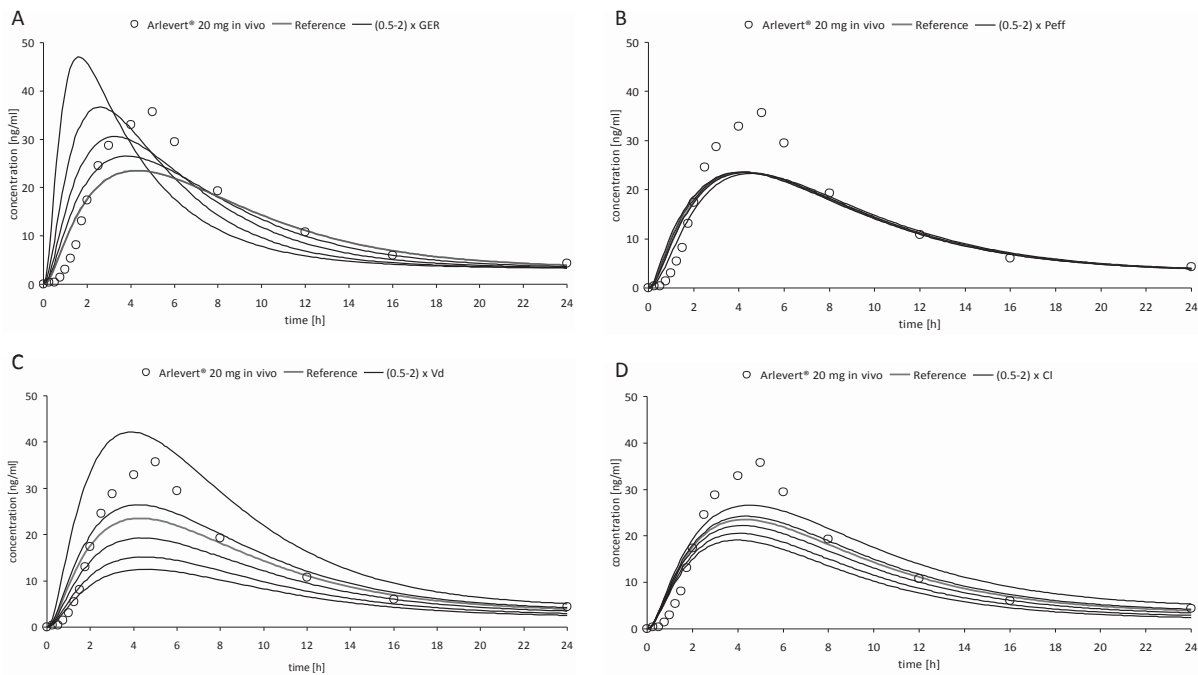


Fig. 7.22: Sensitivity analysis of the gastric emptying (A), the permeability (B), the volume of distribution (C) and the clearance (D) on plasma profile predictions of Arlevert[®] in the fed state using Simcyp[®] predictions of cinnarizine solubility based on its physicochemical properties.

Appendix

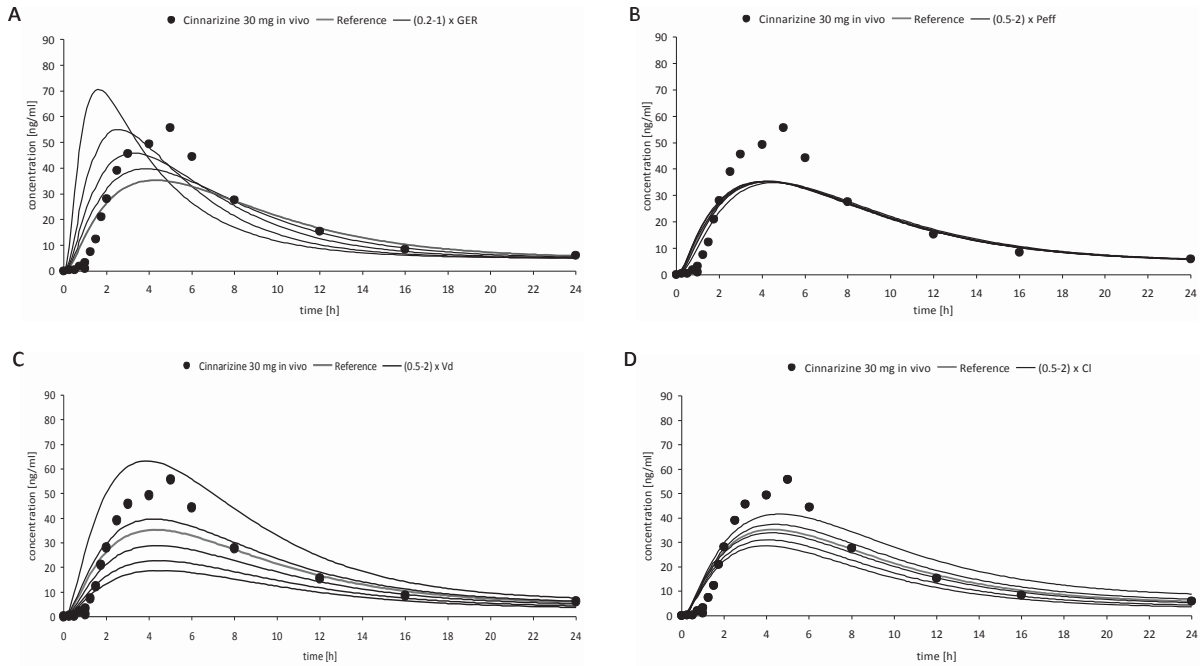


Fig. 7.23: Sensitivity analysis of the gastric emptying (A), the permeability (B), the volume of distribution (C) and the clearance (D) on plasma profile predictions of Cinnarizine 30 mg tablets in the fed state using Simcyp[®] predictions of cinnarizine solubility based on its physicochemical properties.

7.3.4 Simcyp[®] plasma profile predictions of cinnarizine using fitted Vd

Simulations of cinnarizine plasma profiles were performed with a fitted Vd value of 189 L. The value was adjusted by using fed state simulations with the predicted solubility method, where the fraction absorbed value of 1.0 was calculated. The Vd value was adjusted to fit the predictions with the observed plasma profile of Cinnarizine 30 mg tablets. The fitted Vd value was introduced into the simulation methods, which were expected to most reasonably represent the *in vivo* behavior. Hence, the fed state simulations were performed using the dissolution profile method. The fasted state simulations were conducted with the GI solubility method.

Fasted state simulation results are shown in Table 7.11 and Figure 7.24 along with predicted values using the “original” Vd value as comparators. Even with a lower Vd the plasma profiles were underestimated for both, Arlevert[®] and Stugeron[®]. However, the use of the fitted Vd exhibited better estimations than using the “original” value.

Table 7.11: *In vivo* and predicted (*Vd* new and *Vd* old) pharmacokinetic parameters for Arlevert[®] and Stugeron[®] tablets in the fasted state by implementing biorelevant solubility of cinnarizine into the Simcyp[®] gastrointestinal solubility mask

Formulation	AUC ₀₋₂₄ (ng x h/ml)	C _{max} (ng/ml)	t _{max} (h)
Arlevert[®]			
<i>in vivo</i>	218.72	33.0	2.0
<i>predicted (Vd new)</i>	129.21	18.83	1.560
<i>predicted (Vd old)</i>	108.00	13.68	1.681
Stugeron[®]			
<i>in vivo</i>	232.81	29.87	2.0
<i>predicted (Vd new)</i>	96.45	16.23	1.560
<i>predicted (Vd old)</i>	79.54	11.81	1.683

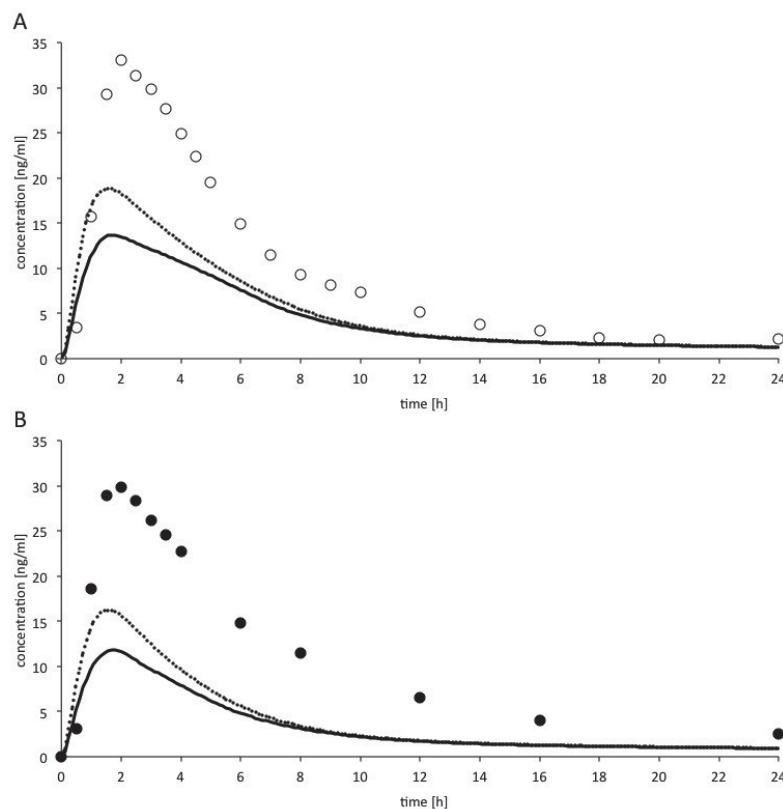


Fig. 7.24: Fasted state plasma profile predictions of Arlevert[®] 20 mg (A) and Stugeron[®] 25 mg (B) by implementing biorelevant solubility of cinnarizine into the Simcyp[®] gastrointestinal solubility mask. The two profiles were simulated using the “old *Vd*” (–) and “new *Vd*” (– –) values.

The plasma profile underestimations of Arlevert[®] and Stugeron[®] may originate from inaccurate supersaturation and precipitation calculations in Simcyp[®]. The program



Appendix

simulates the supersaturation by setting the supersaturation concentration as an initial value. Moreover, the onset of precipitation occurs instantly (without delay), which would underestimate the cinnarizine concentration in the GI tract and hence its *in vivo* performance. The *in vitro* investigation of the dissolution behavior of cinnarizine during simulated gastric emptying (transfer experiments) revealed that the maximum supersaturation concentration was achieved after a considerable time (30 minutes). Moreover, the precipitation took place after the simulated gastric emptying was completed. Thus, the onset of precipitation was delayed. Simulation of such *in vitro* behavior cannot be reflected with Simcyp[®] and may be the reason for these plasma profile underestimations.

The fed state results using the “new” Vd value are presented in Table 7.12 and Figure 7.25 along with outputs from simulations using the “old” Vd value. The use of the fitted Vd value exhibited reasonable simulations of the *in vivo* performance of both Arlevert[®] and Cinnarizine 30 mg tablets, even though the PK parameters were slightly underestimated.

Table 7.12: *In vivo* and predicted (Vd new and Vd old) pharmacokinetic parameters for Arlevert[®] and Cinnarizine 30 mg tablets in the fed state by implementing dissolution profiles in FeSSGF pH 5.0 and FeSSIF-V2 into Simcyp[®]

Formulation	AUC ₀₋₂₄ (ng x h/ml)	C _{max} (ng/ml)	t _{max} (h)
Arlevert[®]			
<i>in vivo</i>	315.22	35.69	5.000
<i>predicted (Vd new)</i>	303.97	33.59	4.690
<i>predicted (Vd old)</i>	232.51	21.66	4.697
Cinnarizine 30 mg			
<i>in vivo</i>	466.50	55.68	5.000
<i>predicted (Vd new)</i>	421.39	47.19	5.170
<i>predicted (Vd old)</i>	321.34	31.20	5.296

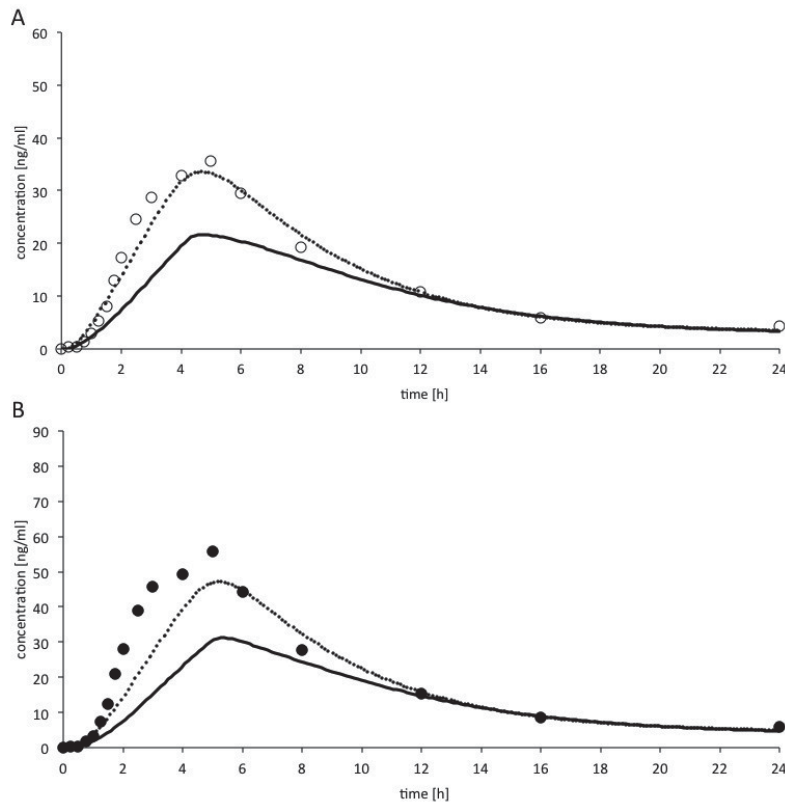


Fig. 7.25: Fed state plasma profile predictions of Arlevert[®] 20 mg (A) and Cinnarizine 30 mg tablets (B) by implementing biorelevant dissolution profiles into the Simcyp[®] mask. The two profiles were simulated using the “old Vd” (–) and “new Vd” (–) values.

Simcyp[®] simulations using biorelevant solubility, dissolution and transfer experiment data exhibited reasonable plasma profile predictions of cinnarizine formulations at different gastric states, especially when the volume of distribution was fitted. The utilization of parameter predictions by Simcyp[®] (predicted solubility, bile salt solubility enhancement) do not seem to be accurate, since only few compound specific physicochemical parameters are used for this purpose. With the parameters used to calculate supersaturation and precipitation behavior in Simcyp[®] one may not expect to obtain accurate simulations of complex dissolution behavior as shown in the transfer experiments with cinnarizine. To accurately simulate the *in vitro* supersaturation and precipitation behavior, additional parameters are required, such as the time of reaching the maximal supersaturation concentration and time of onset of precipitation.



Appendix

Thus, plasma profile simulations of compounds showing similar *in vitro* (and *in vivo*) behavior to cinnarizine may be improved by refining the dissolution, supersaturation and precipitation parameterization in Simcyp®.

7.4 Simcyp® plasma profile predictions of atazanavir

7.4.1 Simcyp® plasma profile predictions of atazanavir in the fasted state

Atazanavir plasma profile predictions in the fasted state were prepared by introducing compound related input parameters into the program mask. These were the molecular weight, the pKa value, the logP value, the plasma protein binding and the melting temperature (Table 7.14). Atazanavir permeability in Caco-2 cell monolayers was introduced along the distribution (Vd/F) and elimination kinetics (Cl/F) obtained from the literature and calculated in WinNonLin® (presented in Table 7.13). Supersaturation values and precipitation kinetics (if observed), which were obtained from transfer experiments, were additionally implemented into the program. Three different approaches, which are presented in the following sections, were utilized to predict the plasma profiles of different atazanavir sulfate doses (Reyataz® capsules).

Table 7.13: Absorption, distribution and elimination parameters of atazanavir implemented into Simcyp®

Parameter	Fasted state	Fed state (light meal)
Permeability (Caco-2)	$1.5\text{-}8 \times 10^{-6}$ cm/s	1.25×10^{-5} cm/s
Vd/F [142]	80.8 L	80.8 L
CL (100 mg)	247.0 L/h	-
CL (200 mg)	77.40 L/h	-
CL (400 mg)	65.99 L/h	34.9 L/h
CL (1200 mg)	63.00 L/h	-

Table 7.14: Standard physicochemical parameters of atazanavir implemented into Simcyp[®]

Parameter	Value
Molecular weight	704 g/mol
pKa	4.7
logP	4.54
Plasma protein binding	0.86
Melting temperature	210° C

Predictions obtained by implementing biorelevant solubility of atazanavir into the Simcyp[®] gastrointestinal solubility mask

Atazanavir plasma profile predictions were performed using GI solubility (Figures 3.14 and 3.15) and distribution and elimination data provided in Table 7.13. The biorelevant solubility values of atazanavir sulfate in the fasted (solubility in FaSSGF pH 1.6 and FaSSIF-V2) were introduced into the Simcyp[®] GI solubility mask. The gastric solubility of 7.488 mg/ml (FaSSGF pH 1.6) and the intestinal solubility of 91 µg/ml (kinetic solubility in FaSSGF pH2.0/FaSSIF-V2 combination after one hour) were implemented for all investigated atazanavir sulfate doses. The equilibrium solubility in FaSSIF-V2 was not chosen, since stable supersaturation was observed in transfer experiments. The supersaturation concentration corresponded to the kinetic solubility in the FaSSGF pH 2.0/FaSSIF-V2(PO₄) (1:2) mixture. On that basis precipitation was not considered in the simulations, resulting in the precipitation constant value of 0. Predictions and *in vivo* observations for all doses are presented in Figure 7.26 and Table 7.15.

Simcyp[®] predictions using the GI solubility method were somewhat similar to the ones obtained using the STELLA[®] model. The simulations of 100 mg dose exhibited an overestimation of the C_{max} value, although the AUC was only slightly overestimated. It is assumed that the calculated high clearance value of 247 L/h for the 100 mg dose could partly include the efflux/extraction and first pass hepatic elimination. Efflux and metabolism kinetics could not be included as it was done in STELLA[®], since concrete *in vitro* data were not available in the literature. Such simulations are only possible with Simcyp[®] when data are available which describe the Michaelis-Menten kinetics (microsomal, P-gp) of the compound.

Appendix

At higher atazanavir sulfate doses the *in vivo* performance was increasingly underestimated. Interestingly, the Simcyp® calculations show only a slightly greater AUC value and a lower C_{max} for the 1200 mg than for the 400 mg dose. Still the simulations lie within the standard deviations of the *in vivo* observations (100 mg dose excluded).

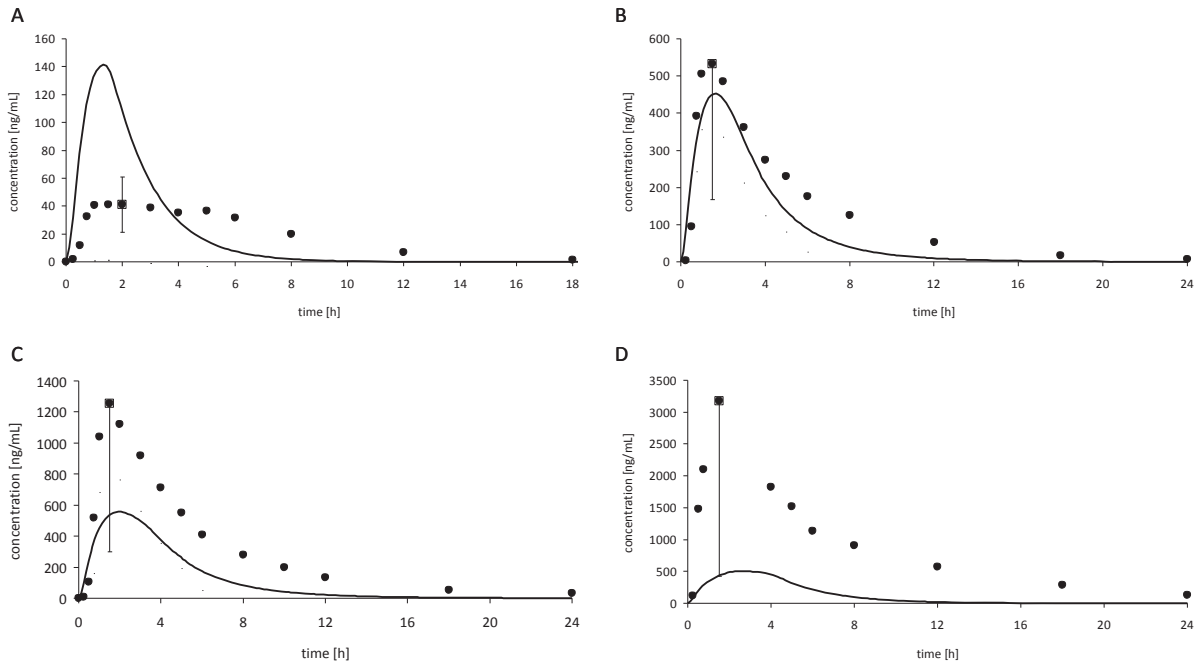


Fig. 7.26: Fasted state plasma profile predictions of atazanavir sulfate 100 mg (A), 200 mg (B), 400 mg (C) and 1200 mg (D) capsules by implementing kinetic biorelevant solubility of atazanavir into the Simcyp® gastrointestinal solubility mask.

Table 7.15: *In vivo* and predicted pharmacokinetic parameters for different doses of atazanavir sulfate in the fasted state by implementing kinetic biorelevant solubility of atazanavir into the Simcyp[®] gastrointestinal solubility mask

Atazanavir sulfate 100 mg	AUC ₀₋₁₈ (ng x h/ml)	C _{max} (ng/ml)	t _{max} (h)
<i>in vivo</i>	311	41	2.0
<i>predicted (no efflux/extraction)</i>	370.94	141.34	1.323

Atazanavir sulfate 200 mg	AUC ₀₋₂₄ (ng x h/ml)	C _{max} (ng/ml)	t _{max} (h)
<i>in vivo</i>	2828	533	1.5
<i>predicted</i>	1822.86	452.33	1.682

Atazanavir sulfate 400 mg	AUC ₀₋₂₄ (ng x h/ml)	C _{max} (ng/ml)	t _{max} (h)
<i>in vivo</i>	6721	1254	1.5
<i>predicted</i>	2766.16	556.57	1.920

Atazanavir sulfate 1200 mg	AUC ₀₋₂₄ (ng x h/ml)	C _{max} (ng/ml)	t _{max} (h)
<i>in vivo</i>	20648	3175	1.5
<i>predicted</i>	2786.46	502.92	2.520

Predictions obtained by using predicted atazanavir solubility by Simcyp[®]

Plasma profile simulations were performed using predicted atazanavir solubility (calculated solubility on basis of data in Table 7.14). Bile salt solubility enhancement was chosen in the model, since *in vitro* results have shown slightly higher solubility values in biorelevant media compared to blank buffers at the same pH. Distribution and elimination data were implemented from Table 3.14. The predicted pH solubility profile in Figure 7.27 shows reasonable solubility values for atazanavir. Plasma profile simulation results are presented in Figure 7.28 and Table 7.16.

Plasma profile predictions were similar to the simulations in which biorelevant solubility of atazanavir was implemented into Simcyp[®] GI solubility mask. Except for 100 mg dose plasma profile predictions lie within the standard deviations of the *in vivo* profile.

Appendix

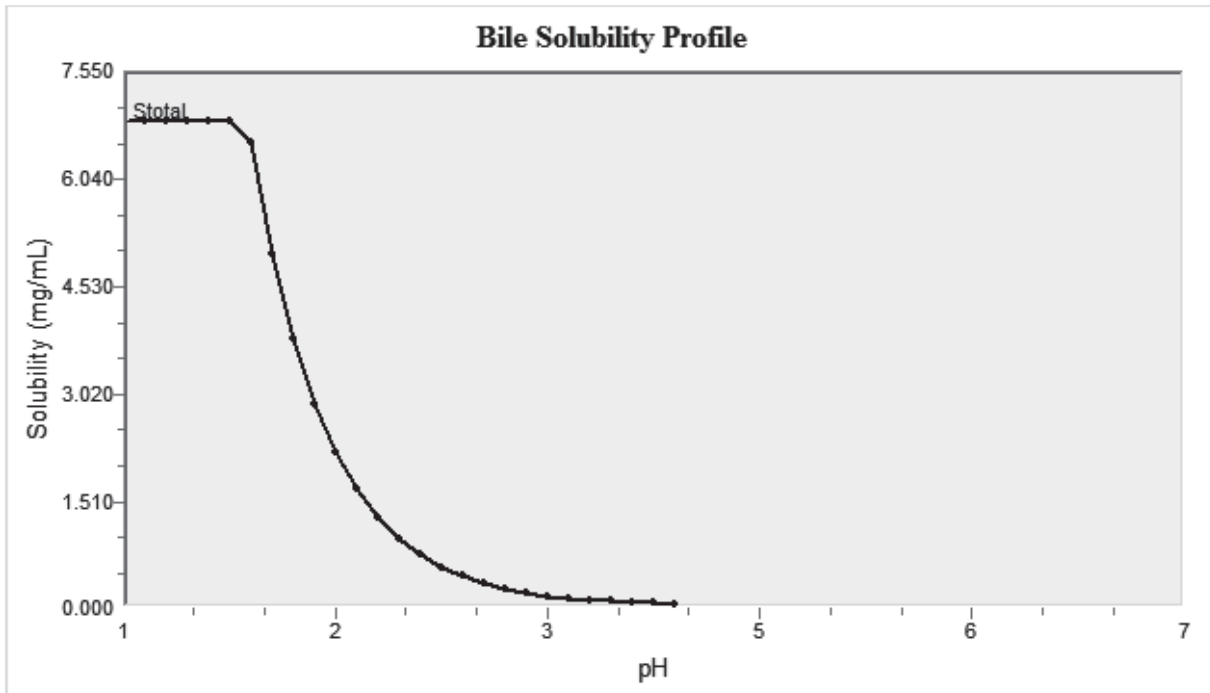


Fig. 7.27: Predicted pH solubility profile for atazanavir in Simcyp®.

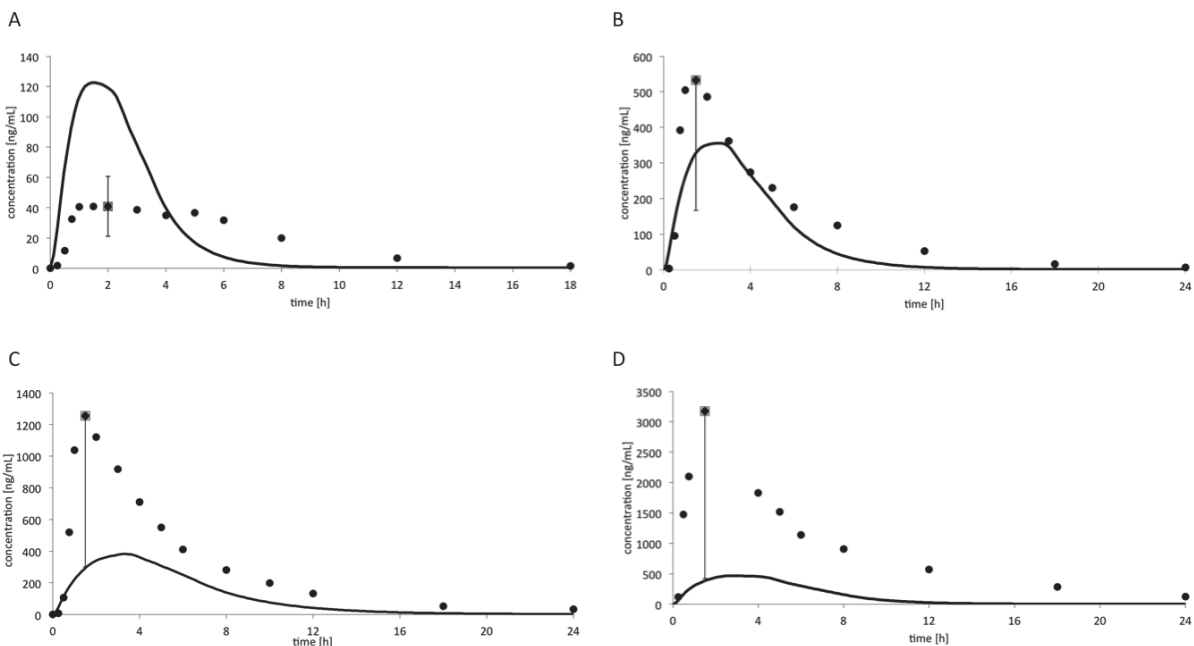


Fig. 7.28: Fasted state plasma profile predictions of atazanavir sulfate 100 mg (A), 200 mg (B), 400 mg (C) and 1200 mg (D) capsules using Simcyp® predictions of atazanavir solubility based on its physicochemical properties.

Table 7.16: *In vivo* and predicted pharmacokinetic parameters for different doses of atazanavir sulfate in the fasted state using Simcyp[®] predictions of atazanavir solubility based on its physicochemical properties

Atazanavir sulfate 100 mg	AUC ₀₋₁₈ (ng x h/ml)	C _{max} (ng/ml)	t _{max} (h)
<i>in vivo</i>	311	41	2.0
<i>predicted (no efflux/extraction)</i>	397.2	122.56	1.56

Atazanavir sulfate 200 mg	AUC ₀₋₂₄ (ng x h/ml)	C _{max} (ng/ml)	t _{max} (h)
<i>in vivo</i>	2828	533	1.5
<i>predicted</i>	1762.63	355.42	2.52

Atazanavir sulfate 400 mg	AUC ₀₋₂₄ (ng x h/ml)	C _{max} (ng/ml)	t _{max} (h)
<i>in vivo</i>	6721	1255	1.5
<i>predicted</i>	2607.0	381.95	3.36

Atazanavir sulfate 1200 mg	AUC ₀₋₂₄ (ng x h/ml)	C _{max} (ng/ml)	t _{max} (h)
<i>in vivo</i>	20648	3175	1.5
<i>predicted</i>	3041.14	466.07	2.88

Predictions obtained by introducing pH dependent solubility of atazanavir into the Simcyp[®] mask

Plasma profile predictions were simulated using equilibrium atazanavir solubility in aqueous buffers at different pH values (Figure 3.14). Since a light bile salt mediated solubility improvement was observed for atazanavir *in vitro*, bile salt solubility enhancement was considered in the simulations.

Simulations using the pH solubility profile resulted in almost the same predictions when using predicted atazanavir solubility by Simcyp[®] (Figure 7.29 and Table 7.17). As it was observed in previous simulations (using biorelevant and predicted solubility values), the C_{max} and AUC values of 100 mg atazanavir sulfate were overestimated. The C_{max} and AUC values were increasingly underestimated with higher doses. Only for the 200 mg and 400 mg doses the predictions were within the standard deviations of the *in vivo* observations.



Appendix

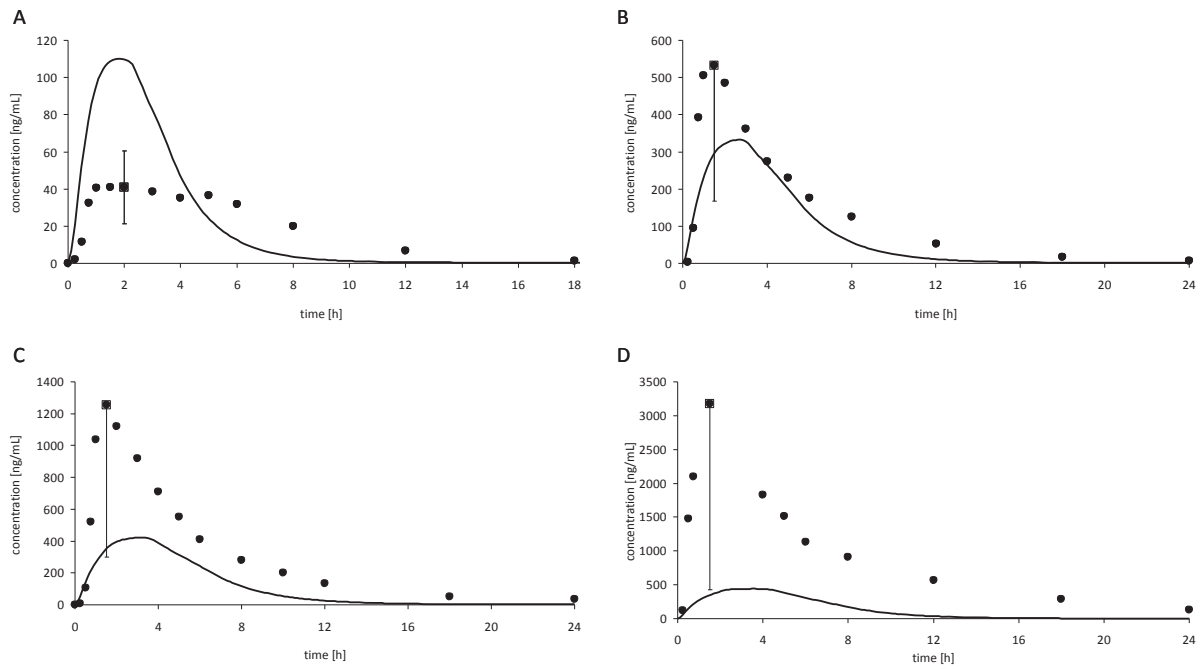


Fig. 7.29: Fasted state plasma profile predictions of atazanavir sulfate 100 mg (A), 200 mg (B), 400 mg (C) and 1200 mg (D) capsules by implementing equilibrium solubilities of atazanavir at different pH values into the Simcyp[®] mask.

Table 7.17: *In vivo* and predicted pharmacokinetic parameters for different doses of atazanavir sulfate in the fasted state by implementing equilibrium solubilities of atazanavir at different pH values into the Simcyp[®] mask.

Atazanavir sulfate 100 mg	AUC ₀₋₁₈ (ng x h/ml)	C _{max} (ng/ml)	t _{max} (h)
<i>in vivo</i>	311	41	2.0
<i>predicted (no efflux/extraction)</i>	397.14	110.05	1.803

Atazanavir sulfate 200 mg	AUC ₀₋₂₄ (ng x h/ml)	C _{max} (ng/ml)	t _{max} (h)
<i>in vivo</i>	2828	533	1.5
<i>predicted</i>	1761.25	333.31	2.760

Atazanavir sulfate 400 mg	AUC ₀₋₂₄ (ng x h/ml)	C _{max} (ng/ml)	t _{max} (h)
<i>in vivo</i>	6721	1255	1.5
<i>predicted</i>	2609.63	423.74	3.240

Atazanavir sulfate 1200 mg	AUC ₀₋₂₄ (ng x h/ml)	C _{max} (ng/ml)	t _{max} (h)
<i>in vivo</i>	20648	3175	1.5
<i>predicted</i>	3039.90	441.09	3.480

7.4.2 Simcyp[®] plasma profile predictions of atazanavir in the fed state

Predictions obtained by implementing biorelevant solubility of atazanavir into the Simcyp[®] gastrointestinal solubility mask

Fed state plasma profile predictions of 400 mg atazanavir sulfate capsules (2 x 200 mg Reyataz[®]) were performed by implementing biorelevant atazanavir solubility (in FeSSGF/FeSSGEm pH 2.75, FeSSIF-V2 and FeSSGF/FeSSGEm pH 2.75 and FeSSIF-V2 (1:2) mixtures) into the Simcyp[®] GI solubility mask. In the case of supersaturation and precipitation observed in *in vitro* experiments (FeSSGEm pH 2.75 as donor compartment), the appropriate supersaturation value and the precipitation constant were introduced into the model.

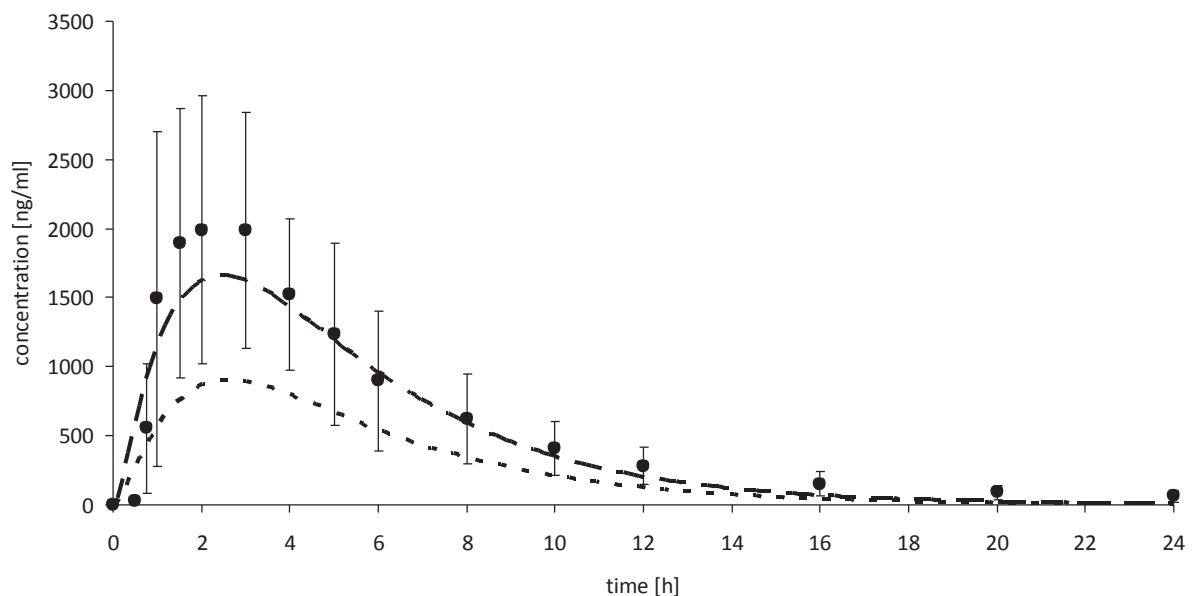


Fig. 7.30: Fed state plasma profile predictions of atazanavir sulfate 400 mg capsules (2 x 200 Reyataz[®]) by implementing biorelevant solubility data into the Simcyp[®] gastrointestinal solubility mask: “worst case” (--) (using FeSSGEm pH 2.75 data) and “best case” (- -) (using FeSSGF pH 2.75 data).

The simulations (Figure 7.30 and Table 7.18) exhibited different outcomes for the two *in vitro* approaches. When using the atazanavir concentrations obtained from transfer experiments utilizing FeSSGF pH 2.75 as the donor compartment the predictions were in a good agreement with the *in vivo* observation ($f_a = 0.98$). Although the C_{max} and AUC values were slightly underestimated, the simulated profiles were lying safely within the standard deviations of the *in vivo* observation.

The simulation using results from the transfer experiment, in which FeSSGEm pH 2.75 was utilized as the donor medium, significantly underestimated *in vivo* plasma profile ($f_a = 0.55$). The reason for this underestimation was the relatively lower atazanavir solubility in FeSSGEm pH 2.75. Additionally, precipitation was observed during transfer experiments utilizing the medium as the donor phase. By contrast, atazanavir solubility in FeSSGF pH 2.75 is considerably higher and no precipitation was observed when the medium was used as the donor phase for transfer experiments.

A mass balance study demonstrated 80% absorption of 400 mg atazanavir sulfate dose under fed conditions [106]. Even in the case of almost 100% atazanavir absorption the predicted plasma profile underestimated the *in vivo* profile. Overestimations of the Vd and/or clearance values by Simcyp[®] are most likely responsible for these underestimations. The sensitivity analysis should give more insight about the parameters that have the biggest relative impact on plasma profile predictions of atazanavir (Section 7.4.3).

Table 7.18: *In vivo* and predicted pharmacokinetic parameters for 400 mg atazanavir sulfate capsules (2 x 200 Reyataz[®]) in the fed state by implementing biorelevant solubility data into the Simcyp[®] gastrointestinal solubility mask: “worst case” (using FeSSGEm pH 2.75 data) and “best case” (using FeSSGF pH 2.75 data)

Atazanavir sulfate 400 mg	AUC ₀₋₂₄ (ng x h/ml)	C _{max} (ng/ml)	t _{max} (h)
<i>in vivo</i>	13232	1988	2.0
<i>best case</i>	11249.20	1658.55	2.52
<i>worst case</i>	6248.47	900.14	2.64

Predictions obtained by using predicted atazanavir solubility by Simcyp[®]

Analogous to fasted state predictions the fed state simulations were performed using predicted solubility of atazanavir (shown in Figure 7.27). For both transfer experiments predictions were almost identical (Figure 7.31 and Table 7.19). Prediction of atazanavir solubility seems to be reasonable for simulations of the fed state plasma profiles. However, the implementation of supersaturation and precipitation kinetics (from transfer experiments using FeSSGEm pH 2.75 as donor compartment) did not have a significant effect on the plasma profile predictions. Still,

Appendix

the incorporation of supersaturation and precipitation data predicted somewhat higher AUC and C_{\max} values than simulations in which the data were excluded.

Both simulations demonstrated 100% atazanavir absorption. Since a mass balance study revealed 80% absorption under fed conditions, it was therefore assumed that the solubility prediction by Simcyp[®] overestimated the *in vivo* performance of the compound in the fed state [106]. Slight plasma profile underestimations were attributed to overestimations of the V_d and/or clearance values (as described in the previous section).

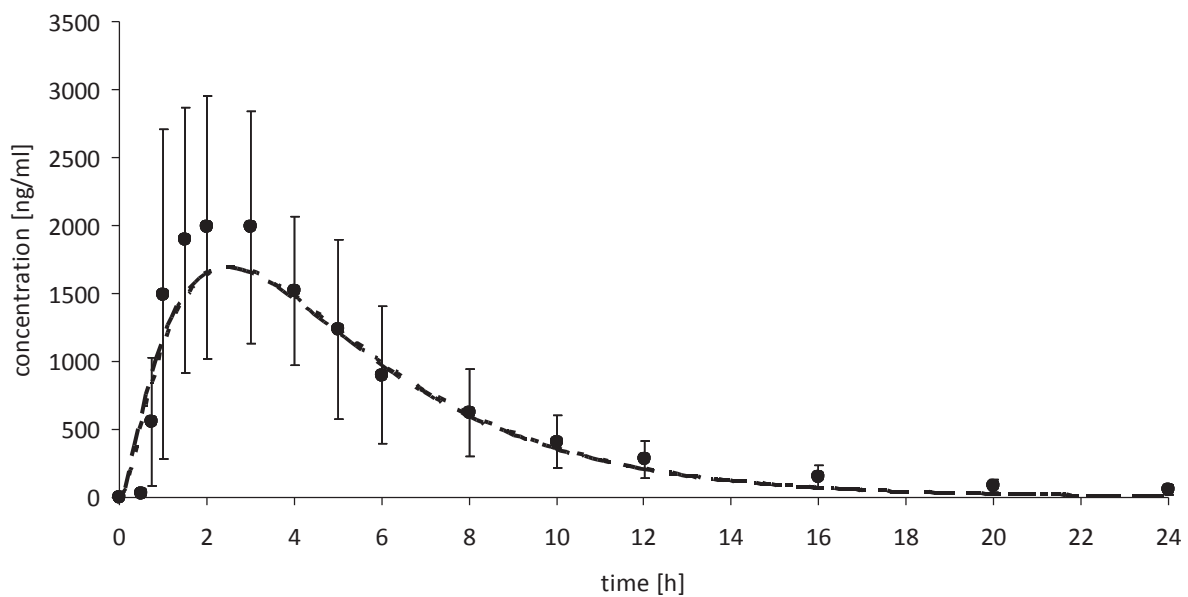


Fig. 7.31: Fed state plasma profile predictions of atazanavir sulfate 400 mg capsules (2 x 200 Reyataz[®]) by using Simcyp[®] predictions of atazanavir solubility based on its physicochemical properties: “worst case” (--) (using FeSSGEm pH 2.75 data) and “best case” (—) (using FeSSGF pH 2.75 data).

Table 7.19: *In vivo* and predicted pharmacokinetic parameters for 400 mg atazanavir sulfate capsules (2 x 200 Reyataz[®]) in the fed state using Simcyp[®] predictions of atazanavir solubility based on its physicochemical properties: “worst case” (using FeSSGEm pH 2.75 data) and “best case” (using FeSSGF pH 2.75 data).

Atazanavir sulfate 400 mg	AUC ₀₋₂₄ (ng x h/ml)	C_{\max} (ng/ml)	t_{\max} (h)
<i>in vivo</i>	13232	1988	2.0
<i>best case</i>	11420.92	1685.82	2.418
<i>worst case</i>	11497.26	1691.27	2.538

Predictions obtained by introducing pH dependent solubility of atazanavir into the Simcyp[®] mask

Using the pH dependent solubility approach the simulations revealed good plasma profile predictions (Figure 7.32 and Table 7.20). Predicted AUC and C_{max} values were close to the parameters observed *in vivo*. However, the t_{max} value was overestimated in both simulations, especially when supersaturation and precipitation were taken into consideration. Both simulations demonstrated 100% atazanavir absorption. The reasons for the slight underestimations of plasma profiles are described in the previous sections (biorelevant solubility used as GI solubility and predicted solubility simulations).

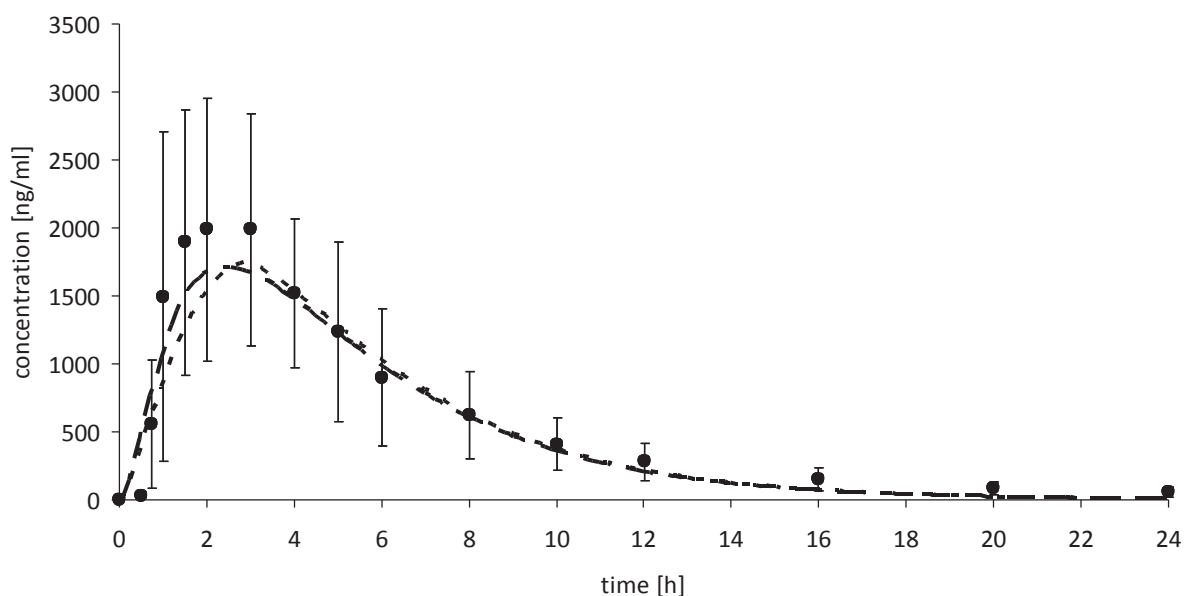


Fig. 7.32: Fed state plasma profile predictions of atazanavir sulfate 400 mg capsules (2 x 200 Reyataz[®]) by implementing equilibrium solubilities of atazanavir at different pH values into the Simcyp[®] mask: “worst case” (--) (using FeSSGEm pH 2.75 data) and “best case” (-·-) (using FeSSGF pH 2.75 data).



Appendix

Table 7.20: *In vivo* and predicted pharmacokinetic parameters for 400 mg atazanavir sulfate capsules (2 x 200 Reyataz[®]) in the fed state by implementing equilibrium solubilities of atazanavir at different pH values into the Simcyp[®] mask: “worst case” (using FeSSGEm pH 2.75 data) and “best case” (using FeSSGF pH 2.75 data).

Atazanavir sulfate 400 mg	AUC ₀₋₂₄ (ng x h/ml)	C _{max} (ng/ml)	t _{max} (h)
<i>in vivo</i>	13232	1988	2.0
best case	11470.95	1707.46	2.404
<i>worst case</i>	11450.26	1741.18	2.882

7.4.3 Simcyp[®] sensitivity analysis of atazanavir plasma profile predictions

The sensitivity analysis was performed for all doses, prandial states and simulation approaches. For the GI solubility approach variations were executed for the intestinal permeability, the gastric emptying rate (GER), the effective permeability (P_{eff}), the volume of distribution (Vd) and the clearance (Cl). When predicted solubility and pH dependent solubility were used for simulations, the GER, P_{eff} , Vd and Cl values were varied. In case of supersaturation and precipitation (k_p) variations of both parameters were additionally performed. All factors were altered from 0.5 to 2 times the initial value, except for the GER value in the fasted state which was varied 0.5-5 fold.

Sensitivity analysis by implementing biorelevant solubility of atazanavir into the Simcyp[®] gastrointestinal solubility mask

Intestinal solubility represents the amount of drug able to dissolve in the intestine in order to be absorbed through the gut wall. C_{max} and t_{max} values were affected through changes of the intestinal solubility (Figures 7.33 to 7.36). Variations of the GER value exhibited the biggest effect on the t_{max} value. Interestingly, the intestinal solubility and GER had the smallest influence on the plasma profile predictions. Permeability represents the rate of drug absorption through the gut wall. Changes to the permeability value exhibited a significant influence on the C_{max} and t_{max}, and finally on the AUC values. Hence, higher flux rates resulted in earlier t_{max}, and higher C_{max} and AUC values. Greatest influences on plasma profiles were exhibited by changes in the post-absorptive factors, volume of distribution and clearance. Since volume of distribution is inversely related to drug concentration in the blood, lower Vd values

demonstrated higher plasma profile predictions. Lower clearance values resulted in higher plasma profile predictions. A decrease of the clearance value would thus exhibit higher C_{max} values, since the elimination of atazanavir is decreased and the compound is accumulated in the blood compartment.

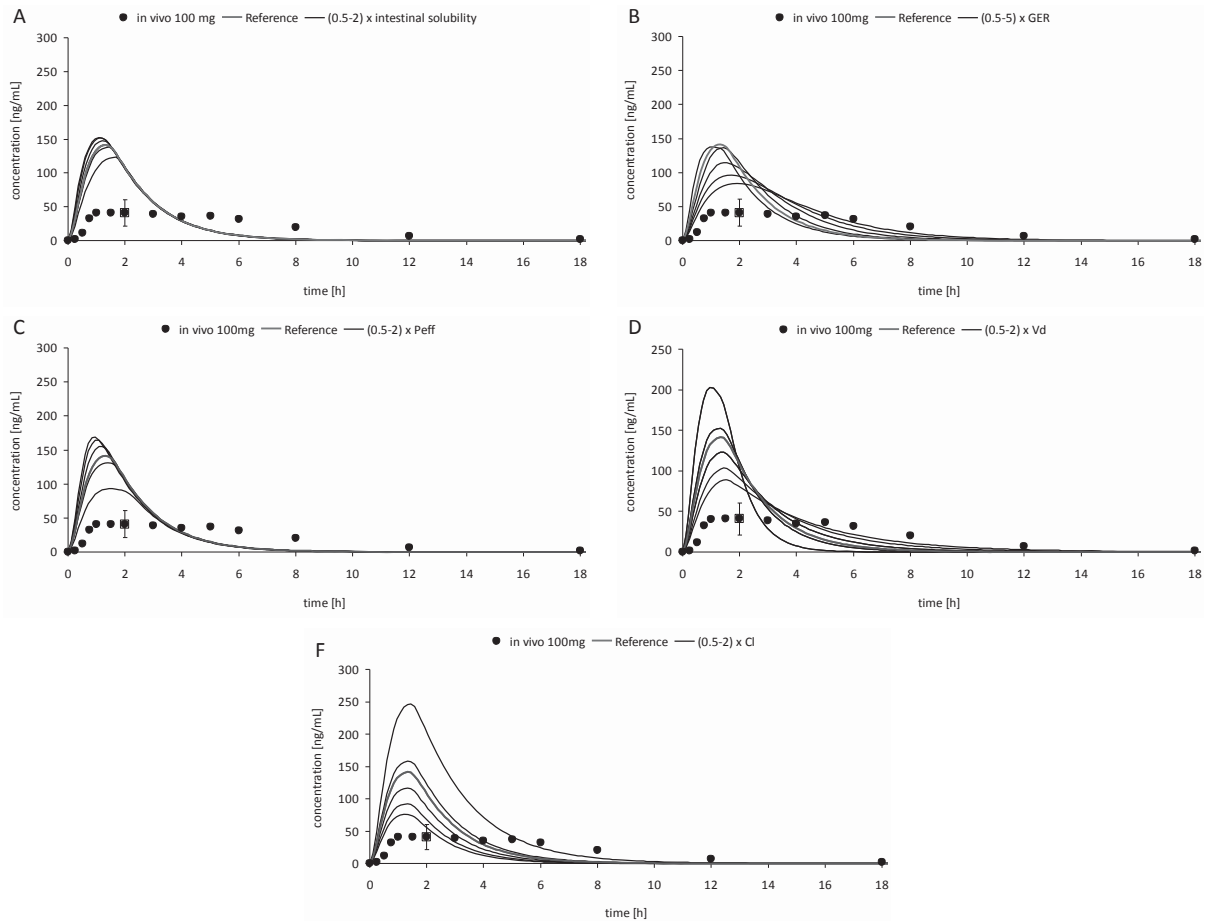


Fig. 7.33: Sensitivity analysis of the intestinal solubility (A), the gastric emptying (B), the permeability (C), the volume of distribution (D) and the clearance (E) on plasma profile predictions of 100 mg atazanavir sulfate in the fasted state by implementing biorelevant solubility of atazanavir into the Simcyp® gastrointestinal solubility mask.

Appendix

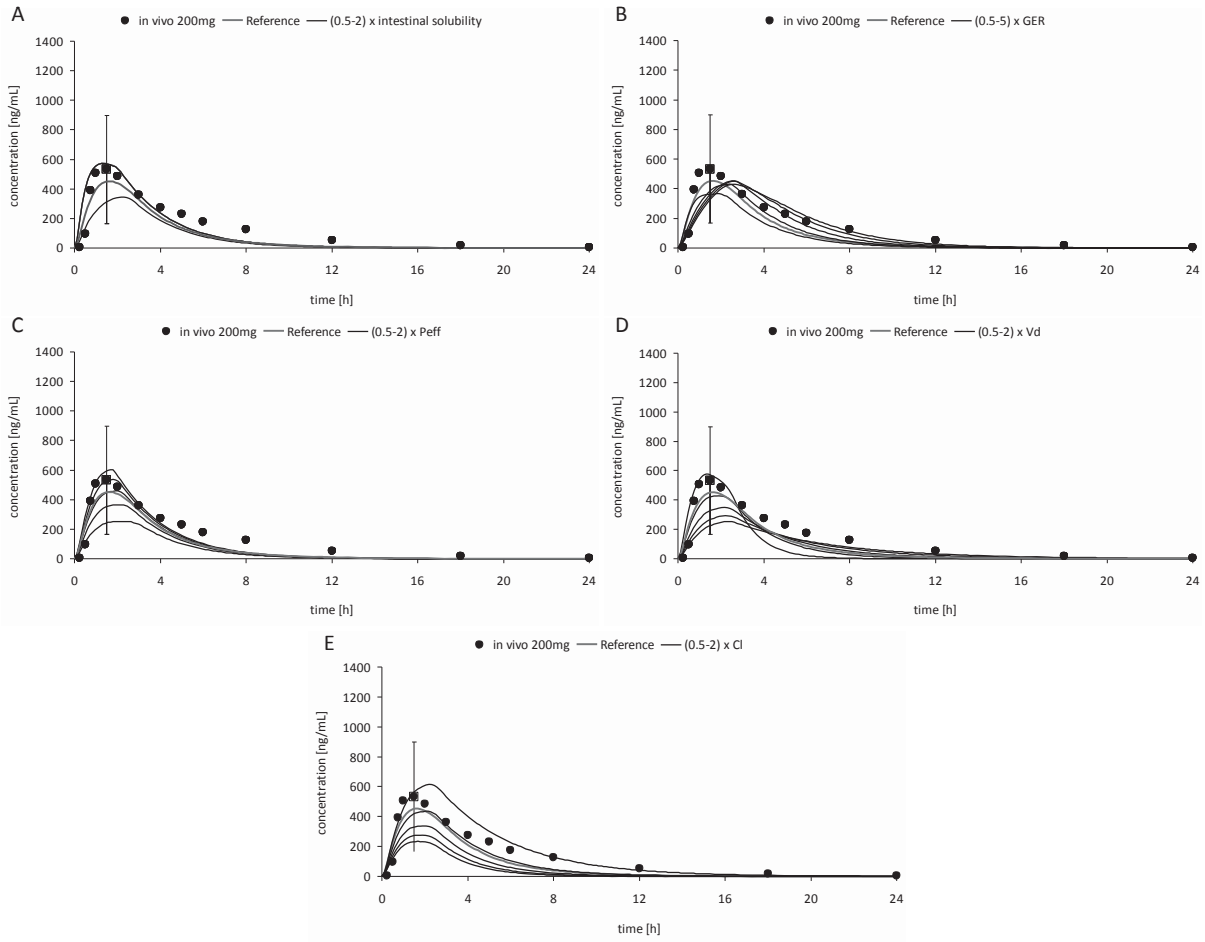


Fig. 7.34: Sensitivity analysis of the intestinal solubility (A), the gastric emptying (B), the permeability (C), the volume of distribution (D) and the clearance (E) on plasma profile predictions of 200 mg atazanavir sulfate in the fasted state by implementing biorelevant solubility of atazanavir into the Simcyp[®] gastrointestinal solubility mask.

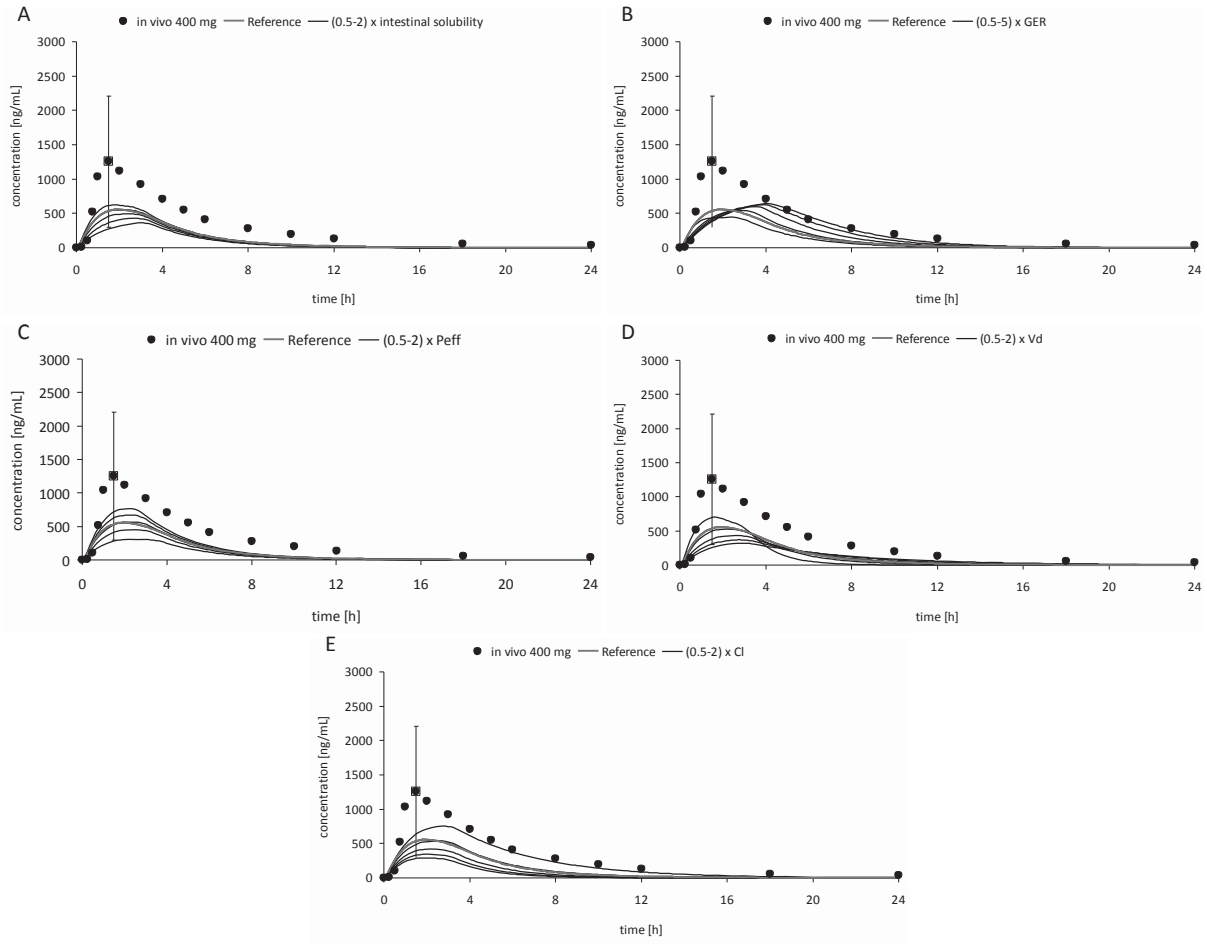


Fig. 7.35: Sensitivity analysis of the intestinal solubility (A), the gastric emptying (B), the permeability (C), the volume of distribution (D) and the clearance (E) on plasma profile predictions of 400 mg atazanavir sulfate in the fasted state by implementing biorelevant solubility of atazanavir into the Simcyp® gastrointestinal solubility mask.

Appendix

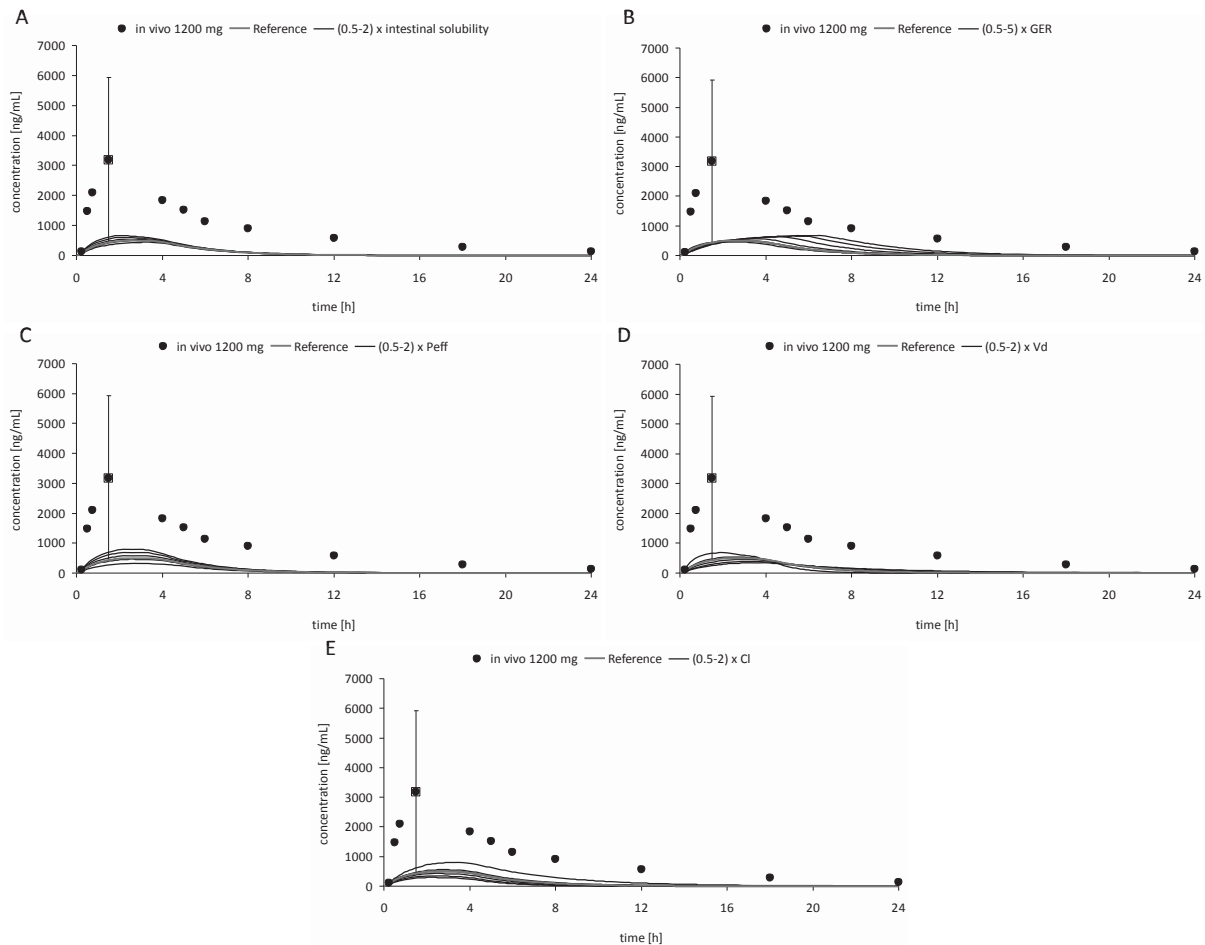


Fig. 7.36: Sensitivity analysis of the intestinal solubility (A), the gastric emptying (B), the permeability (C), the volume of distribution (D) and the clearance (E) on plasma profile predictions of 1200 mg atazanavir sulfate in the fasted state by implementing biorelevant solubility of atazanavir into the Simcyp® gastrointestinal solubility mask.

The sensitivity analysis of the fed state exhibited similar results to those observed in the fasted state (Figures 7.37 and 7.38). Changes of the intestinal solubility and the supersaturation value ("worst case") did not have any influence on the variability of plasma profile simulations. However, variations in the precipitation value ("worst case") had a considerable effect on the C_{max} , and hence the AUC. Alterations of the gastric emptying had a significant effect on the t_{max} value, since gastric emptying in the fed state is subject to zero order kinetics and thus is generally slower than in the fasted state. Shifts of the permeability value had some effect on the predictions of C_{max} and AUC. The most significant influence on the plasma profile predictions was exhibited through changes of the post-absorptive parameters, V_d and Cl .

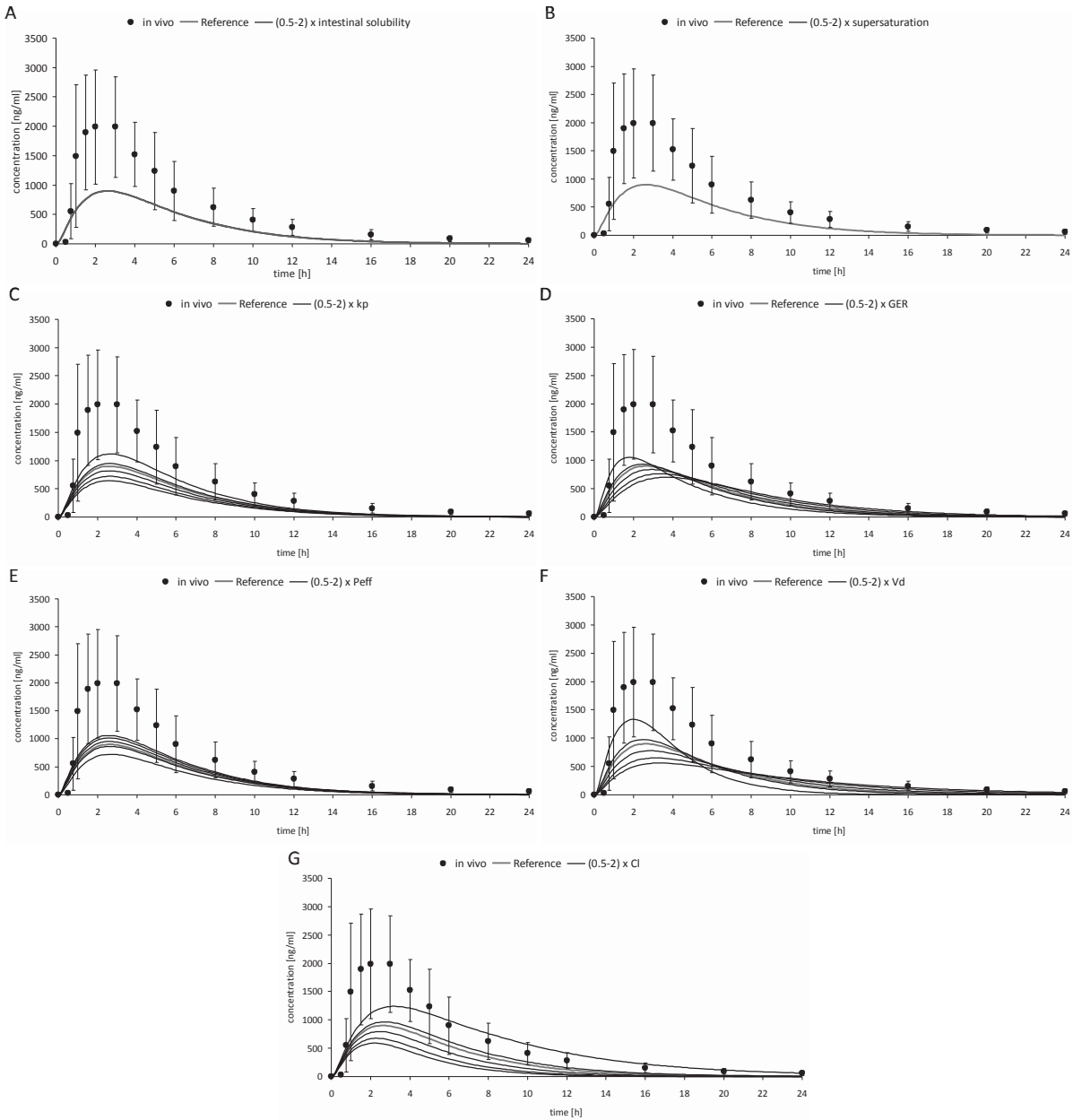


Fig. 7.37: “worst case” example - sensitivity analysis of the intestinal solubility (A), the supersaturation (B), the precipitation (C), the gastric emptying (D), the permeability (E), the volume of distribution (F) and the clearance (G) on plasma profile predictions of 400 mg atazanavir sulfate in the fed state by implementing biorelevant solubility of atazanavir into the Simcyp® gastrointestinal solubility mask.

Appendix

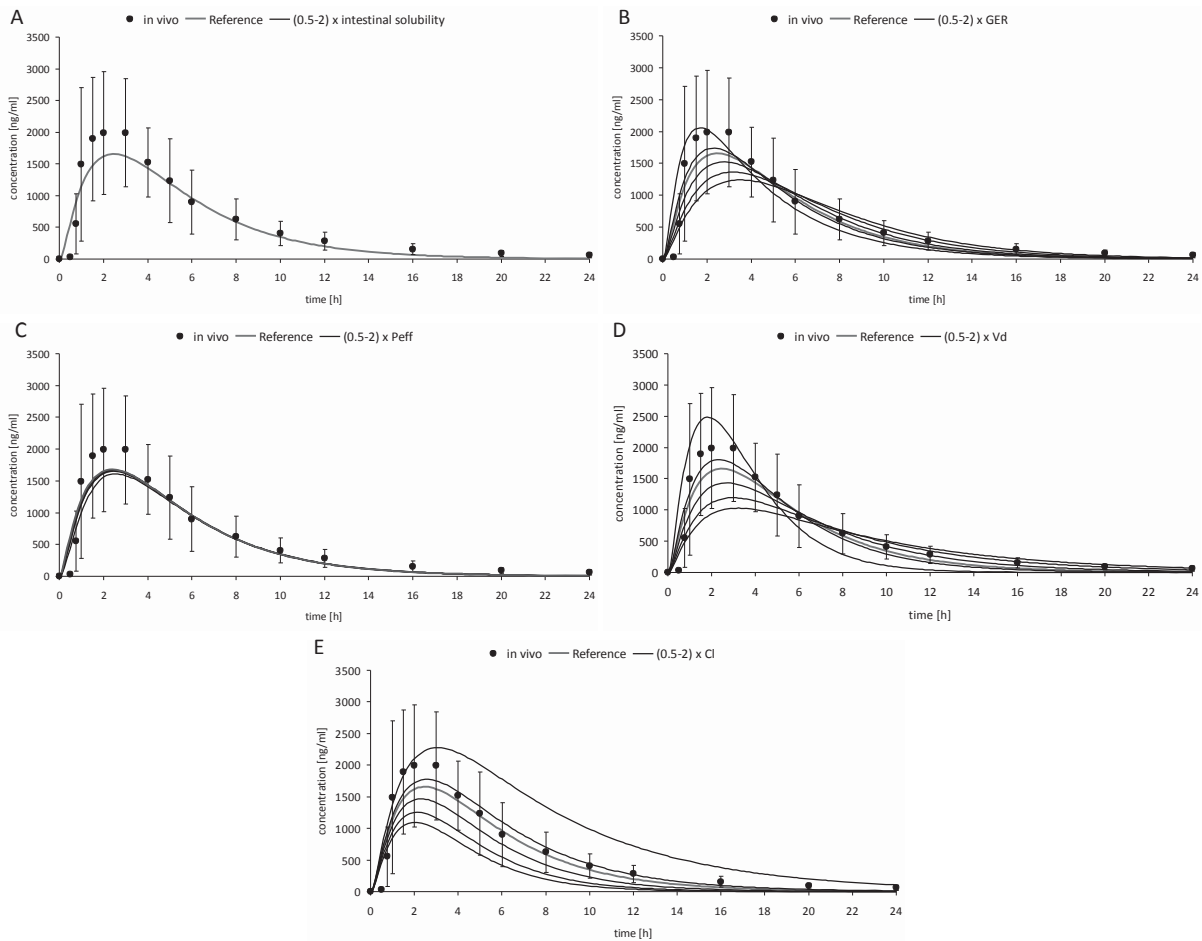


Fig. 7.38: “best case” example - sensitivity analysis of the intestinal solubility (A), the gastric emptying (B), the permeability (C), the volume of distribution (D) and the clearance (E) on plasma profile predictions of 400 mg atazanavir sulfate in the fed state by implementing biorelevant solubility of atazanavir into the Simcyp® gastrointestinal solubility mask.

Sensitivity analysis using predicted atazanavir solubility by Simcyp®

The sensitivity analysis of the fasted state simulations using predicted solubility exhibited similar results to the previous investigation (Figures 7.39 to 7.42). However, changes of the permeability value did not have a significant influence on the plasma profile predictions. Alterations of the GER affected the predictions to a relatively greater extent. The most dominant influence on the plasma profile predictions was observed when both post-absorptive factors, Vd and clearance, were modified.

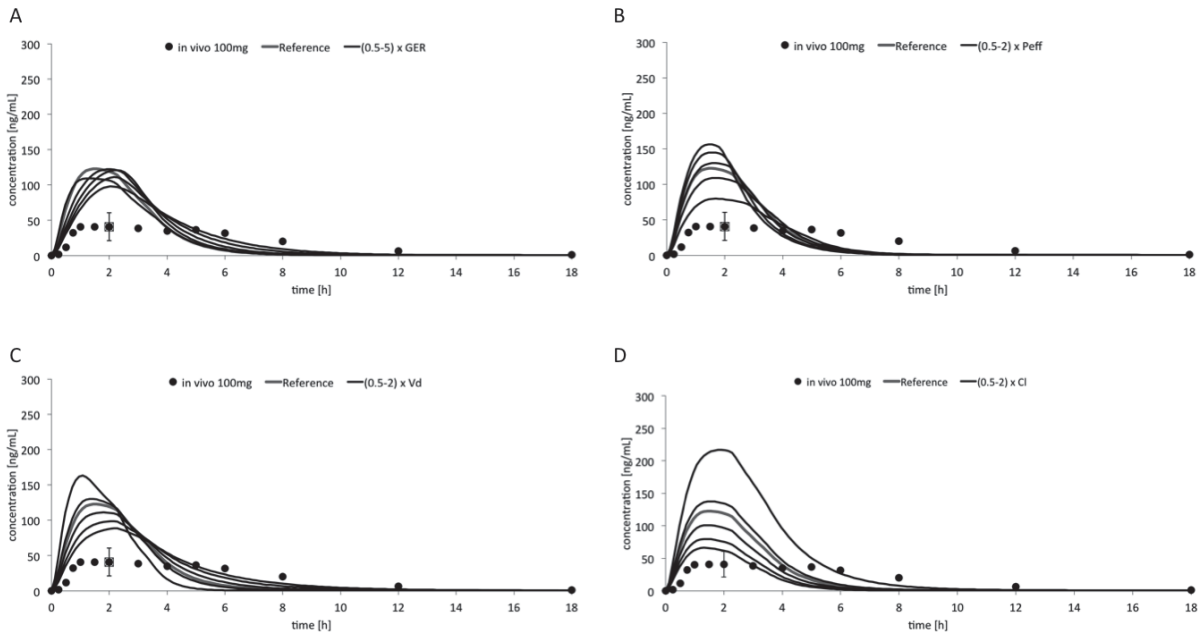


Fig. 7.39: Sensitivity analysis of the gastric emptying (A), the permeability (B), the volume of distribution (C) and the clearance (D) on plasma profile predictions of 100 mg atazanavir sulfate in the fasted state using predicted atazanavir solubility by Simcyp®.

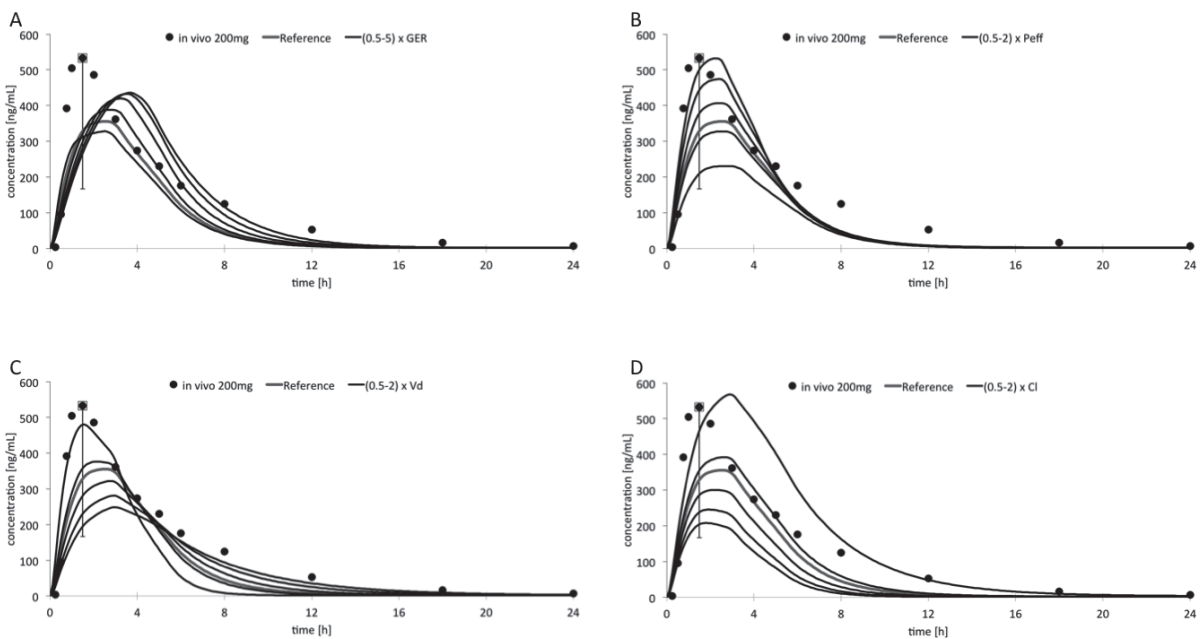


Fig. 7.40: Sensitivity analysis of the gastric emptying (A), the permeability (B), the volume of distribution (C) and the clearance (D) on plasma profile predictions of 200 mg atazanavir sulfate in the fasted state using predicted atazanavir solubility by Simcyp®.



Appendix

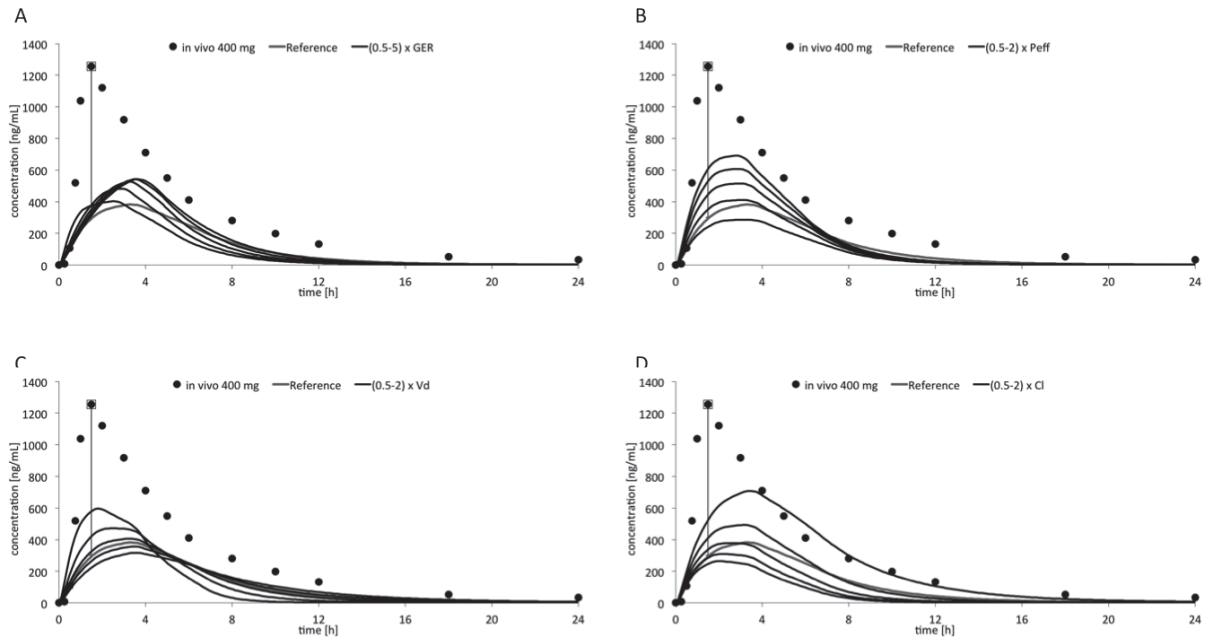


Fig. 7.41: Sensitivity analysis of the gastric emptying (A), the permeability (B), the volume of distribution (C) and the clearance (D) on plasma profile predictions of 400 mg atazanavir sulfate in the fasted state using predicted atazanavir solubility by Simcyp®.

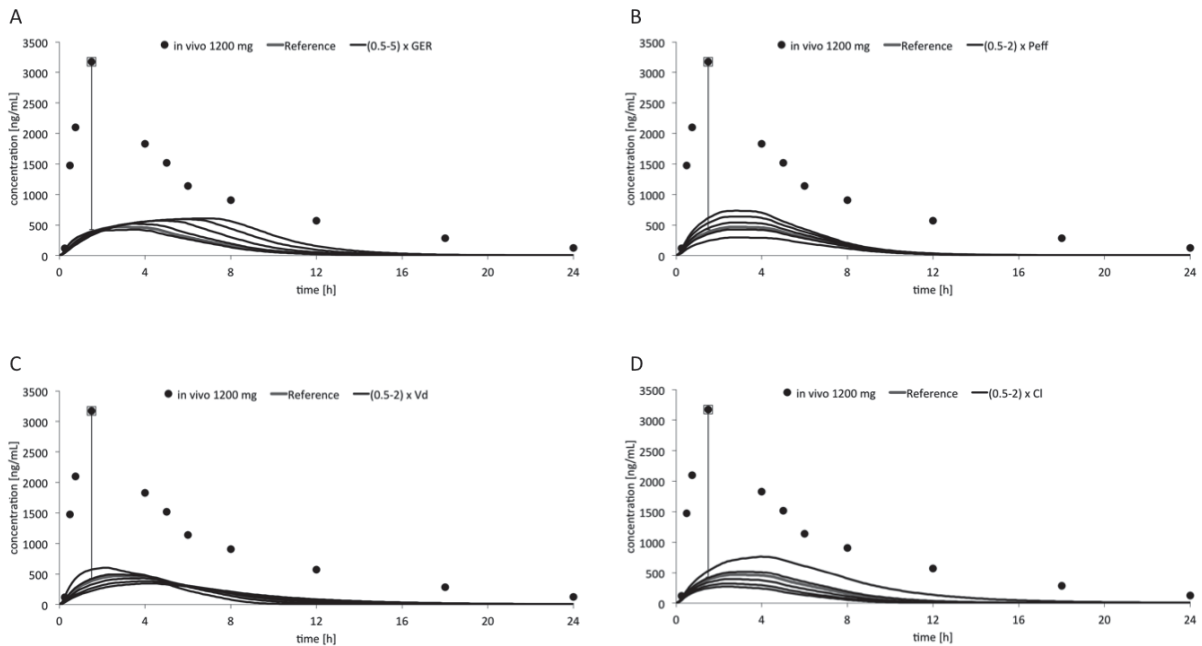


Fig. 7.42: Sensitivity analysis of the gastric emptying (A), the permeability (B), the volume of distribution (C) and the clearance (D) on plasma profile predictions of 1200 mg atazanavir sulfate in the fasted state using predicted atazanavir solubility by Simcyp®.

The fed state sensitivity analysis exhibited similar results to fasted state investigations (Figures 7.43 and 7.44). Interestingly, when investigating the “worst case” alterations of supersaturation and precipitation did not have any effect on the

profile predictions. As it was observed in the fasted state analysis variations of the P_{eff} value had only a minor effect on the predictions, while changes of the GER moderately affected the simulated profiles. Still alterations of the post-absorptive parameters (Vd and clearance) had the strongest influence on the predictions.

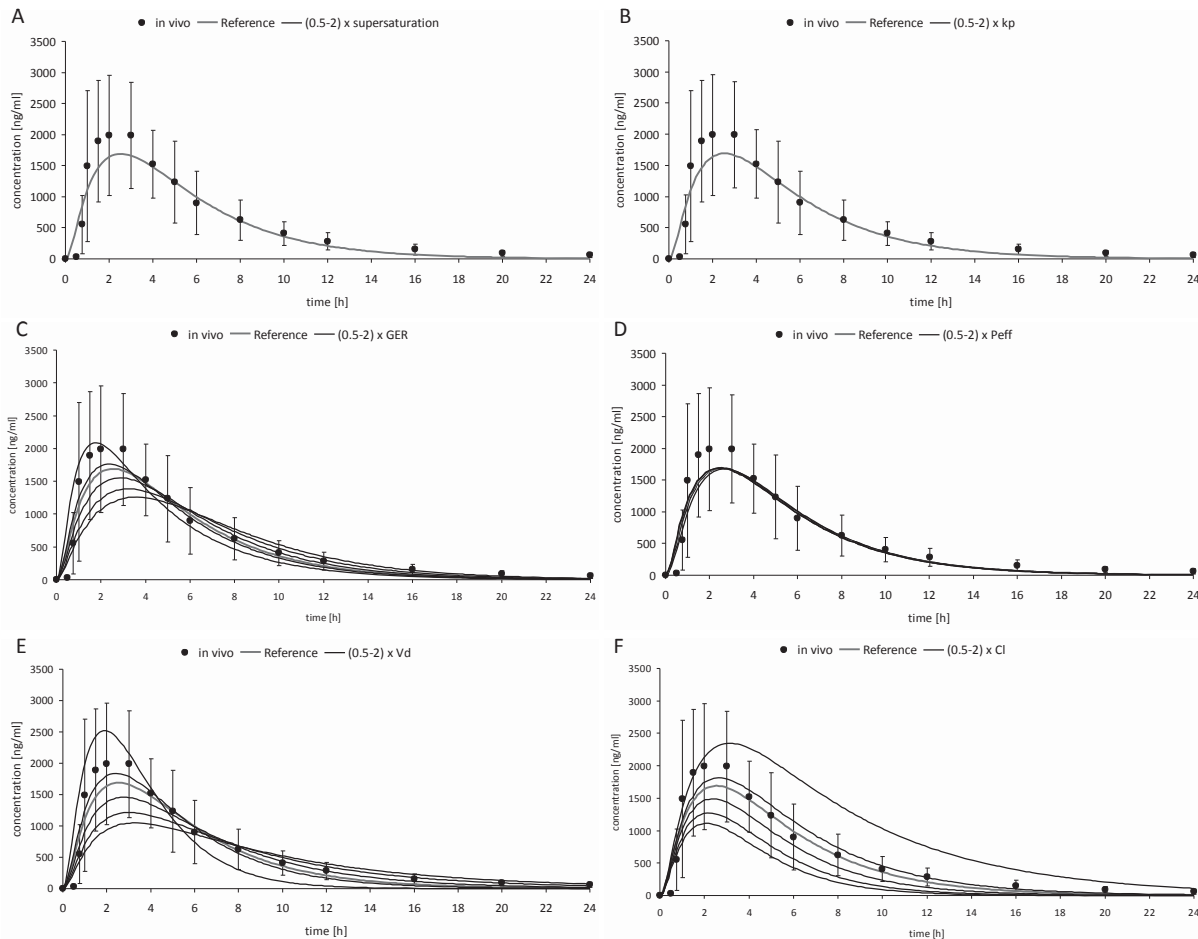


Fig. 7.43: “worst case” example - sensitivity analysis of supersaturation (A), precipitation (B), the gastric emptying (C), the permeability (D), the volume of distribution (E) and the clearance (F) on plasma profile predictions of 400 mg atazanavir sulfate in the fed state using predicted atazanavir solubility by Simcyp®.

Appendix

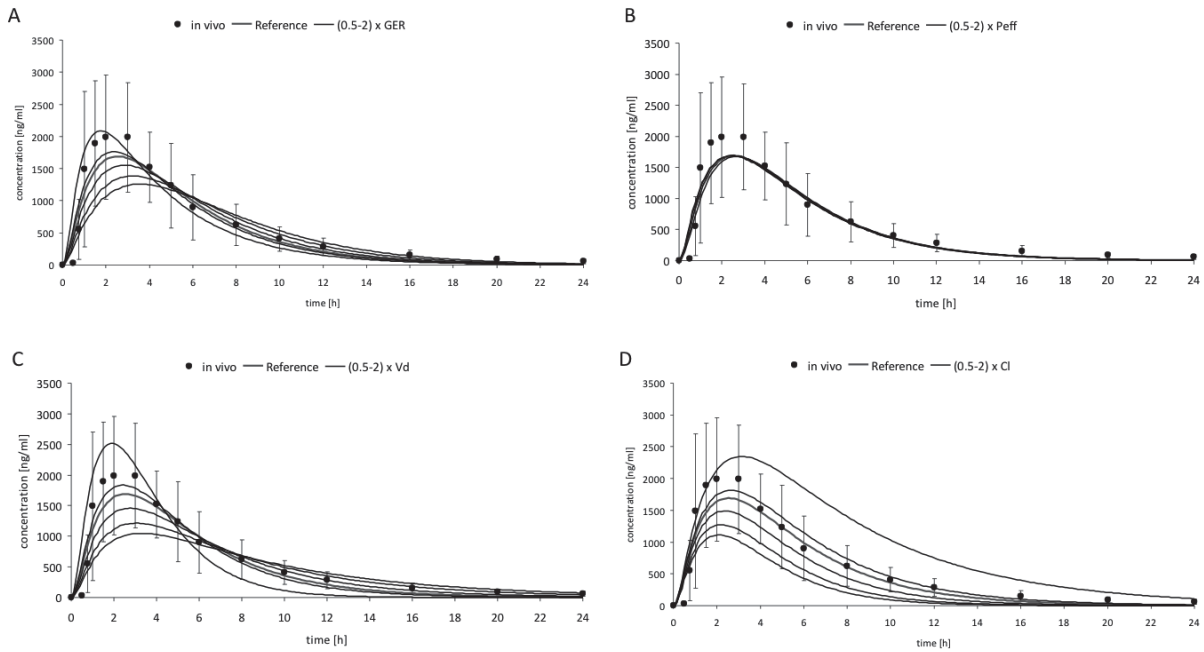


Fig. 7.44: “best case” example - sensitivity analysis of the gastric emptying (A), the permeability (B), the volume of distribution (C) and the clearance (D) on plasma profile predictions of 400 mg atazanavir sulfate in the fed state using predicted atazanavir solubility by Simcyp®.

Sensitivity analysis by implementing equilibrium solubilities of atazanavir at different pH values into the Simcyp® mask

The sensitivity analysis of the fasted state simulations using the pH dependent solubility yields similar results to those from the previous two investigations (Figure 7.45 to 7.48). Alterations of the pre-absorptive (supersaturation, k_p , GER) and absorptive (P_{eff}) parameters had a less significant influence on the plasma profile predictions relative to the post-absorptive parameters, Vd and clearance.

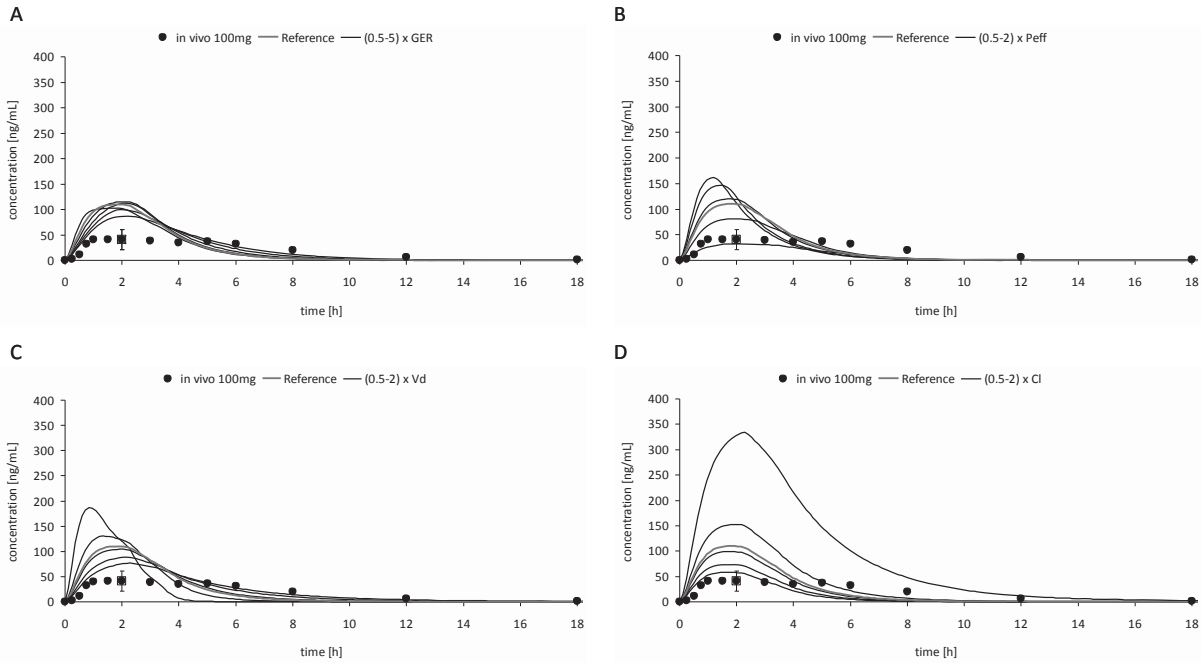


Fig. 7.45: Sensitivity analysis of the gastric emptying (A), the permeability (B), the volume of distribution (C) and the clearance (D) on plasma profile predictions of 200 mg atazanavir sulfate in the fasted state by implementing equilibrium solubilities of atazanavir at different pH values into the Simcyp[®] mask.

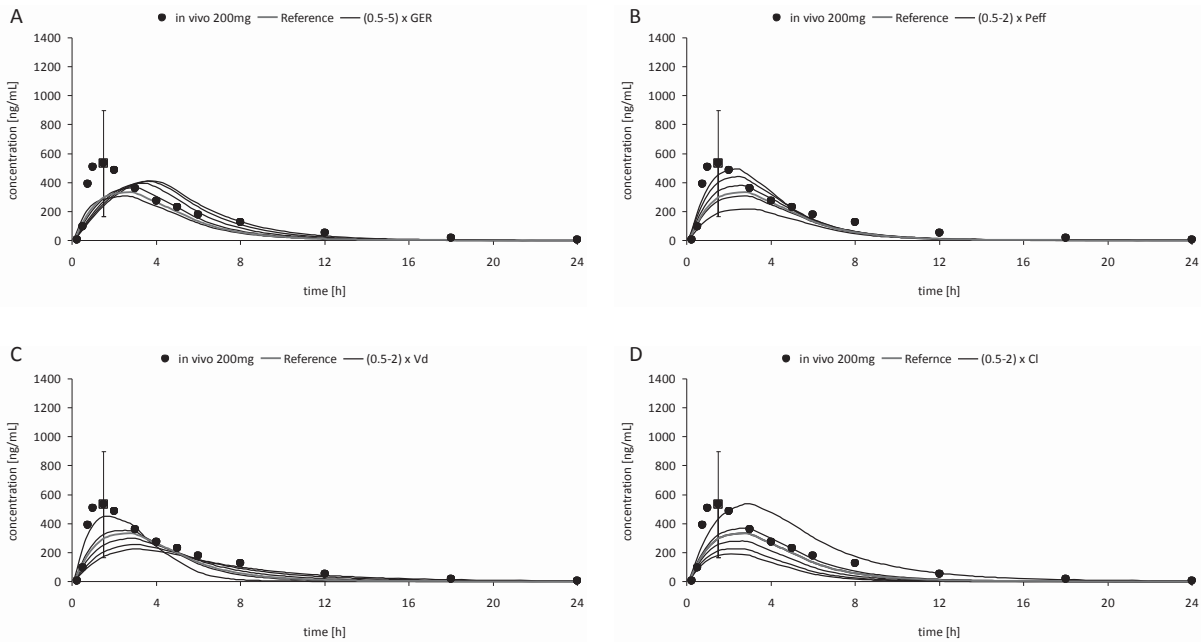


Fig. 7.46: Sensitivity analysis of the gastric emptying (A), the permeability (B), the volume of distribution (C) and clearance (D) on plasma profile predictions of 200 mg atazanavir sulfate in the fasted state by implementing equilibrium solubilities of atazanavir at different pH values into the Simcyp[®] mask.

Appendix

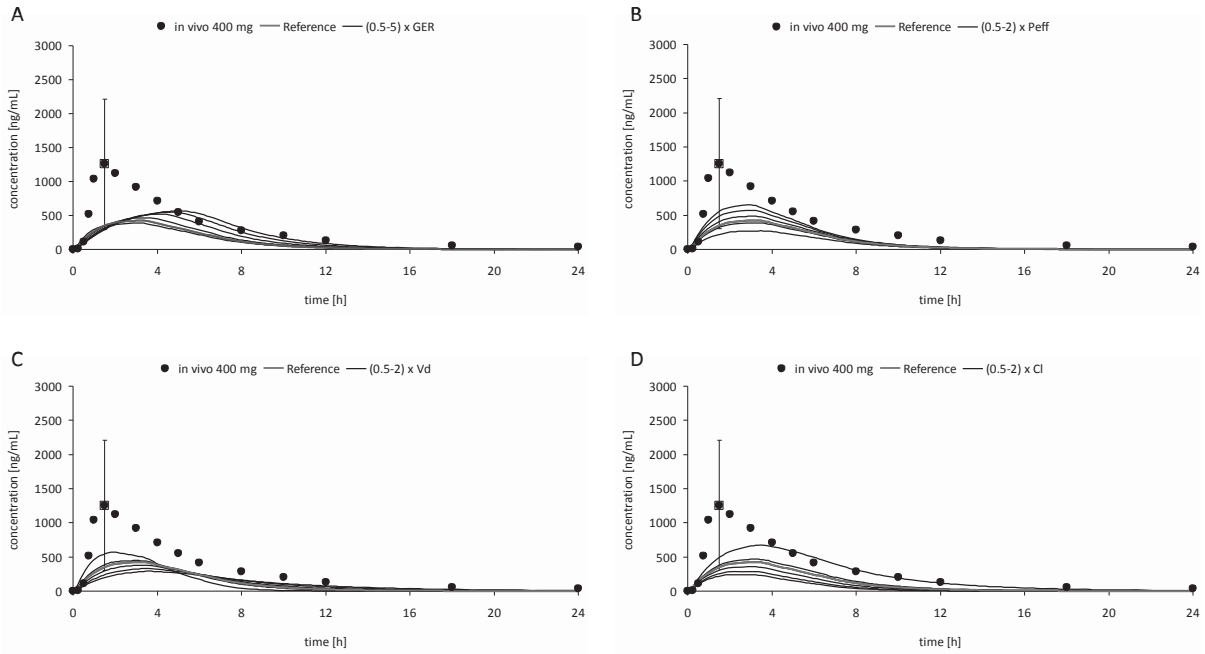


Fig. 7.47: Sensitivity analysis of the gastric emptying (A), the permeability (B), the volume of distribution (C) and the clearance (D) on plasma profile predictions of 400 mg atazanavir sulfate in the fasted state by implementing equilibrium solubilities of atazanavir at different pH values into the Simcyp® mask.

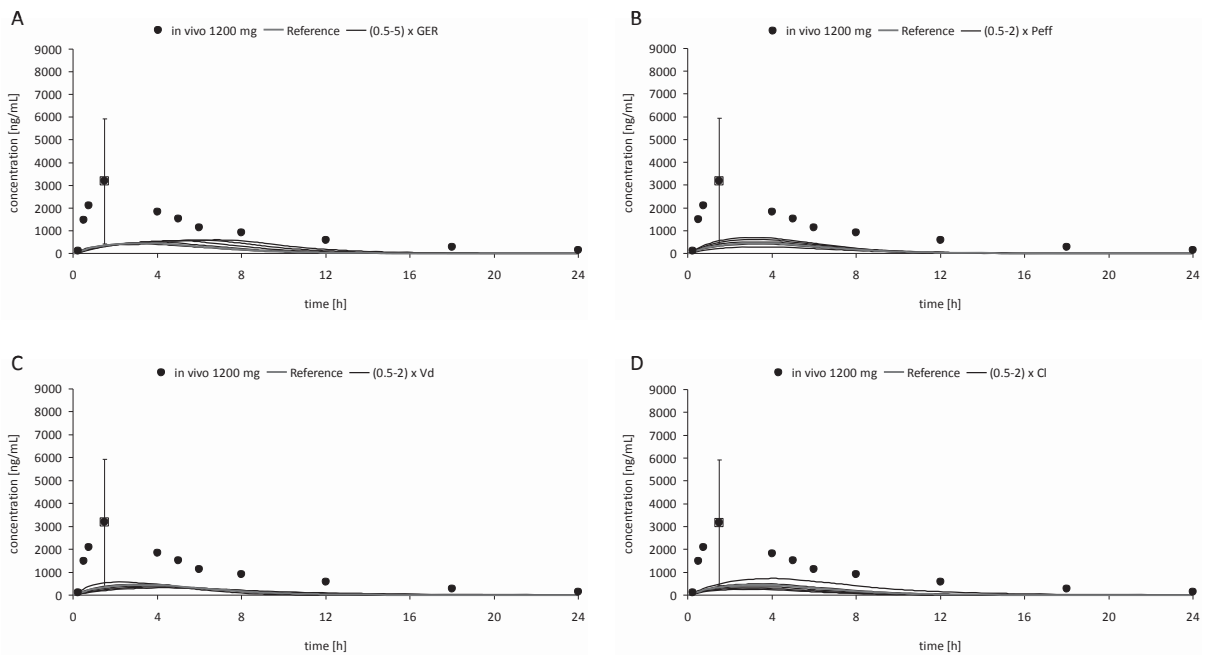


Fig. 7.48: Sensitivity analysis of the gastric emptying (A), the permeability (B), the volume of distribution (C) and the clearance (D) on plasma profile predictions of 1200 mg atazanavir sulfate in the fasted state by implementing equilibrium solubilities of atazanavir at different pH values into the Simcyp® mask.

The fed state sensitivity analysis shows similar outputs as observed in the investigations which utilized predicted atazanavir solubility (Figures 7.49 and 7.50). Supersaturation and precipitation did not have any effect on the predictions. Changes of the GER and the P_{eff} had a moderate influence on the simulations. The strongest influences on the predictions of the *in vivo* performance were seen through alterations of the V_d and clearance values.

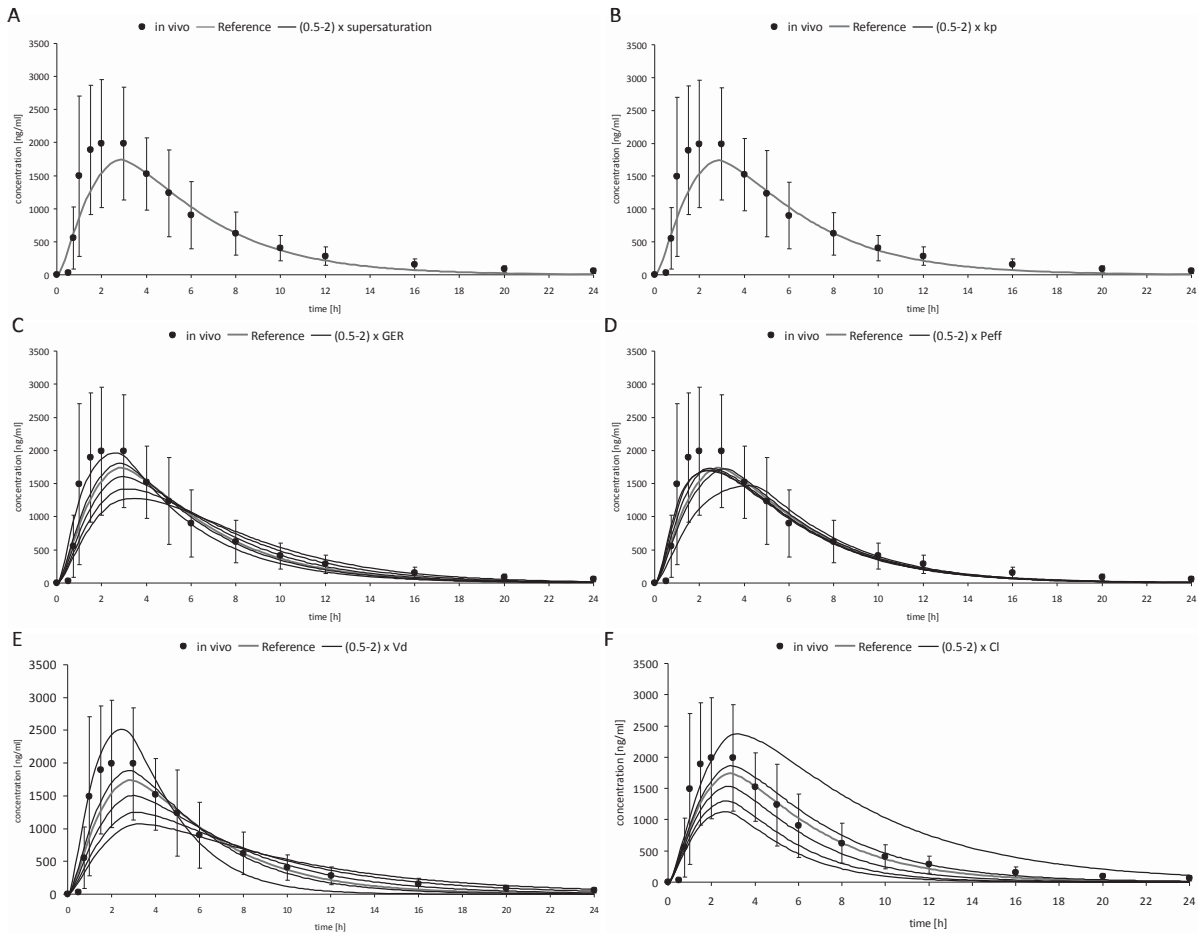


Fig. 7.49: “worst case” example - sensitivity analysis of the supersaturation (A), the precipitation (B), the gastric emptying (C), the permeability (D), the volume of distribution (E) and the clearance (F) on plasma profile predictions of 400 mg atazanavir sulfate in the fed state by implementing equilibrium solubilities of atazanavir at different pH values into the Simcyp® mask.

Appendix

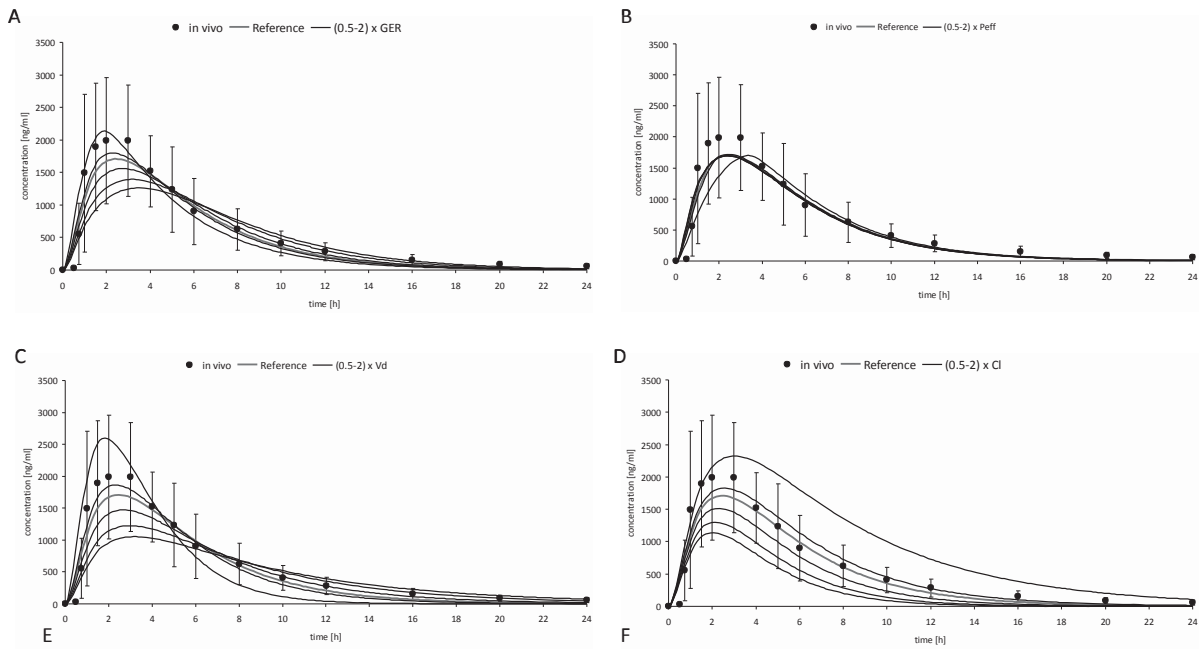


Fig. 7.50: “best case” example - sensitivity analysis of the gastric emptying (A), the permeability (B), the volume of distribution (C) and the clearance (D) on plasma profile predictions of 400 mg atazanavir sulfate in the fed state by implementing equilibrium solubilities of atazanavir at different pH values into the Simcyp[®] mask.

In summary, the sensitivity analysis revealed that atazanavir plasma profile predictions are mostly affected by the two post-absorptive factors, volume of distribution and clearance. Pre-absorptive determinants had a relatively insignificant effect on plasma profiles simulations. Thus, post-absorptive elements such as metabolism and biliary excretion play a crucial role on atazanavir bioavailability, since these factors could be influenced by the atazanavir sulfate dose, the prandial state and co-medication (e.g. ritonavir as booster).

8 References

- [1] E. Stone, An Account of the Success of the Bark of the Willow in the Cure of Agues, *Phil. Trans.*, 53 (1763) 195-200.
- [2] A. Fleming, On the antibacterial action of cultures of a penicillium, with special reference to their use in the isolation of *B. influenzae*. 1929, *Bulletin of the World Health Organization*, 79 (2001) 780-790.
- [3] J.D. McKinney, Reactivity parameters in structure-activity relationship-based risk assessment of chemicals, *Environmental health perspectives*, 104 (1996) 810-816.
- [4] S.H. Kaufmann, Paul Ehrlich: founder of chemotherapy, *Nature reviews. Drug discovery*, 7 (2008) 373.
- [5] D.J. Newman, G.M. Cragg, Natural products as sources of new drugs over the 30 years from 1981 to 2010, *Journal of natural products*, 75 (2012) 311-335.
- [6] G.L. Amidon, H. Lennernas, V.P. Shah, J.R. Crison, A theoretical basis for a biopharmaceutic drug classification: the correlation of in vitro drug product dissolution and in vivo bioavailability, *Pharm Res*, 12 (1995) 413-420.
- [7] J.P. Hughes, S. Rees, S.B. Kalindjian, K.L. Philpott, Principles of early drug discovery, *Br J Pharmacol*, 162 (2011) 1239-1249.
- [8] C.A. Lipinski, Drug-like properties and the causes of poor solubility and poor permeability, *Journal of pharmacological and toxicological methods*, 44 (2000) 235-249.
- [9] L. Di, E.H. Kerns, Solubility Issues in Early Discovery and HTS, in: P. Augustijns, M. Brewster (Eds.) *Solvent Systems and Their Selection in Pharmaceuticals and Biopharmaceutics*, Springer, New York, 2007, pp. 111-136.
- [10] C.A. Bergstrom, R. Holm, S.A. Jorgensen, S.B. Andersson, P. Artursson, S. Beato, A. Borde, K. Box, M. Brewster, J. Dressman, K.I. Feng, G. Halbert, E. Kostewicz, M. McAllister, U. Muenster, J. Thinnes, R. Taylor, A. Mullertz, Early pharmaceutical profiling to predict oral drug absorption: current status and unmet needs, *Eur J Pharm Sci*, 57 (2014) 173-199.
- [11] E.S. Kostewicz, L. Aarons, M. Bergstrand, M.B. Bolger, A. Galetin, O. Hatley, M. Jamei, R. Lloyd, X. Pepin, A. Rostami-Hodjegan, E. Sjogren, C. Tannergren, D.B. Turner, C. Wagner, W. Weitschies, J. Dressman, PBPK models for the prediction of in vivo performance of oral dosage forms, *Eur J Pharm Sci*, (2013).
- [12] H. Lennernas, L. Aarons, P. Augustijns, S. Beato, M. Bolger, K. Box, M. Brewster, J. Butler, J. Dressman, R. Holm, K. Julia Frank, R. Kendall, P. Langguth, J. Sydor, A. Lindahl, M. McAllister, U. Muenster, A. Mullertz, K. Ojala, X. Pepin, C. Reppas, A. Rostami-Hodjegan, M. Verwei, W. Weitschies, C. Wilson, C. Karlsson, B. Abrahamsson, Oral biopharmaceutics tools - time for a new initiative - an introduction to the IMI project OrBiTo, *Eur J Pharm Sci*, 57 (2014) 292-299.
- [13] N. Penner, L.J. Klunk, C. Prakash, Human radiolabeled mass balance studies: objectives, utilities and limitations, *Biopharm Drug Dispos*, 30 (2009) 185-203.
- [14] U.S. Food and Drug Administration, Center for Drug Evaluation and Research. Guidance for Industry: Waiver of In Vivo Bioavailability and Bioequivalence Studies for Immediate-Release Solid Oral Dosage Forms Based on a Biopharmaceutics Classification System. 2000 August. Available from: <http://www.fda.gov/downloads/Drugs/GuidanceComplianceRegulatoryInformation/Guidances/ucm070246.pdf>.



References

- [15] Z.S. Teksin, P.R. Seo, J.E. Polli, Comparison of drug permeabilities and BCS classification: three lipid-component PAMPA system method versus Caco-2 monolayers, *AAPS J*, 12 (2010) 238-241.
- [16] M.L. Chen, G.L. Amidon, L.Z. Benet, H. Lennernas, L.X. Yu, The BCS, BDDCS, and regulatory guidances, *Pharm Res*, 28 (2011) 1774-1778.
- [17] C.Y. Wu, L.Z. Benet, Predicting drug disposition via application of BCS: transport/absorption/ elimination interplay and development of a biopharmaceutics drug disposition classification system, *Pharm Res*, 22 (2005) 11-23.
- [18] J. Konig, F. Muller, M.F. Fromm, Transporters and drug-drug interactions: important determinants of drug disposition and effects, *Pharmacological reviews*, 65 (2013) 944-966.
- [19] J.M. Butler, J.B. Dressman, The developability classification system: application of biopharmaceutics concepts to formulation development, *J Pharm Sci*, 99 (2010) 4940-4954.
- [20] E. Galia, E. Nicolaidis, D. Horter, R. Lobenberg, C. Reppas, J.B. Dressman, Evaluation of various dissolution media for predicting in vivo performance of class I and II drugs, *Pharm Res*, 15 (1998) 698-705.
- [21] M. Vertzoni, J. Dressman, J. Butler, J. Hempenstall, C. Reppas, Simulation of fasting gastric conditions and its importance for the in vivo dissolution of lipophilic compounds, *Eur J Pharm Biopharm*, 60 (2005) 413-417.
- [22] E. Jantratid, N. Janssen, C. Reppas, J.B. Dressman, Dissolution media simulating conditions in the proximal human gastrointestinal tract: an update, *Pharm Res*, 25 (2008) 1663-1676.
- [23] J.B. Dressman, G.L. Amidon, C. Reppas, V.P. Shah, Dissolution testing as a prognostic tool for oral drug absorption: immediate release dosage forms, *Pharm Res*, 15 (1998) 11-22.
- [24] J.B. Dressman, R.R. Berardi, L.C. Dermentzoglou, T.L. Russell, S.P. Schmaltz, J.L. Barnett, K.M. Jarvenpaa, Upper gastrointestinal (GI) pH in young, healthy men and women, *Pharm Res*, 7 (1990) 756-761.
- [25] V.C. Ibekwe, H.M. Fadda, E.L. McConnell, M.K. Khela, D.F. Evans, A.W. Basit, Interplay between intestinal pH, transit time and feed status on the in vivo performance of pH responsive ileo-colonic release systems, *Pharm Res*, 25 (2008) 1828-1835.
- [26] A. Mitra, F. Kesisoglou, Impaired drug absorption due to high stomach pH: a review of strategies for mitigation of such effect to enable pharmaceutical product development, *Mol Pharm*, 10 (2013) 3970-3979.
- [27] S. Gabardi, A. Olyaei, Evaluation of potential interactions between mycophenolic acid derivatives and proton pump inhibitors, *Ann Pharmacother*, 46 (2012) 1054-1064.
- [28] N. Takahashi, M. Miura, T. Niioka, K. Sawada, Influence of H₂-receptor antagonists and proton pump inhibitors on dasatinib pharmacokinetics in Japanese leukemia patients, *Cancer chemotherapy and pharmacology*, 69 (2012) 999-1004.
- [29] V. Bakatselou, R.C. Oppenheim, J.B. Dressman, Solubilization and wetting effects of bile salts on the dissolution of steroids, *Pharm Res*, 8 (1991) 1461-1469.
- [30] T.S. Wiedmann, L. Kamel, Examination of the solubilization of drugs by bile salt micelles, *J Pharm Sci*, 91 (2002) 1743-1764.
- [31] G.A. Magee, J. French, B. Gibbon, C. Luscombe, Bile salt/lecithin mixed micelles optimized for the solubilization of a poorly soluble steroid molecule using statistical experimental design, *Drug development and industrial pharmacy*, 29 (2003) 441-450.
- [32] L. Kalantzi, K. Goumas, V. Kalioras, B. Abrahamsson, J.B. Dressman, C. Reppas, Characterization of the human upper gastrointestinal contents under conditions simulating bioavailability/bioequivalence studies, *Pharm Res*, 23 (2006) 165-176.



- [33] O. Hernell, J.E. Stiggers, M.C. Carey, Physical-chemical behavior of dietary and biliary lipids during intestinal digestion and absorption. 2. Phase analysis and aggregation states of luminal lipids during duodenal fat digestion in healthy adult human beings, *Biochemistry*, 29 (1990) 2041-2056.
- [34] C.M. Mansbach, 2nd, R.S. Cohen, P.B. Leff, Isolation and properties of the mixed lipid micelles present in intestinal content during fat digestion in man, *J Clin Invest*, 56 (1975) 781-791.
- [35] J. Brouwers, J. Tack, F. Lammert, P. Augustijns, Intraluminal drug and formulation behavior and integration in in vitro permeability estimation: a case study with amprenavir, *J Pharm Sci*, 95 (2006) 372-383.
- [36] E.M. Persson, A.S. Gustafsson, A.S. Carlsson, R.G. Nilsson, L. Knutson, P. Forsell, G. Hanisch, H. Lennernas, B. Abrahamsson, The effects of food on the dissolution of poorly soluble drugs in human and in model small intestinal fluids, *Pharm Res*, 22 (2005) 2141-2151.
- [37] Y. Honda, F. Ushigome, N. Koyabu, S. Morimoto, Y. Shoyama, T. Uchiumi, M. Kuwano, H. Ohtani, Y. Sawada, Effects of grapefruit juice and orange juice components on P-glycoprotein- and MRP2-mediated drug efflux, *Br J Pharmacol*, 143 (2004) 856-864.
- [38] C.F. Code, The interdigestive housekeeper of the gastrointestinal tract, *Perspectives in biology and medicine*, 22 (1979) S49-55.
- [39] M.L. Grivel, Y. Ruckebusch, The propagation of segmental contractions along the small intestine, *The Journal of physiology*, 227 (1972) 611-625.
- [40] S.K. Sarna, Cyclic motor activity; migrating motor complex: 1985, *Gastroenterology*, 89 (1985) 894-913.
- [41] J.B. Dressman, Comparison of canine and human gastrointestinal physiology, *Pharm Res*, 3 (1986) 123-131.
- [42] R.L. Oberle, T.S. Chen, C. Lloyd, J.L. Barnett, C. Owyang, J. Meyer, G.L. Amidon, The influence of the interdigestive migrating myoelectric complex on the gastric emptying of liquids, *Gastroenterology*, 99 (1990) 1275-1282.
- [43] J.N. Hunt, I. Macdonald, The influence of volume on gastric emptying, *The Journal of physiology*, 126 (1954) 459-474.
- [44] D.N. Bateman, T.A. Whittingham, Measurement of gastric emptying by real-time ultrasound, *Gut*, 23 (1982) 524-527.
- [45] J.C. Meeroff, V.L. Go, S.F. Phillips, Gastric emptying of liquids in man. Quantification by duodenal recovery marker, *Mayo Clinic proceedings*, 48 (1973) 728-732.
- [46] P.R. McHugh, The control of gastric emptying, *Journal of the autonomic nervous system*, 9 (1983) 221-231.
- [47] N.W. Weisbrodt, J.N. Wiley, B.F. Overholt, P. Bass, A relation between gastroduodenal muscle contractions and gastric emptying, *Gut*, 10 (1969) 543-548.
- [48] J.N. Hunt, D.F. Stubbs, The volume and energy content of meals as determinants of gastric emptying, *The Journal of physiology*, 245 (1975) 209-225.
- [49] H. Minami, R.W. McCallum, The physiology and pathophysiology of gastric emptying in humans, *Gastroenterology*, 86 (1984) 1592-1610.
- [50] W. Brener, T.R. Hendrix, P.R. McHugh, Regulation of the gastric emptying of glucose, *Gastroenterology*, 85 (1983) 76-82.
- [51] M. Horowitz, J. Dent, Disordered gastric emptying: mechanical basis, assessment and treatment, *Bailliere's clinical gastroenterology*, 5 (1991) 371-407.



References

- [52] The United States Pharmacopeia. USP 29., United States Pharmacopeial Convention Inc., Rockville, MD, (2006).
- [53] M. Vertzoni, A. Diakidou, M. Chatzilias, E. Soderlind, B. Abrahamsson, J.B. Dressman, C. Reppas, Biorelevant media to simulate fluids in the ascending colon of humans and their usefulness in predicting intracolonic drug solubility, *Pharm Res*, 27 (2010) 2187-2196.
- [54] C. Reppas, M. Vertzoni, Biorelevant in-vitro performance testing of orally administered dosage forms, *J Pharm Pharmacol*, 64 (2012) 919-930.
- [55] K. Kleberg, J. Jacobsen, A. Mullertz, Characterising the behaviour of poorly water soluble drugs in the intestine: application of biorelevant media for solubility, dissolution and transport studies, *J Pharm Pharmacol*, 62 (2010) 1656-1668.
- [56] J.B. Dressman, C. Reppas, In vitro-in vivo correlations for lipophilic, poorly water-soluble drugs, *Eur J Pharm Sci*, 11 Suppl 2 (2000) S73-80.
- [57] B.M. Lue, F.S. Nielsen, T. Magnussen, H.M. Schou, K. Kristensen, L.O. Jacobsen, A. Mullertz, Using biorelevant dissolution to obtain IVIVC of solid dosage forms containing a poorly-soluble model compound, *Eur J Pharm Biopharm*, 69 (2008) 648-657.
- [58] S. Klein, The use of biorelevant dissolution media to forecast the in vivo performance of a drug, *AAPS J*, 12 (2010) 397-406.
- [59] E.S. Kostewicz, M. Wunderlich, U. Brauns, R. Becker, T. Bock, J.B. Dressman, Predicting the precipitation of poorly soluble weak bases upon entry in the small intestine, *J Pharm Pharmacol*, 56 (2004) 43-51.
- [60] C. Wagner, E. Jantratid, F. Kesisoglou, M. Vertzoni, C. Reppas, B.D. J, Predicting the oral absorption of a poorly soluble, poorly permeable weak base using biorelevant dissolution and transfer model tests coupled with a physiologically based pharmacokinetic model, *Eur J Pharm Biopharm*, 82 (2012) 127-138.
- [61] Y. Fei, E.S. Kostewicz, M.T. Sheu, J.B. Dressman, Analysis of the enhanced oral bioavailability of fenofibrate lipid formulations in fasted humans using an in vitro-in silico-in vivo approach, *Eur J Pharm Biopharm*, (2013).
- [62] Y.E. Arnold, G. Imanidis, M.T. Kuentz, Advancing in-vitro drug precipitation testing: new process monitoring tools and a kinetic nucleation and growth model, *J Pharm Pharmacol*, 63 (2011) 333-341.
- [63] T. Taupitz, J.B. Dressman, S. Klein, In vitro tools for evaluating novel dosage forms of poorly soluble, weakly basic drugs: case example ketoconazole, *J Pharm Sci*, 102 (2013) 3645-3652.
- [64] M. Berlin, K.H. Przyklenk, A. Richtberg, W. Baumann, J.B. Dressman, Prediction of oral absorption of cinnarizine - A highly supersaturating poorly soluble weak base with borderline permeability, *Eur J Pharm Biopharm*, (2014).
- [65] D. Psachoulis, M. Vertzoni, J. Butler, D. Busby, M. Symillides, J. Dressman, C. Reppas, An in vitro methodology for forecasting luminal concentrations and precipitation of highly permeable lipophilic weak bases in the fasted upper small intestine, *Pharm Res*, 29 (2012) 3486-3498.
- [66] C.A. Lipinski, F. Lombardo, B.W. Dominy, P.J. Feeney, Experimental and computational approaches to estimate solubility and permeability in drug discovery and development settings, *Adv Drug Deliv Rev*, 46 (2001) 3-26.
- [67] S. Winiwarter, N.M. Bonham, F. Ax, A. Hallberg, H. Lennernas, A. Karlen, Correlation of human jejunal permeability (in vivo) of drugs with experimentally and theoretically derived parameters. A multivariate data analysis approach, *J Med Chem*, 41 (1998) 4939-4949.



- [68] K. Palm, P. Stenberg, K. Luthman, P. Artursson, Polar molecular surface properties predict the intestinal absorption of drugs in humans, *Pharm Res*, 14 (1997) 568-571.
- [69] G. Subramanian, D.B. Kitchen, Computational approaches for modeling human intestinal absorption and permeability, *Journal of molecular modeling*, 12 (2006) 577-589.
- [70] K. Kiehm, Development of a novel screening tool for the prediction of oral drug absorption based on surface activity profiling, Shaker Verlag, (2009).
- [71] A.C. Petereit, K. Swinney, J. Mensch, C. Mackie, S. Stokbroekx, M. Brewster, J.B. Dressman, Prediction of blood-brain barrier penetration of poorly soluble drug candidates using surface activity profiling, *Eur J Pharm Biopharm*, 75 (2010) 405-410.
- [72] M. Kansy, F. Senner, K. Gubernator, Physicochemical high throughput screening: parallel artificial membrane permeation assay in the description of passive absorption processes, *J Med Chem*, 41 (1998) 1007-1010.
- [73] R.B. van Breemen, Y. Li, Caco-2 cell permeability assays to measure drug absorption, *Expert Opin Drug Metab Toxicol*, 1 (2005) 175-185.
- [74] A. Wikman, J. Karlsson, I. Carlstedt, P. Artursson, A drug absorption model based on the mucus layer producing human intestinal goblet cell line HT29-H, *Pharm Res*, 10 (1993) 843-852.
- [75] E. Walter, S. Janich, B.J. Roessler, J.M. Hilfinger, G.L. Amidon, HT29-MTX/Caco-2 cocultures as an in vitro model for the intestinal epithelium: in vitro-in vivo correlation with permeability data from rats and humans, *J Pharm Sci*, 85 (1996) 1070-1076.
- [76] W.S. Putnam, L. Pan, K. Tsutsui, L. Takahashi, L.Z. Benet, Comparison of bidirectional cephalixin transport across MDCK and caco-2 cell monolayers: interactions with peptide transporters, *Pharm Res*, 19 (2002) 27-33.
- [77] H. Li, S.J. Chung, C.K. Shim, Characterization of the transport of uracil across Caco-2 and LLC-PK1 cell monolayers, *Pharm Res*, 19 (2002) 1495-1501.
- [78] H. Li, H.E. Jin, W.S. Shim, C.K. Shim, An improved prediction of the human in vivo intestinal permeability and BCS class of drugs using the in vitro permeability ratio obtained for rat intestine using an Ussing chamber system, *Drug development and industrial pharmacy*, 39 (2013) 1515-1522.
- [79] T. Teorell, Kinetics of distribution of substances administered to the body, *Arch Int Pharmacodyn Thér*, 57 (1937) 205-240.
- [80] Guidance for industry: drug interaction studies - study design, data analysis, implications for dosing, and labeling recommendations; Draft Guidance, in: F.a.D.A. (FDA) (Ed.), Rockville, MD 2012.
- [81] Guideline on the Investigation of Drug Interactions, in: E.M. Agency (Ed.), London, UK, 2012.
- [82] M. Jamei, G.L. Dickinson, A. Rostami-Hodjegan, A framework for assessing inter-individual variability in pharmacokinetics using virtual human populations and integrating general knowledge of physical chemistry, biology, anatomy, physiology and genetics: A tale of 'bottom-up' vs 'top-down' recognition of covariates, *Drug metabolism and pharmacokinetics*, 24 (2009) 53-75.
- [83] H. Ohtani, Z. Barter, T. Minematsu, M. Makuuchi, Y. Sawada, A. Rostami-Hodjegan, Bottom-up modeling and simulation of tacrolimus clearance: prospective investigation of blood cell distribution, sex and CYP3A5 expression as covariates and assessment of study power, *Biopharm Drug Dispos*, 32 (2011) 498-506.
- [84] C. Gerard, J. Stocco, A. Hulin, B. Blanchet, C. Verstuyft, F. Durand, F. Conti, C. Duvoux, M. Tod, Determination of the most influential sources of variability in tacrolimus trough blood



References

concentrations in adult liver transplant recipients: a bottom-up approach, *AAPS J*, 16 (2014) 379-391.

[85] M. Jamei, S. Marciniak, D. Edwards, K. Wragg, K. Feng, A. Barnett, A. Rostami-Hodjegan, The simcyp population based simulator: architecture, implementation, and quality assurance, *In silico pharmacology*, 1 (2013) 9.

[86] A. Maharaj, N. Fotaki, A. Edginton, Parameterization of small intestinal water volume using PBPK modeling, *Eur J Pharm Sci*, 67 (2015) 55-64.

[87] Y. Shono, E. Jantratid, J.B. Dressman, Precipitation in the small intestine may play a more important role in the in vivo performance of poorly soluble weak bases in the fasted state: case example nelfinavir, *Eur J Pharm Biopharm*, 79 (2011) 349-356.

[88] Y. Shono, E. Jantratid, N. Janssen, F. Kesisoglou, Y. Mao, M. Vertzoni, C. Reppas, J.B. Dressman, Prediction of food effects on the absorption of celecoxib based on biorelevant dissolution testing coupled with physiologically based pharmacokinetic modeling, *Eur J Pharm Biopharm*, 73 (2009) 107-114.

[89] Y. Shono, E. Jantratid, F. Kesisoglou, C. Reppas, J.B. Dressman, Forecasting in vivo oral absorption and food effect of micronized and nanosized aprepitant formulations in humans, *Eur J Pharm Biopharm*, 76 (2010) 95-104.

[90] T. Jarvinen, K. Jarvinen, N. Schwarting, V.J. Stella, beta-cyclodextrin derivatives, SBE4-beta-CD and HP-beta-CD, increase the oral bioavailability of cinnarizine in beagle dogs, *J Pharm Sci*, 84 (1995) 295-299.

[91] K. Peeters, R. De Maesschalck, H. Bohets, K. Vanhoutte, L. Nagels, In situ dissolution testing using potentiometric sensors, *Eur J Pharm Sci*, 34 (2008) 243-249.

[92] S. Branchu, P.G. Rogueda, A.P. Plumb, W.G. Cook, A decision-support tool for the formulation of orally active, poorly soluble compounds, *Eur J Pharm Sci*, 32 (2007) 128-139.

[93] C.A. Bergstrom, C.M. Wassvik, K. Johansson, I. Hubatsch, Poorly soluble marketed drugs display solvation limited solubility, *J Med Chem*, 50 (2007) 5858-5862.

[94] C.H. Gu, D. Rao, R.B. Gandhi, J. Hilden, K. Raghavan, Using a novel multicompartiment dissolution system to predict the effect of gastric pH on the oral absorption of weak bases with poor intrinsic solubility, *J Pharm Sci*, 94 (2005) 199-208.

[95] H. Ogata, N. Aoyagi, N. Kaniwa, A. Ejima, N. Sekine, K. Kitamura, M. Inoue, Gastric acidity dependent bioavailability of cinnarizine from two commercial capsules in healthy volunteers, *International Journal of Pharmaceutics*, 29 (1986).

[96] I. Yamada, T. Goda, M. Kawata, K. Ogawa, [Application of gastric acidity-controlled beagle dog to bioavailability study of cinnarizine], *Yakugaku Zasshi*, 110 (1990) 280-285.

[97] A.T. Larsen, P. Akesson, A. Jureus, L. Saaby, R. Abu-Rmaileh, B. Abrahamsson, J. Ostergaard, A. Mullertz, Bioavailability of Cinnarizine in Dogs: Effect of SNEDDS Loading Level and Correlation with Cinnarizine Solubilization During In Vitro Lipolysis, *Pharm Res*, (2013).

[98] Hennig Arzneimittel - Data on file.

[99] H. Nowacka-Krukowska, M. Rakowska, K. Neubart, M. Kobylinska, High-performance liquid chromatographic assay for cinnarizine in human plasma, *Acta Pol Pharm*, 64 (2007) 407-411.

[100] P.J. Piliero, Atazanavir: a novel HIV-1 protease inhibitor, *Expert Opin Investig Drugs*, 11 (2002) 1295-1301.

[101] D.R. Goldsmith, C.M. Perry, Atazanavir, *Drugs*, 63 (2003) 1679-1693; discussion 1694-1675.

[102] B.L. Musial, J.K. Chojnacki, C.I. Coleman, Atazanavir: a new protease inhibitor to treat HIV infection, *Am J Health Syst Pharm*, 61 (2004) 1365-1374.



- [103] J.J. Orrick, C.R. Steinhart, Atazanavir, *Ann Pharmacother*, 38 (2004) 1664-1674.
- [104] K.F. Croom, S. Dhillon, S.J. Keam, Atazanavir: a review of its use in the management of HIV-1 infection, *Drugs*, 69 (2009) 1107-1140.
- [105] L.Z. Benet, F. Broccatelli, T.I. Oprea, BDDCS applied to over 900 drugs, *AAPS J*, 13 (2011) 519-547.
- [106] Bristol-Myers Squibb Company, Clinical Pharmacology and Biopharmaceutics Review, Application number 21-567, (2002). Available from:
http://www.accessdata.fda.gov/drugsatfda_docs/nda/2003/21-567_Reyataz_BioPharmr_P1.pdf and
http://www.accessdata.fda.gov/drugsatfda_docs/nda/2003/21-567_Reyataz_BioPharmr_P2.pdf.
- [107] P.L. Anderson, C.L. Aquilante, E.M. Gardner, J. Predhomme, P. McDanel, L.R. Bushman, J.H. Zheng, M. Ray, S. MaWhinney, Atazanavir pharmacokinetics in genetically determined CYP3A5 expressors versus non-expressors, *J Antimicrob Chemother*, 64 (2009) 1071-1079.
- [108] M.F. Wempe, P.L. Anderson, Atazanavir metabolism according to CYP3A5 status: an in vitro-in vivo assessment, *Drug Metab Dispos*, 39 (2011) 522-527.
- [109] X. Tao, H. Sevinsky, R. Wang, P. Ravindran, K. Sims, X. Xu, N. Jariwala, R. Bertz, Atazanavir/Cobicistat Fixed-Dose Combination is Bioequivalent to the Separate Agents - Poster Presentation, Conference on Retroviruses and Opportunistic Infections (CROI), Boston, Massachusetts, March 3-6 2014.
- [110] K.A. Lentz, Current methods for predicting human food effect, *AAPS J*, 10 (2008) 282-288.
- [111] K.A. Lentz, M. Quitko, D.G. Morgan, J.E. Grace, Jr., C. Gleason, P.H. Marathe, Development and validation of a preclinical food effect model, *J Pharm Sci*, 96 (2007) 459-472.
- [112] B. Wuyts, J. Brouwers, R. Mols, J. Tack, P. Annaert, P. Augustijns, Solubility profiling of HIV protease inhibitors in human intestinal fluids, *J Pharm Sci*, 102 (2013) 3800-3807.
- [113] O. Kis, J.A. Zastre, M.T. Hoque, S.L. Walmsley, R. Bendayan, Role of drug efflux and uptake transporters in atazanavir intestinal permeability and drug-drug interactions, *Pharm Res*, 30 (2013) 1050-1064.
- [114] O. Kis, S.L. Walmsley, R. Bendayan, In Vitro and In Situ Evaluation of pH-Dependence of Atazanavir Intestinal Permeability and Interactions with Acid-Reducing Agents, *Pharm Res*, (2014).
- [115] X. Wang, M. Boffito, J. Zhang, E. Chung, L. Zhu, Y. Wu, K. Patterson, A. Kashuba, P. Tebas, M. Child, L. Mahnke, R. Bertz, Effects of the H₂-receptor antagonist famotidine on the pharmacokinetics of atazanavir-ritonavir with or without tenofovir in HIV-infected patients, *AIDS patient care and STDs*, 25 (2011) 509-515.
- [116] W. Li, S. Zeng, L.S. Yu, Q. Zhou, Pharmacokinetic drug interaction profile of omeprazole with adverse consequences and clinical risk management, *Therapeutics and clinical risk management*, 9 (2013) 259-271.
- [117] E. Nicolaidis, M. Symillides, J.B. Dressman, C. Reppas, Biorelevant dissolution testing to predict the plasma profile of lipophilic drugs after oral administration, *Pharm Res*, 18 (2001) 380-388.
- [118] D. Juenemann, E. Jantratid, C. Wagner, C. Reppas, M. Vertzoni, J.B. Dressman, Biorelevant in vitro dissolution testing of products containing micronized or nanosized



References

fenofibrate with a view to predicting plasma profiles, *Eur J Pharm Biopharm*, 77 (2011) 257-264.

[119] N. Fotaki, M. Symillides, C. Reppas, Canine versus in vitro data for predicting input profiles of L-sulpiride after oral administration, *Eur J Pharm Sci*, 26 (2005) 324-333.

[120] E.L. McConnell, H.M. Fadda, A.W. Basit, Gut instincts: explorations in intestinal physiology and drug delivery, *Int J Pharm*, 364 (2008) 213-226.

[121] A. Kambayashi, J.B. Dressman, An in vitro-in silico-in vivo approach to predicting the oral pharmacokinetic profile of salts of weak acids: case example dantrolene, *Eur J Pharm Biopharm*, 84 (2013) 200-207.

[122] P. Costa, J.M. Sousa Lobo, Modeling and comparison of dissolution profiles, *Eur J Pharm Sci*, 13 (2001) 123-133.

[123] M. Lindenberg, A biopharmaceutics classification scheme for the development of new drugs, Shaker Verlag, (2008) 126.

[124] G.A. Kossena, W.N. Charman, B.J. Boyd, C.J. Porter, Influence of the intermediate digestion phases of common formulation lipids on the absorption of a poorly water-soluble drug, *J Pharm Sci*, 94 (2005) 481-492.

[125] C. Markopoulos, F. Thoenen, D. Preisig, M. Symillides, M. Vertzoni, N. Parrott, C. Reppas, G. Imanidis, Biorelevant media for transport experiments in the Caco-2 model to evaluate drug absorption in the fasted and the fed state and their usefulness, *Eur J Pharm Biopharm*, 86 (2014) 438-448.

[126] R. Angi, T. Solymosi, Z. Otvos, B. Ordasi, H. Glavinas, G. Filipcsei, G. Heltovics, F. Darvas, Novel continuous flow technology for the development of a nanostructured Aprepitant formulation with improved pharmacokinetic properties, *Eur J Pharm Biopharm*, (2013).

[127] Y. Wu, A. Loper, E. Landis, L. Hettrick, L. Novak, K. Lynn, C. Chen, K. Thompson, R. Higgins, U. Batra, S. Shelukar, G. Kwei, D. Storey, The role of biopharmaceutics in the development of a clinical nanoparticle formulation of MK-0869: a Beagle dog model predicts improved bioavailability and diminished food effect on absorption in human, *Int J Pharm*, 285 (2004) 135-146.

[128] T. Tokumura, Y. Tsushima, M. Kayano, Y. Machida, T. Nagai, Enhancement of bioavailability of cinnarizine from its beta-cyclodextrin complex on oral administration with DL-phenylalanine as a competing agent, *J Pharm Sci*, 74 (1985) 496-497.

[129] T. Tokumura, Y. Tsushima, K. Tatsuishi, M. Kayano, Y. Machida, T. Nagai, Enhancement of the bioavailability of cinnarizine from its beta-cyclodextrin complex on oral administration with L-isoleucine as a competing agent, *Chem Pharm Bull (Tokyo)*, 34 (1986) 1275-1279.

[130] T. Tokumura, Y. Tsushima, K. Tatsuishi, M. Kayano, Y. Machida, T. Nagai, Enhancement of the oral bioavailability of cinnarizine in oleic acid in beagle dogs, *J Pharm Sci*, 76 (1987) 286-288.

[131] T. Tokumura, M. Nanba, Y. Tsushima, K. Tatsuishi, M. Kayano, Y. Machida, T. Nagai, Enhancement of bioavailability of cinnarizine from its beta-cyclodextrin complex on oral administration with DL-phenylalanine as a competing agent, *J Pharm Sci*, 75 (1986) 391-394.

[132] A.T. Larsen, A.G. Ohlsson, B. Polentarutti, R.A. Barker, A.R. Phillips, R. Abu-Rmaleh, P.A. Dickinson, B. Abrahamsson, J. Ostergaard, A. Mullertz, Oral bioavailability of cinnarizine in dogs: relation to SNEDDS droplet size, drug solubility and in vitro precipitation, *Eur J Pharm Sci*, 48 (2013) 339-350.

[133] M.L. Christiansen, R. Holm, J. Kristensen, M. Kreilgaard, J. Jacobsen, B. Abrahamsson, A. Mullertz, Cinnarizine food-effects in beagle dogs can be avoided by administration in a Self Nano Emulsifying Drug Delivery System (SNEDDS), *Eur J Pharm Sci*, 57 (2014) 164-172.



- [134] A.A. Shahba, K. Mohsin, F.K. Alanazi, Novel self-nanoemulsifying drug delivery systems (SNEDDS) for oral delivery of cinnarizine: design, optimization, and in-vitro assessment, *AAPS PharmSciTech*, 13 (2012) 967-977.
- [135] C.J. Achenbach, K.M. Darin, R.L. Murphy, C. Katlama, Atazanavir/ritonavir-based combination antiretroviral therapy for treatment of HIV-1 infection in adults, *Future Virol*, 6 (2011) 157-177.
- [136] Q. Ma, H.A. Gelbard, S.B. Maggirwar, S. Dewhurst, H.E. Gendelman, D.R. Peterson, R. DiFrancesco, J.S. Hochreiter, G.D. Morse, G. Schifitto, Pharmacokinetic interactions of CEP-1347 and atazanavir in HIV-infected patients, *J Neurovirol*, 19 (2013) 254-260.
- [137] Bristol-Myers Squibb Company. REYATAZ® (atazanavir sulfate) Capsules: Prescribing Information. Bristol-Myers Squibb Company; (2013). Available from: http://packageinserts.bms.com/pi/pi_reyataz.pdf.
- [138] Spencer L, Neely M, Mordwinkin N, et al. Intensive pharmacokinetics of zidovudine, lamivudine, and atazanavir and HIV-1 viral load in breast milk and plasma in HIV+ women receiving HAART. Paper presented at: 16th Conference on Retroviruses and Opportunistic Infections; 2009; Montreal, Canada.
- [139] Bristol-Myers Squibb Company, Material Safety Data Sheet: Atazanavir Sulfate.
- [140] Scientific discussion EMA. Accessed October 3, 2014. Available from: http://www.ema.europa.eu/docs/en_GB/document_library/EPAR_Scientific_Discussion/human/000494/WC500056377.pdf.
- [141] S. Colombo, T. Buclin, M. Cavassini, L.A. Decosterd, A. Telenti, J. Biollaz, C. Csajka, Population pharmacokinetics of atazanavir in patients with human immunodeficiency virus infection, *Antimicrob Agents Chemother*, 50 (2006) 3801-3808.
- [142] C. Solas, M.C. Gagnieu, I. Ravoux, M.P. Drogoul, A. Lafeuillade, S. Mokhtari, B. Lacarelle, N. Simon, Population pharmacokinetics of atazanavir in human immunodeficiency virus-infected patients, *Ther Drug Monit*, 30 (2008) 670-673.
- [143] L. Dickinson, M. Boffito, D. Back, L. Waters, L. Else, G. Davies, S. Khoo, A. Pozniak, L. Aarons, Population pharmacokinetics of ritonavir-boosted atazanavir in HIV-infected patients and healthy volunteers, *J Antimicrob Chemother*, 63 (2009) 1233-1243.
- [144] A. Barrail-Tran, F. Mentre, C. Cosson, C. Piketty, C. Chazallon, L. Gerard, P.M. Girard, A.M. Taburet, Influence of alpha-1 glycoprotein acid concentrations and variants on atazanavir pharmacokinetics in HIV-infected patients included in the ANRS 107 trial, *Antimicrob Agents Chemother*, 54 (2010) 614-619.
- [145] Bristol-Myers Squibb Company, BMS-232632, Atazanavir Briefing Document; (2003). Available from: http://www.fda.gov/ohrms/dockets/ac/03/briefing/3950B1_01_bristolmyerssquibb-atazanavir.pdf.
- [146] L.Z. Benet, Predicting drug disposition via application of a Biopharmaceutics Drug Disposition Classification System, *Basic Clin Pharmacol Toxicol*, 106 (2010) 162-167.
- [147] E.S. Perloff, S.X. Duan, P.R. Skolnik, D.J. Greenblatt, L.L. von Moltke, Atazanavir: effects on P-glycoprotein transport and CYP3A metabolism in vitro, *Drug Metab Dispos*, 33 (2005) 764-770.
- [148] L. Bousquet, C. Roucairol, A. Hembury, M.C. Nevers, C. Creminon, R. Farinotti, A. Mabondzo, Comparison of ABC transporter modulation by atazanavir in lymphocytes and human brain endothelial cells: ABC transporters are involved in the atazanavir-limited passage across an in vitro human model of the blood-brain barrier, *AIDS Res Hum Retroviruses*, 24 (2008) 1147-1154.



References

- [149] O. Janneh, T. Anwar, C. Jungbauer, S. Kopp, S.H. Khoo, D.J. Back, P. Chiba, P-glycoprotein, multidrug resistance-associated proteins and human organic anion transporting polypeptide influence the intracellular accumulation of atazanavir, *Antivir Ther*, 14 (2009) 965-974.
- [150] M.B. Lucia, C. Golotta, S. Rutella, E. Rastrelli, A. Savarino, R. Cauda, Atazanavir inhibits P-glycoprotein and multidrug resistance-associated protein efflux activity, *J Acquir Immune Defic Syndr*, 39 (2005) 635-637.
- [151] C.H. Storch, D. Theile, H. Lindenmaier, W.E. Haefeli, J. Weiss, Comparison of the inhibitory activity of anti-HIV drugs on P-glycoprotein, *Biochem Pharmacol*, 73 (2007) 1573-1581.
- [152] J. Drewe, H. Gutmann, G. Fricker, M. Torok, C. Beglinger, J. Huwyler, HIV protease inhibitor ritonavir: a more potent inhibitor of P-glycoprotein than the cyclosporine analog SDZ PSC 833, *Biochem Pharmacol*, 57 (1999) 1147-1152.
- [153] T. Ikezoe, Y. Hisatake, T. Takeuchi, Y. Ohtsuki, Y. Yang, J.W. Said, H. Taguchi, H.P. Koeffler, HIV-1 protease inhibitor, ritonavir: a potent inhibitor of CYP3A4, enhanced the anticancer effects of docetaxel in androgen-independent prostate cancer cells in vitro and in vivo, *Cancer Res*, 64 (2004) 7426-7431.
- [154] S. Klein, J. Butler, J.M. Hempenstall, C. Reppas, J.B. Dressman, Media to simulate the postprandial stomach I. Matching the physicochemical characteristics of standard breakfasts, *J Pharm Pharmacol*, 56 (2004) 605-610.
- [155] G. Singh, R.S. Pai, Optimized self-nanoemulsifying drug delivery system of atazanavir with enhanced oral bioavailability: in vitro/in vivo characterization, *Expert Opin Drug Deliv*, 11 (2014) 1023-1032.
- [156] G. Singh, R.S. Pai, Atazanavir-loaded Eudragit RL 100 nanoparticles to improve oral bioavailability: optimization and in vitro/in vivo appraisal, *Drug Deliv*, (2014) 1-8.
- [157] K. Fukushima, S. Terasaka, K. Haraya, S. Kodera, Y. Seki, A. Wada, Y. Ito, N. Shibata, N. Sugioka, K. Takada, Pharmaceutical approach to HIV protease inhibitor atazanavir for bioavailability enhancement based on solid dispersion system, *Biol Pharm Bull*, 30 (2007) 733-738.
- [158] S. Klein, N.L. Buchanan, C.M. Buchanan, Miniaturized transfer models to predict the precipitation of poorly soluble weak bases upon entry into the small intestine, *AAPS PharmSciTech*, 13 (2012) 1230-1235.
- [159] R.K. Parikh, D.C. Parikh, R.R. Delvadia, S.M. Patel, A Novel Multicompartment Dissolution Apparatus for Evaluation of Floating Dosage Form Containing Poorly Soluble Weakly Basic Drug, *Dissolution Technologies*, (2006) 14-19.
- [160] Food and Drug Administration (FDA), Question-Based Review for CMC Evaluations of ANDAs, Available from: <http://www.fda.gov/Drugs/DevelopmentApprovalProcess/HowDrugsareDevelopedandApproved/ApprovalApplications/AbbreviatedNewDrugApplicationANDAGenerics/ucm120971.htm>, (2014).
- [161] L.X. Yu, Pharmaceutical quality by design: product and process development, understanding, and control, *Pharm Res*, 25 (2008) 781-791.
- [162] C. Schiller, C.P. Frohlich, T. Giessmann, W. Siegmund, H. Monnikes, N. Hosten, W. Weitschies, Intestinal fluid volumes and transit of dosage forms as assessed by magnetic resonance imaging, *Aliment Pharmacol Ther*, 22 (2005) 971-979.
- [163] D.M. Mudie, K. Murray, C.L. Hoad, S.E. Pritchard, M.C. Garnett, G.L. Amidon, P.A. Gowland, R.C. Spiller, G.E. Amidon, L. Marciani, Quantification of gastrointestinal liquid



- volumes and distribution following a 240 mL dose of water in the fasted state, *Mol Pharm*, 11 (2014) 3039-3047.
- [164] T. Shingaki, T. Takashima, Y. Wada, M. Tanaka, M. Kataoka, A. Ishii, Y. Shigihara, Y. Sugiyama, S. Yamashita, Y. Watanabe, Imaging of gastrointestinal absorption and biodistribution of an orally administered probe using positron emission tomography in humans, *Clinical pharmacology and therapeutics*, 91 (2012) 653-659.
- [165] L. Marciani, E.F. Cox, C.L. Hoad, S. Pritchard, J.J. Totman, S. Foley, A. Mistry, S. Evans, P.A. Gowland, R.C. Spiller, Postprandial changes in small bowel water content in healthy subjects and patients with irritable bowel syndrome, *Gastroenterology*, 138 (2010) 469-477, 477 e461.
- [166] E. Placidi, C.L. Hoad, L. Marciani, P.A. Gowland, R.C. Spiller, PTH-045 Effects of an osmotic laxative on the distribution of water between the small and large intestine in humans, *Gut*, 59 (2010).
- [167] Y. Xu, X. Liu, R. Lian, S. Zheng, Z. Yin, Y. Lu, W. Wu, Enhanced dissolution and oral bioavailability of aripiprazole nanosuspensions prepared by nanoprecipitation/homogenization based on acid-base neutralization, *Int J Pharm*, 438 (2012) 287-295.
- [168] R. Holm, L. Andresen, C. Strange, Oral bioavailability of a poorly aqueous drug from three different SBE7-beta-cyclodextrin based formulations in beagle dogs, *Results in pharmaceutical sciences*, 1 (2011) 57-59.
- [169] P. Jarho, A. Urtti, T. Jarvinen, Hydroxypropyl-beta-cyclodextrin increases the aqueous solubility and stability of pilocarpine prodrugs, *Pharm Res*, 12 (1995) 1371-1375.
- [170] S.M. Pathak, P. Musmade, S. Dengle, A. Karthik, K. Bhat, N. Udupa, Enhanced oral absorption of saquinavir with Methyl-Beta-Cyclodextrin-Preparation and in vitro and in vivo evaluation, *Eur J Pharm Sci*, 41 (2010) 440-451.
- [171] R.C. Nagarwal, D.N. Ridhurkar, J.K. Pandit, In vitro release kinetics and bioavailability of gastroretentive cinnarizine hydrochloride tablet, *AAPS PharmSciTech*, 11 (2010) 294-303.
- [172] J. Varshosaz, M. Tabbakhian, M. Zahrooni, Development and characterization of floating microballoons for oral delivery of cinnarizine by a factorial design, *J Microencapsul*, 24 (2007) 253-262.
- [173] S. Verma, K. Nagpal, S.K. Singh, D.N. Mishra, Unfolding type gastroretentive film of Cinnarizine based on ethyl cellulose and hydroxypropylmethyl cellulose, *International journal of biological macromolecules*, 64 (2014) 347-352.
- [174] A. Yadav, D.K. Jain, Gastroretentive microballoons of metformin: Formulation development and characterization, *Journal of advanced pharmaceutical technology & research*, 2 (2011) 51-55.
- [175] S.M. Abouelatta, A.A. Aboelwafa, R.M. Khalil, O.N. ElGazayerly, Floating lipid beads for the improvement of bioavailability of poorly soluble basic drugs: in-vitro optimization and in-vivo performance in humans, *Eur J Pharm Biopharm*, 89 (2015) 82-92.
- [176] R. Takano, K. Sugano, A. Higashida, Y. Hayashi, M. Machida, Y. Aso, S. Yamashita, Oral absorption of poorly water-soluble drugs: computer simulation of fraction absorbed in humans from a miniscale dissolution test, *Pharm Res*, 23 (2006) 1144-1156.
- [177] R. Takano, K. Furumoto, K. Shiraki, N. Takata, Y. Hayashi, Y. Aso, S. Yamashita, Rate-limiting steps of oral absorption for poorly water-soluble drugs in dogs; prediction from a miniscale dissolution test and a physiologically-based computer simulation, *Pharm Res*, 25 (2008) 2334-2344.



References

- [178] B. Hens, J. Brouwers, B. Anneveld, M. Corsetti, M. Symillides, M. Vertzoni, C. Reppas, D.B. Turner, P. Augustijns, Gastrointestinal transfer: in vivo evaluation and implementation in in vitro and in silico predictive tools, *Eur J Pharm Sci*, 63 (2014) 233-242.
- [179] Y. Chen, J.Y. Jin, S. Mukadam, V. Malhi, J.R. Kenny, Application of IVIVE and PBPK modeling in prospective prediction of clinical pharmacokinetics: strategy and approach during the drug discovery phase with four case studies, *Biopharm Drug Dispos*, 33 (2012) 85-98.
- [180] K. Abduljalil, M. Jamei, A. Rostami-Hodjegan, T.N. Johnson, Changes in individual drug-independent system parameters during virtual paediatric pharmacokinetic trials: introducing time-varying physiology into a paediatric PBPK model, *AAPS J*, 16 (2014) 568-576.
- [181] F. Khalil, S. Laer, Physiologically based pharmacokinetic models in the prediction of oral drug exposure over the entire pediatric age range-sotalol as a model drug, *AAPS J*, 16 (2014) 226-239.
- [182] G. Lu, K. Abduljalil, M. Jamei, T.N. Johnson, H. Soltani, A. Rostami-Hodjegan, Physiologically-based pharmacokinetic (PBPK) models for assessing the kinetics of xenobiotics during pregnancy: achievements and shortcomings, *Current drug metabolism*, 13 (2012) 695-720.
- [183] S. Cheeti, N.R. Budha, S. Rajan, M.J. Dresser, J.Y. Jin, A physiologically based pharmacokinetic (PBPK) approach to evaluate pharmacokinetics in patients with cancer, *Biopharm Drug Dispos*, 34 (2013) 141-154.
- [184] N. Djebli, D. Fabre, X. Boulenc, G. Fabre, E. Sultan, F. Hurbin, Physiologically-based Pharmacokinetic Modeling for Sequential Metabolism: Effect of CYP2C19 Genetic Polymorphism on Clopidogrel and Clopidogrel Active Metabolite Pharmacokinetics, *Drug Metab Dispos*, (2015).
- [185] K.R. Yeo, J.R. Kenny, A. Rostami-Hodjegan, Application of in vitro-in vivo extrapolation (IVIVE) and physiologically based pharmacokinetic (PBPK) modelling to investigate the impact of the CYP2C8 polymorphism on rosiglitazone exposure, *Eur J Clin Pharmacol*, 69 (2013) 1311-1320.
- [186] X. Boulenc, O. Nicolas, S. Hermabessiere, I. Zobouyan, V. Martin, Y. Donazzolo, C. Ollier, CYP3A4-based drug-drug interaction: CYP3A4 substrates' pharmacokinetic properties and ketoconazole dose regimen effect, *European journal of drug metabolism and pharmacokinetics*, (2014).
- [187] N. Marsousi, Y. Daali, S. Rudaz, L. Almond, H. Humphries, J. Desmeules, C.F. Samer, Prediction of Metabolic Interactions With Oxycodone via CYP2D6 and CYP3A Inhibition Using a Physiologically Based Pharmacokinetic Model, *CPT: pharmacometrics & systems pharmacology*, 3 (2014) e152.
- [188] B. Xia, A. Barve, T. Heimbach, T. Zhang, H. Gu, L. Wang, H. Einolf, N. Alexander, I. Hanna, J. Ke, J.B. Mangold, H. He, G. Sunkara, Physiologically based pharmacokinetic modeling for assessing the clinical drug-drug interaction of alisporivir, *Eur J Pharm Sci*, 63 (2014) 103-112.
- [189] K. Ball, F. Bouzom, J.M. Scherrmann, B. Walther, X. Decleves, Comparing translational population-PBPK modelling of brain microdialysis with bottom-up prediction of brain-to-plasma distribution in rat and human, *Biopharm Drug Dispos*, 35 (2014) 485-499.
- [190] G. Levy, M. Gibaldi, W.J. Jusko, Multicompartment pharmacokinetic models and pharmacologic effects, *J Pharm Sci*, 58 (1969) 422-424.
- [191] A. Selen, P.A. Dickinson, A. Mullertz, J.R. Crison, H.B. Mistry, M.T. Cruanes, M.N. Martinez, H. Lennernas, T.L. Wigal, D.C. Swinney, J.E. Polli, A.T. Serajuddin, J.A. Cook, J.B.



- Dressman, The biopharmaceutics risk assessment roadmap for optimizing clinical drug product performance, *J Pharm Sci*, 103 (2014) 3377-3397.
- [192] A. Caruso, N. Frances, C. Meille, A. Greiter-Wilke, A. Hillebrecht, T. Lave, Translational PK/PD modeling for cardiovascular safety assessment of drug candidates: Methods and examples in drug development, *Journal of pharmacological and toxicological methods*, 70 (2014) 73-85.
- [193] J.B. Knaak, C.C. Dary, M.S. Okino, F.W. Power, X. Zhang, C.B. Thompson, R. Tornerov-Velez, J.N. Blancato, Parameters for Carbamate Pesticide QSAR and PBPK/PD Models for Human Risk Assessment, *Reviews of environmental contamination and toxicology*, 193 (2008) 53-212.
- [194] H. Mishra, S. Polak, M. Jamei, A. Rostami-Hodjegan, Interaction Between Domperidone and Ketoconazole: Toward Prediction of Consequent QTc Prolongation Using Purely In Vitro Information, *CPT: pharmacometrics & systems pharmacology*, 3 (2014) e130.
- [195] T. Eissing, L. Kuepfer, C. Becker, M. Block, K. Coboeken, T. Gaub, L. Goerlitz, J. Jaeger, R. Loosen, B. Ludewig, M. Meyer, C. Niederalt, M. Sevestre, H.U. Siegmund, J. Solodenko, K. Thelen, U. Telle, W. Weiss, T. Wendl, S. Willmann, J. Lippert, A computational systems biology software platform for multiscale modeling and simulation: integrating whole-body physiology, disease biology, and molecular reaction networks, *Frontiers in physiology*, 2 (2011) 4.
- [196] M. Tubic, D. Wagner, H. Spahn-Langguth, M.B. Bolger, P. Langguth, In silico modeling of non-linear drug absorption for the P-gp substrate talinolol and of consequences for the resulting pharmacodynamic effect, *Pharm Res*, 23 (2006) 1712-1720.
- [197] R. Cristofolletti, J.B. Dressman, Use of physiologically based pharmacokinetic models coupled with pharmacodynamic models to assess the clinical relevance of current bioequivalence criteria for generic drug products containing Ibuprofen, *J Pharm Sci*, 103 (2014) 3263-3275.
- [198] S.M. Huang, M. Rowland, The role of physiologically based pharmacokinetic modeling in regulatory review, *Clinical pharmacology and therapeutics*, 91 (2012) 542-549.
- [199] P. Zhao, L. Zhang, J.A. Grillo, Q. Liu, J.M. Bullock, Y.J. Moon, P. Song, S.S. Brar, R. Madabushi, T.C. Wu, B.P. Booth, N.A. Rahman, K.S. Reynolds, E. Gil Berglund, L.J. Lesko, S.M. Huang, Applications of physiologically based pharmacokinetic (PBPK) modeling and simulation during regulatory review, *Clinical pharmacology and therapeutics*, 89 (2011) 259-267.



9 Curriculum Vitae

9.1 Personal Information

Date of birth	08/05/1984
Place of birth	Vilnius, Lithuania
Citizenships	German, Lithuanian

9.2 Professional experience

Since 07/2015	Business Development at Biorelevant.com Ltd., London, United Kingdom
01/2010– 06/2015	Scientist in the Institute of Pharmaceutical Technology, Goethe University, Frankfurt, Germany
04/2009 – 11/2009	Pharmacist at Internationale Ludwigs-Apotheke (International Pharmacy), Munich, Germany
11/2008 – 04/2009	Pharmacist at Lilly Deutschland GmbH, Medical and scientific department, CNS division, Bad Homburg, Germany
04/2007 – 11/2007	Student trainee at Lilly Deutschland GmbH, Medical and scientific department, diabetes division, Bad Homburg, Germany



9.3 Education

- 09/2012– 06/2015 PhD candidate at the Institute of Pharmaceutical Technology,
Goethe University, Frankfurt, Germany
Group: Prof. Dr. Dressman
Thesis: “Predicting Oral Absorption of Poorly Soluble Weakly
Basic Drugs“
- 09/2007 – 04/2012 Student of Economics and Business Administration at
Goethe University, Frankfurt, Germany
Majors: Management and Marketing
Degree: Bachelor of Science
Bachelor thesis: “Forming Utility and Attention Based
Consideration Sets“
- 12/2009 State-approved pharmaceutical license
- 09/2004 – 09/2008 Student of Pharmacy at Goethe University, Frankfurt,
Germany
Degree: Pharmacist
- 09/1995 – 06/2004 Student at Kaiserin-Friedrich-Gymnasium, Bad Homburg,
Germany
Degree: university-entrance diploma
- 09/2001 – 12/2001 Studying abroad at Bryanston School, Blandford Forum,
United Kingdom
- 01/1995 – 09/1995 Student at Ketteler-Francke-Schule, Bad Homburg, Germany
- 09/1991 – 10/1994 Student at school No. 31 (grades 1.-3.), Vilnius, Lithuania



10 Scientific Publications

10.1 Papers

Berlin M, Ruff A, Kesisoglou F, Xu W, Wang MH, Dressman JB. Advances and challenges in PBPK modeling - Analysis of factors contributing to the oral absorption of atazanavir, a poorly soluble weak base. Eur J Pharm Biopharm. 2015 Jun;93:267-80.

Berlin M, Przyklenk KH, Richtberg A, Baumann W, Dressman JB. Prediction of oral absorption of cinnarizine - a highly supersaturating poorly soluble weak base with borderline permeability. Eur J Pharm Biopharm. 2014 Nov;88(3):795-806.

10.2 Posters

Berlin M, Przyklenk KH, Dressman JB. Prediction of Oral Absorption of Cinnarizine Under Fasted and Fed State Conditions. FIP Pharmaceutical Sciences World Congress. 13-14 April 2014. Melbourne, Victoria, Australia.

Ruff A, Berlin M, Kesisoglou F, Wang MH, Xu W, Dressman JB. Influence of HPMC capsule shells on supersaturation and precipitation in Transfer Experiments. FIP Pharmaceutical Sciences World Congress. 13-14 April 2014. Melbourne, Victoria, Australia.

Berlin M, Dressman JB. *IVISIV* Correlation of Poorly Soluble Weak Bases Using Biorelevant Dissolution and Transfer Methods. AAPS Annual Meeting and Exposition. 10-14 November 2013. San Antonio, TX, USA

11 Academic Teachers

Hennig Blume, Theo Dingermann, Jennifer B. Dressman, Eberhard Ehlers, Axel Helmstädter, Michael Huth, Michael Karas, Jochen Klein, Jörg Kreuter, Günther Lamprecht, Rolf Marschalek, Walter E. Müller, Reinhard Schmidt, Manfred Schubert-Zsilavecz, Martin Schulz, Holger Stark, Dieter Steinhilber.



